Physical behaviour of Greenlandic rock flour, soils and rock flour amended soils

Particle, pore-network and mechanical properties

Pesch, Charles

DOI (link to publication from Publisher):
10.54337/aau495048349

Publication date:
2022

Document Version
Publisher's PDF, also known as Version of record

PHYSICAL BEHAVIOUR OF GREENLANDIC ROCK FLOUR, SOILS AND ROCK FLOUR AMENDED SOILS

PARTICLE, PORE-NETWORK AND MECHANICAL PROPERTIES

BY
CHARLES PESCH

DISSERTATION SUBMITTED 2022

AALBORG UNIVERSITY
DENMARK

Physical behaviour of Greenlandic rock flour, soils and rock flour amended soils

Particle, pore-network and mechanical properties

Charles Pesch

June 2022

Dissertation submitted in partial fulfilment
of the requirements for the degree of
Doctor of Philosophy (PhD) in Civil Engineering
at the
Faculty of Engineering and Science
Aalborg University

Dissertation submitted: June 2022

PhD supervisor: Prof. Per Moldrup
Aalborg University, Denmark

Assistant PhD supervisor: Prof. Lis Wollesen de Jonge
Aarhus University, Denmark

PhD committee: Associate Professor Francesco Ferri
Aalborg University, Denmark

Adjunct Professor, Principal Scientific Officer
David Robinson
Center for Ecology & Hydrology Environment
Centre Wales, United Kingdom

Professor Thomas Keller
Swedish University of Agricultural Sciences, Sweden

PhD Series: Faculty of Engineering and Science, Aalborg University

Department: Department of the Build Environment

ISSN (online): 2446-1636
ISBN (online): 978-87-7573-882-3

Published by:
Aalborg University Press
Kroghstræde 3
DK – 9220 Aalborg Ø
Phone: +45 99407140
aauf@forlag.aau.dk
forlag.aau.dk

Printed in Denmark by Stibo Complete, 2022

List of supporting papers

Paper I Pesch, C., Weber, P. L., Moldrup, P., de Jonge, L. W., Arthur, E., & Greve, M. H. (2022). Physical characterization of glacial rock flours from fjord deposits in South Greenland–Toward soil amendment. *Soil Science Society of America Journal*, *86*(2), 407–422. doi: 10.1002/saj2.20352

Paper II Pesch, C., Lamandé, M., de Jonge, L. W., Norgaard, T., Greve, M. H., & Moldrup, P. (2020). Compression and rebound characteristics of agricultural sandy pasture soils from South Greenland. *Geoderma*, *380*, 114608. doi: 10.1016/j.geoderma.2020.114608

Paper III Pesch, C., Weber, P. L., de Jonge, L. W., Greve, M. H., Norgaard, T., & Moldrup, P. (2021). Soil–air phase characteristics: Response to texture, density, and land use in Greenland and Denmark. *Soil Science Society of America Journal*, *85*(5), 1534–1554. doi: 10.1002/saj2.20284

Paper IV Pesch, C., Weber, P. L., de Jonge, L. W., Greve, M. H., Lamandé, M., & Moldrup, P. (n.d.). Changes in pore-network and mechanical properties after Greenlandic rock flour addition to repacked sands and soils [submitted]. *Soil Science Society of America Jounal*, *n/a*(n/a)

Other work by the author

- Weber, P. L., Hermansen, C., Norgaard, T., Pesch, C., Moldrup, P., Greve, M. H., Müller, K., Arthur, E., & de Jonge, L. W. (2021). Moisture-dependent water repellency of Greenlandic cultivated soils. *Geoderma*, *402*, 115189. doi: 10.1016/j.geoderma.2021.115189
- Weber, P. L., Hermansen, C., Nørgaard, T., Pesch, C., Moldrup, P., Greve, M. H., Arthur, E., & de Jonge, L. W. (2022). Evaluating the particle densities of subarctic soils using pedotransfer functions and vis–NIR spectroscopy. *Soil Science Society of America Journal*, *n/a*(n/a), 1–15. doi: 10.1002/saj2.20410
- Weber, P. L., Blæsbjerg, N. H., Pesch, C., Hermansen, C., Greve, M. H., de Jonge, L. W., & Moldrup, P. (n.d.-a). Organic matter controls water retention and plant available water in cultivated soils from four regions in South Greenland [submitted]. *Soil Science Society of America Journal*, *n/a*(n/a)
- Weber, P. L., Hermansen, C., Pesch, C., Moldrup, P., Greve, M. H., Blæsbjerg, N. H., Romero, G. M., Arthur, E., & de Jonge, L. W. (n.d.-b). Glacial rock flour reduces the hydrophobicity of Greenlandic cultivated soils [submitted]. *Soil Science Society of America Journal*, *n/a*(n/a)

Summary

The interactions between the three main soil phases (solids, water, air) are complex and not fully understood. The solid phase can be subdivided into mineral and organic phases, each of which interacts very differently with the water and air phases. These interactions are further affected and complicated by external factors like climate and soil management. To understand and improve soil health and functions during climate change, more knowledge about this is needed, especially in the less investigated soil regions on Earth.

For the last three decades, the Arctic has warmed at around twice the rate compared to the entire Earth. This has dramatic consequences for the local environment and population. Although Greenland is considered the largest island on the planet, arable land is rare, and the soils exhibit low plant-available water and nutrient levels and long turn-over times for organic matter, which is also not well incorporated into the soil matrix. If the protection from the vegetation cover is missing, the coarse-textured soils are highly vulnerable to erosion. Agricultural activity in southwest Greenland needs to adapt to those challenges.

This PhD dissertation focused mainly on the mechanical properties and air-phase characteristics of repacked and intact, sandy cultivated pasture soils from South Greenland. Additionally, the physico-chemical properties of glacially abraded mineral rock powder (glacial rock flour, GRF) were investigated in the perspective of future use as a soil amendment towards creating healthy and robust arable soils.

The investigated GRFs showed good potential for future soil amendment by providing the mineral phase of the soil with additional surface area and charge to facilitate soil aggregation and soil organic matter protection. The mapped amounts of GRF would be largely sufficient to provide the entire Greenlandic agricultural area currently in use with enough glacial rock flour to be utilised as a soil amendment.

The Greenlandic pasture soils showed both resistance and resilience to compaction, which was mainly attributed to the high organic matter contents of the soil matrix and the dense root zone of the soil cover. As expected, soil-structure

indices derived from measurements of air-phase parameters revealed a pronounced lack of well-developed soil structure of all the investigated Greenlandic soils. In line with this, results and conclusions from intact and repacked soils agreed fairly well throughout this study.

At low GRF application rates ($< 5\,\%$ w/w), the plant available water content of repacked sandy soils was not affected but decreased significantly at high application rates ($> 10\,\%$ w/w). GRF amendment reduced gas diffusivity and increased pore network tortuosity without affecting the effective pore diameter for convective gas transport, implying a complex pore-network change with GRF application. It was shown that present models for predicting the soil-gas diffusion coefficient in non-amended soils can still predict gas diffusion accurately after GRF application, merely by taking the GRF effects on water retention and compaction into account. The soil compressibility increased at high GRF application rates, whereas the short-term recovery from compaction was not affected.

This PhD study provided the first details on the mechanical and pore-network parameters from the until now less investigated agricultural soils from sub and low-arctic South Greenland. Furthermore, the possible effect of glacial rock flour amendment on soil's pore network and mechanical stability was described for the first time.

Resumé

Interaktioner mellem jordens 3 faser (partikler, vand, luft) er komplekse, og det er ikke endnu fuldt belyst, hvordan de påvirker jordens sundhed og kvalitet. Partikelfasen kan yderligere inddeles i de mineralske partikler og jordens organiske stof; hver af disse to partikelfaser interagerer meget forskelligt med jordens vand- og luftfaser. Fase-interaktioner og -funktioner er yderligere påvirket og kontrolleret af eksterne faktorer som klima og jordbearbejdning. For at forstå og forbedre jordens sundhed og produktivitet under et skiftende klima, skal der skabes en bedre forståelse af jordens fasefunktioner og de styrende parametre for disse, især i de mindre undersøgte landområder såsom Arktis.

I de sidste tre dekader har Arktis været udsat for en global opvarmning, der er ca. dobbelt så stor som for Jordkloden som helhed. Dette har dramatiske konsekvenser for både det lokale miljø og befolkningen. Selvom Grønland betragtes som den største ø på Jordkloden, er dyrkbar jord ressourcen sparsom, og den potentielt dyrkbare jord er karakteriseret ved lavt indhold af plantetilgængeligt vand og næringsstoffer. Jordene udviser samtidig en meget langsom omsætning af organisk stof, og det organiske stof er ikke tilstrækkeligt indbygget i jordmatricen, hvilket skaber strukturløse jorde. De betydelige landområder, der derudover er både sandede og mangler beskyttelse fra et plantedække er derfor meget sårbare overfor vind- og vand-erosion. En fremtidig landbrugsproduktion i Sydgrønland vil kræve en smart adaptering til disse store jord- og klimaudfordringer.

Denne PhD afhandling fokuserer på jordens mekaniske og porenetværk (luft fase) parametre i både pakkede og intakte prøver fra dyrkede jorde og græsningsarealer i Sydgrønland. Derudover blev de fysiske og kemiske karakteristika af en række forskellige typer gletsjermel (GM; sedimenter af finkornet mineralsk materiale) fra de Grønlandske fjorde undersøgt med henblik på at anvende Grønlandsk GM som lokalt og bæredygtigt jordforbedringsmiddel for sandede, strukturløse jorde hen imod at skabe sunde og robuste dyrkningsjorde.

De undersøgte GM materialer udviste et højt potentiale som jordforbedringsmiddel i forhold til at tilføre jorde yderlige mineralsk overfladeareal og dermed skabe mulighed for dannelse af komplekser (aggregater) mellem GM og det typisk høje indhold af organisk stof i jordene. Denne aggregatdannelse vil være helt

essentiel, da den potentielt vil forbedre både geniltning og indhold af plantetilgængeligt vand og tilgang til næringsstoffer i jordene. En foreløbig kortlægning af GM forekomster viste, at der er tilstrækkeligt GM til jordforbedring af hele det Grønlandske dyrkningsareal nu og i fremtiden.

De Grønlandske jorde udviste både styrke og modstandskraft (robusthed) overfor mekaniske påvirkninger. dette skyldes især det typisk høje indhold af organisk stof og sand kombineret med et tæt rodnet af græsrødder. Som forventet illustrerede porenetværks-parameter udledt fra målinger af gasdiffusion og luftpermeabilitet en lavt udviklet jordstruktur. Derfor var der også generelt god overensstemmelse mellem målinger og resultater fra pakkede og intakte jorde i denne afhandling.

Tilsætning af relativt lave og realistiske mængder af GM til jordene gav ikke en påvirkning på jordenes indhold af plantetilgængeligt vand. Tilsætning af meget høje GM koncentrationer reducerede derimod indholdet af plantilgængeligt vand, fordi GM tilsætning skabte mere hårdt bundet (ikke plantetilgængeligt) vand, og der ikke samtidigt skete aggregatdannelse i disse korttidsforsøg. GM tilsætning reducerede gasdiffusivitet (forholdet mellem gasdiffusionskoefficient i jord og i ren luft) og gav øget snoethed af jordens porenetværk, men gav ikke umiddelbart en ændring i den beregnede effektive pore diameter for konvektiv gas transport.

Resultaterne viser, at GM tilsætning giver komplekse ændringer i jordens porenetværks-struktur. Samtidigt er det en vigtig konklusion fra denne afhandling, at eksisterende modeller for gasdiffusivitet i jord meget præcist kunne forudsige ændringer i jordenes gasdiffusivitet ved tilsætning af GM blot ud fra kendskab til, hvordan GM tilsætningen ændrer jordenes vandretention og fasefordelingen mellem partikler, vand og luft. Jordenes potentielle kompakteringsniveau steg efter høje tilsætninger af GM, mens jordenes (typisk meget gode) korttidsevne til at komme sig (rebounde) efter kompaktering ikke blev påvirket.

Denne PhD afhandling præsenterer de første meget detaljerede undersøgelser af mekaniske og porenetværks funktioner for disse indtil videre meget lidt undersøgte Arktiske jorde fra Sydgrønland. Desuden er mulige positive og negative effekter fra tilsætning af lokalt gletsjermel som jordforbedringsmiddel målt og diskuteret.

Preface

This dissertation has been submitted for assessment in partial fulfilment of the PhD degree. As part of the assessment, co-author statements have been made available to the assessment committee and are also available at the Faculty.

The present three-year PhD study was part of the research project *NewLand* financed by the Danish Council for Independent Research (Technology and Production Sciences) and was carried out at Aalborg University, Department of the Built Environment, Division of Water and Environment. Most of the laboratory work associated with the study was carried out at Aarhus University, Department of Agroecology, Research Center Foulum.

The dissertation is based on three papers (Paper I, Paper II and Paper III) and one submitted manuscript (Paper IV). All the papers were prepared in close cooperation with the Research Center Foulum.

The contents and scientific findings of the papers are briefly discussed in the extended summary of this dissertation. Additionally, background information that could not be included in the papers will be presented.

Acknowledgements

First and foremost I would like to thank Per Moldrup for giving me the chance to prepare this dissertation under his supervision. I also would like to thank Lis Wollesen de Jonge, not only for providing access to the research facilities at the Research Center Foulum, but also for preventing Per and myself from digressing.

I would like to thank my co-authors from Foulum Trine, Emmanuel, Mathieu and Mogens for sharing their knowledge and giving valuable comments and advice to produce well received articles.

Without the help of Peter, this dissertation could not have been accomplished. The amount of time he spent in the laboratory and, not to forget, the time he spent organising the trips to Greenland was extraordinary. It has been a pleasure working with you.

I also would like to thank my colleagues from Aalborg University, especially Alvise with whom I spent many hours in the office, and not to forget Kirstine, Lucian, Jesper, Claudia, Rupa, Fan, Rasmus, Sorin, and many more.

I also would like to thank Annette who helped me during the final stages in the laboratory.

Without the help and constant support during my studies from Robert, Liz and my family, especially my mother, I would not have been able to accomplish this dissertation.

Contents

1. Introduction

The DFF (Danmarks Frie Forskningsfond [Independent Research Fund Denmark]) funded research project –*NewLand*– investigates the potential of glacial rock flour as an environment-friendly soil amendment to improve Greenlandic agricultural soils. The the project's main objective is to determine the benefits of rock flour amendment on physical and chemical soil properties and the repercussions on agricultural production. Furthermore, the glacial rock flours and agricultural soils found in South Greenland should be mapped and characterised.

Objectives

The specific objectives of this dissertation and the supporting papers were:

(a) Basic soil characterisation and preliminary studies to detect future changes in soil properties (background soil screening, Paper II and Paper III)

(b) Physico-chemical characterisation of glacial rock flour and its availability for regional exploitation (Paper I)

(c) Application of mass transport models to characterise soil structure with focus on Greenlandic soils (Paper III)

(d) Effect of glacial rock flour amendment on functional and mechanical soil properties on repacked soil samples (Paper IV)

The extended summary of the dissertation includes relevant background information and data that could not be included in the supporting papers:

(i) Climate monitoring

(ii) Site characterisation

(iii) Comparing intact and repacked soils

The soil-related data was measured on soil samples collected during four field trips to Greenland (June 2019, August 2019, August 2020 and September 2021).

1.1. Farming in South Greenland

The colonisation of Greenland by the Norse started at around 985 AD and lasted until the end of the fifteenth century (Berglund, 1986; Buckland et al., 2009); it concurred with the Medieval Warm Period (MWP) (Kuijpers et al., 1999). The Norse introduced agriculture for food procurement, and at the peak of the medieval agricultural activity, approximately 2 000 to 3 000 settlers occupied around 500 farms (Bichet et al., 2013). Norse agriculture was mainly based on livestock (cattle and sheep) and the required winter forage (hay) production (Berglund, 1986). Evidence from pollen analysis additionally indicated attempts to produce cereals (Edwards et al., 2008; Schofield et al., 2007). The land management of the Norse included irrigation and manuring (Berglund, 1986; Buckland et al., 2009).

Figure 1: Typical farm in south Greenland (South Igaliku).

During the fifteenth century, however, the Norse colonies vanished, and the reason for this remains a debate among the scientific community. Several reasons were presented for the rapid decline of Norse activity. The onset of the Little Ice Age (LIA) accompanied by lower temperatures and redistribution of precipitation (Christiansen, 1998) following the MWP coincides with the disappearance of the Norse settlements. The associated environmental changes may have led to a decline in agricultural activity and subsequently to shortages in food production (Ledger et al., 2013). Several studies (Bichet et al., 2013; Massa et al., 2012) investigated lake sediments across South Greenland and revealed massive soil erosion from land clearance and overgrazing combined with climatic changes. Other studies showed that socio-economic factors might have played an equally important role in the demise of Norse settlements in Greenland (Dugmore et al., 2007; Lynnerup, 1996). Most likely, the exodus of the Norse from Greenland resulted from a complex interplay of all of the above circumstances.

After approximately three centuries of no agricultural activity in Greenland, it was reintroduced in the eighteenth century by the Danish and intensified in 1924

at the urging of the Danish government. The current form of livestock management with summer pastures for grazing sheep and winter indoor husbandry dates back to the 1960s and the mechanisation of forage production to the 1980s (Bichet et al., 2013). Currently (2020), 36 farms accommodate approximately 20 000 sheep (ewes), the offspring is generally sold to the central slaughterhouse located in Narsaq. The cultivated area extends on approximately 1 100 ha (Austrheim et al., 2008; Bojesen et al., 2019) and mainly consists of cultivated pastures (occasionally tilled for resowing) and regularly tilled farmlands (oat, rye and barley) for winter forage (silage) production (Lehmann et al., 2016). The cultivated farmlands are generally found at low altitudes and in direct vicinity to the fjords, whereas an additional 200 000 ha are used for summer pasture, i.e., sheep grazing in the mountainous areas and on plateaus not suited for cultivation (Austrheim et al., 2008).

Several authors studied the potential for intensification and expansion of agriculture in Greenland (Bojesen et al., 2019; Caviezel et al., 2017; Lehmann et al., 2016; Michelsen et al., 2014; Munk et al., 2009; Westergaard-Nielsen et al., 2015). Generally, the authors pointed out the risk of detrimental effects of intensive agriculture on soil health. The risk of further soil acidification, nutrient leaching, and the introduction of pests from overseas and changes in the soil's microbial community structure pose a major concern for future agricultural activity, especially in view of rising temperatures due to climate change (Hassol, 2004).

1.2. Main soil and climate challenges of Greenlandic pasture soils

Soils in South Greenland are characterised by a lack of clay minerals or fine mineral particles in general and a high contents of weakly decomposed organic matter. The combined effect of low clay and high organic matter contents results in particularly critical soil conditions, especially during dry periods (Jacobsen, 1987). The soils developing on glacial till and crystalline bedrock are often shallow and high in stone and gravel contents, leaving the crops with a restricted root zone and thus limited plant available water (PAW). The nutrient and water holding capacities of such soils are almost entirely dependent on the quality and amount of organic matter (Doran et al., 1994; Libohova et al., 2018), thus revealing the paramount role of the latter for soil health and crop growth.

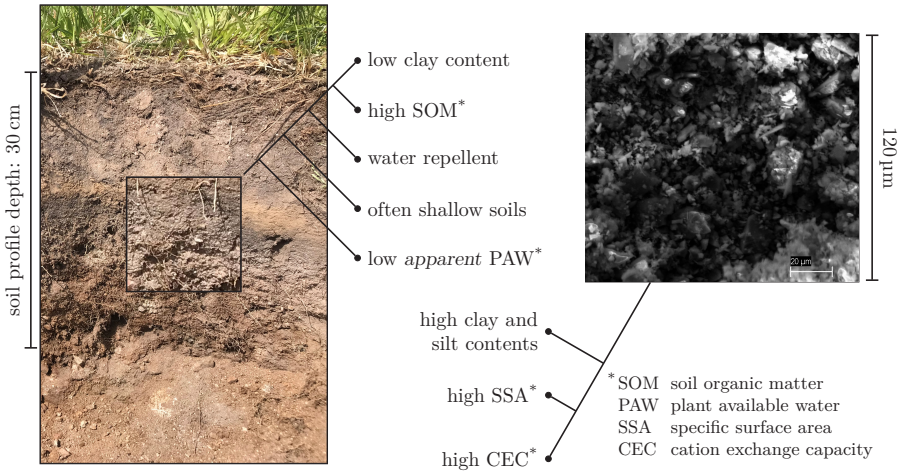

Figure 2: Overview of possible or already described challenges faced by South Greenlandic soil resources, left: soil profile from field-plot experiment Itinnera (IT-FE, see Figure 5); right: SEM micrograph of a glacial rock flour from Greenland (IK-4, Paper I).

Dry periods, especially during the growing season, are a common phenomenon in South Greenland. Strong falling winds originating from the inland ice sheet (katabatic winds, *piteraq*) causing exceptionally high evaporation rates (Jacobsen, 1987) aggravate crop water stress further. According to Christensen et al. (2016), the frequency of drought events in South Greenland will markedly increase in the course of the current century.

Soil melioration techniques by addition of mineral material has a long tradition in agriculture, and several studies showed the positive effects on soil-physical and chemical properties (Cann, 2000; Hall et al., 2010; Roper et al., 2015; Tahir et al., 2016; Ward et al., 1993). Generally, the substrate is amended with material rich in clay minerals due to their large specific surface area (SSA) and cation exchange capacity (CEC) and the resulting high reactivity with other soil components (Arthur et al., 2020; Eusterhues et al., 2003; Petersen et al., 1996; Tuller et al., 2005).

In Greenland, the movement of the glaciers constantly scrapes the underlying bedrock, producing vast amounts of fine, mechanically abraded rock flour (glacial rock flour, GRF), which are eventually evacuated from the basement of the glacier by outwash streams into periglacial lakes or fjords (Bennike et al., 2019). Paper I investigated some physical and chemical characteristics of these glacial rock flour deposits in South Greenland towards their use as a local soil

amendment and reported promising results. The rock flours are characterised by large amounts of fine particles and thus high specific surface area and cation exchange capacity compared to the soils found in South Greenland. A few studies investigated the use of Greenlandic rock flour as soil amendment and reported promising results (Gunnarsen, 2020; Gunnarsen et al., 2019; Sukstorf et al., 2020).

The mechanical stability of the Greenlandic soils was recently assessed by Paper II. The authors ascertained high bearing capacity (following Horn et al., 2003), high resilience to and recovery from compaction to the Greenlandic pasture soils. They concluded that the dense root zone of the grass-cover, together with the large amounts of particulate organic matter contents were the main reasons for the high mechanical stability of these soils. Once the grass-cover removed, due to changes in soil management or land use for example, the mechanical stability of these soils would be reduced, potentially leading to detrimental effects regarding soil functional properties. The borderline soil aeration of Greenlandic pasture soils, reported by Weber et al. (2020) and Paper III will be aggravated by reducing the total and effective porosities following potential compaction due to increased field traffic (Pulido-Moncada et al., 2019). Figure 3 illustrates the potential effect of rock flour amendment, represented by the increasing clay content, on the mechanical soil strength (precompression stress).

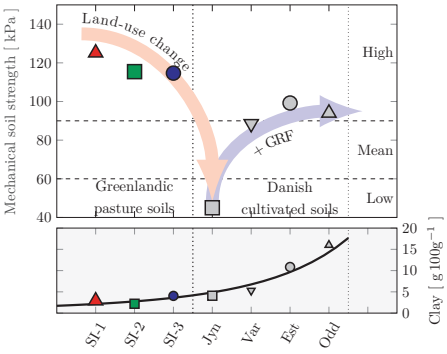

Figure 3: Robustness challenge: Change of bearing capacity after a potential future land-use change; data from Paper II.

The increase of soil strength is closely related to soil aggregation and soil structure development (Rücknagel et al., 2007), which are, in turn, governed by the potential of soil to form organo-mineral complexes (Christensen, 1995; Emerson et al., 1986). The lack of fine mineral particles providing chemically active surfaces for soil aggregation has thus also repercussions on soil structural development. The degree of soil structurality may be assessed by the soil air-phase parameters (air-filled porosity, diffusivity and air permeability; Arthur et al., 2013b;

Kawamoto et al., 2006; Moldrup et al., 2003a, 2003b; Resurreccion et al., 2007). Weber et al. (2020) and Paper III clearly showed that the Greenlandic pasture soils did not exhibit significant soil-structure development. Soil aggregation was minimal and governed by the high organic matter contents solely. Figure 4 illustrates the potential effect of rock-flour addition on soil structural development in relation to the ratio of fine particles to organic matter contents, expressed by the *Dexter* $m = (\text{clay} + \text{silt})/\text{OC}$ according to Schjønning et al. (2010).

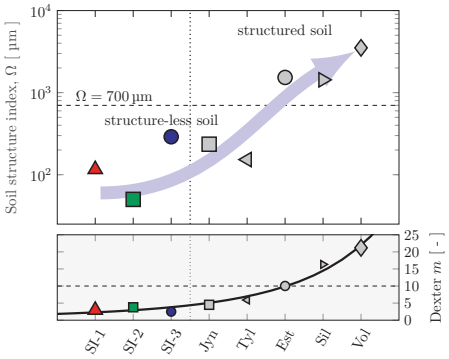

FIGURE 4: Pore-network challenge: Soil structure index $\Omega = k_a/(D_p/D_o)$ and Dexter $m = (\text{clay+silt})/\text{OC}$. $\Omega = 700\,\mu\text{m}$ is the threshold at which soil structure effects on air functions are predominant; data from Paper III

Other negative impacts of high organic matter contents in combination with a lack of fine minerals are, e.g., water repellency (de Jonge et al., 1999; Doerr et al., 2000), impeding water infiltration and homogeneous soil water distribution within the soil matrix and reduced soil aeration due to enhanced pore-network tortuosity and a disconnected air-phase (Freijer, 1994; Hamamoto et al., 2012; Iiyama et al., 2005; Weber et al., 2020). Furthermore, the protection of soil organic matter towards degradation is closely related to the content of fine particles (clay or clay + silt, i.e., particles $< 20\,\mu\text{m}$) and the associated surface charge (Kögel-Knabner et al., 2008; Lehmann et al., 2015; Lellei-Kovács et al., 2016; Schmidt et al., 2011). The compounds formed by complexation of the organic matter with the mineral phase govern many soil-physical and chemical properties (Dexter et al., 2008; Schjønning et al., 2010), and an adequate balance between the two compounds has a major impact on the soil's quality.

Providing Greenlandic sandy soils with fine-grained (clay and silt sized) mineral particles might thus alleviate some of the soil properties unfavourable for agricultural production.

2. Presentation of the study area and regional climate

2.1. Major study area

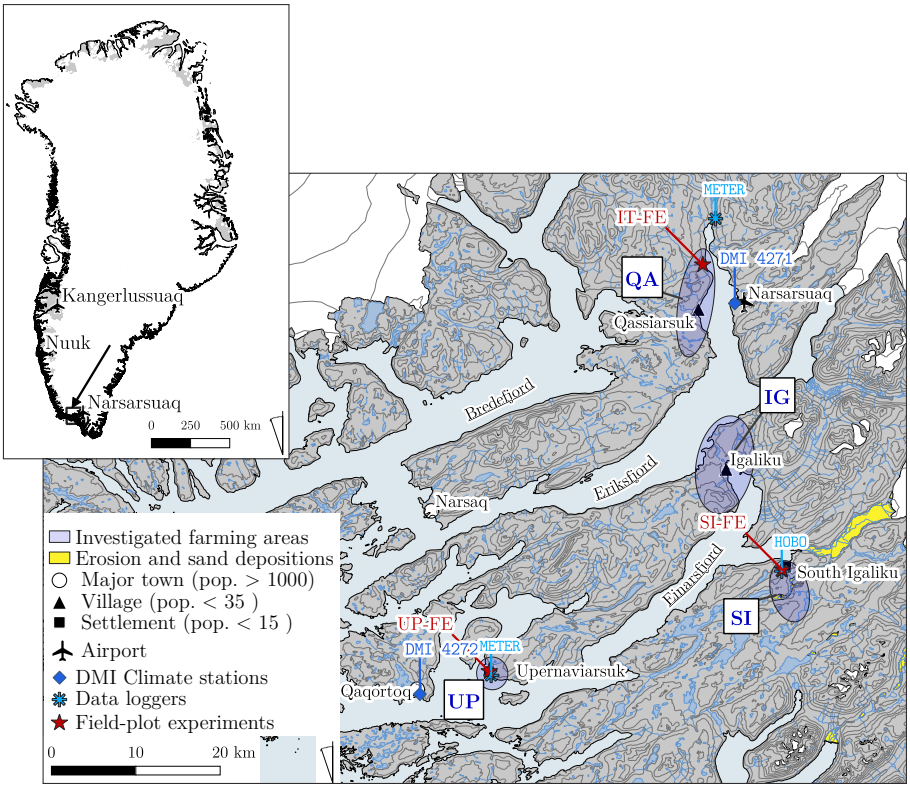

FIGURE 5: Map of the study area in south Greenland with the main agricultural areas Qassiarsuk (QA), Igaliku (IG), South Igaliku (SI) and Upernaviarsuk (UP) (north to south). The two DMI climate monitoring stations at Narsarsuaq airport and Qaqortoq and the currently installed soil-moisture and temperature monitoring stations.

The study area is located in southwest Greenland and is part of the recently appointed UNESCO World Heritage with the title: *Kujataa: A Norse and Inuit farming landscape on the Edge of the Ice Cap*. The most significant towns are Qaqortoq and Narsaq, with a population of 3 000 and 1 000 people, respectively. Notable historic sites from the Norse are abundant, and today's settlements are generally located on or close by historic Norse and Inuit settlements (Figure 5).

The study area is transected by three major fjord systems (north to south:

Bredefjord [Ikersuaq], Eriksfjord [Tunulliarfik] and Einarsfjord [Igalikup Kangerlua]) and mountain ranges up to 1 700 m. The region has been ice-free prior to 10 ka, and the isostatic uplift of the crust following deglaciation summed up to around 40 m (Bennike et al., 2002; Fleming et al., 2004). Permafrost only exists locally on upland plateaus (Zhang et al., 1999).

The geological background of the study area is diverse and is dominated by the Julianehåb batholith and intrusive complexes referred to as the *Gardar Domain* (Wegmann, 1938). The region is rich in rare and rare earth elements (Au, U, Hf, Zr, Nb, La, Ce, Nd, Sm, Eu, Tb, Yb, Lu, Y), and the geological provinces have been studied in detail regarding their geochemistry, mineralogy and lithology (Kolb et al., 2016; Steenfelt, 2012). The Julianehåb igneous complex was formed approximately 1 850 Ma to 1 780 Ma ago and consists of plutonic rocks which are crossed by numerous dykes and sills from later eras. The intrusive Gardar province comprises sedimentary and magmatic rocks which were emplaced during several events between circa 1 300 Ma and 1 140 Ma ago (Steenfelt et al., 2016).

The rocks found in the study area include igneous (both plutonic and volcanic), metamorphic and sedimentary types with, e.g., granite, granodiorite, diorite, basalt, syenite, nepheline syenite, carbonatite, gneiss, amphibolite, quartzite, sandstone, breccia and tuff (Kokfelt et al., 2019; Kolb et al., 2016; Steenfelt et al., 2016)

Natural vegetation mainly consists of dwarf-shrub heath communities, including species like grey willow (*Salix glauca* L.), shrub birch (*Betula glandulosa* Michx.) and bog blueberry (*Vaccinium uliginosum* L.). In protected valleys with low sheep density, small-growing (maximum height up to 10 m) open forests composed mainly of mountain birch (*Betula pubescens* Ehrh.), Greenland mountain-ash (*Sorbus groenlandica* Á. Löve & D. Löve) and mountain alder (*Alnus crispa* Ehrh.) may develop (Austrheim et al., 2008; Böcher, 1979; Damgaard et al., 2016).

2.2. Climate observations for two selected regions within the study area

The ice-free parts of south-west Greenland are characterised by contrasting climatic conditions, which are governed by the distance to the open sea and to the inland ice-sheet (Hanna et al., 2002). According to Beck et al. (2018)

and Feilberg (1984), the coastal areas (outer-fjord) can be classified as oceanic, low Arctic, whereas the inland areas (inner-fjord, closer to the inland ice-sheet) are classified as sub-oceanic to continental, sub-Arctic. The inner-fjord regions exhibit larger seasonal temperature variations during the year (colder winters and warmer summers) compared to the outer-fjord. The Danish Meteorological Institute (DMI) operates approximately 25 meteorological stations across Greenland, two of which are located in the study area (Narsarsuaq [DMI 4271] and Qaqortoq [DMI 4272]). The DMI regularly publishes the meteorological observations, and the herein used data was compiled from Cappelen et al. (2001) and Cappelen (2021) and half-hourly time-series, which were obtained form the DMI operated API (DMI, 2021).

Long term climate observations: climate normals

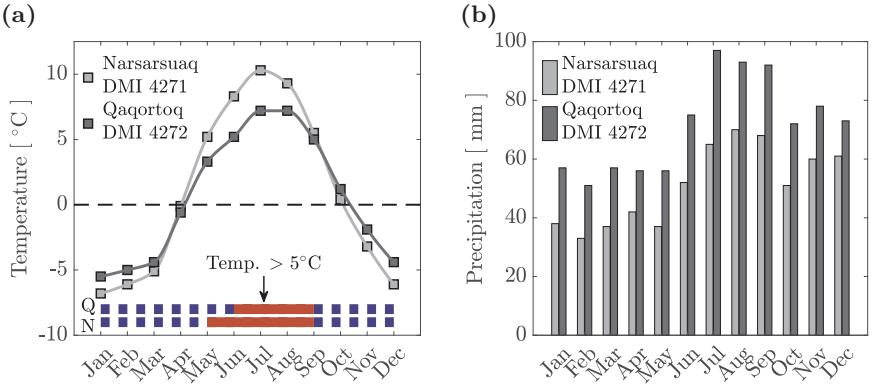

Figure 6: (a) Temperature and (b) precipitation for the climate normal 1961 – 1990 in Narsarsuaq (DMI 4271, inner fjord) and Qaqortoq (DMI 4272, outer fjord). See Figure 5 for the exact positions of the DMI weather stations.

The climate records from 1961 to 1991 illustrate the differences between the outer- and inner-fjord area climatic conditions (Figure 6 and Table 1). The two stations are only approximately 60 km apart from each other, but temperature and precipitation differ markedly. The higher seasonal variation in temperature revealed the continentality effect in Narsarsuaq compared to Qaqortoq. Comparing the temperate normals from 1961-1990 and 1981-2010, an increase for both temperature and precipitation could be observed. The absolute temperature ranges for the period 1961-1990 were −39.8 °C to 24.0 °C and −30.0 °C to

Table 1: Annual mean temperature and accumulated precipitation at inner and outer fjord stations for the indicated periods. The exact position of the DMI weather stations can be found in Figure 5

	1961–1990		1981–2010	
Station	Temperature	Precipitation	Temperature	Precipitation
Narsarsuaq (4271)	0.97	614	1.08	641
Qaqortoq (4272)	0.61	857	0.80	963

22.0 °C for the stations in Narsarsuaq and Qaqortoq, respectively. The precipitation peaked in July, August and September at both locations. Table 1 lists the annual mean temperatures and cumulative precipitations of the two 30–year periods $1961-1990$ and $1981-2010$, unveiling an increase in temperature and precipitation.

The growing season, which was defined as period exhibiting daily mean air temperatures above 5 °C, does generally not exceed 120 days; however, climate projections predict a significant increase of the growing season by the end of this century of around two months (Christensen et al., 2016; Westergaard-Nielsen et al., 2015). Although precipitation peaks during summer, the increasing variability in precipitation patterns during the growing season has led to dry spells and consequently to shortages in winter fodder production (Caviezel et al., 2017).

Similar to the foehn winds occurring in alpine regions, katabatic winds from the ice sheet (*piteraq*) occur time by time and may lead to considerable soil water evaporation from the agriculturally used lands, significantly facilitating wind erosion. Jacobsen (1987), for example, measured evaporation rates up to $1\,\mathrm{mm\,h^{-1}}$ on the first day of such a foehn event with average wind speeds of $40\,\mathrm{m\,s^{-1}}$. On the second day, under the same meteorological conditions, the evaporation rate dropped to $0.4\,\mathrm{mm\,h^{-1}}$. The top-soil had dried out, and its coarse-grained texture did not allow for capillary attraction of water from the sub-soil. The impact on the soil-water balance by such events is considerable, and dry soil conditions are thus not necessarily only a result of a lack of precipitation but also a consequence of high evaporation. This effect is enhanced if the soil cover is insufficient following, e.g., soil cultivation or overgrazing (Allen, 1990; Li et al., 2017).

Relative humidity during the study period and potential impact on soil moisture

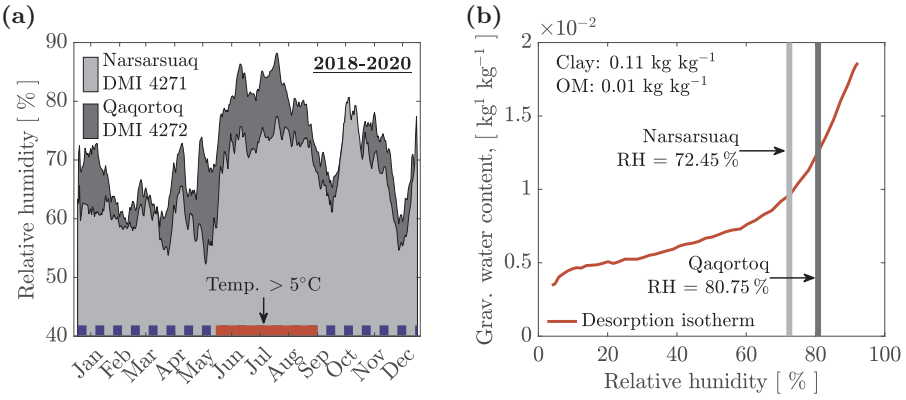

FIGURE 7: (a) Daily relative humidity (RH) averaged over the three years 2018-2020 measured at the weather stations in Narsarsuaq and Qaqortoq. The red bar indicates the period exhibiting temperatures above 5 °C common to both locations. (b) Water vapour sorption isotherm of an agricultural soil to exemplify the particle surface-bound water as a function of RH and indicated average RH measured at the two stations.

A considerable lower relative humidity characterises the inner-fjord's meso-climate (Narsarsuaq) during the growing season (defined here as the period with daily air temperatures above 5 °C) than the outer-fjord (Qaqortoq). Figure 7 a shows the mean daily relative humidities averaged over three years ($2018-2020$) for the meteorological stations at Narsarsuaq and Qaqortoq. The observed average RH for the period exhibiting $> 5\,°C$ were 80.75 and 72.45 % for the inner and outer-fjord, respectively. An analysis of variance proved that the mean RH of the two regions for the two regions were significantly different from each other (ANOVA result $F(1, 208) = 257.13, p < .001$). The effect of changes in water activity on the particle-bound water of a typical agricultural soil is shown by the vapour sorption isotherm in Figure 7 b. Small changes within the observed RH-range lead to considerable changes in the gravimetric water contents of the soil. This effect is, of course, massively weakened by the soil cover and the limited gas exchange between soil and atmosphere, but the example illustrated the drying effect of reduced RH on the upper centimetres of, e.g., a fallow or recently tilled soil.

2.3. Microclimate and soil monitoring installations

The topography in South Greenland creates diverse habitats exhibiting differing microclimates within short distances (Böcher, 1979). Among others, exposition, slope, the orientation of the associated fjord system towards prevailing wind directions, distance to the inland ice influence the local climate and soil conditions like soil temperature, soil moisture and energy state of the soil water.

In August 2020, a soil-monitoring system to record soil temperature and matric potential at two depths (15 cm and 30 cm) was installed in Upernaviarsuk (field UP-FE, see map in Figure 5). The measurement time-series cover August 2020 to August 2021. The sensors (TEROS 21, METER Group) were controlled by a data logger (ZL6, METER Group), which additionally measured atmospheric pressure and air temperature at 1.5 m height.

The relevant meteorological data (precipitation, atmospheric temperature and pressure, relative humidity) was obtained from the closest weather monitoring station located in Qaqortoq (QA, DMI-4272, see map in Figure 5). The meteorological station is located approximately 10 km southwest of Upernaviarsuk.

The combined display of the matric potential, ψ in hPa, or expressed as the decadal logarithm of $|\psi|$ (pF $= \log(|\psi|)$) as proposed by Schofield (1935), and soil temperature at two depths (15 and 30 cm) for the monitored period is shown in Figure 8. Additionally, the atmospheric temperature measured by the internal temperature sensor of the data-logger and the precipitation recorded by the DMI weather station at Qaqortoq (DMI 4272) are shown. The TEROS 21 measures the dielectric permittivity of a known material with a static matrix of pores (ceramic discs) in contact with the surrounding soil; the second law of thermodynamics states that two systems in contact with each other will eventually reach energetic equilibrium (here: hydraulic equilibrium). The dielectric permittivity depends on the amount of water present in the ceramic discs, and since the moisture characteristics curve of the used ceramic material is well known, the water potential of the ceramic discs can be inferred from their water contents, which will be equal to the potential of the soil water (Campbell, 1988; METER Group AG, 2020). The matric potential measurement is thus independent of soil type, as the device only measures the potential of the ceramic discs.

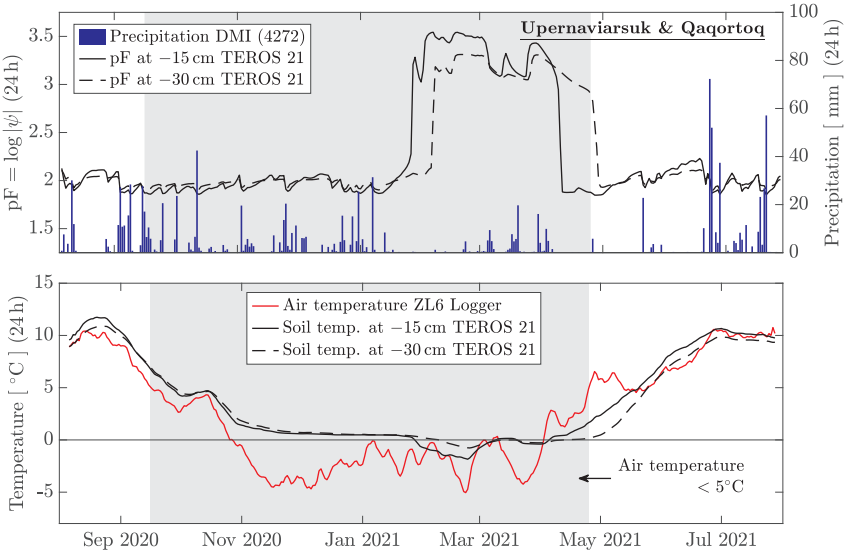

Figure 8: Monitoring station Upernaviarsuk – field-plot experiment (UP-FE). Temperatures and matric potential ($pF = \log|\psi|$, ψ in hPa) data from UP data logger; precipitation from DMI climate station Qaqortoq (DMI 4272). pF and precipitation are daily averages and cumulative sum, respectively; temperatures: 15-day moving mean. The shaded area depicts the period with temperatures $< 5\,°C$.

The insulation-effectiveness of snow cover was clearly revealed by comparing the winter air and soil temperatures (November to April). Although the daily air temperatures were continuously below freezing point from November onwards, the soil temperatures only dropped below 0 °C in February. The abrupt increase of the matric potential corresponded to freezing soil conditions; the dielectric permittivity of ice is very low compared to liquid water (Spaans et al., 1996), which implies that the sensor can no longer measure the water content of the ceramic discs accurately.

Figure 9 shows an excerpt of the recorded matric potential and precipitation for the period in 2021, exhibiting air temperatures $> 5\,°C$ (May 1, 2021 to July 31, 2021). The cumulative precipitation amounted to 376 mm, and the average daytime (8 am to 8 pm) temperatures ranged from 0.3 °C to 21.7 °C with a mean value of 10.2 °C.

The soil temperatures (15 cm soil depth) ranged from 1.2 °C to 11.7 °C with a mean value of 7.9 °C. At 30 cm soil depth, the mean temperature during the

observation period dropped to 6.9 °C covering a range from 0.3 °C to 10.8 °C.

The matric potential at 15 cm soil depth during the observed period ranged from −187.9 hPa to −70.5 hPa (pF 2.27 to pF 1.85) with a mean value of −103.3 hPa (pF 2.01). At 30 cm soil depth, the amplitude of the matric potential was higher than at 15 cm soil depth, ranging from −134.6 hPa to −77.6 hPa (pF 2.13 to pF 1.89) with a mean value of −100.8 hPa (pF 2.0).

The matric potential during non-freezing soil conditions levelled out at approximately $\psi = -100$ hPa or pF 2, indicating that the field capacity of the investigated soil was reached at similar potentials as found by Aljibury et al. (1965) and Richards et al. (1944) for intact and repacked sandy soils from temperate regions. This important information might be used in the future for modelling plant available water and fluid transport through the soil matrix of Greenlandic soils.

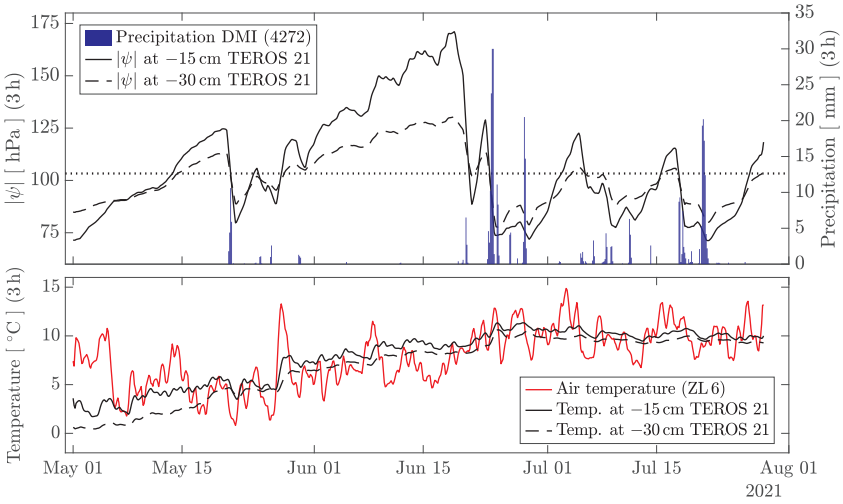

Figure 9: Excerpt of the micro-climate time-series recorded in Upernaviarsuk (May 2021 to August 2021) – field-plot experiment (UP-FE). 3 h average air and soil temperatures (7-day moving mean); the matric potential (ψ in hPa) data from UP data logger; ψ and precipitation 3 h averages and cumulative sum, respectively.

3. Characterisation of Greenlandic soils and rock flour (GRF)

3.1. Overview of the soils found in the major study area

The south Greenlandic soils are characterised by a relatively coarse texture and high organic matter contents (Caviezel et al., 2017; Jacobsen, 1987; Weber et al., 2020; Weber et al., 2021, Paper II, Paper III). Signs of medieval agriculture can be found throughout the study area in the form of old pasture fields with well-developed organic horizons (from manuring) and polypedons with well-developed podzols overlain by aeolian sediments (Jakobsen, 1989). The soil reaction is generally strongly acidic with recorded pH values as low as 3.0 (Rutherford, 1995).

The diverse geology of the study area leads to various parent materials on which weakly developed soils are found. The low temperatures result in low soil activity and long turnover times for organic material resulting in high amounts of particulate, fibrous and not-complexed organic matter (Paper II; Paper III; Caviezel et al., 2017; Ogrič et al., 2019; Weber et al., 2020; Weber et al., 2021).

The time and temperature dependence of the formation of secondary clay minerals from primary silicates, described by the Goldich dissolution series (Goldich, 1938), can conclusively explain the findings of Kelly et al. (1961), who investigated the weathering of silicate rocks in cold environments. They reported that the mineralogical composition of the initial rock was not significantly altered throughout the observed weathering sequence, and that no clay was formed during the weathering process. These findings can partly be transferred to Arctic soils, considering the environmental conditions, and explain, to some extent, the lack of clay minerals in Greenlandic soils. Furthermore, Kelly et al. (1961) reported that the only noticeable change involving an original constituent of the rock was the oxidation of ferrous iron (Fe^{2+}) into iron sulphide (pyrrhotite), biotite and iron (hydr)oxides, which were found to be relatively abundant in the herein investigated soils (XRD analyses of Greenlandic soils, data not shown).

Figure 10: Typical soil profiles from three cultivated pastures developed on different parent material: (a) Qassiarsuk (profile depth: 30 cm, photo credit: Peter L. Weber), (b) Itinnera (IT, profile depth: 30 cm) and (c) South Igaliku (SI, profile depth: 60 cm). (b) and (c) show soils from the field-plot experiments. Note the wetting front in the SI profile.

Qassiarsuk

The soils from Qassiarsuk developed on the sandstones and basalts of the Eriksfjord formation (Weber et al., 2021) and hornblende and biotite bearing granites of the Julianehåb batholith (Kokfelt et al., 2019). They were characterised by high organic matter contents ranging from 0.054 kg kg^{-1} to 0.324 kg kg^{-1} and relatively high clay contents compared to soils which developed granite-derived parent materials alone. The soil type ranged from sandy loam to loam. The basalt content of the parent material was also likely to be responsible for the considerably higher pH-values than those observed for soils developed on granite and similar rocks (Gillman et al., 2001; Priyono et al., 2004). One typical soil profile developed on the biotite-bearing, striking red parent material of the Qassiarsuk region is shown in Figure 10 a. Figure 10 b shows a profile from Itinnera (IT-FE), developed on colluvium of biotite-bearing granites of the Julianehåb batholith.

Igaliku

The parent material found in the Igaliku region are sandstones and basalts of the Eriksfjord formation, granite of the Julianehåb batholith and undifferentiated alluvium and colluvium in more or less protected valleys (Kokfelt et al., 2019). The investigated soils showed relatively high organic matter contents and particularly low dry bulk densities (Table 2). The soil types ranged from loamy sand to sandy loam and were classified as humic Cambisols (Paper II and Paper III).

Table 2: Texture and densities of soils found in the major study area (see Figure 5).

Parameter		Qassiarsuk	Igaliku	South Igaliku	Upernaviarsuk
SOM		0.162 (0.117)	0.096 (0.011)	0.044 (0.004)	0.070 (0.006)
Clay	($< 2\,\mu m$)	0.091 (0.007)	0.064 (0.038)	0.031 (0.007)	0.044 (0.014)
Silt	($2 - 50\,\mu m$)	0.307 (0.021)	0.249 (0.069)	0.234 (0.043)	0.284 (0.055)
Sand	($50 - 2000\,\mu m$)	0.476 (0.112)	0.686 (0.098)	0.694 (0.051)	0.671 (0.075)
ρ_s		2.500 (0.204)	2.480 (0.035)	2.640 (0.017)	2.550 (0.050)
ρ_b		No data	0.935 (0.050)	1.157 (0.182)	1.210 (0.130)
pH		6.210 (0.905)	5.580 (0.310)	4.970 (0.310)	5.700 (0.730)
N		54	58	74	70

SOM: soil organic matter, ρ_s: particle density, ρ_b: bulk density, N: number of samples
SOM, Clay, Silt and Sand in $kg\,kg^{-1}$; ρ_s and ρ_b in $Mg\,m^{-3}$

South Igaliku

The soils from South Igaliku developed on the granite of the Julianehåb batholith, overlain by aeolian sediments, originating from the same parent material and hornblende-bearing diorite and gabbro, syenite including olivine (Kokfelt et al., 2019). The soils developed on the massive aeolian deposits are deep and well-drained and were classified as arenic Cambisols to brunic Arenosols (Paper II and Paper III). The soil types ranged from sand to loamy sand. The layering of the soil profile shown in Figure 10 c could be easily identified; it was the result of multiple deposition events of aeolian sediments on top of the organic A horizon.

Upernaviarsuk

The only regularly tilled (yearly) field presented in this dissertation developed on a mix of granodioritic gneiss and granites (including Leucogranite) and is part of the agricultural school located in Upernaviarsuk. The soil has been classified as humic Umbrisol (Bradley-Cook et al., 2016; Hermansen et al., 2017), and the vegetation cover at the time of sampling consisted of common oat (*Avena sativa* L.) for forage production.

3.2. Water and air-phase related properties

The high organic matter contents of the investigated soils result in high total porosities and high macro-porosities (Paper II; Paper III; Caviezel et al., 2017; Weber et al., 2020). The plant available water (PAW) measured on the 100 cm^3 soil core cylinders collected from top-soils thus showed high to very high PAW. However, considering the generally shallow soil depths and the often high gravel contents, the apparent plant available water contents may rather be low. The observed water and air contents of the Greenlandic soils were compared to those of well-known soils from Denmark (Danish Soil Library, DSL; Hansen, 1976; Resurreccion et al., 2011).

Water retention and air-phase characteristics

The *van Genuchten* water retention function (Equation 1; van Genuchten, 1980) was fitted to the measured volumetric water contents (θ in $m^3\,m^{-3}$) and a rearranged *van Genuchten* air content function (Equation 2) to the air-filled porosities (ε in $m^3\,m^{-3}$).

$$\theta(\psi) = \theta_r + \frac{\theta_s - \theta_r}{[1 + (\alpha|\psi|)^n]^{1-m}} \tag{1}$$

$$\varepsilon(\psi) = \varepsilon_r - \frac{\varepsilon_r - \varepsilon_s}{[1 + (\alpha|\psi|)^n]^{1-m}}. \tag{2}$$

The fitting parameters common to both equations (although not equal) were α, n and m; α was related to the matric potential at air entry, n and m were parameters related to the shape of the water retention (air content) curve. θ_s represented the water content at saturation and θ_r was referred to as the residual water content. The corresponding ε-parameters used in Equation 2 were referred to as air-filled porosity at air-dry conditions (ε_r), which might be set equal to the total porosity and ε_s, the air-filled porosity at water saturation (which might be set

Table 3: Overview of basic soil properties of the Danish Soil Library (DSL, Hansen, 1976).

Statistic	SOM	Clay	Silt	Sand	ρ_b
mean	0.014	0.109	0.107	0.770	1.511
SD	0.010	0.068	0.070	0.130	0.107
min	0.003	0.016	0.009	0.475	1.240
max	0.041	0.276	0.244	0.971	1.750

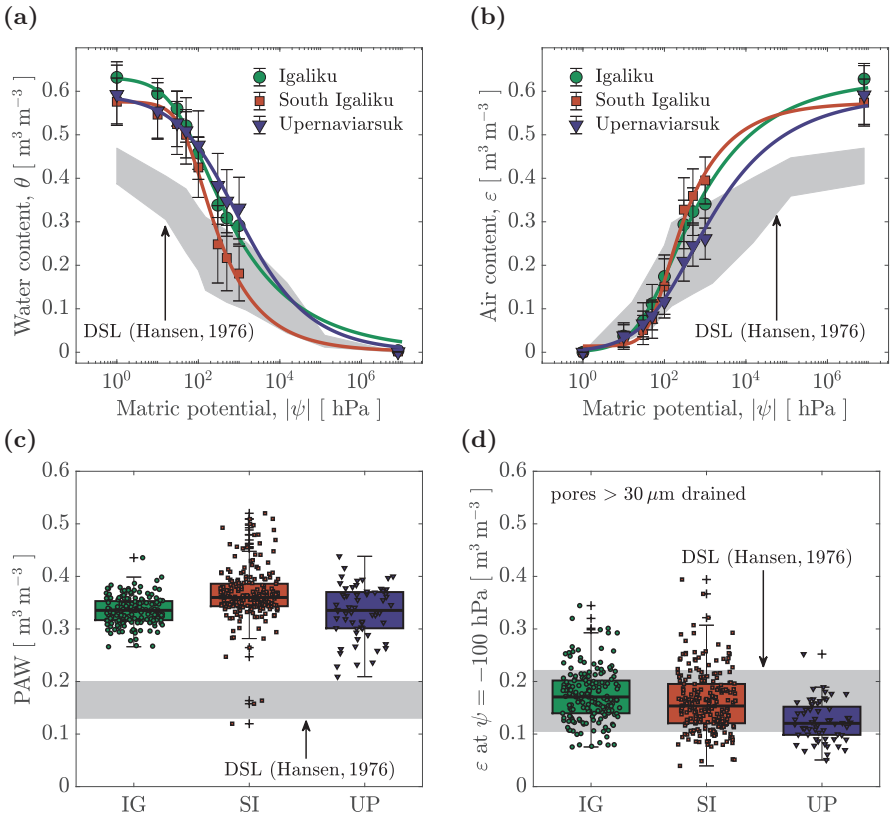

Figure 11: (a) Soil-water retention and (b) soil-air characteristic curves for three selected regions/fields (Igaliku: 2 fields, 174 samples; South Igaliku: 3 fields, 222 samples; Upernaviarsuk: 1 field, 60 samples). Box plots of (c) the plant available water content (PAW) and (d) the air-filled porosity at $\psi = -100\,\mathrm{hPa}$ (pF 2; macro-porosity, pores $> 30\,\mu\mathrm{m}$).

to null). The fitted water and air content functions to three representative soil groups found in the study area are shown in Figure 11 a and Figure 11 b. The shaded area in the figures corresponds to the water and air contents of the DSL, which basic soil characteristics are listed in Table 3. The comparison data from the DSL consisted of top and subsoils from 15 different soil profiles (40 observations in total) covering the ranges of texture and organic matter contents of soils found throughout Denmark.

The plant available water (PAW) was calculated for each sample individually as the difference between the water content at field capacity (FC, at $\psi = -100\,\mathrm{hPa}$ or pF 2.0) and the water content at the permanent wilting point (PWP, at

$\psi = -15\,000$ hPa or pF 4.2). Figure 11 c shows the markedly higher PAW of the Greenlandic soils compared to the soils from the Danish Soil Library (shaded area). The air-filled porosity at field capacity, which also represents the macroporosity (pores > 30 µm in diameter) of both the Danish and the Greenlandic datasets overlapped as seen in Figure 11 c.

Hydraulic conductivity and air permeability

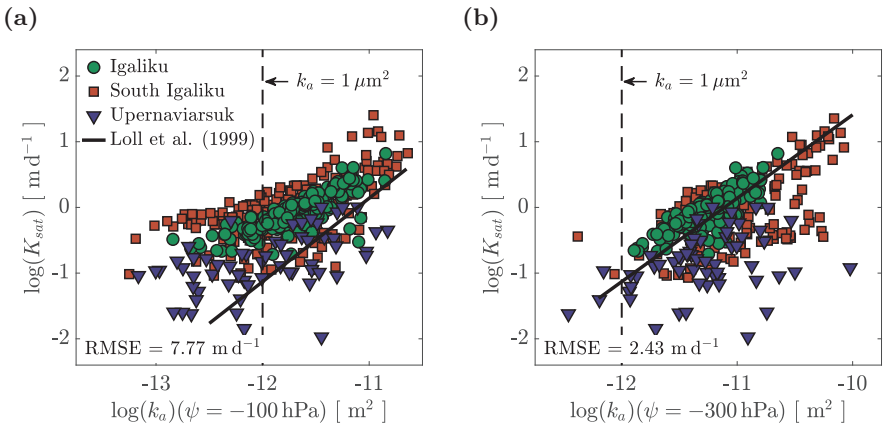

Figure 12: log(K_{sat}) versus log(k_a) with k_a at (a) $\psi = -100$ hPa and at (b) $\psi = -300$ hPa and indicated model for temperate soils from Loll et al. (1999). The vertical dotted line at $k_a = 1$ µm^2 indicates the lower boundary for air exchange.

Loll et al. (1999) derived a prediction model for the saturated hydraulic conductivity (K_{sat}) of cultivated fields from measurements of the air permeability (k_a) on intact, 100 cm^3 soil cores samples. Despite exhibiting similar macroporosity, as shown in Figure 11 c, the model generally under-predicted the K_{sat} of the Greenlandic soils at the reference matric potential of $\psi = -100$ hPa (Figure 12 a). A large number of observations for which $k_a < 1$ µm^2 (lower boundary for gas exchange; Ball, 1981) revealed the disconnected nature of the pore network of the Greenlandic pasture soils. The performance of the model increased (RMSE decreased from 7.77 to 2.43 m d^{-1}) if the K_{sat} was related to the k_a measured at $\psi = -300$ hPa. Ahuja et al. (1984) defined the effective porosity for water transport as the air-filled pore space available at $\psi = -330$ hPa, which is reasonably close to the chosen matric potential for the k_a measurements ($\psi = -300$ hPa) in Figure 12 b. This result is considerably

different from the estimation of the effective porosity obtained from the in-situ measurement of the matric potential (matric potential sensors; Section 2.3). One reason for the discrepancy between the derived effective porosities was the scale dependence of the measuring procedures, which was found to be particularly pronounced for pore network-related properties, like, e.g., K_{sat} (Hopmans et al., 2002; Warrick et al., 1977).

3.3. The 16 glacial rock flours

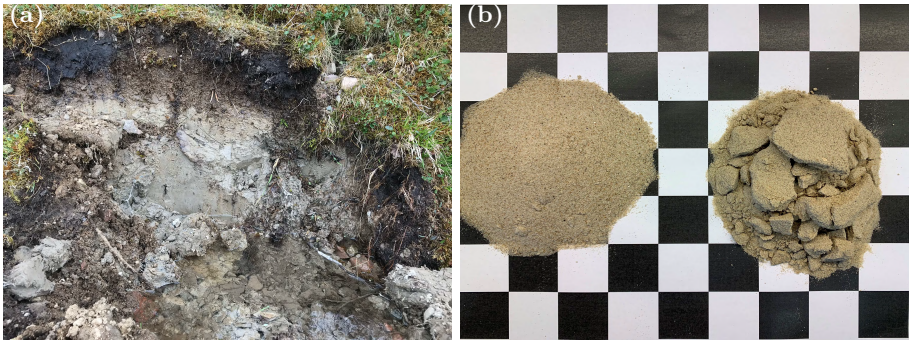

Figure 13: (a) Glacial rock flour deposition (Qinngua, QI-2, see Paper I) with the overlying debris from rock slope erosion and aeolian deposits on which a thick O horizon has formed. (b) Marked increase of the apparent cohesion of a geotechnical sand by addition of 3.5 % w/w rock flour.

The potential of the GRF-amendment for the amelioration of the agricultural properties of Greenlandic soils has been analysed by Paper I and the benefits for plant production regarding the effect of GRF amendment on nutrient uptake and nutrient efficiency by Gunnarsen (2020), Gunnarsen et al. (2019) and Sukstorf et al. (2020).

Paper I gives a detailed overview of the physico-chemical properties of selected glacial rock flours found in the study area. The material generally exhibited high contents of clay and silt-sized particles (particles exhibiting $< 20\,\mu m$ in diameter), as shown in Figure 14 a. The mineralogical characterisation revealed that the fine fraction contained large amounts of quartz and feldspars, but only low contents of primary and secondary clay minerals compared to the total amount of fine particles (Paper I; Belmonte, 2015).

Soil aggregation, soil structure development and organic matter protection might be improved by introducing high surface-active mineral material compared to the low surface activity of the mineral phase of the Greenlandic pasture soils (Dexter et al., 2008; Oades, 1984; Schjønning et al., 2010; Wagner et al., 2007). The average SSA of the GRFs amounts to $31.41\,m^2\,g^{-1}$ (sample QI-3 excluded, see Figure 13 b) and a significant correlation between the SSA and the CEC was found in Paper I ($r = 0.83$). The CEC of selected typical Greenlandic soils

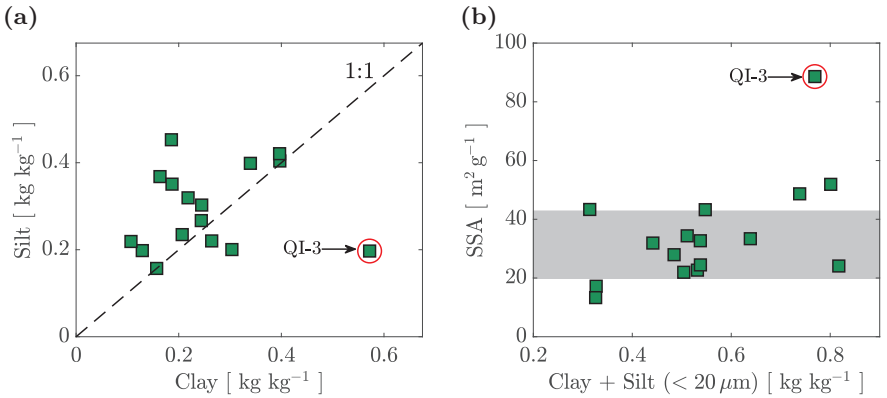

Figure 14: The 16 glacial rock flours. (a) Gravimetric clay versus silt contents and (b) specific surface area (SSA) versus fine particle contents (< 20 µm); shaded area depicts mean SSA ± SD, sample QI-3 excluded. Data from Paper I.

was low (CEC = 11.83(4.42) cmol kg^{-1}), despite exhibiting high organic matter contents (OM = 0.08(0.04) kg kg^{-1}).

The benefits of the GRF-amendment for soil structure development and organic matter stabilisation in perspective of increasing temperatures is, however, mainly dependent on the not well understood long-term interaction between the mineral and organic phases, which includes the formation of organo-mineral complexes and the weathering of primary minerals into clay minerals during soil development (Folkoff et al., 1987).

The volumetric water contents during twelve days of drainage of repacked fine sandy soils, amended with four levels of GRF (0, 5, 10 and 15 % by weight), are shown in Figure 15 a; between the different application rates, no apparent differences in the water-release dynamics could be observed, although the not-amended and 5 %-amended samples exhibited consistently higher volumetric water contents throughout the drainage period.

The addition of 5 % GRF by weight significantly increased the volumetric water content at field capacity ($\psi = -100$ hPa); however, higher GRF concentrations reduced the water content at field capacity to a level not significantly different from the not treated soil as shown in Figure 15 b. In Paper I the plant available water content (PAW) was estimated, and a slight increase (not statistically significant compared to the not-amended soil) was found at application rates below 5 % by weight; at higher rates, the PAW was significantly reduced

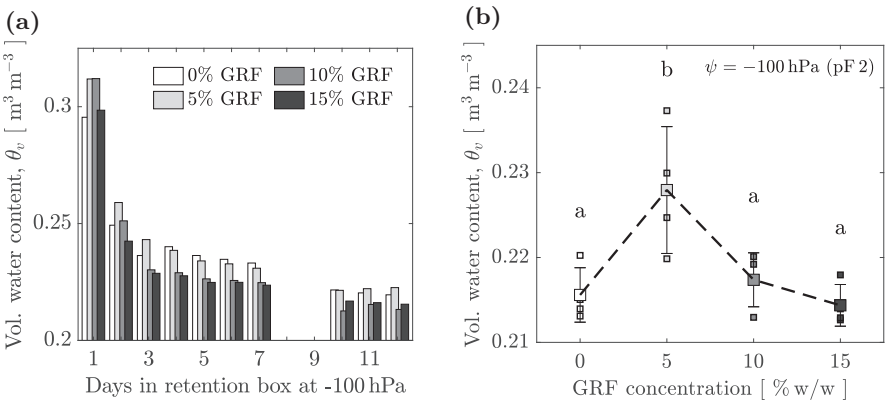

Figure 15: Water retention of GRF amended repacked soils. (a) dynamics of water release during twelve days, and (b) equilibrium water content at field capacity ($\psi = -100$ hPa, days 11 and 12 combined). Big squares are the mean values; whiskers represent the standard deviation. Means bearing the same letters are not statistically different from each other at the 5% significance level.

compared to the not-treated soil. The reduction of the PAW at high application rates was thus solely due to the increase of the water content at the permanent wilting point ($\psi = -15\,000$ hPa).

The short-term effects of high GRF application rates on plant available water might thus be negative, and only well-controlled field-plot experiments can assess the mid- to long-term effects on the water balance of Greenlandic soils.

One beneficial short-term effect of the GRF-amendment might be the reduction of the high water repellency of the Greenlandic soils (Weber et al., 2021). The addition of fine mineral material to agricultural soil effectively reduced hydrophobicity, as shown by several studies, mainly from dry-land agriculture (Cann, 2000; McKissock et al., 2002; Roper et al., 2015).

4. Mechanical and pore-network characteristics of Greenlandic soils

The mechanical and pore-network properties of Greenlandic pastures soils will be illustrated on unpublished data from two fields exhibiting contrasting texture and organic matter contents.

4.1. Field-plot experiments

During field trips in 2019 and 2020, three field-plot experiments were installed in three of the major agricultural areas of South Greenland. The chosen fields represented the general soil type in the selected area and were not taken out of agricultural production. The purpose of installing field-plot experiments is to investigate the effect of GRF amendment on soil properties, yield and nutrient contents of the crop systematically. The results of the ongoing experiments will be published elsewhere. The herein used samples were collected prior to the amendment and do not contain glacial rock flour. The fields were named according to the local place names, and the suffix –FE– (field experiment) was added to avoid confusion with other fields in the same region.

Site presentation and experimental setup

The set-up of the experiments is illustrated in Figure 16, and the design corresponds to a randomised block design. Each plot extended on $9\,\mathrm{m}^2$ ($3\,\mathrm{m} \times 3\,\mathrm{m}$) and was amended with glacial rock flour with either one of the concentrations $0, 50, 100, 300$ or $500\,\mathrm{t\,ha}^{-1}$. After the amendment, the parcel of land was tilled (disc harrowed) and resown with the typical local grass mixture consisting of colonial bentgrass (*Agrostis tenuis* L.), red fescue (*Festuca rubra* L.), perennial ryegrass (*Lolium perenne* L.), timothy (*Phleum pratense* L.) and Kentucky bluegrass (*Poa pratensis* L.) (Weber et al., 2021).

Prior to the GRF amendment, duplicates of intact $100\,\mathrm{cm}^3$ soil core samples from two field-plot experiments were collected: Itinnera (IT-FE, 20 plots, 40 soil core samples) and South Igaliku (SI-FE, 15 plots, 30 soil core samples) and brought to the laboratory for further analysis. The schematics of the experimental set-ups are shown in Figure 16. A third field-plot experiment is located in Upernaviarsuk (UP-FE, 20 plots), but no data was available at the

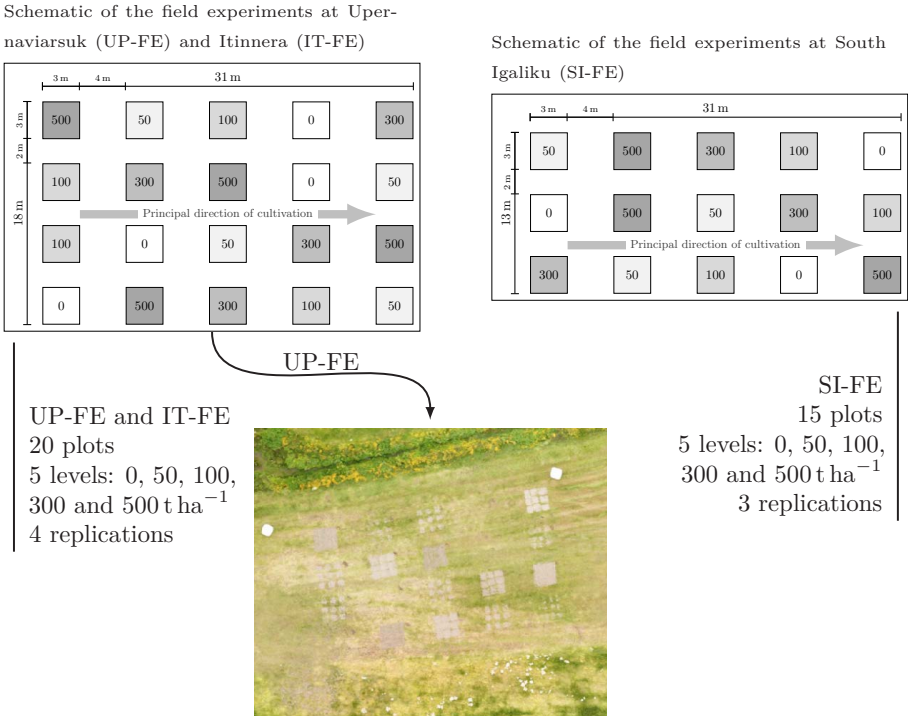

Figure 16: Schematics of the field-plot experimental sites installed in 2019 and 2020 in South Greenland. Drone picture of the field-plot experiment in Upernaviarsuk during instalment in spring 2019. Photo credits: Peter L. Jensen.

time of writing. The sites are depicted by red stars on the map of the study area in Figure 5.

The coarse-grained soils from IT-FE developed on glacial till and exhibited a well-graded particle size distribution. SI-FE on the other hand developed on aeolian deposits with approximately 90 % of the particles $< 200\,\mu m$.

Phase distribution

The particle size distribution was determined for each soil core individually by dry sieving. After sieving, the organic matter content (OM_{LOI}) of each grain-size fraction was determined by loss on ignition (LOI at 550 °C for 12 h); additionally, the total organic matter was determined on a subsample of the not sieved soil using the same method (Table 4). The weighted sum of the organic matter contents per size fraction agreed well with the organic matter

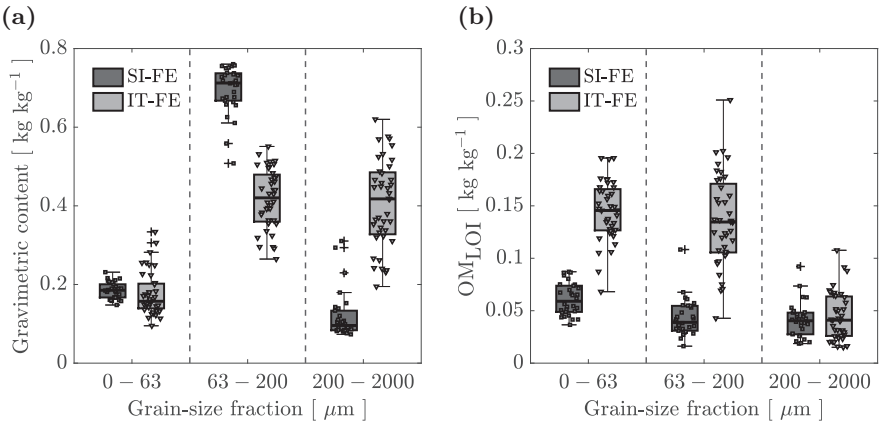

Figure 17: (a) Texture and (b) associated organic matter contents of the soils from the field-plot experiments.

contents determined on the bulk soil ($r = 0.98$). Figure 17 shows the grain size distribution and the organic matter contents associated with each grain-size fraction. The soil from IT-FE was additionally characterised by a considerably higher gravel content (particles $> 2\,000\,\mu m$) with mean gravimetric contents of $0.085\,(0.054)\,kg\,kg^{-1}$ compared to $0.007\,(0.010)\,kg\,kg^{-1}$ for the soil from SI-FE.

The particle densities (ρ_s, oven-dry at 105 °C) and mineral densities (ρ_{min}, after removal of the organic matter by LOI at 550 °C) for each size fraction

Table 4: Average particle (ρ_s) and mineral (ρ_{min}) densities for different particle size fractions; bulk density (ρ_b) and organic matter content (OM_{LOI}).

Parameter	Size-fraction [µm]	SI-FE mean (std)	IT-FE mean (std)
ρ_s	0–2 000	2.625 (0.021)	2.508 (0.030)
ρ_{min}	0–2 000	2.718 (0.045)	2.696 (0.008)
ρ_s	< 63	2.643 (0.040)	2.441 (0.012)
ρ_{min}	< 63	2.752 (0.011)	2.708 (0.024)
ρ_s	63–200	2.685 (0.016)	2.464 (0.034)
ρ_{min}	63–200	2.707 (0.036)	2.708 (0.007)
ρ_s	200–2 000	—	2.561 (0.027)
ρ_{min}	200–2 000	2.663 (0.014)	2.660 (0.007)
ρ_b	—	1.328 (0.086)	1.189 (0.178)
OM_{LOI}	—	0.045 (0.012)	0.097 (0.035)

ρ_s, ρ_{min} and ρ_b in $Mg\,m^{-3}$; OM_{LOI} in $kg\,kg^{-1}$

were determined on a subsample (6 samples per field) covering the range of organic matter contents of each soil (Table 4). Although thermally induced phase transitions during the organic matter removal eventually alter part of the soil minerals (Sjöström et al., 2019), the knowledge of the mineral density reveals differences in parent mineral material and soil organic matter quality (Rühlmann et al., 2006). The consistently higher ρ_s of the SI-FE than those of the samples from IT-FE could be explained by the lower organic matter contents of the former. The ρ_{min} of both fields were reasonably close to each other and approached the theoretical ρ_{min}-value of quartz ($2.65\,\mathrm{Mg\,m^{-3}}$) for the coarse sand fraction ($200 - 2000\,\mu\mathrm{m}$).

The bulk densities (ρ_b), determined on the oven-dry soil cores (105 °C for 24 h), were relatively high compared to other Greenlandic pasture soils (see, e.g., Paper II and Paper III). Following an analysis of variance, the soil from SI-FE exhibited significantly higher bulk densities than the soil from IT-FE (Table 4). Figure 18 a shows the variation of the dry bulk density with changes in organic matter content, and a Grigal et al. (1989)-type exponential model [$\rho_b = a + b \cdot \exp(c \cdot \mathrm{OM_{LOI}})$, with fitting coefficients a, b and c] to predict ρ_b from $\mathrm{OM_{LOI}}$ fitted to each dataset individually.

Figure 18 b shows the linear increase of the void ratio, e_0 [with $e_0 = \rho_s/\rho_b - 1$], with increasing $\mathrm{OM_{LOI}}$, a finding also reported by other studies (e.g., Arthur

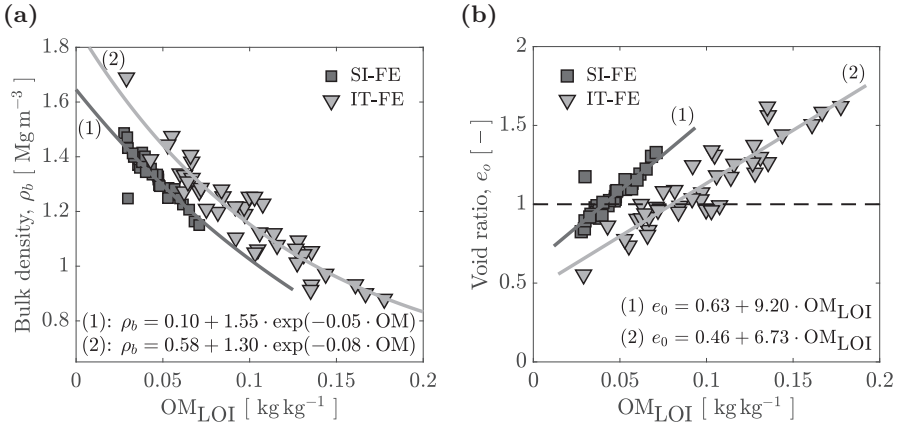

FIGURE 18: Solid and phase distribution as related to $\mathrm{OM_{LOI}}$. (a) Relationship between dry bulk density (before compression) and $\mathrm{OM_{LOI}}$ and fitted exponential models (OM replaced $\mathrm{OM_{LOI}}$ due to space constraints); (b) the initial solid to void ratio, e_0, versus $\mathrm{OM_{LOI}}$ and fitted linear models.

et al., 2013a; Soane, 1990). An analysis of variance of both fitted linear relationships revealed that the dependence of e_0 on OM_{LOI} did not differ significantly between the two fields (the slopes were not different at the 5 % significance level).

4.2. Mechanical properties of Greenlandic pasture soils

The mechanical parameters, compression index (C_c, compressibility of the soil), precompression stress (σ_p, maximum bearing capacity of the soil) and rebound (ΔE, recovery from compaction) were determined on the compression curves measured by uniaxial confined compression tests using a constant strain rate of $1\,\mathrm{mm\,min^{-1}}$ as proposed by Lamandé et al. (2017) and a maximum applied stress of 1 000 kPa. Prior to the compression tests, the samples were drained on suction plates to a matric potential of $\psi = -100$ hPa. Detailed information about the measuring procedure can be found in Paper II and Paper IV.

Figure 19 a shows the compression curves of the tested samples in the semi-logarithmic stress-compressive extension ($\log\sigma - E$) domain, with the stress, σ, expressed in kPa and the extension, E, in mm. The solid line represents the median of the curves per field combined, the shaded area depicts the interquartile range of the pooled measurements. The C_c was calculated as the slope of the

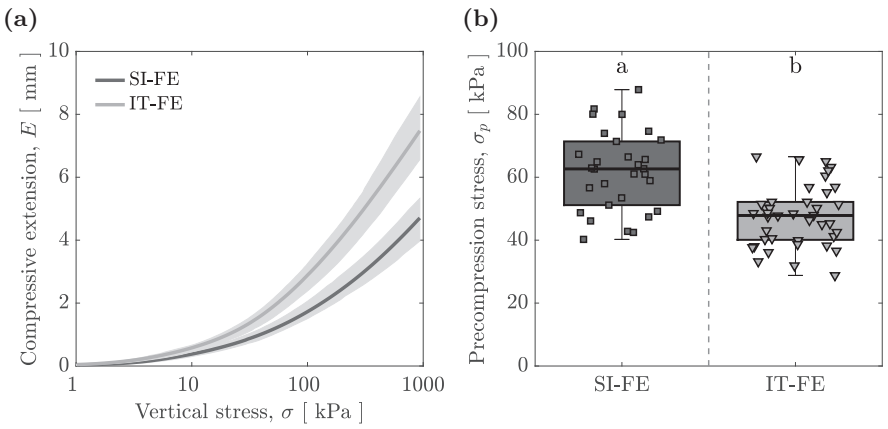

Figure 19: (a) Compression curves for SI-FE and IT-FE. Solid lines represent the median value of 30 (SI-FE) and 40 (IT-FE) UCCT curves; the shaded areas depict the interquartile range. (b) Box-whisker plots of the precompression stress. Boxes bearing the same letter were not statistically different from each other at the 5 % significance level.

virgin compression line (VCL, Keller et al., 2011), which describes the plastic deformation of the soil (here set to $\sigma > 200\,\mathrm{kPa}$). The precompression stress (σ_p) was set to the intersection of the swelling line (SL, part of the compression curve for $\sigma < 25\,\mathrm{kPa}$) and the VCL, according to da Silva et al. (2016). The rebound was actively measured by recording the soil sample's expansion after compression by application of a small applied normal load of 1 N (for details, see Paper II and Paper IV).

An analysis of variance showed that the precompression stress (σ_p) of the samples from SI-FE were significantly higher than those measured on the samples from IT-FE [$F(1, 68) = 29.18$, $p < 0.001$] with mean values of 61.83 (12.52) kPa and 47.55 (9.62) kPa, respectively (figures in parentheses depict the standard deviation). Figure 19 b shows the measured σ_p for both fields; interestingly, the samples from SI-FE exhibited higher variation although exhibiting a more uniform particle size distribution and lower organic matter ranges. The σ_p of the samples from SI-FE were significantly correlated to $\mathrm{OM_{LOI}}$ ($r = 0.64$), whereas no such significant correlation could be found for the samples from IT-FE ($r = 0.07$).

The compression index (C_c) of the samples from SI-FE were significantly lower than those from IT-FE [$F(1, 68) = 46.52$, $p < 0.001$] with mean values of 3.45 (0.86) mm 10kPa^{-1} and 5.08 (1.08) mm 10kPa^{-1}, respectively. An increase of the compressibility with increasing organic matter contents was in accordance

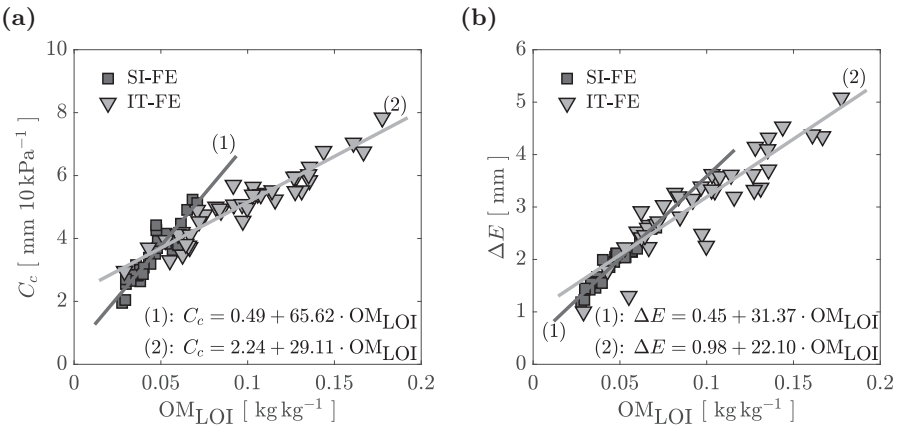

Figure 20: Dependence of the (a) compression index (C_c) and (b) rebound after stress release (ΔE) on the organic matter ($\mathrm{OM_{LOI}}$).

with the findings of Paper II, Arthur et al. (2013a), Soane (1990) and Zhang et al. (2005). Figure 20 a shows the different linear relationship between the C_c and the OM_{LOI} of the two fields (significantly different slopes at the 5 % significance level).

The rebound after compression (ΔE) of the SI-FE samples was significantly lower than those measured on the IT-FE samples [$F(1, 68) = 56.55$, $p < 0.001$], with mean values of 1.86 (0.40) mm and 3.13 (0.86) mm, respectively. The two fields exhibited significantly different linear relationships between the ΔE and the OM_{LOI} as shown in Figure 20 b (significantly different slopes at the 5 % significance level, $p = 0.047$).

High organic matter contents, resulting in high porosities, might increase the amount of plastic deformation (high C_c); however, Paper II and Zhang et al. (2005) also revealed that high organic matter contents increase the recovery from compaction (high ΔE). Zhang et al. (2005) and Paper II attributed this property to the elastic spring effect caused by the organic matter within the soil matrix. This shows that the separation between purely elastic (low applied normal stress, $\sigma < \sigma_p$) and purely plastic (high applied normal stress, $\sigma > \sigma_p$) deformation during compression events is not necessarily valid for soils exhibiting high organic matter contents.

4.3. Soil-air phase characteristics of Greenlandic pasture soils

The air phase was characterised by the gas diffusivity, D_p/D_o [–], and the air permeability, k_a [µm^2], both measured at $\psi = -100$ hPa and before and after compression and readjustment to $\psi = -100$ hPa. Further details of the measuring apparatus and methods can be found in Paper III and Paper IV.

Pore-network characteristics

The pore network tortuosity was characterised by the connectivity-tortuosity parameter, X, first derived by Buckingham (1904) and calculated according to Equation 3 or by using its log-transformed version, given in Equation 4

$$D_p/D_o = \varepsilon^X \tag{3}$$

$$X = \frac{\log(D_p/D_o)}{\log \varepsilon}. \tag{4}$$

The diameter of pores allowing gas transport through the soil was calculated according to Ball (1981) and Millington et al. (1964) using Equation 5

$$d_{eff} = 2 \cdot \sqrt{\frac{8 \cdot k_a}{(D_p/D_o)}}. \tag{5}$$

The measured gas diffusivities (D_p/D_o) and air permeabilities (k_a) of the intact samples are shown in Figure 21 a and Figure 21 c, respectively. The measured D_p/D_o and k_a after compression, rebound and readjustment to $\psi = -100$ hPa were depicted by red marker-outlines in the figures.

According to Schjønning et al. (2003) and Stepniewski (1981), adequate soil aeration and aerobic microbial activity are impeded if the gas diffusion coefficients are below 0.005 and 0.02, depending on texture and bulk density (Weber et al., 2020). After compression, however, the mean D_p/D_o of SI-FE and IT-FE were 0.005 (0.002) and 0.003 (0.003), respectively. Similar results were obtained for the k_a measurements after compression, with mean values of 0.42 (0.19) µm^2 and 0.28 (0.39) µm^2 for SI-FE and IT-FE, respectively. Such low air permeabilities indicated impermeable soil conditions for soil-gas transport, according to Ball (1981); furthermore, the accuracy of the used apparatus was significantly

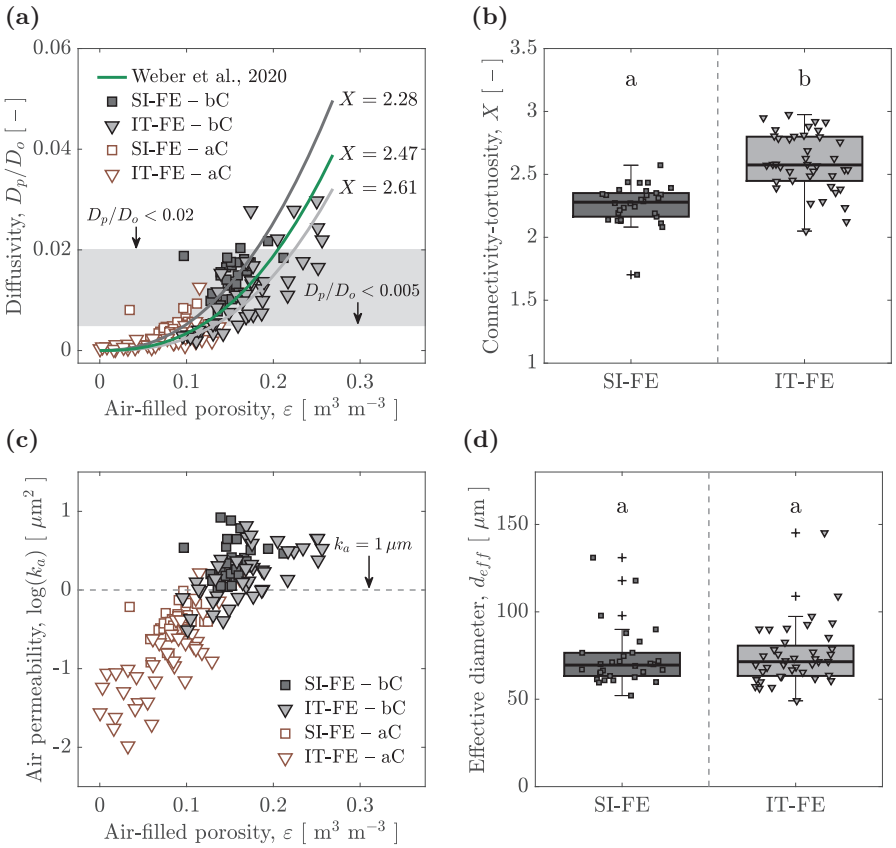

FIGURE 21: Air-phase parameters of the field-plot experiments. (a) Diffusivity (D_p/D_o) with fitted X (Equation 3); (b) connectivity-tortuosity parameter calculated for each sample individually (Equation 4). (c) Air permeability (k_a) and (d) effective diameter for gas transport (d_{eff}) were calculated for each sample individually (Equation 5). Boxes bearing the same letter were not statistically different from each other at the 5 % significance level.

reduced at such low permeabilities (Schjønning et al., 2017). The D_p/D_o and k_a measurements after compression were thus not further analysed.

Figure 17 a shows the fitted Buckingham (1904) X (Equation 3) to the measured D_p/D_o values (before compression) of each field. Comparison with the D_p/D_o measurements of the comprehensive dataset of intact Greenlandic pasture soils investigated by Weber et al. (2020) reveals that the herein shown soils exhibited similar pore-network properties. The best-fit of the Buckingham-type X model (Equation 3) to the Weber et al. (2020) dataset was plotted in Figure 21 a for reference.

The tortuosity-connectivity parameter, X, was determined for each sample individually using Equation 4 and is shown in Figure 21 b. SI-FE exhibited significantly lower X-values than IT-FE [$F(1, 68) = 45.76$, $p < 0.001$] with mean X-values of 2.26 (0.16) and 2.59 (0.23), respectively. The tortuosity-connectivity parameter of the combined dataset exhibited a significant positive correlation with the organic matter content ($r = 0.68$), which is in accordance with the findings of Paper III and, e.g., Hamamoto et al. (2012).

The effective diameter (d_{eff}) was not statistically different between the two fields, exhibiting mean values of 73.53 (17.01) µm and 74.84 (17.15) µm for the samples from SI-FE and IT-FE, respectively.

For undisturbed cultivated pasture soils, the organic matter was the main driver, markedly affecting the phase distribution (solid–water–air), and by that, the mechanical parameters and the properties of the pore network.

5. Effects of rock flour on soil gas transport properties

5.1. Intact and GRF-amended repacked soils compared

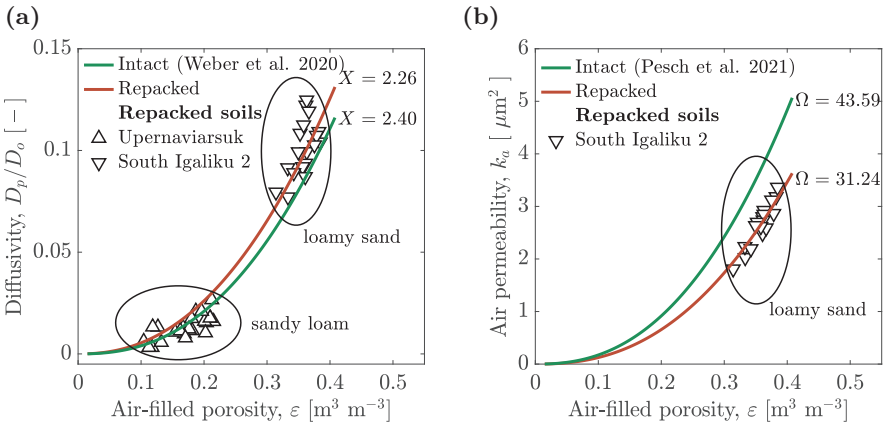

FIGURE 22: Air-phase parameters of intact and repacked samples compared. (a) D_p/D_o: X for the intact samples was taken from Weber et al. (2020); data for repacked soils from Paper IV. (b) k_a: Ω for the intact samples was taken from Paper III; data for repacked soils from Paper IV. All the soils were equilibrated to $\psi = -300$ hPa.

In Paper IV the air-phase functions of repacked and GRF amended soils were investigated. Weber et al. (2020) measured D_p/D_o on intact soil core samples from Upernaviarsuk (U) and South Igaliku Site 2 (S), which were issued from the same fields as the ones used for repacking in Paper IV; thus, a direct comparison between the measured D_p/D_o of the two studies was possible. In Paper III, the k_a of South Igaliku Site 2 was measured, and a direct comparison with the k_a of the repacked samples was possible; unfortunately, no k_a measurements were available for the soils from Upernaviarsuk.

Figure 23 shows that the air-phase parameters measured on the repacked samples were reasonably close to those measured on undisturbed samples. The similarity of the air-phase functions of repacked and intact samples pointed towards the lack of developed soil structure of the Greenlandic soils. Furthermore, these similarities made it possible to draw conclusions on repacked samples that were then likely to be correct for intact samples.

5.2. Effects of GRF addition on soil-gas diffusivity

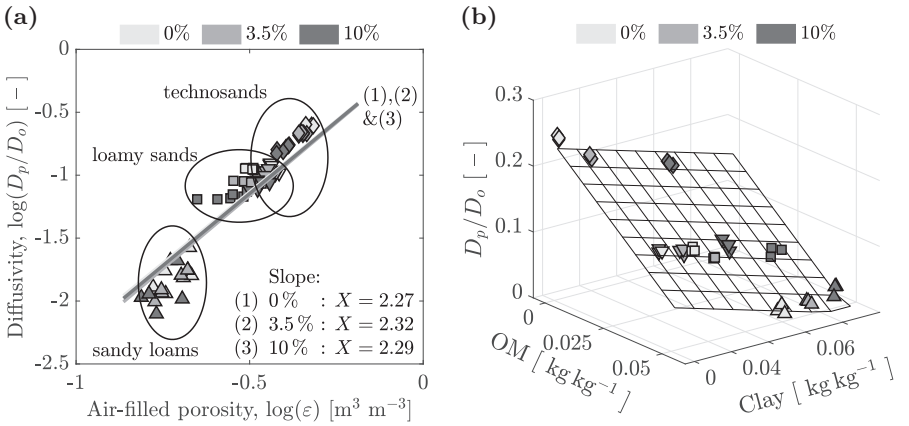

Figure 23: (a) Effect of GRF on gas diffusivity (modified from Paper IV) and (b) response of D_p/D_o to changes in organic matter (OM_{LOI}) and Clay (as a continuous measure for GRF addition). GRF concentrations (in % w/w) above plot areas.

In Paper IV soils and sands were amended with three levels of GRF (0, 3.5 and 10 % per weight) and repacked into soil core cylinders. The soils consisted of a sandy loam (Upernaviarsuk) and a loamy sand (South Igaliku 2), both from Greenland, a coarse sand from Denmark (Jyndevad) and a geotechnical sand from Sweden (Baskarp). The organic matter was set equal to the loss on ignition at 550 °C (OM). According to Paper I, the clay contents were estimated from laser diffraction measurements of the particle size distribution and set equal to the fraction of particles < 4.5 µm in diameter.

Figure 23 a shows the gas diffusivity versus the air-filled porosity in a $\log - \log$ domain. The slope of the best-fit line represents the connectivity-tortuosity parameter (Equation 4).

For the different soil types combined, the relationship between the decadal logarithms of ε and D_p/D_o did not show any significant and directed response to the GRF concentration, which was visualised by the three overlapping linear regressions, fitted to each GRF application rate group, in Figure 23 a. However, separating the sources of variance by a linear model including the initial soil (4 levels) and GRF concentration (3 levels) as categorical predictors followed by an analysis of variance revealed that the GRF concentration indeed significantly reduced the magnitude of D_p/D_o, although it was still the initial

Table 5: ANOVA table for D_p/D_o as affected by the soil/sand type and by the GRF concentration.

Factor/model	Sum of Squares	DF	Mean Square	F	p
Linear model:	$D_p/D_o \sim 1$ + soil/sand + GRF conc.				
soil/sand	12.461	3	4.153	761.705	<0.001
GRF conc.	0.273	2	0.136	24.999	<0.001
Error	0.343	63	0.005		
Total	12.927	68			

soil type, which had the biggest influence on the magnitude of D_p/D_o. Table 5 shows the result of the analysis of variance. The marginal means of the GRF induced reduction of the magnitude of D_p/D_o were as follows: 0.12 (0 %) > 0.10 (3.5 %) > 0.08 (10 %).

The addition of GRF to the soils changed the particle size distribution and led to changes in the solid phase. The low to null organic matter contents of the GRF replaced the amount of organic matter associated to the replaced soil (dilution of OM), which affected the functional properties of the soil. The response of D_p/D_o towards changes in organic matter and clay (as a proxy for GRF addition) is shown in Figure 23 b. The multiple regression to construct the response surface resulted in excellent goodness of fit, with an RMSE of 0.012 and an adjusted R^2 of 0.97.

As elaborated in Section 3.3 and visualised in Figure 15, the addition of GRF changed the water retention characteristics and thus the air phase in two ways: (i) by acting on the pore size distribution and reducing the pore space available for gas and water transport (air-filled porosity and total porosity), and (ii)

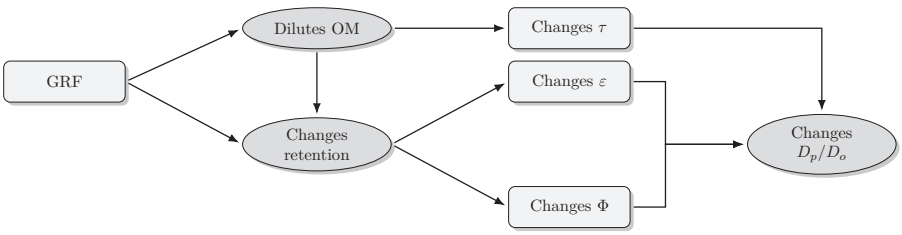

Figure 24: Flow chart to visualise the effects of GRF addition on the phase distribution and subsequently on gas diffusivity. (GRF, glacial rock flour; OM, organic matter; τ, tortuosity; ε, air-filled porosity; Φ, total porosity; D_p/D_o, diffusivity)

by reducing the OM content, which affected the water content itself and the tortuosity ($\tau = L_e/L$, the ratio of effective transport length and total length of the porous medium; Moldrup et al., 2001) of the pore space. Figure 24 shows a flow chart of the affected phases and their consequences for diffusivity-relevant properties by GRF addition to soil.

6. Conclusions, perspectives and outlook

First, the general and most important conclusions of the supporting papers will be presented before recapitulating the major findings of the extended summary.

Conclusions – supporting papers

(a) Basic soil characterisation and preliminary studies:

Some mechanical properties of intact samples from Greenlandic pasture soils were determined by uniaxial confined compression tests. The results showed that the pasture soils exhibited higher bearing capacities (precompression stress) than similar-textured cultivated soils from Denmark. The resilience to and recovery from compaction (swelling index and rebound after compression) were found to be significantly higher for the Greenlandic pasture soils than comparable Danish cultivated soils. The compression index, as a measure of irreversible soil deformation following compression, was higher than those of comparable Danish soils. The mechanical properties of the sandy Greenlandic soils were closely related to the organic matter contents, and it was suggested that the high resilience to and recovery from compaction was mainly due to the high content of fibrous organic material present in the soil matrix.

(b) Physico-chemical characterisation of glacial rock flour:

The GRF showed good potential for use as a soil amendment. The surface properties (specific surface area, cation exchange capacity) were on the line with or higher than agricultural soils from temperate regions bearing similar kaolinitic-dominated clay contents. The water sorption at the dry end of the water retention curve was low compared to typical temperate soils, which suggest that the addition of GRF to soil would not increase the water content at the permanent wilting point. At low application rates ($< 5\,\%$ per weight), the plant available water content was significantly increased, whereas no significant differences compared to the not-treated soils were found for higher application rates.

(c) Application of mass transport models to characterise soil structure:

The soil structural development of intact South Greenlandic soils was assessed by investigating the air-phase characteristics (air-filled porosity, soil-gas diffusivity and air permeability). The results showed that the Greenlandic pasture soils exhibited a highly tortuous and disconnected pore network, which might lead to inadequate soil-aeration conditions for plant growth if the current soil equilibrium would be changed by, e.g., changes in land management. The reasons for these suboptimal soil conditions were the high, uncomplexed organic matter contents, inducing highly tortuous pores, and the lack of fine-grained, surface-active minerals resulting in low aggregation potential and thus a lack of soil structure.

(d) Effect of glacial rock flour amendment on functional and mechanical soil properties of repacked soils:

The effect of glacial rock flour amendment on the soil's air phase and on its mechanical properties was studied on repacked and GRF-amended soils from Greenland and Denmark. The addition of low-organic fine mineral material replaced the same amount of soil exhibiting high organic matter contents, reducing the available space for gas transport and slightly increasing the pore network's tortuosity. An increase of the application rate from 3.5 % to 10 % by weight only had minimal effect on the measured mechanical and pore network properties.

Conclusions – extended summary

(i) Climate monitoring

Tow distinct climatic zones could be identified within a relatively small area exhibiting large gradients in precipitation, temperature and relative humidity. The impact of high evaporation rates in combination with coarse-textured soils on the water balance might not be sufficiently taken into account by climate and evapotranspiration models. The matric potential at field capacity was found to be close to $\psi = -100\,\mathrm{hPa}$, an important finding for modelling purposes.

(ii) Site characterisation

The plant available water contents were high compared to Danish agricultural soils, mainly because of high total porosities due to high organic matter contents on the one hand, and low water contents at the permanent wilting point due to low contents of fine particles on the other hand. Based on the relationship between air permeability and saturated hydraulic conductivity, the effective porosity for water-transport was found to be closer to $\psi = -300\,\text{hPa}$ as opposed to $\psi = -100\,\text{hPa}$ following the in-situ measurements of the matric potential. Scale effects and the not captured variability of porosity by the ($100\,\text{cm}^3$) soil core cylinders compared to the in-situ matric potential measurements, measuring a considerably larger volume of soil, definitely had a significant impact on the magnitude of the derived effective porosity.

(iii) Comparing intact and repacked soils

The air-phase parameters measured on repacked soil cores corresponded well to those measured on intact soil cores. The dilution effect on the organic matter, the change of pore size distribution (and probably pore shape) following a change in particle size distribution, and the increased tortuosity due to GRF amendment affected the air phase, which was eventually reflected in lower gas diffusivity measurements.

Perspectives – understanding the effects of GRF addition

The low aggregation potential of most Greenlandic soils results in a four-phase system with clearly separated phases: mineral, organic, water and air phases. This constellation facilitates detrimental effects on the organic matter due to, e.g., climate change or changes in soil management and on the mineral phase by, e.g., facilitating erosion.

Will the GRF, with time, act like inherent clay and provide the soil with additional surface charge to promote soil aggregation and structure formation? Figure 25 illustrates how the GRF might incorporate into the soil system and possibly interact with the different phases of soil. The effect of GRF addition to a technical sand has been assessed in Section 3.3, and it has been empirically shown that the GRF markedly increased the apparent cohesion of the sand particles. Matus (2021) and Schjønning et al. (2010) identified the fine mineral fraction (clay + silt; $< 20\,\mu\text{m}$) to be the major component defining the upper

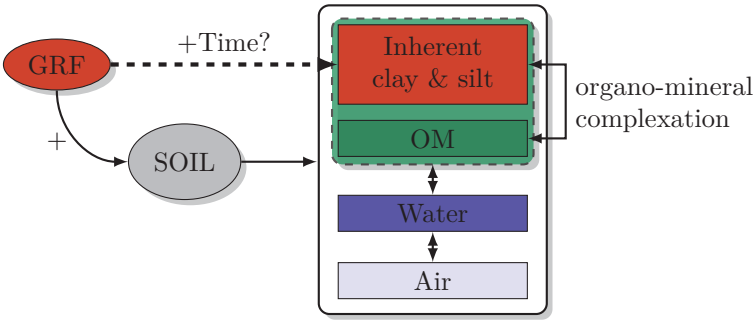

Figure 25: GRF incorporation into the soil and conversion of GRF into clay to facilitate OM-mineral complexation and soil aggregation.

(complexed) organic carbon level in soil. Furthermore, Matus (2021) reported that the organic carbon contents in the silt and clay fraction were independent of clay mineralogy, which is promising, regarding the (short term) GRF's potential to protect soil organic matter.

However, many favourable soil properties promoting soil health and fertility are indeed dependent on clay mineralogy. The chemical weathering of silicates in northern latitudes is rather slow, and it might take a considerable amount of time (Folkoff et al., 1987). Similar to the explanation of the lack of clay minerals in Greenlandic soils (see Section 3.1), the transformation of the primary silicates into secondary clay minerals might be inhibited by the initial mineralogy of the GRF and the prevailing climatic conditions (Palandri et al., 2004). The large specific surface area of the mechanically abraded glacial rock flour and the moderate to strong acidic soil conditions, however, might accelerate the formation of secondary clay minerals (Correns, 1961; Hawkins et al., 1963; White, 1995).

Besides organic carbon sequestration by increasing and protecting the soil organic matter pools, the chemical weathering of rock dust has been considered as geoengineering tool to mitigate climate change by CO_2 removal from the atmosphere, as initially suggested by Seifritz (1990) and Lackner et al. (1995). The process is referred to as *enhanced weathering* and consists of the carbonisation of silicate rocks, which is strongly dependent on the rock's mineral composition (preferably mafic to ultramafic material, cf. Goldich dissolution series), temperature and precipitation (both preferably high) (Hartmann et al., 2013). The high contents of K-feldspars and granite (both felsic) in the fine

fraction of the GRF reduces the suitability of GRF as agent for enhanced weathering, however, the high amount of clay and silt-sized particles makes the energy intensive milling process redundant, which would be a significant advantage (Renforth, 2012). Recently, Beerling et al. (2020), investigated the potential of terrestrial large scale CO_2 removal by enhanced weathering and reported promising results.

Outlook

The most valuable short- and mid-term results of GRF amendment are likely to be obtained from the analysis of yield and nutrient content of crop (grass) from the field-plot experiments.

Measurements of water retention and air-phase properties on intact soil core samples collected shortly after GRF application might point towards detrimental effects on plant available water and soil aeration. For that reason, it is crucial to investigate soil aggregation and soil structure development of GRF amended soils in controlled laboratory experiments, including, e.g., freeze-thaw experiments to simulate long-term effects, the investigation of silicate weathering in cold climates and the interaction of GRF with soil organic matter.

Another critical parameter is the effect of the GRF amendment on the thermal regime of the soil. The short vegetation period necessitates that the soil heats up as fast as possible during spring, enabling an early start of plant growth. Changes in particle size distribution and the pore network will have an impact on the thermal properties of the growing medium which needs to be assessed.

The cardinal role of the soil microbiome in biogeochemical cycles and on soil health (e.g., soil structure) is widely acknowledged by the scientific community but has been neglected throughout this thesis. Recent studies have revealed that the microbial communities in the Arctic are more diverse and abundant than formerly thought. A decline in microbial abundance and diversity due to GRF application should be excluded by appropriate testing.

Further research is needed for greater food security given the increasing environmental stress imposed by climate change in Greenland. Furthermore, additional steps towards greater self-sufficiency of agricultural products for the Greenlandic nation should include: identification and mapping of potential

future arable land, establish an effective irrigation strategy to reduce crop water stress (including hydrophobicity), increase the selection of arable crops and vegetables available for fodder and food production, and improve and strengthen the knowledge exchange between and across research and local farmers.

References

Ahuja, L. R., Naney, J. W., Green, R. E., & Nielsen, D. R. (1984). Macroporosity to characterize spatial variability of hydraulic conductivity and effects of land management. *Soil Science Society of America Journal*, *48*(4), 699–702.

Aljibury, F. K., & Evans, D. D. (1965). Water permeability of saturated soils as related to air permeability at different moisture tensions. *Soil Science Society of America Journal*, *29*(4), 366–369.

Allen, S. J. (1990). Measurement and estimation of evaporation from soil under sparse barley crops in northern Syria. *Agricultural and Forest Meteorology*, *49*(4), 291–309.

Arthur, E., Schjønning, P., Moldrup, P., Tuller, M., & de Jonge, L. W. (2013a). Density and permeability of a loess soil: Long-term organic matter effect and the response to compressive stress. *Geoderma*, *193-194*, 236–245.

Arthur, E., Moldrup, P., Schjønning, P., & de Jonge, L. W. (2013b). Water retention, gas transport, and pore network complexity during short-term regeneration of soil structure. *Soil Science Society of America Journal*, *77*(6), 1965–1976.

Arthur, E., Tuller, M., Moldrup, P., & de Jonge, L. W. (2020). Clay content and mineralogy, organic carbon and cation exchange capacity affect water vapour sorption hysteresis of soil. *European Journal of Soil Science*, *71*(2), 204–214.

Austrheim, G., Asheim, L., Bjarnason, G., Feilberg, J., Fosaa, A. M., Holand, O., Høegh, K., Jónsdóttir, I., Magnusson, B., Mortensen, L., Mysterud, A., Olsen, E., Skonhoft, A., Steinheim, G., & Thorhallsdottir, A. (2008). Sheep grazing in the North Atlantic region: A long term perspective on management, resource economy and ecology. *Rapport Zoology Series*, *3*, 1–82.

Ball, B. C. (1981). Modelling of soil pores as tubes using gas permeabilities, gas diffusivities and water release. *Journal of Soil Science*, *32*(4), 465–481.

Beck, H. E., Zimmermann, N. E., McVicar, T. R., Vergopolan, N., Berg, A., & Wood, E. F. (2018). Present and future Köppen-Geiger climate classification maps at 1-km resolution. *Scientific Data*, *5*(1), 180214.

Beerling, D. J., Kantzas, E. P., Lomas, M. R., Wade, P., Eufrasio, R. M., Renforth, P., Sarkar, B., Andrews, M. G., James, R. H., Pearce, C. R., Mecure, J.-F., Pollitt, H., Holden, P. B., Edwards, N. R., Khanna, M., Koh, L., Quegan, S., Pidgeon, N. F., Janssens, I. A., ... Banwart, S. A. (2020). Potential for large-scale CO_2 removal via enhanced rock weathering with croplands. *Nature*, *583*(7815), 242–248.

Belmonte, L. J. (2015). *Use of Greenlandic resources for the production of bricks* (Doctoral dissertation) [R-315]. Technical University of Denmark, Department of Civil Engineering.

Bennike, O., Björck, S., & Lambeck, K. (2002). Estimates of South Greenland late-glacial ice limits from a new relative sea level curve. *Earth and Planetary Science Letters*, *197*(3), 171–186.

Bennike, O., Jensen, J. B., Næsby Sukstorf, F., & Rosing, M. T. (2019). Mapping glacial rock flour deposits in Tasersuaq, southern West Greenland. *GEUS Bulletin*, *43*.

Berglund, J. (1986). The decline of the Norse settlements in Greenland. *Arctic Anthropology*, *23*(1/2), 109–135.

Bichet, V., Gauthier, É., Massa, C., Perren, B., Richard, H., Petit, C., & Mathieu, O. (2013). The history and impacts of farming activities in south Greenland: An insight from lake deposits. *Polar Record*, *49*(3), 210–220.

Böcher, T. W. (1979). Birch woodlands and tree growth in southern Greenland. *Ecography*, *2*(4), 218–221.

Bojesen, M. H., & Olsen, A. (Eds.). (2019). *Agriculture in Greenland – possibilities and needs for future development and research* (Vol. 1) [Synthesis Report for Greenland Agricultural Initiative (GRAIN) in cooperation with Greenland Perspective].

Bradley-Cook, J. I., & Virginia, R. A. (2016). Soil carbon storage, respiration potential, and organic matter quality across an age and climate gradient in southwestern Greenland. *Polar Biology*, *39*(7), 1283–1295.

Buckingham, E. (1904). *Contributions to our knowledge of the aeration of soils* (tech. rep. No. 25). Bureau of Soils, US Deptartment of Agriculture. Washington.

Buckland, P. C., Edwards, K. J., Panagiotakopulu, E., & Schofield, J. E. (2009). Palaeoecological and historical evidence for manuring and irrigation at Garðar (Igaliku), Norse Eastern Settlement, Greenland. *The Holocene*, *19*(1), 105–116.

Campbell, G. S. (1988). Soil water potential measurement: An overview. *Irrigation Science*, *9*(4), 265–273.

Cann, M. A. (2000). Clay spreading on water repellent sands in the south east of South Australia – promoting sustainable agriculture. *Journal of Hydrology*, *231-232*, 333–341.

Cappelen, J., Jørgensen, B. V., Laursen, E. V., Stannius, L. S., & Thomsen, R. S. (2001). *The observed climate of Greenland, 1958–1999 — with climatological standard normals, 1961–90.* (Technical Report No. 00-18). Danish Meteorological Institute, Ministry of Transport. Copenhagen.

Cappelen, J. (2021). *Greenland-DMI Historical climate data collection 1784-2019* (Technical Report No. 21-04). DMI, Danish Meteorological Institute. Copenhagen.

Caviezel, C., Hunziker, M., & Kuhn, N. J. (2017). Bequest of the Norseman—The potential for agricultural intensification and expansion in southern Greenland under climate change. *Land*, *6*(4), 1–20.

Christensen, B. T. (1995). Carbon in primary and secondary organomineral complexes. In M. R. Carter & B. A. Stewart (Eds.), *Structure and Organic Matter Storage in Agricultural Soils* (pp. 97–165). CRC Press.

Christensen, J. H., Olesen, M., Boberg, F., Stendel, M., & Koldtoft, I. (2016). *Fremtidigeklimaforandringer i Grønland: Kujalleq Kommune* (tech. rep.) [online 13th June 2022, in Danish]. Danish Meteorological Institute. Copenhagen.

Christiansen, H. H. (1998). 'Little Ice Age' nivation activity in northeast Greenland. *The Holocene*, *8*(6), 719–728.

Correns, C. W. (1961). The experimental chemical weathering of silicates. *Clay Minerals Bulletin*, *4*(26), 249–265.

Damgaard, C., Raundrup, K., Aastrup, P., Langen, P. L., Feilberg, J., & Nabe-Nielsen, J. (2016). Arctic resilience: No evidence of vegetation change in response to grazing and climate changes in South Greenland. *Arctic, Antarctic, and Alpine Research*, *48*(3), 531–549.

da Silva, A. R., & de Lima, R. P. (2016). Comparison of methods for determining precompression stress based on computational simulation. *Revista Brasileira De Ciencia Do Solo Journal*, *40*, e0150164.

de Jonge, L. W., Jacobsen, O. H., & Moldrup, P. (1999). Soil water repellency: Effects of water content, temperature, and particle size. *Soil Science Society of America Journal*, *63*(3), 437–442.

Dexter, A. R., Richard, G., Arrouays, D., Czyż, E. A., Jolivet, C., & Duval, O. (2008). Complexed organic matter controls soil physical properties. *Geoderma*, *144*(3), 620–627.

Doerr, S. H., Shakesby, R. A., & Walsh, R. P. D. (2000). Soil water repellency: Its causes, characteristics and hydro-geomorphological significance. *Earth-Science Reviews*, *51*(1), 33–65.

Doran, J. W., & Parkin, T. B. (1994). Defining and assessing soil quality. In J. Doran, D. Coleman, D. Bezdicek & B. Stewart (Eds.), *Defining Soil Quality for a Sustainable Environment* (pp. 1–21). John Wiley & Sons, Ltd.

Dugmore, A. J., Keller, C., & McGovern, T. H. (2007). Norse Greenland settlement: Reflections on climate change, trade, and the contrasting fates or human settlements in the North Atlantic islands. *Arctic Anthropology*, *44*(1), 12–36.

Edwards, K. J., Schofield, J. E., & Mauquoy, D. (2008). High resolution paleoenvironmental and chronological investigations of Norse landnám at Tasiusaq, Eastern Settlement, Greenland. *Quaternary Research*, *69*(1), 1–15.

Emerson, W. W., Foster, R. C., & Oades, J. M. (1986). Organo-mineral complexes in relation to soil aggregation and structure. In P. M. Huang & M. Schnitzer (Eds.), *Interactions*

of Soil Minerals with Natural Organics and Microbes (pp. 521–548). John Wiley & Sons, Ltd.

Eusterhues, K., Rumpel, C., Kleber, M., & Kögel-Knabner, I. (2003). Stabilisation of soil organic matter by interactions with minerals as revealed by mineral dissolution and oxidative degradation. *Organic Geochemistry*, *34*(12), 1591–1600.

Feilberg, J. (1984). A phytogeographical study of South Greenland. Vascular plants. In G. S. Mogensen (Ed.), *Meddelelser om Grønland: Bioscience (Geoscience, Man & Society)* (p. 72). Kommissionen for Videnskabelige Undersøgelser i Grønland.

DMI. (2021). DMI Open Data [data retrieved from: https://confluence.govcloud.dk/].

Fleming, K., & Lambeck, K. (2004). Constraints on the Greenland Ice Sheet since the Last Glacial Maximum from sea-level observations and glacial-rebound models. *Quaternary Science Reviews*, *23*(9), 1053–1077.

Folkoff, M. E., & Meentemeyer, V. (1987). Climatic control of the geography of clay minerals genesis. *Annals of the Association of American Geographers*, *77*(4), 635–650.

Freijer, J. I. (1994). Calibration of jointed tube model for the gas diffusion coefficient in soils. *Soil Science Society of America Journal*, *58*(4), 1067–1076.

Gillman, G. P., Burkett, D. C., & Coventry, R. J. (2001). A laboratory study of application of basalt dust to highly weathered soils: Effect on soil cation chemistry. *Soil Research*, *39*(4), 799–811.

Goldich, S. S. (1938). A study in rock-weathering. *The Journal of Geology*, *46*(1), 17–58.

Grigal, D. F., Brovold, S. L., Nord, W. S., & Ohmann, L. F. (1989). Bulk density of surface soils and peat in the North Central United States. *Canadian Journal of Soil Science*, *69*(4), 895–900.

Gunnarsen, K. C. (2020). *Plant nutritional value of Greenlandic glacial rock flour: An amendment to improve weathered and nutrient poor soils* (Doctoral dissertation). University of Copenhagen, Department of Plant and Environmental Sciences.

Gunnarsen, K. C., Jensen, L. S., Gómez-Muñoz, B., Rosing, M. T., & de Neergaard, A. (2019). Glacially abraded rock flour from Greenland: Potential for macronutrient supply to plants. *Journal of Plant Nutrition and Soil Science*, *182*(5), 846–856.

Hall, D., Jones, H., Crabtree, W., & Daniels, T. (2010). Claying and deep ripping can increase crop yields and profits on water repellent sands with marginal fertility in southern Western Australia. *Australian Journal of Soil Research*, *48*(2), 178–187.

Hamamoto, S., Moldrup, P., Kawamoto, K., & Komatsu, T. (2012). Organic matter fraction dependent model for predicting the gas diffusion coefficient in variably saturated soils. *Vadose Zone Journal*, *11*(1).

Hanna, E., & Cappelen, J. (2002). Recent climate of southern Greenland. *Weather*, *57*(9), 320–328.

Hansen, L. (1976). Jordtyper ved statens forsøgsstationer - Soil types at the Danish state experimental stations. Beretning fra statens forsøgsvirksomhed i plantekultur. *Særtryk af Tidsskrift for Planteavl*, *80*, 742–758.

Hartmann, J., West, A. J., Renforth, P., Köhler, P., De La Rocha, C. L., Wolf-Gladrow, D. A., Dürr, H. H., & Scheffran, J. (2013). Enhanced chemical weathering as a geoengineering strategy to reduce atmospheric carbon dioxide, supply nutrients, and mitigate ocean acidification. *Reviews of Geophysics*, *51*(2), 113–149.

Hassol, S. (2004). *Impacts of a warming Arctic - Arctic climate impact assessment* (tech. rep.). Arctic Council. Cambridge University Press.

Hawkins, D. B., & Rustum, R. (1963). Experimental hydrothermal studies on rock alteration and clay mineral formation. *Geochimica et Cosmochimica Acta*, *27*(10), 1047–1054.

Hermansen, C., Knadel, M., Moldrup, P., Greve, M. H., Karup, D., & de Jonge, L. W. (2017). Complete soil texture is accurately predicted by visible near-infrared spectroscopy. *Soil Science Society of America Journal*, *81*(4), 758–769.

Hopmans, J. W., Nielsen, D. R., & Bristow, K. L. (2002). How useful are small-scale soil hydraulic property measurements for large-scale vadose zone modeling? *American Geophysical Union Geophysical Monograph Series*, *129*, 247–258.

Horn, R., & Fleige, H. (2003). A method for assessing the impact of load on mechanical stability and on physical properties of soils. *Soil & Tillage Research*, *73*(1-2), 89–99.

Iiyama, I., & Hasegawa, S. (2005). Gas diffusion coefficient of undisturbed peat soils. *Soil Science and Plant Nutrition*, *51*(3), 431–435.

Jacobsen, N. K. (1987). Studies on soils and potential for soil erosion in the sheep farming area of South Greenland. *Arctic and Alpine Research*, *19*(4), 498–507.

Jakobsen, B. H. (1989). Evidence for translocations into the B horizon of a subarctic Podzol in Greenland. *Geoderma*, *45*(1), 3–17.

Kawamoto, K., Moldrup, P., Schjønning, P., Iversen, B. V., Komatsu, T., & Rolston, D. E. (2006). Gas transport parameters in the vadose zone: Development and tests of power-law models for air permeability. *Vadose Zone Journal*, *5*(4), 1205–1215.

Keller, T., Lamandé, M., Schjønning, P., & Dexter, A. R. (2011). Analysis of soil compression curves from uniaxial confined compression tests. *Geoderma*, *163*(1), 13–23.

Kelly, W. C., & Zumberge, J. H. (1961). Weathering of a quartz diorite at Marble Point, McMurdo Sound, Antarctica. *The Journal of Geology*, *69*(4), 433–446.

Kögel-Knabner, I., Ekschmitt, K., Flessa, H., Guggenberger, G., Matzner, E., Marschner, B., & Lützow, M. v. (2008). An integrative approach of organic matter stabilization in temperate soils: Linking chemistry, physics, and biology. *Journal of Plant Nutrition and Soil Science*, *171*(1), 5–13.

Kokfelt, F. T., Weng, L. W., & Willerslev, E. (2019). *Geological map of South and South West Greenland – 1 : 100 000* (tech. rep.). Geological Survey of Denmark and Greenland (GEUS). Copenhagen.

Kolb, J., Keiding, J. K., Steenfelt, A., Secher, K., Keulen, N., Rosa, D., & Stensgaard, B. M. (2016). Metallogeny of Greenland. *Ore Geology Reviews*, *78*, 493–555.

Kuijpers, A., Abrahamsen, N., Hoffmann, G., Hühnerbach, V., Konradi, P., Kunzendorf, H., Mikkelsen, N., Thiede, J., & Weinrebe, W. (1999). Climate change and the Viking-age fjord environment of the Eastern Settlement, South Greenland. *Geology of Greenland Survey Bulletin*, *183*, 61–67.

Lackner, K. S., Wendt, C. H., Butt, D. P., Joyce, E. L., & Sharp, D. H. (1995). Carbon dioxide disposal in carbonate minerals. *Energy*, *20*(11), 1153–1170.

Lamandé, M., Schjønning, P., & Labouriau, R. (2017). A novel method for estimating soil precompression stress from uniaxial confined compression tests. *Soil Science Society of America Journal*, *81*(5), 1005–1013.

Ledger, P. M., Edwards, K. J., & Schofield, E. J. (2013). Shieling activity in the Norse Eastern Settlement: Palaeoenvironment of the 'Mountain Farm', Vatnahverfi, Greenland. *The Holocene*, *23*(6), 810–822.

Lehmann, J. O., Sharif, B., Kjeldsen, C., Plauborg, F., Olesen, J. E., Mikkelsen, M. H., Aastrup, P., Wegeberg, S., Kristensen, T., & Greve, M. H. (2016). *Muligheder for klimatilpasning i landbrugserhvervet - status og handlemuligheder.* (tech. rep.) [in Danish]. Aarhus Universitet, Institut for Agroøkologi / Naalakkersuisut: The Government of Greenland. Foulum, Tjele.

Lehmann, J., & Kleber, M. (2015). The contentious nature of soil organic matter. *Nature*, *528*(7580), 60–68.

Lellei-Kovács, E., Botta-Dukát, Z., De Dato, G., Estiarte, M., Guidolotti, G., Kopittke, G. R., Kovács-Láng, E., Kröel-Dulay, G., Larsen, K. S., Peñuelas, J., Smith, A. R., Sowerby, A., Tietema, A., & Schmidt, K. I. (2016). Temperature dependence of soil respiration modulated by thresholds in soil water availability across European shrubland ecosystems. *Ecosystems*, *19*(8), 1460–1477.

Li, X., Hou, X., Liu, Z., Guo, F., Ding, Y., & Duan, J. (2017). Long-term overgrazing-induced changes in topsoil water-retaining capacity in a typical steppe. *Rangeland Ecology & Management*, *70*(3), 324–330.

Libohova, Z., Seybold, C., Wysocki, D., Wills, S., Schoeneberger, P., Williams, C., Lindbo, D., Stott, D., & Owens, P. R. (2018). Reevaluating the effects of soil organic matter and other properties on available water-holding capacity using the National Cooperative Soil Survey Characterization Database. *Journal of Soil and Water Conservation*, *73*(4), 411–421.

Loll, P., Moldrup, P., Schjønning, P., & Riley, H. (1999). Predicting saturated hydraulic conductivity from air permeability: Application in stochastic water infiltration modeling. *Water Resources Research*, *35*(8), 2387–2400.

Lynnerup, N. (1996). Paleodemography of the Greenland Norse. *Arctic Anthropology*, *33*(2), 122–136.

Massa, C., Bichet, V., Gauthier, É., Perren, B. B., Mathieu, O., Petit, C., Monna, F., Giraudeau, J., Losno, R., & Richard, H. (2012). A 2500 year record of natural and anthropogenic soil erosion in South Greenland. *Quaternary Science Reviews*, *32*, 119–130.

Matus, F. J. (2021). Fine silt and clay content is the main factor defining maximal C and N accumulations in soils: A meta-analysis. *Scientific Reports*, *11*(6438).

McKissock, I., Gilkes, R. J., & Walker, E. L. (2002). The reduction of water repellency by added clay is influenced by clay and soil properties [Clay Research in Australia and New Zealand]. *Applied Clay Science*, *20*(4), 225–241.

METER Group AG. (2020). *TEROS 21 (GEN 2) Manual*. München, Germany.

Michelsen, C. F., Pedas, P., Glaring, M. A., Schjoerring, J. K., & Stougaard, P. (2014). Bacterial diversity in Greenlandic soils as affected by potato cropping and inorganic versus organic fertilization. *Polar Biology*, *37*(1), 61–71.

Millington, R. J., & Quirk, J. M. (1964). Formation factor and permeability equations. *Nature*, *202*, 143–145.

Moldrup, P., Olesen, T., Komatsu, T., Schjønning, P., & Rolston, D. E. (2001). Tortuosity, diffusivity, and permeability in the soil liquid and gaseous phases. *Soil Science Society of America Journal*, *65*(3), 613–623.

Moldrup, P., Yoshikawa, S., Olesen, T., Komatsu, T., & Rolston, D. E. (2003a). Air permeability in undisturbed volcanic ash soils. *Soil Science Society of America Journal*, *67*(1), 32–40.

Moldrup, P., Yoshikawa, S., Olesen, T., Komatsu, T., & Rolston, D. E. (2003b). Gas diffusivity in undisturbed volcanic ash soils. *Soil Science Society of America Journal*, *67*(1), 41–51.

Munk, L., Neergaard, E., Stougaard, P., & Høegh, K. Climatic changes and agriculture in Greenland: Plant diseases in potatoes and grass fields. In: In *Climate change. global risks, challenges & decisions, copenhagen, denmark.* 2009.

Oades, J. M. (1984). Soil organic matter and structural stability: Mechanisms and implications for management. *Plant and Soil*, *76*(1), 319–337.

Ogrič, M., Knadel, M., Kristiansen, S. M., Peng, Y., de Jonge, L. W., Adhikari, K., & Greve, M. H. (2019). Soil organic carbon predictions in Subarctic Greenland by visible–near infrared spectroscopy. *Arctic, Antarctic, and Alpine Research*, *51*(1), 490–505.

Palandri, J. L., & Kharaka, Y. K. (2004). *A compilation of rate parameters of water-mineral interaction kinetics for application to geochemical modeling* (Report No. 2004-1068). U.S. Geological Survey.

Pesch, C., Lamandé, M., de Jonge, L. W., Norgaard, T., Greve, M. H., & Moldrup, P. (2020). Compression and rebound characteristics of agricultural sandy pasture soils from South Greenland. *Geoderma*, *380*, 114608.

Pesch, C., Weber, P. L., de Jonge, L. W., Greve, M. H., Lamandé, M., & Moldrup, P. (n.d.). Changes in pore-network and mechanical properties after Greenlandic rock flour addition to repacked sands and soils [submitted]. *Soil Science Society of America Jounal*, *n/a*(n/a).

Pesch, C., Weber, P. L., de Jonge, L. W., Greve, M. H., Norgaard, T., & Moldrup, P. (2021). Soil–air phase characteristics: Response to texture, density, and land use in Greenland and Denmark. *Soil Science Society of America Journal*, *85*(5), 1534–1554.

Pesch, C., Weber, P. L., Moldrup, P., de Jonge, L. W., Arthur, E., & Greve, M. H. (2022). Physical characterization of glacial rock flours from fjord deposits in South Greenland–Toward soil amendment. *Soil Science Society of America Journal*, *86*(2), 407–422.

Petersen, L. W., Møldrup, P., Jacobsen, O. H., & Rolston, D. E. (1996). Relations between specific surface area and soil physical and chemical properties. *Soil Science*, *161*, 1–13.

Priyono, J., & Gilkes, R. J. (2004). Dissolution of milled-silicate rock fertilisers in the soil. *Soil Research*, *42*(4), 441–448.

Pulido-Moncada, M., Munkholm, L. J., & Schjønning, P. (2019). Wheel load, repeated wheeling, and traction effects on subsoil compaction in northern Europe. *Soil and Tillage Research*, *186*, 300–309.

Renforth, P. (2012). The potential of enhanced weathering in the UK. *International Journal of Greenhouse Gas Control*, *10*, 229–243.

Resurreccion, A. C., Kawamoto, K., Komatsu, T., Moldrup, P., Sato, K., & Rolston, D. E. (2007). Gas diffusivity and air permeability in a volcanic ash soil profile: Effects of organic matter and water retention. *Soil Science*, *172*(6), 432–443.

Resurreccion, A. C., Moldrup, P., Tuller, M., Ferré, T. P. A., Kawamoto, K., Komatsu, T., & de Jonge, L. W. (2011). Relationship between specific surface area and the dry end of the water retention curve for soils with varying clay and organic carbon contents. *Water Resources Research*, *47*(6).

Richards, L. A., & Weaver, L. R. (1944). Moisture retention by some irrigated soils as related to soil-moisture tension. *Journal of Agricultural Research*, *69*, 215–235.

Roper, M., Davies, S., Blackwell, P., Hall, D., Bakker, D., Jongepier, R., & Ward, P. (2015). Management options for water-repellent soils in Australian dryland agriculture. *Soil Research*, *53*(7), 786–806.

Rücknagel, J., Hofmann, B., Paul, R., Christen, O., & Hülsbergen, K.-J. (2007). Estimating precompression stress of structured soils on the basis of aggregate density and dry bulk density. *Soil and Tillage Research*, *92*(1), 213–220.

Rühlmann, J., Körschens, M., & Graefe, J. (2006). A new approach to calculate the particle density of soils considering properties of the soil organic matter and the mineral matrix. *Geoderma*, *130*(3), 272–283.

Rutherford, G. K. (1995). Soils of some Norse settlements in southwestern Greenland. *Arctic*, *48*(4), 324–328.

Schjønning, P., de Jonge, L. W., Moldrup, P., Christensen, B. T., & Olesen, J. E. (2010). Searching the critical soil organic carbon threshold for satisfactory tilth conditions – test of the Dexter clay:carbon hypothesis. *Proceedings of the 1st international conference and exploratory workshop on soil architecture and physico-chemical functions "Cesar"*, 341–346.

Schjønning, P., & Koppelgaard, M. (2017). The Forchheimer approach for soil air permeability measurement. *Soil Science Society of America Journal*, *81*(5), 1045–1053.

Schjønning, P., Thomsen, I. K., Moldrup, P., & Christensen, B. T. (2003). Linking soil microbial activity to water- and air-phase contents and diffusivities. *Soil Science Society of America Journal*, *67*(1), 156–165.

Schmidt, M. W. I., Torn, M. S., Abiven, S., Dittmar, T., Guggenberger, G., Janssens, I. A., Kleber, M., Kögel-Knabner, I., Lehmann, J., Manning, D. A. C., Nannipieri, P., Rasse, D. P., Weiner, S., & Trumbore, S. E. (2011). Persistence of soil organic matter as an ecosystem property. *Nature*, *478*(7367), 49–56.

Schofield, E. J., Edwards, K. J., & McMullen, A. J. (2007). Modern pollen–vegetation relationships in subarctic southern Greenland and the interpretation of fossil pollen data from the Norse landnám. *Journal of Biogeography*, *34*(3), 473–488.

Schofield, R. K. The pF of the water in soil. In: In *Transactions of the Third International Congress of Soil Science. 2.* International Society of Soil Science. Oxford: Thomas Murby & Company, 1935, 37–48.

Seifritz, W. (1990). CO_2 disposal by means of silicates. *Nature*, *345*(6275), 486.

Sjöström, J. K., Bindler, R., Granberg, T., & Kylander, M. E. (2019). Procedure for organic matter removal from peat samples for XRD mineral analysis. *Wetlands*, *39*(3), 473–481.

Soane, B. D. (1990). The role of organic matter in soil compactibility: A review of some practical aspects [A Tribute to Prof. IR. H. Kuipers]. *Soil and Tillage Research*, *16*(1), 179–201.

Spaans, E. J. A., & Baker, J. M. (1996). The soil freezing characteristic: Its measurement and similarity to the soil moisture characteristic. *Soil Science Society of America Journal*, *60*(1), 13–19.

Steenfelt, A. (2012). Rare earth elements in Greenland: known and new targets identified and characterised by regional stream sediment data. *Geochemistry: Exploration, Environment, Analysis*, *12*(4), 313–326.

Steenfelt, A., Kolb, J., & Thrane, K. (2016). Metallogeny of South Greenland: A review of geological evolution, mineral occurrences and geochemical exploration data. *Ore Geology Reviews*, *77*, 194–245.

Stepniewski, W. (1981). Oxygen diffusion and strength as related to soil compaction. II. Oxygen diffusion coefficient. *Polish Journal of Soil Science*, *14*, 3–13.

Sukstorf, F. N., Bennike, O., & Elberling, B. (2020). Glacial rock flour as soil amendment in subarctic farming in South Greenland. *Land*, *9*(6).

Tahir, S., & Marschner, P. (2016). Clay amendment to sandy soil – effect of clay concentration and ped size on nutrient dynamics after residue addition of low C/N ratio residue. *Journal of Soil Science and Plant Nutrition*, *16*(4), 864–875.

Tuller, M., & Or, D. (2005). Water films and scaling of soil characteristic curves at low water contents. *Water Resources Research*, *41*(9), W09403.

van Genuchten, M. T. (1980). A closed-form equation for predicting the hydraulic conductivity of unsaturated soils. *Soil Science Society of America Journal*, *44*(5), 892–898.

Wagner, S., Cattle, S. R., & Scholten, T. (2007). Soil-aggregate formation as influenced by clay content and organic-matter amendment. *Journal of Plant Nutrition and Soil Science*, *170*(1), 173–180.

Ward, P. R., & Oades, J. M. (1993). Effect of clay mineralogy and exchangeable cations on water repellency in clay-amended sandy soils. *Soil Research*, *31*(3), 351–364.

Warrick, A. W., Mullen, G. J., & Nielsen, D. R. (1977). Scaling field-measured soil hydraulic properties using a similar media concept. *Water Resources Research*, *13*(2), 355–362.

Weber, P. L., Blæsbjerg, N. H., Pesch, C., Hermansen, C., Greve, M. H., de Jonge, L. W., & Moldrup, P. (n.d.-a). Organic matter controls water retention and plant available water in cultivated soils from four regions in South Greenland [submitted]. *Soil Science Society of America Journal*, *n/a*(n/a).

Weber, P. L., de Jonge, L. W., Greve, M. H., Norgaard, T., & Moldrup, P. (2020). Gas diffusion characteristics of agricultural soils from South Greenland. *Soil Science Society of America Journal*, *84*(5), 1606–1619.

Weber, P. L., Hermansen, C., Nørgaard, T., Pesch, C., Moldrup, P., Greve, M. H., Arthur, E., & de Jonge, L. W. (2022). Evaluating the particle densities of subarctic soils using pedotransfer functions and vis–NIR spectroscopy. *Soil Science Society of America Journal*, *n/a*(n/a), 1–15.

Weber, P. L., Hermansen, C., Norgaard, T., Pesch, C., Moldrup, P., Greve, M. H., Müller, K., Arthur, E., & de Jonge, L. W. (2021). Moisture-dependent water repellency of Greenlandic cultivated soils. *Geoderma*, *402*, 115189.

Weber, P. L., Hermansen, C., Pesch, C., Moldrup, P., Greve, M. H., Blæsbjerg, N. H., Romero, G. M., Arthur, E., & de Jonge, L. W. (n.d.-b). Glacial rock flour reduces the hydrophobicity of Greenlandic cultivated soils [submitted]. *Soil Science Society of America Journal*, *n/a*(n/a).

Wegmann, C. E. (1938). Geological investigations in southern Greenland. Part I. On the structural divisions of southern Greenland. *Meddelelser om Grønland*, *113*, 148pp.

Westergaard-Nielsen, A., Bjørnsson, A. B., Jepsen, M. R., Stendel, M., Hansen, B. U., & Elberling, B. (2015). Greenlandic sheep farming controlled by vegetation response today and at the end of the 21st century. *Science of The Total Environment*, *512-513*, 672–681.

White, A. F. (1995). Chemical weathering rates of silicate minerals in soils. In A. F. White & S. L. Brantley (Eds.), *Chemical weathering rates of silicate minerals* (pp. 407–462). De Gruyter.

Zhang, B., Horn, R., & Hallett, P. D. (2005). Mechanical resilience of degraded soil amended with organic matter. *Soil Science Society of America Journal*, *69*(3), 864–871.

Zhang, T., Barry, R. G., Knowles, K., Heginbottom, J. A., & Brown, J. (1999). Statistics and characteristics of permafrost and ground-ice distribution in the Northern Hemisphere. *Polar Geography*, *23*(2), 132–154.

Supporting Papers

A. Paper I

published as:
Pesch, C., Weber, P. L., Moldrup, P., de Jonge, L. W., Arthur, E., & Greve, M. H. (2022). Physical characterization of glacial rock flours from fjord deposits in South Greenland–Toward soil amendment. *Soil Science Society of America Journal*, *86*(2), 407–422. doi: 10.1002/saj2.20352

Received: 6 July 2021 | Accepted: 4 November 2021

DOI: 10.1002/saj2.20352

Soil Science Society of America Journal

PEDOLOGY

Physical characterization of glacial rock flours from fjord deposits in South Greenland–Toward soil amendment

Charles Pesch[1] | **Peter Lystbæk Weber**[2] | **Per Moldrup**[1] | **Lis Wollesen de Jonge**[2] | **Emmanuel Arthur**[2] | **Mogens Humlekrog Greve**[2]

[1] Dep. of the Built Environment, Aalborg Univ., Thomas Manns Vej 23, DK-9220, Aalborg, Denmark

[2] Dep. of Agroecology, Aarhus Univ., Blichers Allé 20, P.O. Box 50, DK-8830, Tjele, Denmark

Correspondence
Charles Pesch, Dep. of the Built Environment, Aalborg Univ., Thomas Manns Vej 23, DK-9220, Aalborg, Denmark.
Email: cmep@build.aau.dk

Assigned to Associate Editor Travis Nauman.

Funding information
Teknologi og Produktion, Det Frie Forskningsråd, Grant/Award Number: 8022-00184B

Abstract

Greenlandic fjords contain vast amounts of glacially derived mineral material (glacial rock flour [GRF]), which may be used to amend structureless, low-clay, and water-repellent agricultural soils in South Greenland and elsewhere. In this study, we investigate key physical amendment properties of GRF from 16 different deposits in South Greenland. The clay-sized fraction varied largely (range, 0.11–0.57 kg kg^{-1}), and the particles were mostly angular. The specific surface area (SSA) determined by either ethylene glycol monomethyl ether (EGME, polar liquid) (range, 13.32–88.06 m^2 g^{-1}) or water-vapor adsorption (range, 10.62–63.82 m^2 g^{-1}) agreed well (r = .90) and were comparable to kaolinitic-clay dominated cultivated soils (KA-soils) with clay content similar to the GRFs. The cation exchange capacities (CECs) (range, 4.25–21.91 cmol kg^{-1}) were similar to or higher than those of the KA-soils. The water content at the permanent wilting point (PWP) for the GRFs were considerably lower than those of the KA-soils. The addition of 5% GRF to a sandy soil from Greenland showed a tendency (although not statistically significant) to increase plant available water (PAW). However, very high GRF addition (10 and 15%) significantly decreased the PAW. The specific surface charge (CEC/SSA) of the GRFs were higher than for comparable KA-soils, suggesting a good soil amendment potential. The results from this study are valuable toward designing sustainable GRF amendment strategies, matching a given cultivated soil with the right amount and type of GRF.

1 | INTRODUCTION

The South Greenlandic soils are characterized by a relatively coarse texture and moderate to high organic matter (OM) content and show little to moderate soil development (Jakobsen, 1991); Caviezel et al., 2017; Weber et al., 2020; Pesch et al., 2021). In a recent study, Weber et al. (2021) revealed the hydrophobic tendency of Greenlandic agricultural soils, which was attributed to the combination of coarse soil texture and high OM content. Furthermore, Pesch et al.

Abbreviations: CEC, cation exchange capacity; DSL, Danish Soil Library; EC, electrical conductivity; EGME, ethylene glycol monomethyl ether; GRF, glacial rock flour; IL, illite; KA, kaolinite; KA-soils, kaolinitic-clay-dominated cultivated soils; LD, laser diffraction; MO, montmorillonite; OM, organic matter; PAW, plant available water; PSD, particle size distribution; PWP, permanent wilting point; RH, relative humidity; SP, sieve and pipette; SSA, specific surface area; SSA_w, specific surface area estimated from water vapor sorption isotherms; SSC, specific surface charge; WSI, water vapor sorption isotherm; Ψ, soil-water potential

(2021) revealed the quasi absence of any soil aggregation and Weber et al. (2020) pointed out the complexity of adequate soil aeration because of pronounced pore network tortuosity. The cold environment, relatively coarse soil texture, and the lack of soil development result in large amounts of noncomplexed OM (Pesch et al., 2020), which will be prone to degradation following increasing temperatures (Kirschbaum, 1995) or changes in soil management (Besnard et al., 1996).

To counteract such unfavorable soil conditions for productive agriculture, different soil amelioration strategies have shown more or less promising results (Maslov, 2009). Intentional or unintentional soil conditioning has a long history in agriculture (Simonson, 1959), and in recent years, the use of chemically untreated mineral rock dust has been given more attention (van Straaten, 2007).

It is well known that the soil's fine particle content governs its functional, physical, and chemical properties. Among others, McKissock et al. (2002) reported that the addition of small amounts of clay (≤1.6% w/w) effectively reduced water repellency in sandy soils even though for coarse soils, the finer fractions often exhibit highest water repellency because of the higher OM content of the finer fractions (de Jonge et al., 1999). This corroborates with Tahir and Marschner (2016), who reported increased OM retention in Australian farmlands after clay amendment. Dexter et al. (2008), Schjønning et al. (2010), Oades (1984), and Wagner et al. (2007) pointed out the importance of the specific surface area (SSA) and thus the content of fine particles of the mineral soil fraction for OM protection and soil aggregate stability. The soil's nutrient holding capacity is largely dependent on the OM and the fine mineral fraction and the associated cation exchange capacity (CEC), as concluded by Matus (2021) and Nguyen and Marschner (2013). Last but not least, the effect of the fine solid fraction on soil-water retention and plant-available water is widely acknowledged (e.g., Rawls & Brakensiek, 1982; Karup et al., 2017).

Throughout the former glaciated parts of the northern hemisphere, the perpetual movement of the ice sheet produced vast amounts of fine-grained mineral material by abrading the crystalline bedrock with debris embedded in its basement (Belmonte, 2015). The sediments were discharged via the glacial outwash streams into periglacial lakes or into the marine environment, where the particles settled and formed thick bottom layers of fine-grained material, referred to as glacial rock flour (GRF). Investigations on sediments originating from Alaska (Ramesh & D'Anglejan, 1995), Canada (Bentley & Smalley, 1979), Scandinavia (Roaldset, 1972), and South Greenland (Belmonte, 2015) revealed that they shared similar mineralogical properties with varying clay content between 20 and 90% (w/w). Under specific circumstances, the low internal cohesion of the sediments of the raised seabeds can lead to dangerous landslides and serious subsidence; therefore, their geotechnical properties have been investigated in detail (Belmonte, 2015). Generally, the abraded and mechanically weathered mineral material mainly consisted of the primary minerals quartz, feldspars, and amphiboles, which were also found in relatively high abundances in the clay fraction (<2 μm). Pederstad and Jørgensen (1985) and Belmonte (2015) reported the presence of illite and kaolinite in the clay-sized fraction as well as expandable clays (e.g., smectite and vermiculite) and concluded that the material underwent subaerial postglacial chemical weathering.

Core Ideas

- We analyzed fine-grained, glacially abraded mineral material from Greenland.
- The surface area was comparable with similar-textured, kaolinitic-clay-dominated soils (KA-soils).
- The water content at the permanent wilting point was lower than that of KA-soils.
- The cation exchange capacity was similar to or higher than that of KA-soils
- The properties of the glacial rock flour suggest that it can be used as mineral soil amendment.

There are only a few studies that investigated the use of Greenlandic GRF as a potential soil fertilizer. Gunnarsen et al. (2019) applied GRF as mineral fertilizer in controlled laboratory experiments and concluded that the GRF could act as slow-release potassium and magnesium source for crops. Furthermore, Gunnarsen (2020) concluded that high rates of GRF application increased biomass production in active soil environments following enhanced weathering of the mineral material. Sukstorf et al. (2020) presented the results of a one-season (2 mo) field experiment in Greenland and concluded that an amendment with only GRF was not suited as short-term fertilizer; however, a combination of GRF and artificial N–P–K fertilizer significantly increased the yields. Regarding the slow dissolution rates of the primary silicates found in the GRF, especially in cold environments, the results of Sukstorf et al. (2020) were expected. In contrast to conventional soil amendments, for example, organic and artificial fertilizers, or liming, the addition of a fine-grained mineral material to soil is a long-term and profound intervention on the soil, and any negative effect on the latter needs to be assessed before large-scale application.

This study is a first step toward the availability and characterization of GRF deposits across South Greenland in the perspective of their suitability as soil conditioner for the local farmland. The focus was put on potential soil–GRF interactions after application to (a) promote soil development in terms of aggregation and structure development, (b) increase

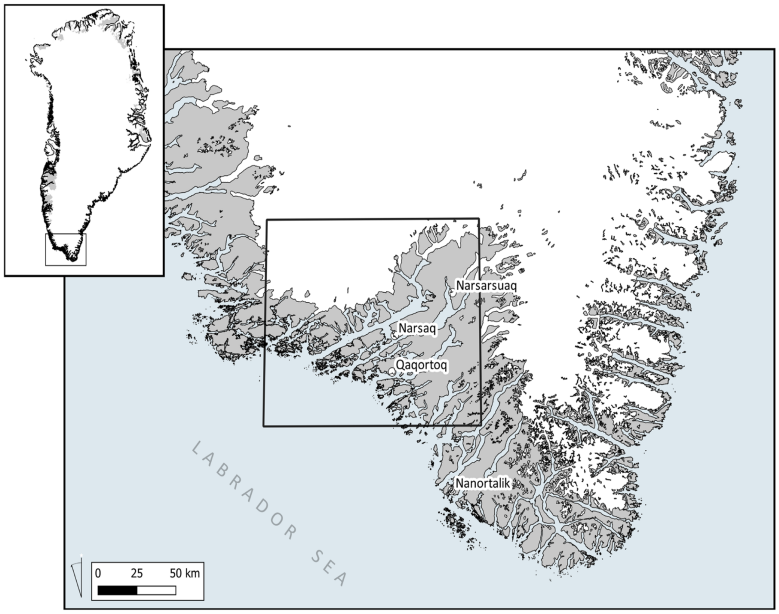

FIGURE 1 Overview of the investigated area in South Greenland. Detailed map of the marked area in Figure 2

mineral fertilizer efficiency, and (c) exclude negative effects on water-holding capacity. For this purpose, we analyzed the particle-size distribution, the SSA, and CEC of 16 selected GRF deposits found in the vicinity of the present agricultural area in South Greenland. Additionally, the bulk mineralogy and several basic soil chemical and physical properties were determined and discussed.

2 | MATERIAL AND METHODS

2.1 | Geological description of the study area

The investigated area (Figure 1) lies within the diverse geological Gardar province, which formed 1.2 Ga BP. It is surrounded by the Ketilidian fold belt (1.8 Ga) and joins the Archaean block further north (3.8 Ga). The crystalline bedrock (Julianehåb batholith) mainly consists of biotite and hornblende-bearing granite and gneiss (Berrangé, 1966) bearing intrusions of intermediate metavolcanic rocks (plagioclase phenocrysts) and light-colored, small-grained granites (leucocratic quartzo-feldspathic and aplitic rocks) (Kalsbeek et al., 1990). The GRF studied here thus consists of some of the oldest geological surface materials on Earth (Henriksen, 2008).

Agriculture in Greenland mainly consists of sheep husbandry with summer pastures and indoor production during winter. The region is the only important agriculturally exploited area in Greenland totaling ~1,100 ha of occasionally cultivated lands (Westergaard-Nielsen et al., 2015) mainly used for winter fodder production.

The subglacial watersheds encompass large areas, and the abraded mineral material suspended in the outwash streams is thus a mix of the bedrock found throughout the watershed. This assumption corroborates with the findings of Andrews (2011) and White et al. (2016), who investigated the mineralogy of marine sediments along the west coast of Greenland. They reported a general similarity of the mineral composition of the collected samples, which suggests that the sediments originate from a similar parent material.

The formation of the investigated GRF deposits took place in the estuaries of the glacial outwash streams (Bennike et al., 2019; Andrews, 2011) and appeared at the surface only after the isostatic rebound because of reduced load following deglaciation. Considerable continental uplift occurred since the end of the Pleistocene (~11 ka BP), with 20–40 m close to the current inland ice margin (inner-fjord) and 60–80 m in the outer-fjord regions (Bennike et al., 2002). According to Bennike et al. (2002), most of the investigated area was deglaciated prior to 10 ka BP. With time, the deposits were covered by combined solifluction of slope deposits and fluvial and aeolian sediments and thus partly protected from extensive erosion (see photograph in Figure 2).

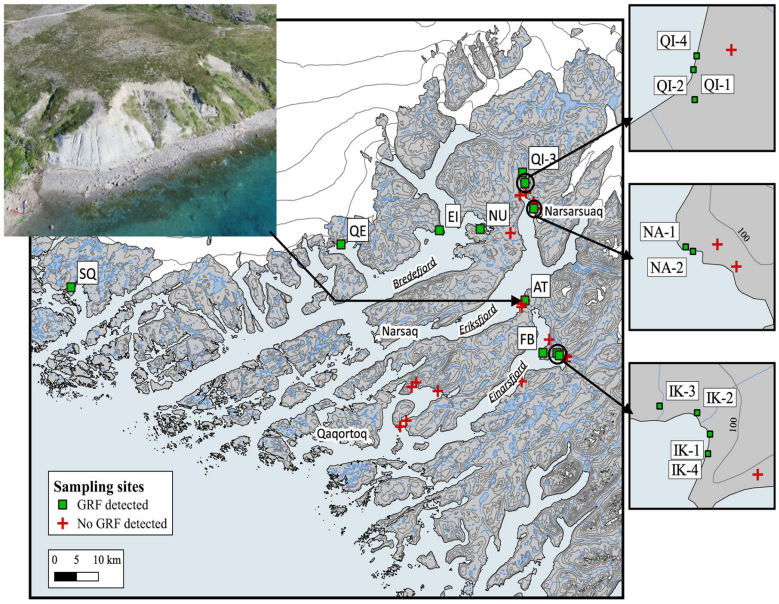

FIGURE 2 Detailed map of the area marked in Figure 1. The approved and discarded sampling sites (green squares and red crosses, respectively) in South Greenland. Top left photograph shows deposition Ataarnasit (AT); its horizontal extent covers ~250 m. EI, Eqaluit Ilulat; FB, Fox Bay; GRF, glacial rock flour; IK, Iterlak; NA, Narsarsuaq; NU, Nunakullak; QE, Qeqertaasaq; QI, Quinngua; SQ, Sioraq

In this study, a total of 16 GRF deposits were either identified from aerial images or reported from locals and sampled during two sampling campaigns in 2018 and 2019 (see map in Figure 1).

We used two datasets from literature as comparative material: the Danish Soil Library (DSL), consisting of 41 agricultural top- and subsoils from Denmark (Hansen, 1976; Resurreccion et al., 2011), and 18 soil samples that have differing clay mineralogy from across the United States and Denmark (Arthur et al., 2020).

2.2 | Laboratory methods

Prior to the laboratory analyses, the air-dry material was carefully crushed in a mortar and presieved to <2 mm. Generally, we found little to no particles >2 mm in the untreated material.

2.2.1 | Texture and organic matter

The texture was determined using a combination of wet sieving and pipette (SP), according to Gee and Or (2002). For total carbon determination, the samples were ball-milled before oxidization of the carbon at 950 ˚C using an elemental analyzer combined with a thermal conductivity detector (Thermo Fisher Scientific) (Nelson & Sommers, 1996). No carbonates were detected; the total carbon could be set equal to the total organic carbon. The OM was obtained by multiplying the total organic carbon with a conversion factor set to 2 as suggested by Pribyl (2010).

The particle size distribution (PSD) was additionally determined by laser diffraction (LD), using a Hydro 2000MU wet dispersion unit coupled to a Mastersizer 2000 (Malvern Instruments Ltd). The samples were dispersed using 0.1 M tetrasodium pyrophosphate ($Na_4P_2O_7$). Further dispersion was achieved by sonication for a period of 60 s. The recorded diffraction pattern was evaluated by the built-in software, using the Mie-scattering theory for which the real and imaginary parts of the refractive index were set to 1.53 and 0.1, respectively, as suggested by Ryżak and Bieganowski (2011). The software stored the result as frequency distribution from which the cumulative PSD was calculated.

2.2.2 | Scanning electron microscopy for particle shape analysis

The shape of the fine fraction of the studied material was visualized by scanning electron microscopy. The pictures were

taken on the air-dried and presieved (<2 mm) material using a Zeiss EVO 60 (Carl Zeiss AG). No additional sample treatments prior to the measurement were performed.

2.2.3 | X-ray diffraction for mineral phase identification

The mineralogical composition of the sediments was determined by X-ray (Cu Kα, 40 mA, 45 kV) powder diffraction analysis (XRD) on the bulk samples using a Malvern Panalytical Empyrean diffractometer mounted with a PIXcel1D detector (Malvern Instruments Ltd). Prior to the measurement, the material was carefully ground in a mortar. No standard for quantitative analysis was added. The step size was set to 0.02 Å with an exposure time of 60 s per step. The semiquantitative mineral phase distribution was determined by Rietveld full-pattern refinement for 2θ degrees ranging from 5 to 65° using the software *Profex* (Doebelin & Kleeberg, 2015).

2.2.4 | Specific surface area and water vapor sorption isotherms

The SSA was determined by the standard ethylene glycol monomethyl ether (EGME) method according to Petersen et al. (1996) and referred to as SSA_{EGME} ($m^2\ g^{-1}$) throughout the text.

The water vapor sorption isotherms (WSIs) were determined using a vapor sorption analyzer (METER Group Inc.). Arthur et al. (2014) include detailed information about the device and procedure. The SSAs were estimated from the WSIs following the procedures as described in the section below and referred to as SSA_w.

2.2.5 | Supporting physical–chemical parameters

The total CEC (cmol kg^{-1}) was measured using the ammonium acetate extraction method according to Sumner and Miller (1996). The acidity of the sediments was assessed by the hydrogen ion activity (pH) measured by a glass electrode on a 1:4 soil/water (pH_w) and soil–0.01 M $CaCl_2$ (pH_{CaCl2}) suspension according to Thomas (1996). The electrical conductivity (EC, μS cm^{-1}) as a measure of salinity was determined with a conductivity cell on a 1:9 soil/water suspension according to Rhoades (1996). The specific surface charge (SSC, cmol m^{-2}) was calculated as the ratio of CEC to SSA_{EGME}.

2.3 | Water vapor sorption isotherm model

The Guggenheim–Anderson–de Boer model (van den Berg & Bruin, 1981), as given in Equation 1, was fitted to the desorption WSIs for water activities (a_w) ranging from 0.2 to 0.8, corresponding to relative humidities (RHs) between 20 and 80% as suggested by Akin and Likos (2014) and Arthur et al. (2018).

$$\theta_m = \frac{\theta_0 \times C \times K \times a_w}{\left[\left(1 - K \times a_w\right)\left(1 - K \times a_w + K \times C \times a_w\right)\right]} \quad (1)$$

where θ_m is the gravimetric water content, θ_0 is the free-fitting parameter representing the gravimetric water content at monolayer coverage, and C and K are related to the thermodynamics of the liquid–solid interactions.

The SSA could eventually be determined from the relation between θ_0 (kg kg^{-1}), the surface covered by one water molecule ($A = 10.8 \times 10^{-20}$), Avogadro's constant ($N_a = 6.02 \times 10^{23}\ mol^{-1}$), and the molar weight of water ($M_w = 0.018$ kg mol^{-1}) according to Newman (1983) and Quirk and Murray (1999) as given in Equation 2:

$$SSA_w = \frac{\theta_0 \times N_a \times A}{M_w} \quad (2)$$

2.4 | Numerical and statistical analysis

The linear relation between two variables was determined by least-squares regression as implemented in MATLAB (The MathWorks, 2018). The goodness of fit was assessed by the coefficient of determination, R^2, and the RMSE, as given in Equation 3:

$$RMSE = \sqrt{\sum_{i=1}^{n} \frac{(\hat{y}_i - y_i)^2}{n}} \quad (3)$$

where n is the number of observations, and y_i and $\hat{y}_i$ are the ith observation and ith predicted value, respectively. The linear correlation between two variables was given as the Pearson linear correlation coefficient r.

The nonlinear least-squares regression to fit the Guggenheim–Anderson–de Boer model to the WSIs was performed using the trust–region–reflective algorithm as implemented in MATLAB and Optimization Toolbox (The MathWorks, 2018).

The significance of differences in means was assessed by ANOVA, and the post-hoc pairwise comparisons by Tukey's HSD test (Tukey, 1977).

TABLE 1 Physical and chemical properties. Texture classes according to Soil Survey Division Staff (1999)

Sample	Class	Clay[a]	fSilt[b]	cSilt[c]	Organic matter	SSA_{EGME}	CEC	EC	pH_w	pH_{CaCl_2}	Volume
		kg kg^{-1}				m^2 g^{-1}	cmol kg^{-1}	µS cm^{-1}	H^+		× 10^3 m^3
AT	L	0.21	0.23	0.12	nd	31.90	8.52	12.01	7.19	6.05	1400
EI	SiL	0.16	0.37	0.16	0.002	22.68	6.04	7.23	6.39	4.91	nd
FB	L	0.24	0.27	0.16	nd	34.36	6.66	18.96	7.17	6.12	nd
IK-1	SiCL	0.40	0.40	0.09	nd	51.90	11.35	21.10	7.35	6.31	175
IK-2	SiL	0.19	0.45	0.15	0.005	33.38	7.55	12.73	6.36	4.85	250
IK-3	L	0.22	0.32	0.17	0.002	32.69	7.16	17.67	7.48	6.16	290
IK-4	SiCL	0.34	0.40	0.10	nd	48.67	9.21	15.34	7.27	6.02	360
NA-1	SiL	0.19	0.35	0.16	0.006	24.46	6.90	8.63	5.56	4.52	nd
NA-2	L	0.13	0.20	0.18	nd	17.21	4.25	10.77	6.40	5.10	nd
NU	SL	0.16	0.16	0.11	nd	43.34	9.92	9.93	7.38	6.15	140
QE	L	0.11	0.22	0.16	0.012	13.32	5.43	6.61	5.61	4.63	nd
QI-1	L	0.24	0.30	0.19	nd	43.26	7.97	13.19	7.16	6.05	nd
QI-2	L	0.26	0.22	0.16	0.001	27.93	14.25	58.10	6.70	6.26	200
QI-3	C	0.57	0.20	0.09	nd	88.60	21.91	10.02	7.53	5.95	nd
QI-4	CL	0.30	0.20	0.15	0.002	21.95	7.11	89.10	6.73	6.26	60
SQ	SiCL	0.40	0.42	0.01	0.012	24.09	9.25	2204.00	6.71	6.48	nd

Note. AT, Ataarnasit; C, clay; CEC, cation exchange capacity; CL, clay loam; EC, electrical conductivity; EI, Eqaluit Ilulat; FB, Fox Bay; IK, Iterlak; NA, Narsarsuaq; nd, below detection limit or not determined; NU, Nunakullak; QE, Qeqertaasaq; QI, Quinngua; SiCL, silty clay loam; SiL, silty loam; L, loam; SL, sandy loam; SQ, Sioraq; SSA_{EGME}, specific surface area determined by the standard EGME-method (ethylene glycol monomethyl ether). Volumes estimated from drone pictures.

[a]Clay, <2 µm.

[b]fSilt, 2–20 µm.

[c]cSilt, 20–50 µm.

3 | RESULTS AND DISCUSSION

3.1 | Identification and sampling of the GRF deposits

Figure 2 shows the map of the investigated area and the identified deposits. Some of the deposits were only accessible by water because of the lack of terrestrial infrastructure in Greenland caused by the rugged terrain. The area was dominated by the three major fjord systems: Bredefjord, Eriksfjord, and Einarsfjord (from north to south). A typical GRF deposition is shown in the photograph insert in Figure 2 (site AT); the overlying coarser sediments bearing the vegetation cover protecting the GRF from very fast erosion can be clearly identified. Generally, the probability of finding GRF decreased with increasing distance to the current ice margin, which could be explained with longer exposure to erosion of the outer-fjord deposits.

In the field, the texture of the deposits was assessed by feel partly following Thien (1979). Sediments with high fine particle content were sampled and brought to the laboratory for further analysis; sediments with high sand content were discarded (red crosses on the map in Figure 2). The GRF deposits were generally overlain by sand and gravel, which was removed prior to sampling; ~2 kg of field moist material was collected from a depth of ~30 cm from each deposit and stored in plastic bags.

In total, 16 from 32 investigated deposits with acceptable levels of fine particle content were retained and further analyzed in the laboratory (green squares in Figure 2). The different deposits were named according to local place names: SQ, Sioraq; QE, Qeqertaasaq; EI, Eqaluit Ilulat; NU, Nunakullak, QI-1 to QI-4, Quinngua; NA-1 and NA-2, Narsarsuaq; AT, Ataarnasit; FB, Fox Bay; and IK-1 to IK-4, Iterlak. The volumes of selected deposits were approximated from georeferenced aerial (drone) photographs and ranged from 60,000 m^3 (QE) to 1,400,000 m^3 (AT) with a median value of 225,000 m^3 (see Table 1).

In 2014, the total cultivated area in Greenland was ~1,100 ha (Lehmann et al., 2016) and the total estimated volume of selected deposits amounted to 2,875 × 10^3 m^3, which would be enough to cover the entire cultivated area with a theoretical surface application height of 25 cm.

3.2 | Grain geometry and mineralogy

The shape of the natural, untreated material was found to be mostly angular as shown in the example micrograph for

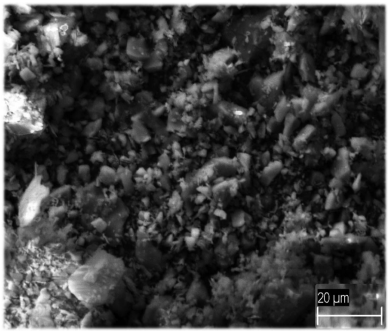

FIGURE 3 Scanning electron microscopy micrographs of sample Iterlak (IK-4)

sample IK-4 in Figure 3. This was expected because the crystal structure of the material was not altered during the physical weathering. The disintegration into smaller fragments happened along the cleavage planes, partly reflecting the shape of the unit cell crystal structure of the basic material. The X-ray diffraction analysis revealed that feldspars dominated the mineral composition of the sediments. The feldspars crystallize in mono- and triclinic crystal structures, exhibiting relatively sharp edges and plane surfaces (Smith & Brown, 1988). The resulting particles followed the shape of the unit cell crystal structure resulting in generally angular shapes.

Figure 4 a shows a typical diffractogram of a GRF exemplified by sample QI-3, the full-pattern Rietveld fit, and the resulting error in the bottom subplot. Supplemental Figure S1 shows the diffractograms of the 16 GRFs individually, and Supplemental Table S1 shows the relative abundance of the primary minerals following the Rietveld refinement.

The mineral assemblage of the sediments was dominated by feldspars (anorthite, oligoclase, and microcline, 72.5 ± 3.7%) and quartz (14.4 ± 4.1%); additionally, diffraction peaks of amphiboles (hornblende and arfvedsonite, 6.3 ± 1.4%) and micas (biotite and muscovite, 6.9 ± 2.0%) were identified and common to all of the 16 GRF samples. The origin of the broad hump at low diffraction angles (range 5–20° 2θ) was not clearly identified; it was either an instrument artifact or the result of the presence of nonidentified amorphous phases.

The similarity between the mineral assemblages of the 16 GRF deposits indicated common parent material (see Supplemental Table S1). The results were in accordance with the primary mineral compositions reported by Belmonte (2015) who also reported the presence of clay minerals associated to the chlorite–vermiculite group as well as illite and kaolinite for a GRF deposit sampled near Narsaq (see map in Figure 2). Generally, Belmonte (2015) and Pederstad and Jørgensen (1985) found high abundance of feldspars and quartz in the clay fraction (<2 µm), which indicated intense mechanical weathering.

3.3 | Texture and surface properties

The gravimetric clay content varied greatly among the 16 GRFs. The samples were identified as loamy sediments with generally high silt-to-clay content according to Soil Survey Division Staff (1999). The OM content were low to null (below detection limit).

The EC clearly reflected that the sediments were non-saline, except for sample SQ, which could be classified as very slightly saline according to Soil Survey Division Staff (1993). The pH values in water and $CaCl_2$ suggested slightly to moderately acidic conditions. The measured SSA_{EGME} of the GRFs were markedly lower than those reported for agriculturally used soils from Denmark (DSL) (Hansen, 1976; Resurreccion et al., 2011), exhibiting similar gravimetric clay and OM content. As a reference, soils from the DSL exhibiting OM <1.2% (13 soils) were plotted together with the GRFs in Figure 5a and b.

The total CEC of the GRFs was generally lower than those of agriculturally used soils exhibiting similar texture and OM content (Figure 5b). The SSA_{EGME} and the CEC correlated well with the gravimetric clay content (r = .77 and r = .80 for the SSA_{EGME} and CEC, respectively). Simple linear regressions yielded satisfactory results; the regression equations are given in the plot areas of Figure 5. Similar linear correlations between SSA_{EGME} and gravimetric clay content were reported by other studies, although the linear dependence of SSA_{EGME} on the gravimetric clay content was generally stronger (e.g., Petersen et al., 1996). Omitting sample QI-3, the correlation coefficients and significance levels (p values) between gravimetric clay content and SSA_{EGME} and CEC dropped to r = .49, p = .049 and r = .57, p = .028, respectively. The CEC was positively correlated to the SSA_{EGME} (r = .83), similar to the findings of Curtin and Smillie (1976) and Petersen et al. (1996).

3.4 | Extended physical characterization using laser diffraction

Figure 6a exemplifies the PSD measured by laser diffraction (LD, solid lines) and conventionally by a combination of the sieve and pipette (SP) methods (filled squares). The multimodality of the PSD of the GRFs was well depicted by the frequency distribution (FD) determined by LD (FD_{LD}).

The first and second modes occurred within the narrow size ranges around a mean value of 4.02 ± 1.17 and 27.82 ± 12.78 µm (sample SQ excluded), respectively. The particle size distributions of the different GRFs were thus very

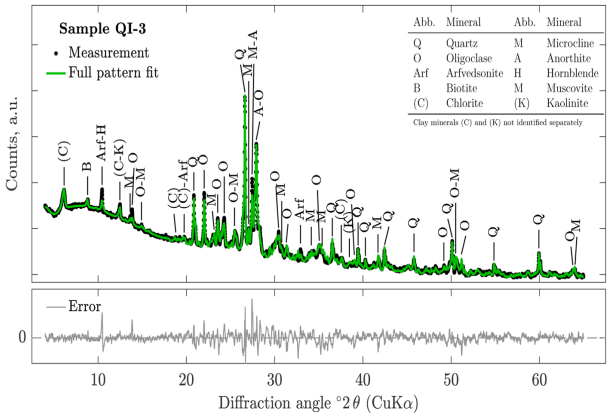

FIGURE 4 Example X-ray diffraction diffractogram for sample Quinngua (QI)-3. Counts per second (black dots) and Rietveld fit (green) and the corresponding error (grey) in the bottom subplot. The phyllosilicates chlorite (C) and kaolinite (K) were not identified separately on the <2-µm fraction, but their potential diffraction peaks were indicated

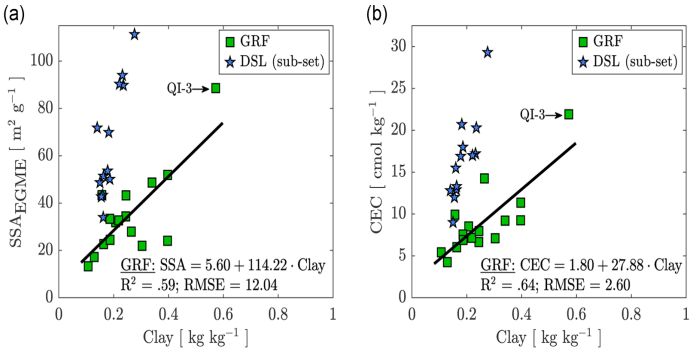

FIGURE 5 (a) Specific surface area (SSA_{EGME}) ($m^2\ g^{-1}$) and (b) cation exchange capacity (CEC) ($cmol\ kg^{-1}$) of the glacial rock flours (GRFs) as a function of the gravimetric clay. A subset of the Danish soil library dataset (DSL) (13 out of 41 soils) with similar clay and organic matter content was added for reference

similar in terms of their principal mode locations (first and second modes). The individual PSDs of all the GRFs are shown in Supplemental Figure S2. Figure 6b shows the PSD_{LD} of all the 16 GRFs measured by LD. The smallest particle diameter averaged over all the samples was detected at d_{min} = 0.60 ± 0.08 µm, sample QI-3 excluded (d_{min} = 0.07 µm).

In this study, the relationship between the conventionally determined gravimetric clay fraction (Clay) and the volumetric fraction <2 µm, $F(d < 2\ \mu m)$, determined by LD could be described by Clay = 0.02 + 2.57 × $F(d < 2\ \mu m)$, with R^2 = 0.68 and RMSE = 0.07 (data not shown), and was in the same order of magnitude as the findings of Konert and Vandenberghe (1997), for example, although the relationship found in this study exhibited lower goodness of fit.

The gravimetric clay content was best represented by the volumetric fraction of particles exhibiting a diameter <3.38 µm as shown in Figure 7a; it was reasonably close to the first mode of the FD_{LD} as derived earlier (d = 4.02 µm). As shown in Figure 7, the volumetric fraction of particles with diameter <2.38 µm was an excellent predictor of the SSA_{EGME} and the CEC, exhibiting coefficients of determination (R^2) of .89 and .81, respectively.

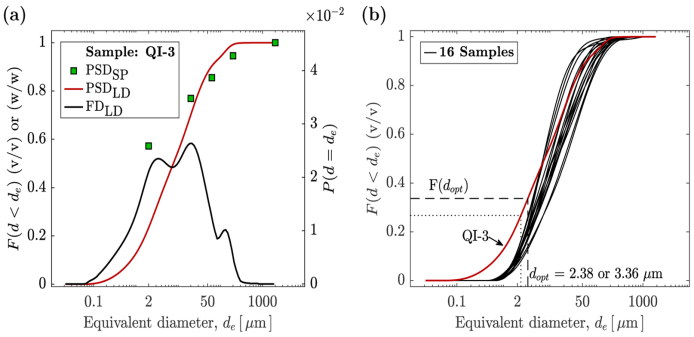

FIGURE 6 (a) Combined plot of the particle size distribution (PSD) measured by laser diffraction (LD, solid lines) and sieve and pipette (SP, filled squares); the cumulative particle size distributions (PSD_{SP} and PSD_{LD}) and the frequency distribution (FD_{LD}), exemplified by sample Quinngua (QI)-3. (b) PSD_{LD} of the 16 glacial rock flours and indicated volumetric fraction, $F(d_{opt})$, at d_{opt} = 2.38 µm and d_{opt} = 3.36 µm shown explicitly for the sample QI-3 by the dashed lines

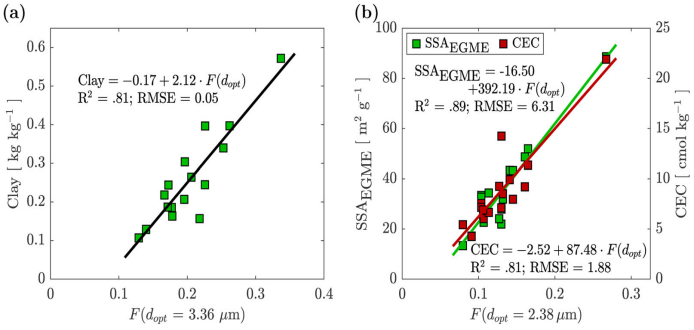

FIGURE 7 (a) Best agreement between particle size distribution measured by laser diffraction (PSD_{LD}) fraction and gravimetric clay determined conventionally (found at d_{opt} = 3.36 µm, based on minimum RMSE) and the best-fit line. (b) Best agreement between PSD_{LD} fraction and specific surface area determined by the standard EGME-method (ethylene glycol monomethyl ether) (SSA_{EGME}) or cation exchange capacities (CEC) (found at d_{opt} = 2.38 µm)

3.5 | Extended physical characterization using water vapor sorption

The WSIs determined on the GRFs exhibited minimum and maximum equilibrium RH between 7.2 ± 5.7 and 92.6 ± 0.3%, corresponding to a soil-water potential (ψ) range of −360 to −10 MPa. Besides samples SQ and QI-3, the WSIs of the GRFs shared similar geometry with a relatively low degree of hysteresis as shown in Figure 8a. The individual sorption isotherms are shown in Supplemental Figure S3. The distinct shape of both ad- and desorption isotherms of sample SQ could be explained by the salinity, that is, the relatively high EC compared with the other samples (Chen et al., 2020). The generally higher θ_m throughout the whole RH range of sample QI-3 could be attributed to the significantly higher clay content. No apparent correlation between the mineralogy and the shape or θ_m level of the WSIs could be found.

Figure 8b, c, and d show the WSIs of selected GRFs compared with agriculturally used soils in which the gravimetric clay fraction was dominated by either montmorillonite (MO), illite (IL), or kaolinite (KA). The comparative soil samples were taken from Arthur et al. (2020) and selected such that the soil samples exhibited clay content as close as possible to the minimum (b), median (c), and maximum (d) clay content of the GRFs. The WSIs of the GRFs closely followed the ones of the KA-soils for RH <80%. For the given RH ranges, the water content of the 2:1 clays (IL and MO) were considerably higher.

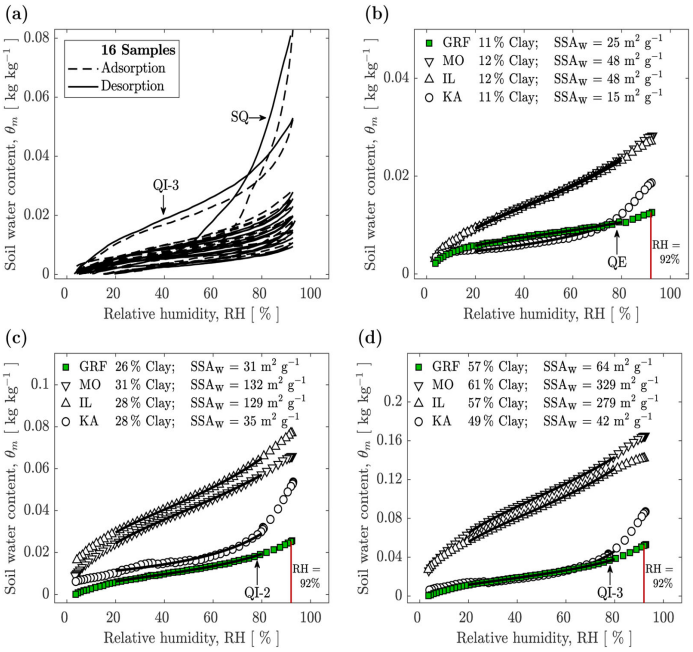

FIGURE 8 (a) Water vapor sorption isotherms of the 16 glacial rock flours (GRFs). Desorption isotherms for (b) low, (c) median, and (d) high clay-level GRFs (green filled squares) and soils bearing similar levels of montmorillonitic (MO), illitic (IL), and kaolinitic (KA) dominated clay content. Fitted Guggenheim–Anderson–de Boer (GAB) model (solid black lines). The red vertical line indicates the water content at relative humidity (RH) = 0.92 ($\psi \approx -11$ MPa). Some isotherms were partly hidden by others. Note the differences in *y* axis limits

The estimated SSA_w of the GRFs were in line with the SSA_w of the KA-soils. The IL- and MO-soils exhibited, as expected, significantly larger surface areas for given clay content. For reference, the slopes of the trend lines were given in the plot area of Figure 9a. As reported by other studies (Akin & Likos, 2014; Arthur et al., 2018), the SSA_w and the SSA_{EGME} were significantly correlated; a linear regression, excluding the sample SQ, exhibited acceptable goodness of fit (Table 2). However, considering only the KA-soils from Arthur et al. (2020), the regression coefficients of the best fit line were very close to those obtained for the GRFs (Table 2).

3.6 | Towards soil amendment

A linear relationship between the water content at the permanent wilting point (PWP) at $\psi = -1.5$ MPa (RH = 98.9%) and the water content at RH = 92.1% (highest equilibrium RH of the WSIs common to all the GRFs) was established from measurements of the soil-water retention at low water content of the DSL-dataset (Resurreccion et al. (2011). The regression resulted in an excellent fit, with a coefficient of determination (R^2) of 0.96. The regression was not dependent on the OM content as shown in Figure 10a. Thus, the relationship could directly be used to estimate the PWP of the GRFs and the Arthur et al. (2020) comparison soils. The PWPs of the DSL dataset were taken from the water-retention measurements directly.

Figure 10b clearly depicted the linear dependence of the PWP on the gravimetric clay content and the distinctively different relationship obtained for the GRFs, depicted by the substantially different slopes of the trend lines. The direct identification of the reason for the considerably different behavior was hidden by the effect of the OM on the PWP of the comparison soils.

To investigate the effect of GRF on the plant available water (PAW) content, we amended a sandy soil from South Greenland (clay, 1.33%; OM, 2.33%) with four levels of GRF from deposit QI-3 (0, 5, 10, and 15% w/w). For each binary mix, we repacked five replicates into soil-core cylinders (diam., 60.5 mm; height, 34.8 mm; volume, 100 cm^3) to a dry bulk density of 1.4 Mg m^{-3}. The samples were saturated in a retention box and equilibrated to $\psi = -100$ hPa corresponding to

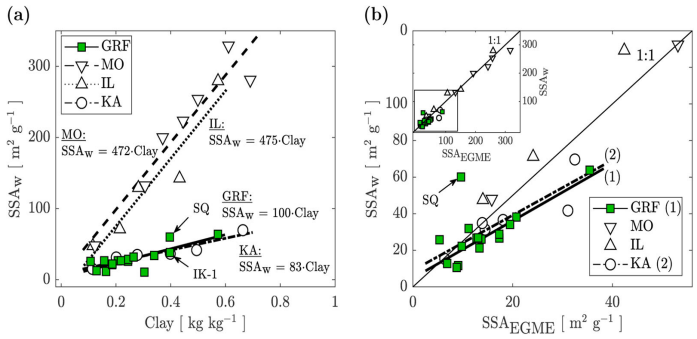

FIGURE 9 Properties determined on the water-vapor sorption isotherms. (a) Specific surface area estimated from water vapor sorption isotherms (SSA_w) as a function of gravimetric clay content and trend lines for the four different materials (only slope of the trend line given as reference); (b) SSA_w vs. the specific surface area determined by the standard EGME method (SSA_{EGME}) and the best fit line of the glacial rock flours (GRFs) (excluding sample SQ) and the kaolinite (KA) soils (see Table 2)

TABLE 2 Regression equations and goodness of fit for Figure 9b. Result of regression for combined illitic (IL) and montmorillonitic (MO) soils given for completeness

Reference	Material	Regression equation	R^2	RMSE
				$m^2\ g^{-1}$
(1) Figure 9b	GRF (− site SQ)	$SSA_w = 4.79 + 0.63 \times SSA_{EGME}$	.80	5.94
(2) Figure 9b	KA	$SSA_w = 8.79 + 0.60 \times SSA_{EGME}$	.76	9.65
(−) Figure 9b	IL + MO	$SSA_w = 20.50 + 0.88 \times SSA_{EGME}$	.98	14.33

Note. GRF, glacial rock flour; KA, kaolinitic clay dominated soils; SQ, Sioraq; SSA_w, specific surface area estimated from water vapor sorption isotherms; SSA_{EGME}, specific surface area determined by the standard ethylene glycol monomethyl ether method.

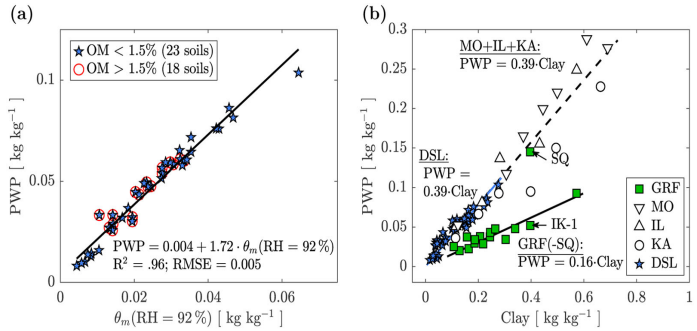

FIGURE 10 (a) Estimation of water content at the wilting point (PWP) based on the Danish soil library dataset (DSL, 41 soils), and (b) linear relation between PWP and gravimetric clay of the glacial rock flours (GRFs) and comparison soils. IL, illitic; KA, kaolinitic; MO, montmorillonitic; OM, organic matter; RH, relative humidity

the field capacity of sandy soils (Aljibury & Evans, 1965). We estimated the PWP of the binary mixtures from the clay content, according to Hansen (1976) (PWP = 0.336 × clay + 0.973, based on 209 Danish soils). The PAW was then calculated as the difference between water content at field capacity and the PWP. Figure 11 shows the resulting mean PAW for each GRF concentration. The one-way ANOVA revealed that there was a significant effect at the $p < .05$ level of

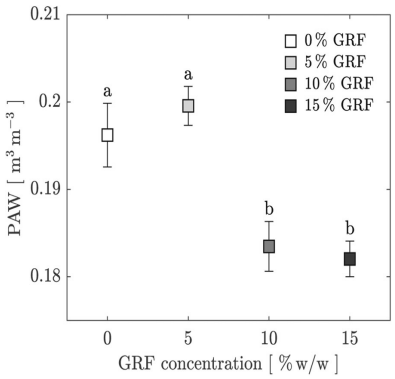

FIGURE 11 Plant available water (PAW) of a repacked, glacial rock flour (GRF) amended, sandy soil from Greenland. Symbols (mean PAW values) bearing the same letters are not statistically significant form each other. The whiskers represent the standard deviation

the GRF concentration on the PAW [$F(3,16) = 51.3$, $p < .001$]. The post-hoc pairwise comparisons (Tukey's HSD test) are displayed by letter notation in Figure 11. Although not statistically significant, the addition of 5% GRF showed a tendency for PAW increase. The reduction in PAW for the two highest GRF concentrations vs. the 0 and 5% levels mainly were due to lower water content at field capacity resulting from a reduction of meso-sized pores because of a shift in the PSD.

Figure 12a gives the overview of the CEC measurements obtained for the different materials as a function of the gravimetric clay content. The CEC of pure MO (100 cmol kg^{-1}) and pure KA (5 cmol kg^{-1}) (Carroll, 1959) were added as a visual guide. According to Schnitzer (1965), the OM contributes significantly (30–60%) to the CEC; although exhibiting higher OM content, the CEC of the KA-soils (mean OM, 0.5%) were generally lower than the CEC of the GRFs (mean OM, 0.3%). The presence of 2:1 clay minerals and micas in the mineral composition were likely the reason for the slightly higher CEC (Carroll, 1959). Belmonte (2015) found high content of primary minerals in the clay-sized fraction of comparable sediments, which explained the lower CEC than the IL- and MO-soils for given clay content.

The SSC of the GRFs were similar to or slightly higher than the SSC of comparable soils exhibiting low OM content. As a reference, all the soils from the DSL were added to Figure 12b; samples exhibiting OM > 1.5% were highlighted by red circles to expose the paramount influence of the OM on the SSC.

4 | CONCLUSIONS

The study characterized 16 GRF deposits located across South Greenland in the perspective of their suitability as soil conditioner for the local farmland. From the results, we conclude the following:

(1) Based on the estimated volumes of the GRF deposits, the exploitation for local agricultural use should be feasible. The deposits QI-3, AT, and IK-4, close to major agricultural areas, are easily accessible and high in clay content (0.21–0.57 kg kg^{-1}) and thus well suited for exploitation.
(2) The scanning electron microscopy micrographs showed that the particles were mostly angular in shape.
(3) The X-ray diffractograms revealed that the GRF shared similar mineralogies and contained large fractions of primary minerals (quartz and feldspars).
(4) The LD granulometry revealed the multimodality of the PSDs; the surface properties (SSA_{EGME} and CEC) of the GRFs could be accurately predicted by LD-determined volumetric fractions of particles exhibiting a diameter <2.38 µm.
(5) The GRF exhibited low water vapor sorption, comparable with soils dominated by kaolinitic clay and much lower compared with 2:1 clay-dominated soils. For given clay content, the SSA_{EGME} and the SSA_{w} were in line with KA-dominated soils.
(6) The water content at the PWP of Greenlandic soils is unlikely to be increased by the addition of GRF because of the low sorption activity.
(7) Five percent GRF addition to a sandy, cultivated soil from South Greenland showed a tendency to increase PAW content, whereas very high amendments of 10–15% decreased PAW.
(8) Despite the lack of OM, the GRF exhibited relatively high CEC and SSC compared with soils dominated by KA-clay.

This study showed promising results in view of the use of GRF as a soil conditioner and amendment for sandy agricultural soils in South Greenland. It is likely that GRF amendment reduces water repellency in a relatively short period of time and increases the soil's nutrient holding capacity.

Future research should investigate the long-term effect of GRF amendment on soil aggregation potential and water-holding capacity of sandy and structurally low developed subarctic agricultural soils. In perspective, to give local farmers advice on application rates and suitable soils for GRF amendment, field-plot experiments covering the major soil types in Greenland are necessary.

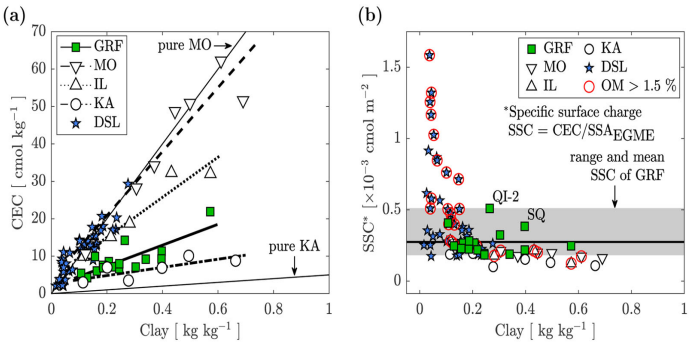

FIGURE 12 (a) Cation exchange capacity (CEC) of the three used datasets vs. gravimetric clay. The two solid black lines indicate the CEC levels of pure kaolinite (KA) (5 cmol kg^{-1}) and montmorillonite (MO) (100 cmol kg^{-1}). (b) Specific exchangeable surface charge (SSC = CEC/specific surface area [SSA]) of the three datasets as a function of gravimetric clay

ACKNOWLEDGMENTS

The research was financed by the Danish Council for Independent Research, Technology, and Production Sciences via the project "Glacial Flour as a New, Climate-Positive Technology for Sustainable Agriculture in Greenland: NewLand." We would like to thank Donghong Yu (Aalborg University, Department of Chemistry and Bioscience) and Thomas Sørensen Quaade (Aalborg University, Department of Materials and Production) for providing access to the XRD and for the help with the SEM, respectively. We also would like to thank the editor and reviewers for their valuable comments to improve the quality of the paper.

AUTHOR CONTRIBUTIONS

Charles Pesch: Conceptualization; Data curation; Formal analysis; Investigation; Methodology; Resources; Validation; Visualization; Writing-original draft; Writing-review & editing. Peter Lystbæk Weber: Conceptualization; Data curation; Formal analysis; Investigation; Methodology; Resources; Validation. Per Moldrup: Conceptualization; Data curation; Formal analysis; Funding acquisition; Investigation; Methodology; Project administration; Resources; Supervision; Validation; Writing-review & editing. Lis de Jonge: Conceptualization; Data curation; Funding acquisition; Methodology; Project administration; Resources; Supervision; Writing-review & editing. Emmanuel Arthur: Conceptualization; Data curation; Formal analysis; Investigation; Methodology; Resources; Validation; Writing-review & editing. Mogens Humlekrog Greve: Conceptualization; Funding acquisition; Investigation; Project administration; Validation; Writing-review & editing.

CONFLICT OF INTEREST

The authors report no conflicts of interest.

ORCID

Charles Pesch https://orcid.org/0000-0003-4120-0239
Peter Lystbæk Weber https://orcid.org/0000-0001-9249-0796
Per Moldrup https://orcid.org/0000-0003-1619-1457
Lis Wollesen de Jonge https://orcid.org/0000-0003-2874-0644
Emmanuel Arthur https://orcid.org/0000-0002-0788-0712
Mogens Humlekrog Greve https://orcid.org/0000-0001-9099-8940

REFERENCES

Akin, I. D., & Likos, W. (2014). Specific surface area of clay using water vapor and EGME sorption methods. *Geotechnical Testing Journal*, *37*, 1016–1027. https://doi.org/10.1520/GTJ20140064

Aljibury, F. K., & Evans, D. D. (1965). Water permeability of saturated soils as related to air permeability at different moisture tensions. *Soil Science Society of America Journal*, *29*, 366–369. https://doi.org/10.2136/sssaj1965.03615995002900040008x

Andrews, J. T. (2011). Unraveling sediment transport along glaciated margins (the Northwestern Nordic Seas) using quantitative X-ray diffraction of bulk (2 mm) sediment. In F. Bhuiyan (Ed.), *Sediment transport* (pp. 225–248). IntechOpen.

Arthur, E., Tuller, M., Moldrup, P., & de Jonge, L. W. (2014). Evaluation of a fully automated analyzer for rapid measurement of water vapor sorption isotherms for applications in soil science. *Soil Science Society of America Journal*, *78*, 754–760. https://doi.org/10.2136/sssaj2013.11.0481n

Arthur, E., Tuller, M., Moldrup, P., & de Jonge, L. W. (2020). Clay content and mineralogy, organic carbon and cation exchange capacity affect water vapour sorption hysteresis of soil. *European Journal of Soil Science*, *71*, 204–214. https://doi.org/10.1111/ejss.12853

Arthur, E., Tuller, M., Moldrup, P., Greve, M. H., Knadel, M., & de Jonge, L. W. (2018). Applicability of the Guggenheim–Anderson–Boer water vapour sorption model for estimation of soil specific surface area. *European Journal of Soil Science*, *69*, 245–255. https://doi.org/10.1111/ejss.12524

Belmonte, L. J. (2015). *Use of Greenlandic resources for the production of bricks* (PhD thesis, Technical University of Denmark, Department of Civil Engineering).

Bennike, O., Björck, S., & Lambeck, K. (2002). Estimates of South Greenland late-glacial ice limits from a new relative sea level curve. *Earth and Planetary Science Letters*, *197*, 171–186. https://doi.org/10.1016/S0012-821X(02)00478-8

Bennike, O., Jensen, J. B., Næsby Sukstorf, F., & Rosing, M. T. (2019). Mapping glacial rock flour deposits in Tasersuaq, southern West Greenland. *GEUS Bulletin*, *43*. https://doi.org/10.34194/GEUSB-201943-02-06

Bentley, S. P., & Smalley, I. J. (1979). Mineralogy of a leda/champlain clay from Gloucester (Ottawa, Ontario). *Engineering Geology*, *14*, 209–217. https://doi.org/10.1016/0013-7952(79)90086-3

Berrangé, J. P. (1966). *The bedrock geology of Vatnahverfi, Julianehåb district, South Greenland*. Kobenhavn.

Besnard, E., Chenu, C., Balesdent, J., Puget, P., & Arrouyas, D. (1996). Fate of particulate organic matter in soil aggregates during cultivation. *European Journal of Soil Science*, *47*, 495–503. https://doi.org/10.1111/j.1365-2389.1996.tb01849.x

Carroll, D. (1959). Ion exchange in clays and other minerals. *GSA Bulletin*, *70*, 749–779. https://doi.org/10.1130/0016-7606(1959)70%5b749:IEICAO%5d2.0.CO;2

Caviezel, C., Hunziker, M., & Kuhn, N. J. (2017). Bequest of the Norseman—The potential for agricultural intensification and expansion in southern Greenland under climate change. *Land*, *6*, 87. https://doi.org/10.3390/land6040087

Chen, M., Zeng, W., Arthur, E., Gaiser, T., Lei, G., Zha, Y., Ao, C., Fang, Y., Wu, J., & Huang, J. (2020). Relating soil salinity, clay content and water vapour sorption isotherms. *European Journal of Soil Science*, *71*, 399–414. https://doi.org/10.1111/ejss.12876

Curtin, D., & Smillie, G. W. (1976). Estimation of components of soil cation exchange capacity from measurements of specific surface and organic matter. *Soil Science Society of America Journal*, *40*, 461–462. https://doi.org/10.2136/sssaj1976.03615995004000030041x

de Jonge, L. W., Jacobsen, O. H., & Moldrup, P. (1999). Soil water repellency: Effects of water content, temperature, and particle size. *Soil Science Society of America Journal*, *63*, 437–442. https://doi.org/10.2136/sssaj1999.03615995006300030003x

Dexter, A. R., Richard, G., Arrouays, D., Czyż, E. A., Jolivet, C., & Duval, O. (2008). Complexed organic matter controls soil physical properties. *Geoderma*, *144*, 620–627. https://doi.org/10.1016/j.geoderma.2008.01.022

Doebelin, N., & Kleeberg, R. (2015). Profex: A graphical user interface for the Rietveld refinement program BGMN. *Journal of Applied Crystallography*, *48*, 1573–1580. https://doi.org/10.1107/S1600576715014685

Gee, G. W., & Or, D. (2002). 2.4 particle-size analysis. In J. H. Dane & C. G. Topp (Eds.), *Methods of soil analysis: Part 4 physical methods, 5.4* (pp. 255–293). Soil Science Society of America. https://doi.org/10.2136/sssabookser5.4.c12

Gunnarsen, K. C. (2020). *Plant nutritional value of Greenlandic glacial rock flour: An amendment to improve weathered and nutrient poor soils* (PhD thesis, Department of Plant and Environmental Sciences, Faculty of Science, University of Copenhagen).

Gunnarsen, K. C., Jensen, L. S., Gómez-Muñoz, B., Rosing, M. T., & de Neergaard, A. (2019). Glacially abraded rock flour from Greenland: Potential for macronutrient supply to plants. *Journal of Plant Nutrition and Soil Science*, *182*, 846–856. https://doi.org/10.1002/jpln.201800647

Hansen, L. (1976). Jordtyper ved statens forsøgsstationer - Soil types at the Danish state experimental stations. Beretning fra statens forsøgsvirksomhed i plantekultur. (In Danish with English abstract) *Særtryk af Tidsskrift for Planteavl*, *80*, 742–758.

Henriksen, N. (2008). *Geological history of Greenland: Four billion years of earth evolution*. Geological Survey of Denmark and Greenland (GEUS).

Jakobsen, B. H. (1991). Multiple processes in the formation of subarctic podzols in Greenland. *Soil Science*, *152*, 414–426. https://doi.org/10.1097/00010694-199112000-00003

Kalsbeek, E., Larsen, L. M., & Bondam, J. (1990). *Descriptive text to 1:500000 sheet 1, Sydgrønland*. Grønlands Geologiske Undersøgelse.

Karup, D., Moldrup, P., Tuller, M., Arthur, E., & de Jonge, L. W. (2017). Prediction of the soil water retention curve for structured soil from saturation to oven-dryness. *European Journal of Soil Science*, *68*, 57–65. https://doi.org/10.1111/ejss.12401

Kirschbaum, M. U. F. (1995). The temperature dependence of soil organic matter decomposition, and the effect of global warming on soil organic C storage. *Soil Biology and Biochemistry*, *27*, 753–760. https://doi.org/10.1016/0038-0717(94)00242-S

Konert, M., & Vandenberghe, J. (1997). Comparison of laser grain size analysis with pipette and sieve analysis: A solution for the underestimation of the clay fraction. *Sedimentology*, *44*, 523–535. https://doi.org/10.1046/j.1365-3091.1997.d01-38.x

Lehmann, J. O., Sharif, B., Kjeldsen, C., Plauborg, F., Olesen, J. E., Mikkelsen, M. H., Aastrup, P., Wegeberg, S., Kristensen, T., & Greve, M. H. (2016). *Muligheder for klimatilpasning i landbrugserhvervet - status og handlemuligheder*. Technical report. (In Danish) Aarhus Universitet, Institut for Agroøkologi/Naalakkersuisut: The Government of Greenland.

Maslov, B. S. (Ed.). (2009). *Agricultural land improvement: Amelioration and reclamation - Volume II*. EOLSS publications.

MATLAB and Optimization Toolbox (2018). *MATLAB and Optimization Toolbox, version 9.5.0 (R2018b)*. The MathWorks Inc.

Matus, F. J. (2021). Fine silt and clay content is the main factor defining maximal C and N accumulations in soils: A meta-analysis. *Scientific Reports*, *11*, 6438. https://doi.org/10.1038/s41598-021-84821-6

McKissock, I., Gilkes, R. J., & Walker, E. L. (2002). The reduction of water repellency by added clay is influenced by clay and soil properties. *Applied Clay Science*, *20*, 225–241. Clay Research in Australia and New Zealand. https://doi.org/10.1016/S0169-1317(01)00074-6

Nelson, D. W., & Sommers, L. E. (1996). Total carbon, organic carbon, and organic matter. In D. L. Sparks, A. L. Page, P. A. Helmke, & R. H. Loeppert (Eds.), *Methods of soil analysis: Part 3 chemical methods, 5.3* (pp. 961–1010). SSSA. https://doi.org/10.2136/sssabookser5.3.c34

Newman, A. C. D. (1983). The specific surface of soils determined by water sorption. *Journal of Soil Science*, *34*, 23–32. https://doi.org/10.1111/j.1365-2389.1983.tb00809.x

Nguyen, T.-T., & Marschner, P. (2013). Addition of a fine-textured soil to compost to reduce nutrient leaching in a sandy soil. *Soil Research*, *51*, 232–239. https://doi.org/10.1071/SR13105

Oades, J. M. (1984). Soil organic matter and structural stability: Mechanisms and implications for management. *Plant and Soil*, *76*, 319–337. https://doi.org/10.1007/BF02205590

Pederstad, K., & Jørgensen, P. (1985). Weathering in a marine clay during postglacial time. *Clay Minerals*, *20*, 477–491. https://doi.org/10.1180/claymin.1985.020.4.04

Pesch, C., Lamandé, M., de Jonge, L. W., Norgaard, T., Greve, M. H., & Moldrup, P. (2020). Compression and rebound characteristics of agricultural sandy pasture soils from South Greenland. *Geoderma*, *380*, 114608. https://doi.org/10.1016/j.geoderma.2020.114608

Pesch, C., Weber, P. L., de Jonge, L. W., Greve, M. H., Norgaard, T., & Moldrup, P. (2021). Soil–air phase characteristics: Response to texture, density, and land use in Greenland and Denmark. *Soil Science Society of America Journal*, *85*, 1534–1554. https://doi.org/10.1002/saj2.20284

Petersen, L. W., Møldrup, P., Jacobsen, O. H., & Rolston, D. E. (1996). Relations between specific surface area and soil physical and chemical properties. *Soil Science*, *161*, 9–12. https://doi.org/10.1097/00010694-199601000-00003

Pribyl, D. W. (2010). A critical review of the conventional SOC to SOM conversion factor. *Geoderma*, *156*, 75–83. https://doi.org/10.1016/j.geoderma.2010.02.003

Quirk, J. P., & Murray, R. S. (1999). Appraisal of the ethylene glycol monoethyl ether method for measuring hydratable surface area of clays and soils. *Soil Science Society of America Journal*, *63*, 839–849. https://doi.org/10.2136/sssaj1999.634839x

Ramesh, R., & D'Anglejan, B. (1995). Mineralogy, chemistry and particle size interrelationships in some post-glacial marine deposits of the St. Lawrence Lowlands. *Journal of Coastal Research*, *11*, 1167–1179.

Rawls, W. J., & Brakensiek, D. L. (1982). Estimating soil water retention from soil properties. *Journal of the Irrigation and Drainage Division*, *108*, 166–171. https://doi.org/10.1061/JRCEA4.0001383

Resurreccion, A. C., Moldrup, P., Tuller, M., Ferré, T. P. A., Kawamoto, K., Komatsu, T., & de Jonge, L. W. (2011). Relationship between specific surface area and the dry end of the water retention curve for soils with varying clay and organic carbon contents. *Water Resources Research*, *47*. https://doi.org/10.1029/2010WR010229

Rhoades, J. D. (1996). Salinity: Electrical conductivity and total dissolved solids. In D. L. Sparks, A. L. Page, P. A. Helmke, R. H. Loeppert, P. N. Soltanpour, M. A. Tabatabai, C. T. Johnston, & M. E. Sumner (Eds.), *Methods of soil analysis: Part 3 chemical methods, 5.3* (pp. 417–435). SSSA. https://doi.org/10.2136/sssabookser5.3.c14

Roaldset, E. (1972). Mineralogy and geochemistry of Quaternary clays in the Numedal area, southern Norway. *Norsk Geologisk Tidsskrift*, *52*, 335–369.

Ryżk, M., & Bieganowski, A. (2011). Methodological aspects of determining soil particle-size distribution using the laser diffraction method. *Journal of Plant Nutrition and Soil Science*, *174*, 624–633. https://doi.org/10.1002/jpln.201000255

Schjønning, P., de Jonge, L. W., Moldrup, P., Christensen, B. T., & Olesen, J. E. (2010). Searching the critical soil organic carbon threshold for satisfactory tilth conditions – test of the Dexter clay:carbon hypothesis. In *Proceedings of the 1st International conference and exploratory workshop on soil architecture and physico-chemical functions "Cesar"* (pp. 341–346). Aarhus University, Faculty of Agricultural Sciences.

Schnitzer, M. (1965). Contribution of organic matter to the cation exchange capacity of soils. *Nature*, *207*, 667–668. https://doi.org/10.1038/207667a0

Simonson, R. W. (1959). Outline of a generalized theory of soil genesis. *Soil Science Society of America Journal*, *23*, 152–156. https://doi.org/10.2136/sssaj1959.03615995002300020021x

Smith, J. V., & Brown, W. L. (1988). *Feldspar minerals vol. 1, crystal structure, physical, chemical and microtextural properties*. Springer.

Soil Survey Division Staff. (1993). *Soil survey handbook*. Agricultural Handbook 18. NRCS, USDA.

Soil Survey Division Staff (1999). *A basic system of soil classification for making and interpreting soil surveys*. Agricultural Handbook 436. NRCS, USDA.

Sukstorf, F. N., Bennike, O., & Elberling, B. (2020). Glacial rock flour as soil amendment in subarctic farming in South Greenland. *Land*, *9*, 198. https://doi.org/10.3390/land9060198

Sumner, M. E., & Miller, W. P. (1996). Cation exchange capacity and exchange coefficients. In D. L. Sparks, A. L. Page, P. A. Helmke, R. H. Loeppert, P. N. Soltanpour, M. A. Tabatabai, C. T. Johnston, & M. E. Sumner (Eds.), *Methods of soil analysis: Part 3 chemical methods, 5.3* (pp. 1201–1229). SSSA. https://doi.org/10.2136/sssabookser5.3.c40

Tahir, S., & Marschner, P. (2016). Clay amendment to sandy soil – effect of clay concentration and ped size on nutrient dynamics after residue addition of low C/N ratio residue. *Journal of Soil Science and Plant Nutrition*, *16*, 864–875. https://doi.org/10.4067/S0718-95162016005000061

Thien, S. J. (1979). A flow diagram for teaching texture-by-feel analysis. *Journal of Agronomic Education*, *8*, 54–55. https://doi.org/10.2134/jae.1979.0054

Thomas, G. W. (1996). Soil pH and soil acidity. In D. L. Sparks, A. L. Page, P. A. Helmke, R. H. Loeppert, P. N. Soltanpour, M. A. Tabatabai, C. T. Johnston, & M. E. Sumner (Eds.), *Methods of soil analysis: Part 3 chemical methods, 5.3* (pp. 475–490). SSSA. https://doi.org/10.2136/sssabookser5.3.c16

Tukey, J. W. (1977). *Exploratory data analysis*. Addison-Wesley.

van den Berg, C., & Bruin, S. (1981). Water activity and its estimation in food systems: Theoretical aspects. In L. B. Rockland & G. F. Stewart (Eds.), *Water activity: Influences on food quality* (pp. 1–61). Academic Press.

van Straaten, P. (2007). *Agroecology: The use of rocks for crops*. Enviroquest.

Wagner, S., Cattle, S. R., & Scholten, T. (2007). Soil-aggregate formation as influenced by clay content and organic-matter amendment. *Journal of Plant Nutrition and Soil Science*, *170*, 173–180. https://doi.org/10.1002/jpln.200521732

Weber, P. L., de Jonge, L. W., Greve, M. H., Norgaard, T., & Moldrup, P. (2020). Gas diffusion characteristics of agricultural soils from South Greenland. *Soil Science Society of America Journal*, *84*, 1606–1619. https://doi.org/10.1002/saj2.20114

Weber, P. L., Hermansen, C., Norgaard, T., Pesch, C., Moldrup, P., Greve, M. H., Müller, K., Arthur, E., & de Jonge, L. W. (2021). Moisture-dependent water repellency of Greenlandic cultivated soils. *Geoderma*, *402*, 115189. https://doi.org/10.1016/j.geoderma.2021.115189

Westergaard-Nielsen, A., Bjørnsson, A. B., Jepsen, M. R., Stendel, M., Hansen, B. U., & Elberling, B. (2015). Greenlandic sheep farming controlled by vegetation response today and at the end of the 21st Century. *Science of The Total Environment*, *512–513*, 672–681. https://doi.org/10.1016/j.scitotenv.2015.01.039

White, L. F., Bailey, I., Foster, G. L., Allen, G., Kelley, S. P., Andrews, J. T., Hogan, K., Dowdeswell, J. A., & Storey, C. D. (2016). Tracking the provenance of Greenland-sourced, Holocene aged, individual sand-sized ice-rafted debris using the Pb-isotope compositions of feldspars and 40Ar/39Ar ages of hornblendes. *Earth and Planetary Science Letters*, *433*, 192–203. https://doi.org/10.1016/j.epsl.2015.10.054

SUPPORTING INFORMATION

Additional supporting information may be found in the online version of the article at the publisher's website.

How to cite this article: Pesch, C., Weber, P. L., Moldrup, P., de Jonge, L. W., Arthur, E., & Greve, M. H. (2022). Physical characterization of glacial rock flours from fjord deposits in South Greenland–Toward soil amendment. *Soil Sci Soc Am J*, 1–15. https://doi.org/10.1002/saj2.20352

B. Paper II

published as:
Pesch, C., Lamandé, M., de Jonge, L. W., Norgaard, T., Greve, M. H., & Moldrup, P. (2020). Compression and rebound characteristics of agricultural sandy pasture soils from South Greenland. *Geoderma*, *380*, 114608. doi: 10.1016/j.geoderma.2020.114608

Geoderma 380 (2020) 114608

Contents lists available at ScienceDirect

Geoderma

journal homepage: www.elsevier.com/locate/geoderma

Compression and rebound characteristics of agricultural sandy pasture soils from South Greenland

Charles Pesch[a,*], Mathieu Lamandé[b,c], Lis Wollesen de Jonge[b], Trine Norgaard[b], Mogens Humlekrog Greve[b], Per Moldrup[a]

[a] Aalborg University, Department of the Built Environment (BUILD), Thomas Manns Vej 23, DK-9220 Aalborg, Denmark
[b] Aarhus University, Department of Agroecology, Research Center Foulum, Blichers Allé 20, P.O. Box 50, DK-8830 Tjele, Denmark
[c] Norwegian University of Life Sciences, Faculty of Environmental Sciences and Natural Resource Management, Campus Ås, Universitetstunet 3, 1430 Ås, Norway

ARTICLE INFO

Keywords:
Arctic pasture soils
Temperate cultivated soils
Precompression stress
Compression index
Swelling index
Rebound

ABSTRACT

The reduction of permafrost areas and a prolonged vegetation period, both due to the ongoing climate change, open up new possibilities for agricultural activities in the circumpolar region. Presently, not much is known about the physical and functional properties of subarctic agricultural soils, making it challenging to evaluate soil impacts from increased agricultural activity. This study aims at assessing the mechanical properties of sandy Greenlandic pasture soils regarding a potential future land-use change.

The compression curves of 210 undisturbed soil core samples of three pasture fields in South Greenland and, as comparison, four intensively cultivated agricultural fields in Denmark were generated by uniaxial confined compression tests (UCCT). Four soil mechanical properties were determined: the precompression stress (σ_{pc}) as a measure of soil strength, the compression index (C_c) as a measure of compressibility, the swelling index (C_s) as a measure of resilience to compaction and the rebound ($\Delta\varepsilon$) after a relaxation time of 60 s as a measure of short-time recovery from compaction.

The Greenlandic pasture soils exhibited significantly higher σ_{pc} than the Danish cultivated soils despite their significantly lower initial bulk density, ρ_b. The C_c negatively correlated with ρ_b, and the Greenlandic soils showed higher C_c values than the Danish soils. The C_s showed a reciprocal correlation with ρ_b and, partly due to lower ρ_b of the Greenlandic soils, higher C_s than the Danish soils. The South Greenlandic sandy pasture soils showed compression and rebound characteristics on level with Danish loamy cultivated soils, likely due to a high content of particulate organic matter (non-degraded organic matter, including grass root-mat residues).

1. Introduction

The ongoing climate change in the northern circumpolar region has consequences for the native population. The reduction of permafrost areas and an extending vegetation period, due to rising temperatures (Park et al., 2016) along with advances in plant breeding, can be useful for self-support in agricultural goods (Reykdal et al., Apr. 2016). Healthy soil is the primary element to allow and maintain a sustainable and productive agriculture. The effects of intensifying agricultural production, for example, of cattle grazing on the young and rather undeveloped Greenlandic soils, showed increased soil erosion (Jacobsen, 1987; Austrheim et al., 2008). The land-use intensification eventually will lead to an increase of fodder production and, thus, to higher and more frequent mechanical loads applied during traffic and tillage in the fields.

Existing literature suggests that agricultural traffic is a major source of detrimental soil compaction (Håkansson et al., 1988; Schjønning et al., 2015). Additionally, the change from perennial grassland to arable land will make soil tillage more frequent and may contribute to degrading changes in the soil's physical and functional properties by disturbing the present soil-ecological equilibrium.

Soil compaction negatively affects most of the soil physical (Horn, 2003), chemical (Lipiec and Stepniewski, 1995) and biological (Whalley et al., 1995; Beylich et al., 2010) properties, what almost unexceptionally leads to a decrease in yield (Alakukku and Elonen, 1995). Other studies on similar soils investigating the effect of grazing and trampling on pasture soils in circumpolar regions (Peth and Horn, 2006), attributed the negative impact of agricultural use on those lands not primarily to the compaction caused by trampling, but more to the change of soil cover, respectively a shift in cover-constituting plant

* Corresponding author.
E-mail address: cp@civil.aau.dk (C. Pesch).

https://doi.org/10.1016/j.geoderma.2020.114608
Received 2 March 2020; Received in revised form 7 July 2020; Accepted 16 July 2020
Available online 18 August 2020
0016-7061/

communities due to grazing and a resulting change in the thermal and water-retention properties.

Only a few studies have investigated soil mechanical properties of arable land transformed to permanent pasture. Ajayi and Horn (2016) found a significant increase in mechanical soil resilience as well as an increase in pore rigidity. The opposite process, changing permanent grassland to arable land, therefore, should decrease the soils resilience to compaction and increase the susceptibility to compaction. The removal of the well developed dense root-zone created by perennial crops, mainly by grass, where a large number of small roots contributes more to the soil stabilization than a small number of large roots (Trükmann et al., 2009), may result in a reduction of the bearing capacity of the soil.

Soil organic matter is well known to play a crucial role in the soil's ability to withstand applied mechanical stresses; indirectly, by forming stable aggregates in conjunction with the soil mineral phase and by that, enhancing the structural stability of soils (Zhang and Hartge, 1990; Barral et al., 1998; Wiesmeier et al., 2012; Sandén et al., 2017). But also the sheer presence of unbound organic matter in the soil, contributing significantly to the soil's ability to absorb applied mechanical stresses in the form of elastic energy and release it after compaction as potential energy (McBride and Watson, 1990; Zhang et al., May 2005), enables the soil to self-recover from compaction.

Several authors investigated the effect of tillage on different soil organic matter pools. Besnard et al. (1996); Six et al. (1998) and Chan (2001) revealed that tillage has a significant effect on soil organic matter. Especially the more labile particulate organic matter pools are affected to a greater extent by tillage and thus, eventually reducing the soil's resilience to compaction. Rising temperatures have a similar effect on the different soil organic matter pools than tillage. There is evidence that rising temperatures affect the particulate organic matter pools to a greater extent than the mineral-associated organic matter fractions (Kirschbaum, 1995; Zhang et al., 2007; Benbi et al., 2014). Both tillage and rising temperatures and especially the combination of both might, therefore, have critical negative repercussions on the soil mechanical properties.

In perspective of combined land-use change and climate change in the subarctic, the objective of this study was to compare the mechanical behaviour of pasture soils from South Greenland and cultivated typical soils from a temperate region. Uniaxial confined compression tests (UCCT) on 210 undisturbed soil core samples from three pasture fields in South Greenland and four cultivated areas across Denmark were carried out. The Danish soils were chosen to cover the ranges of textures and organic matter contents of the Greenlandic soils.

2. Material and methods

2.1. Study sites and soil sampling

The three Greenlandic fields are located in southern Greenland, near the small settlement of South Igaliku (Igaliku Kujalleq), about 15 km south of Igaliku. Fields South-Igaliku 1 and South-Igaliku 2 (SI-1 and SI-2 respectively, N60°53'29.2" W45°16'27.8") are in direct proximity to the Einarsfjord (Igalikup Kangerlua), whereas field South-Igaliku 3 (SI-3, N60°51'39.1" W45°16'26.4") is located about 4.5km in southern inland direction (Fig. 1). The soils of SI-1 and SI-2 developed on granite (biotite- and hornblende bearing), overlain by aeolian and fluvial sands (Henriksen et al., 2009) and were classified as Arenic Umbrisols, according to IUSS Working Group WRB (2015). The soils of SI-3 developed on a mix of fluvial and aeolian sands originating form the deposition of the erosion belt created by the tunnelled falling winds and the meltwater stream from the inland ice and was classified as an Loamic Umbrisol.

Climate data showed an annual mean temperature of 1.2 °C with January being the coldest and July being the warmest moths with mean temperatures of −6.4 °C and 10.7 °C, respectively. The annual average total precipitation was 612.9 mm a^{-1}. The vegetation period only covers about three months considering the minimum average annual temperature for the considered period, assuming a minimum temperature of 3 °C necessary for plant growth (Inouye, 2000). Precipitation is highest in September with an average value of 75.4 mm and lowest in May with an average of 34.6 mm.

Fields SI-1 and SI-2 are used as pastures, mainly for sheep grazing during the summer months and have not been tilled recently. The third Greenlandic field, SI-3, has regularly (3–4 years interval) been cultivated (disc harrowed) since 1998 and is used as a forage grass source. Additionally, the area is drained by surface ditches, due to the proximity to a nearby stream, resulting in fairly different water availability conditions throughout the year, compared to the other two fields. Mineral fertiliser is applied once per year (early summer); the application of organic fertiliser is not a common practice in the region.

The sampling was carried out in August 2015, and all the three Greenlandic fields were sampled in regular grids, with 15 × 15 m for SI-1 and SI-3 and 7.5 × 7.5 m for SI-2. In total, 74 (32, 18 and 24 for SI-1, SI-2 and SI-3 respectively) undisturbed top-soil (10–20 cm depth) core samples (height 34.2 mm, inner diameter 60.1 mm, volume 100 cm^3) were collected with 2 replicates for each sampling point.

The Danish sampling sites are located throughout Jutland. From four differently textured agricultural fields, 62 undisturbed soil core samples between 10 to 20 cm depth with the same soil core dimensions as for the Greenlandic soils were collected during different sampling campaigns. All the Danish soils are from cultivated agricultural fields, subjected to conventional tillage.

The soil at the Jyndevad sampling site (N54°53' E9°;7') developed on a fluvioglacial outwash plain of the Weichselian ice sheet (Lindhardt et al., 2001; Masís-Mendélez et al., 2014) and was classified as an Arenic Podzol (IUSS Working Group WRB, 2015). In total, 19 undisturbed soil core samples were collected from this site. The soil at the Varde sampling site (N55°37' E8°28') developed on an eroded moraine landscape form the Saalian glaciation period with fluvioglacial and aeolian (loess) components from the Weichselian glaciation period. In total, 20 undisturbed soil core samples were collected from this site, classified as Arenic Podzol. The soil at the Estrup sampling site (N55°29' E9°4') developed on a moraine landscape from the Saale glaciation (Lindhardt et al., 2001; Paradelo et al., 2015) and was classified as Stagnic Podzol; in total, 16 undisturbed soil core samples were collected. The soil at the Odder sampling site (N55°58' E10°6') developed on moraine material from the last glaciation period (Weichsel glacial) and could be classified as Cambisol. From this site, seven undisturbed soil core samples were used.

The climate normals (1961–1991) for Denmark show an annual mean temperature of 7.7 °C with January being the coldest and July being the warmest months with mean temperatures of 0.0 °C and 15.7 °C, respectively. The annual average total precipitation for the mentioned period was 712 mm a^{-1}, with a decline in total annual precipitation from west to east (823 to 584 mm a^{-1}, Cappelen (2008)).

In addition to the intact soil core samples, bulk soil was collected for each sampling point (Greenland and Denmark) for further analysis in the laboratory.

2.2. Methods

The mechanical properties of agricultural top-soils are often determined using uniaxial confined compression tests (UCCT), as the lateral confinement simulates quasi isotropic stress conditions (Lamandé et al., 2017). Depending on the purpose of the study, different loading times may be applied. For simulating traffic by agricultural machinery, where the duration of the stress application is generally less than one second (Keller and Lamandé, 2010), a strain-controlled, in contrast to a stress-controlled, compression test should be carried out.

The result of a UCC-tests is generally presented as a stress-

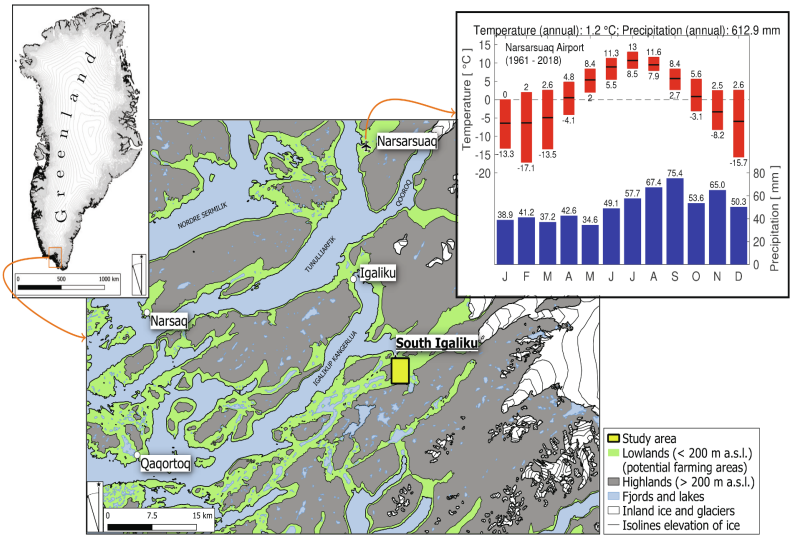

Fig. 1. The study area indicated by the filled square, next to the small settlement of South Igaliku (Styrelsen for Dataforsyning og Effektivisering, 2018). Climate diagram for the climate station at Narsarsuaq airport (monthly averages from 1961 to 2018), extend of the boxes drawn for the temperature variation corresponds to the average minimum and maximum temperatures for the considered period, the black line represents the mean monthly temperature. Climate data from Cappelen (2019).

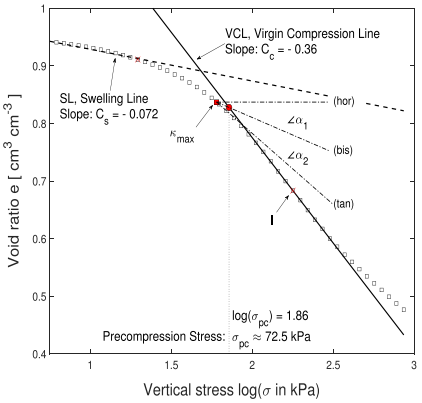

Fig. 2. Obtaining the compression characteristics on the stress-void ratio curve: Compression index (C_c, kPa^{-1}), precompression stress (σ_{pc}, kPa) and swelling index (C_s, kPa^{-1}) from UCCT-experiments; σ_{pc} as proposed by Casagrande (1936) and following Gregory et al. (2006) and Keller et al. (2011) for C_c and C_s, respectively. Sample from Jyndevad as illustration. Table 1 lists the parameter explanation.

deformation curve (Koolen, 1974). Expressed in a semi-logarithmic domain (stress, σ, in log-scale), an ideal compression curve can be divided into two regions, wherein each, the deformation follows a more or less linear path. Casagrande (1936) referred to it as a (bi-linear) elasto-plastic model: a linear elastic (reversible) deformation, described by the swelling or recompression line (SL) and a linear plastic (irreversible) deformation, represented by the virgin compression line (VCL) (Fig. 2).

The SL and VCL are connected by a transition point known as the precompression stress (or pre-consolidation stress), σ_{pc}, first introduced by Casagrande (1936). It is a measure of the soil's maximum bearing capacity before irreversible deformation occurs within the soil (Lebert and Horn, 1991; Horn et al., 1995). Several methods to determine the soil's bearing capacity exist, including the graphical method introduced by Casagrande (1936), simple linear regressions (Junior and Pierce, 1995), fitting non-linear functions (Gregory et al., 2006) and numerical methods (Lamandé et al., 2017). Apart from the regression methods, σ_{pc} depends primarily on the point of maximum curvature, κ_{max}, of the compression curve.

Apart from σ_{pc}, three additional mechanical properties were considered in this study. The compression index, C_c, as the slope of the VCL, is a measure of the soil's susceptibility to compaction (compressibility) and describes the irreversible deformation of the soil during compaction (Imhoff et al., 2004). The swelling or recompression index, C_s, as the slope of the SL, is a measure of the soil's mechanical resilience (Stone and Larson, 1980), and following the ideal elasto-plastic model, the deformation described by C_s is reversible. Finally, the rebound, $\Delta\varepsilon$, as a measure of short term resilience or the soil's ability to recover from compaction. It was measured as the vertical expansion of the compacted soil sample, 60 s after the release of the applied normal load.

2.2.1. Uniaxial confined compression tests (UCCT) and rebound after compression

Prior to the compression test, the samples were drained on a suction table to a soil water potential of $\psi = -100$ hPa (pF2), corresponding to the definition of the matric potential at field capacity for sandy soils (Al Majou et al., 2008).

A fully automated dual column table frame extensometer (Instron series 5960, Illinois Tool Works Inc.) was used to perform the UCC-tests. The device was mounted with a 5 kN static load cell and a 59 mm i.d. compression piston. The test procedure consisted in a strain-controlled stress application with a constant strain rate of 1mm min^{-1}, as

Table 1
Parameter explanation table for Fig. 2. κ_{max} is the point of maximum curvature, and I is the inflection point of the logσ − e curve for $\sigma > \sigma_{pc}$.

Stress – void ratio curve $\log(\sigma)$ **– e – graphical method**				Fig. 2
Symbol	Unit	Description	Formula/Relation	Reference
e	$cm^3\ cm^{-3}$	Void ratio	$\rho_s/\rho_b - 1$	Gupta et al. (2002)
σ_{pc}	kPa	Precompression stress	$VCL \cap$ bis	Casagrande (1936)
		hor: horizontal line passing through κ_{max} bis: bisector ($\angle\alpha_1 = \angle\alpha_2$) tan: tangent to κ_{max}		Dawidowski and Koolen (1994)
C_s	kPa^{-1}	Swelling/ recompression index	$C_s = (e_{1kPa} - e_{20kPa})/\log(20kPa)$	Keller et al. (2011)
C_c	kPa^{-1}	Compression index	$C_c = \tan(I, e)$	Gregory et al. (2006)

suggested by Koolen (1974) and Lamandé et al. (2017). The device's software recorded the displacement of the piston (extension in mm), positive in the downward direction, and the resulting load at the load cell (in N). The subsequent data analysis was entirely performed in the proprietary software MATLAB and Statisticsand Statistics Toolbox (2018).

The soil core sample was subjected to a small preload (5 N) to ensure full contact between piston and soil, and after balancing the load readings to zero, the actual compaction started together with the data recording. The test procedure was executed in several steps. The first step consisted in applying a normal stress to a maximum value of 800 kPa at a constant strain rate of 1 mm min^{-1}. After the maximum value was reached, the piston retracted instantaneously to its initial position for a 60 s waiting time. During this waiting time, hereafter relaxation time, the compacted soil was able to regain in volume (one-dimensional expansion in the vertical direction, rebound $\Delta\varepsilon$). The final step was then to determine the amount of the vertical expansion by measuring the difference between the extension at the maximum applied stress (800 kPa) and the extension after the relaxation time (60 s). For this purpose, the cross-head moved down to the soil core cylinder again, and the displacement of the cylinder was recorded after preload (5 N). The simultaneous measurements of the applied normal load and compressive extension (d) were converted to applied vertical stress, σ (in kPa), and change in void ratio, e, according to Eq. (1),

$$e = (\rho_s/\rho_b)[(H - d)/H] - 1 \text{ and } e_0 = [\rho_s/\rho_b] - 1 \quad (1)$$

with H being the initial height of the soil sample in the same unit as d, e_0 the initial void ratio and ρ_b and ρ_s the dry bulk and the average particle densities, respectively.

2.2.2. Numerical determination of the four mechanical parameters

The precompression stress, σ_{pc}, was determined using the graphical method introduced by Casagrande (1936), and its essential part is the determination of the point of maximum curvature (κ_{max}) of the compression curve. The numerical method recently introduced by Lamandé et al. (2017) is robust in finding κ_{max} without imposing a predefined shape on the stress-deformation curve and served as input for further calculations of the precompression stress via the Casagrande-method. The numerical method consists of fitting a polynomial of form $e = a{\cdot}(\log\sigma) + b{\cdot}(\log\sigma)^2$ to a neighbouring subset of equidistant points of the log(stress)-void ratio curve. The second derivative of a function is a measure for the degree of curvature of a continuous curve, and as the second derivative of the above equation is equal to $2b$, it immediately leads to the point of maximum curvature, which is at the point where b has its maximum. The minimum number of neighbouring points used for the fitting was determined by simultaneously finding the maximum of the coefficient of determination R^2 (close to 1) and a significance of the t-test (assessed by its p-value) of the regression coefficient b below 0.001 as a function of the number of pairs of stress–strain points that were included in the regression. A detailed description of the procedure can be found in Lamandé et al. (2017). This approach reduced the subjectivity of finding κ_{max} to a minimum compared to fitting (Arvidsson and Keller, 2004; Gregory et al., 2006) or even visual methods. The used procedure for finding the three lines needed for determining σ_{pc} followed Dawidowski and Koolen (1994).

The compression index, C_c, defined here as the slope of the tangent at the inflection point of the stress-void ratio curve (following Gregory et al. (2006), where C_c is given by the slope of the tangent at the inflection point of the fitted Gompertz-function), can also be determined using the numerical approach. Considering the applied polynomial for the local regressions and its second derivative, a necessary condition of a point to be an inflection point is that the second derivative at this point vanishes. Thus, finding the location where $b = 0$ at higher applied stresses than the precompression stress, gives a potential inflection point; the determination of the slope of its tangent is straightforward. The assumption that the necessary condition of the existence of an inflection point is also sufficient is valid in this case, because it is expected that the second derivative exists and changes sign at that point. If the second derivative does not vanish at any point right to κ_{max}, the slope of the tangent of the points where b is closest to zero is set as the compression index. In that case, the expression is reduced to the slope of the tangent of the compression curve at high applied loads. The advantage of this method compared to fitting methods is that no subjective assumptions about manually setting the reference points for linear regression are involved.

The swelling index, C_s, was calculated following Keller et al. (2011) as the average slope of the $\sigma - e$ curve between applied vertical stresses of 1 and 20 kPa. Keller et al. (2011) set the upper boundary for the determination of C_s to 25 kPa, in this study, however, it had to be lowered to 20 kPa as some of the determined precompression stresses were lower than 25 kPa (Jyndevad).

The rebound, $\Delta\varepsilon$, was calculated as the difference of the measured displacement of the cross-head from its initial position to the soil surface at an applied vertical stress of 800 kPa, d_{end} (end of compression) with the corresponding compressive strain $\varepsilon_{end} = d_{end}/H$ and the displacement to the soil sample's surface after a relaxation time of 60 s without any applied vertical stress, d_{final} ($\varepsilon_{final} = d_{final}/H$). Thus the rebound expressed in unit strain equals: $\Delta\varepsilon = \varepsilon_{final} - \varepsilon_{end}$.

2.2.3. Supporting basic measurements

After the compression tests, the soil samples were oven-dried for 24 h at 105 °C for dry bulk density (ρ_b) determination. The oven-dried samples were subsequently destroyed for a visual inspection of the presence and abundance of scarcely decomposed organic fragments.

On the air-dry and 2 mm pre-sieved bulk samples, the particle size distribution (PSD) was determined using wet sieving in combination with the hydrometer method, according to Gee and Or (2002). The total carbon content was determined using a LECO carbon analyser coupled to an infrared CO_2 Flash 2000 NC detector, and as the soils were free of carbonates, the organic carbon (OC) could be set equal to the total carbon content. The average particle density (ρ_s) of the Danish soils was estimated based on the gravimetric clay and organic matter contents, according to Schjønning et al. (2017), and for the Greenlandic soils, ρ_s was measured by the water displacement method, according to Flint

and Flint (2002).

2.3. Statistical analysis

The relationships between the initial bulk density (ρ_b, independent variable, IV) and the soil mechanical properties (σ_{pc}, C_c, C_s and $\Delta\varepsilon$, dependent variables, DV) were investigated by linear regressions, if applicable. The goodness of fit of the linear regressions was quantified by the ordinary coefficient of determination, R^2, and the root mean square error, RMSE, calculated, according to Hollander et al. (2013). The level of significance was denoted by stars according to *** for $p < 0.001$, ** for $p < 0.01$, * for $p < 0.05$ and none for $p \geqslant 0.05$.

Pearson's linear correlation coefficient r was used to express the linear correlation between two variables (Hollander et al., 2013).

Box-whisker plots (Tukey, 1977) were used to visualise the relative differences or similarities between the measured mechanical parameters.

To test the land-use-specific difference in medians of the different soil mechanical parameters for significance, the Kruskal–Wallis test was used. It is a non-parametric method and does neither assume normally distributed observations, nor homoscedasticity and allows unbalanced datasets to test the hypothesis, that the medians of two groups come from the same distribution (Kruskal and Wallis, 1952). The result of the test was given by the χ^2-statistic and its p-value. If significant differences in values among the medians of the different groups were found, the Mann–Whitney-Wilcoxon U test (Mann and Whitney, 1947) served as the post hoc test to identify the significance of the pairwise comparisons. The p-values were corrected for inflation of type I errors by using the Bonferroni method (Dunnett, 1955).

3. Results and discussion

3.1. Texture, organic carbon contents and initial bulk densities

The soil type of the three Greenlandic fields ranged from sand to loamy sand, according to Soil Survey Staff (1999), with the dominant type being sandy loam (77% of the Greenlandic dataset). Average OC ranged between 0.0145 g g^{-1} (SI-2) and 0.0313 g g^{-1} (SI-3) with a median value of 0.0223 g g^{-1} and clay contents ranging between 0.022 g g^{-1} (SI-2) and 0.041 g g^{-1} (SI-3) with a median value of 0.029 g g^{-1}. The site-specific basic soil properties are given in Table 2.

The soil types of the Danish soils were coarse sand (Jyndevad), loamy sand to sandy loam (Varde), sandy loam to loam (Estrup) and sandy loam to clay loam (Odder). The average OC contents of the Danish soils ranged from 0.0157 (Odder) to 0.0339 (Estrup) g g^{-1}, with Estrup exhibiting the highest variation in OC contents, see also Table 2.

Fig. 3A shows a box-whisker plot of the gravimetric OC contents for all the soil used in this study. The chosen Danish arable fields covered the texture range of the Greenlandic ones (Fig. 3B). Among the Greenlandic dataset, SI-3 exhibited the highest OC and fine particle contents (particles with equivalent diameter <50 μm).

Dexter et al. (2008) reported that the amount of complexed and non-complexed soil organic carbon contents play a crucial role in the soil's physical and functional behaviour. The clay-OC ratio for a given soil (Dexter n) should be below 10 to ensure that all the organic matter is bound to the clay minerals. For all the soils from Greenland, the majority of the organic carbon was not bound to the clay fraction due to the overabundance of organic material relative to the available surface area of the clay content (Dexter $n < 1.5$, cf. Table 2). Hence, relatively large amounts of non-complexed organic carbon were available within the soil matrix.

The visual examination of the sub-Arctic Greenlandic pasture soil samples revealed that they contained relatively large amounts of root and other scarcely decomposed plant litter fragments, in contrast to the Danish samples issued from permanently cultivated temperate lands. Although Dexter n of most of the Danish soils was well below ten (cf. Table 2), the absence of larger amounts of particulate organic matter was associated to the land-use and management (Chan, 2001; Ramesh et al., 2019), as well as to the enhanced organic matter turnover in temperate compared to subarctic environments (Benbi et al., 2014). The content of particulate organic matter was found to be positively correlated with soil stability and resilience to compaction (Bachmann and Zhang, 1991; Zhang et al., May 2005). A reduction in particulate organic matter, therefore, should eventually lead to decreasing mechanical stability.

The initial dry bulk density, ρ_b, of the Greenlandic soils ranged between 1.08 and 1.27 g cm^{-3} (for SI-3 and SI-2, respectively, Table 2). Similar values for South Greenlandic pasture soils were found by Caviezel et al. (2017). The low values could partly be attributed to the high OC, showing a significant negative correlation (Greenland: $r = -0.74$***, Denmark: $r = -0.54$***) with ρ_b, as also reported in other studies (Gupta and Larson, 1979; Federer et al., 1993; Perie and Ouimet, 2008). A Kruskal–Wallis test indicated that ρ_b of the Greenlandic soils (mean rank = 1.15 g cm^{-3}, $n = 148$) was statistically significantly lower than the ρ_b of the Danish dataset (mean rank = 1.43 g cm^{-3}, $n = 62$), $z = -9.45$, $p < 0.0001$.

The high OC content is, however, not the only factor affecting ρ_b of the Greenlandic soils. Among others, land-use influences ρ_b as other studies found lower ρ_b when comparing cultivated agricultural soils to perennial grasslands (Ajayi and Horn, 2016). Specific for the investigated region, temperature effects resulting in intense freeze and thaw cycles, leading to a high amount of voids in the soil matrix due to

Table 2
Basic soil properties related to texture and structure of the soils used in this study. Median values of gravimetric fractions of clay (< 2μm), silt (2–50 μm) and sand (50–2000 μm) in g g^{-1}, organic carbon content (OC, g g^{-1}), average particle density (ρ_s, g cm^{-3}) and initial dry bulk density (ρ_b, g cm^{-3}). Clay-OC ratio Dexter n according to Dexter et al. (2008); N is the number of samples per site. Soil type according to Soil Survey Soil Survey Staff (1999) with S – Sand, lS – loamy Sand, sL – sandy Loam, L – Loam, cL – clay Loam. The figures in brackets denote the interquartile range (IQR = 75% quartile – 25% quartile). Medians in the same column bearing the same letter are not statistically different on a 5% significance level.

		Soil Type	Particle Size Distribution				Densities		Ratio
Data set/ Site	N	USDA	Clay	Silt	Sand	OC	ρ_s	ρ_b	Dexter n
				× 10^{-2} [g g^{-1}]			[g.cm^{-3}]		[–]
Greenlandic Soils (SI)	148		2.9 (1.2)	23.1 (3.5)	70.4 (4.4)	2.23 (1.51)	2.64 (0.04)	1.15 (0.23)	1.31 (0.38)
South-Igaliku 1 (SI-1)	64	lS-sL	2.9 (0.7)	22.4 (2.5)	71.4 (4.2)	2.09 (0.84)	2.64 (0.02)	1.12 (0.22) a	1.32 (0.38)
South-Igaliku 2 (SI-2)	36	lS-sL	2.2 (0.4)	23.8 (1.6)	71.6 (1.7)	1.45 (0.46)	2.66 (0.01)	1.27 (0.12) b	1.40 (0.78)
South-Igaliku 3 (SI-3)	48	lS-sL	4.1 (1.0)	24.1 (6.9)	65.3 (7.5)	3.13 (0.93)	2.62 (0.02)	1.08 (0.19) a	1.18 (0.40)
Danish Soils (DK)	62		5.7 (6.3)	16.8 (21.9)	73.4 (31.8)	2.18 (0.83)	2.58 (0.03)	1.43 (0.15)	2.52 (1.11)
Jyndevad	19	S	4.1 (0.5)	4.8 (0.4)	87.7 (1.0)	1.92 (0.27)	2.59 (0.01)	1.43 (0.07) c	2.16 (0.60)
Varde	20	lS-sL	5.3 (0.9)	16.6 (1.5)	73.6 (2.8)	2.29 (0.55)	2.58 (0.02)	1.44 (0.25) c	2.41 (0.64)
Estrup	16	sL-L	10.9 (2.0)	28.7 (2.5)	54.6 (3.9)	3.39 (2.87)	2.54(0.12)	1.39 (0.27) c	3.12 (3.01)
Odder	7	sL-cL	16.0 (15.5)	26.7 (8.7)	54.6 (28.0)	1.57 (1.15)	2.62 (0.02)	1.52 (0.14) c	9.85 (0.64)

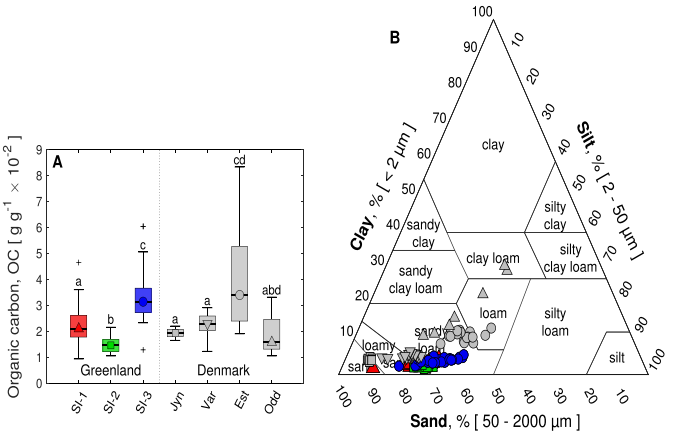

Fig. 3. Texture and organic carbon contents of the soils used in this study. **A**; Box-whisker plot of the gravimetric organic carbon content (OC, g g^{-1}). Columns bearing the same letters were not statistically different on a 5% significance level. The horizontal line within the rectangular box represents the median value of each site, the upper and lower extension of the box depicts the first and third quartiles, respectively, and the whiskers extend to the minimum and maximum of the population cleared from outliers. Outliers are values that are more than three scaled median absolute deviations away from the population median (Rousseeuw and Croux, 1993) and depicted by black crosses. **B**; USDA soil texture triangle. Greenland: ▲ South-Igaliku 1 (SI-1), ■ South-Igaliku 2 (SI-2), ● South-Igaliku 3 (SI-3); Denmark: □ Jyndevad (Jyn), ○ Estrup (Est), ▽ Varde (Var) and △ Odder (Odd).

the expanding freezing water (Xie et al., 2015).

3.2. Precompression stress

The field-specific average of the precompression stress, σ_{pc}, of the Greenlandic soils ranged between 114.7 (SI-3) and 125.2 (SI-1) kPa with an overall median of 119.8 kPa. The site-specific σ_{pc} are listed in Table 3. A Kruskal–Wallis test indicated that the σ_{pc} of the pooled Greenlandic soils (mean rank = 119.64 kPa, n = 148) were statistically significantly higher than the σ_{pc} of the pooled Danish dataset (mean rank = 71.74 kPa, n = 62), χ^2 = 27.15, p < 0.0001. Fig. 4A shows a box-whisker plot of σ_{pc} for the different sites, and following the pairwise comparison test, only the samples from the Jyndevad site had significantly lower σ_{pc}.

Following the classification for the bearing capacity of top-soils proposed by Horn and Fleige (2003), σ_{pc} of the three Greenlandic fields could be classified as *high*. Fig. 4B shows the variation of σ_{pc} with ρ_b and a slight positive tendency of σ_{pc} with increasing ρ_b can be observed; a significant linear correlation between the two variables could only be found for the samples from field SI-1 (r = 0.74**).

A similar weak but significant positive correlation between σ_{pc} and ρ_b could be observed for the Danish cultivated soils (r = 0.42***) what is in accordance to the findings of other studies (Salire et al., 1994; Rücknagel et al., 2007) investigating the mechanical soil properties of cultivated soils. Interestingly, despite having significantly lower ρ_b, the Greenlandic soils exhibited significantly higher σ_{pc} compared to those determined on the Danish soils as revealed above by the Wilcoxon ranked-sum test.

Fig. 4B clearly shows that the dependence of σ_{pc} on ρ_b of the Greenlandic soils followed the same positive trend with increasing ρ_b as the Danish soils, but on a different level. Ajayi and Horn (2016) found an increased pore rigidity for soils under grassland compared to cultivated soils, which may affect the bearing capacity of the soil. The relatively large amounts of particulate organic matter and scarcely decomposed litter fragments found in the Greenlandic soils (cf Section 3.1) may be partly responsible for the significantly higher σ_{pc}. Omitting the soils from Jyndevad from the Danish dataset, the remaining soils (Varde, Estrup and Odder) showed no statistically significant differences in σ_{pc}, but still, the Greenlandic soils showed significantly lower ρ_b (cf. Table 2). This indicated that the pore rigidity due to the plant cover (grass) and the soil-matrix elasticity provided by the unbound organic fragments, both missing in the Danish soils, had a significant positive effect on the Greenlandic soil's strength.

3.3. Compression index

Field-specific average C_c of the Greenlandic soils ranged between 0.196 (SI-2) and 0.319 (SI-3) kPa^{-1} with an overall median of 0.280 kPa^{-1} (absolute values). The site specific C_c are listed in Table 3. Fig. 5A shows a box-whisker plot of C_c for the different sites. The pair-

Table 3
Soil mechanical characteristics of the soils presented in this study. Median values of the precompression stress (σ_{pc}, kPa), the compression index (C_c, kPa^{-1}) and the swelling (recompression) index (C_s, kPa^{-1}) determined on the stress-void ratio curve (logσ - e), the rebound ($\Delta\varepsilon$, –) expressed in terms of unit strain and the recovery ($\Delta\rho$, %) expressed in percent of initial ρ_b. N is the number of samples per site. The figures in brackets denote the interquartile range (IQR = 75% quartile – 25% quartile). Medians in the same column bearing the same letter are not statistically different on a 5% significance level.

Data set/ Site	N	σ_{pc}	C_c	C_s	$\Delta\varepsilon$	$\Delta\rho$
		[kPa]	× 10^{-1} [kPa^{-1}]	× 10^{-2} [kPa^{-1}]	× 10^{-2} [–]	%
Greenlandic Soils (SI)	148	119.8 (55.6)	2.80 (1.77)	4.56 (3.03)	7.77 (3.56)	48.50 (6.66)
South-Igaliku 1 (SI-1)	64	125.2 (75.2)	3.10 (2.05)	4.60 (3.69)	7.94 (3.31) a	48.50 (5.90)
South-Igaliku 2 (SI-2)	36	115.5 (39.9)	1.96 (0.78)	3.59 (1.09)	5.67 (1.52) b	44.54 (4.69)
South-Igaliku 3 (SI-3)	48	114.7 (46.5)	3.19 (1.18)	5.64 (2.64)	9.14 (2.61) a	50.95 (6.82)
Danish Soils (DK)	62	75.6 (53.9)	1.73 (1.34)	3.66 (2.19)	5.23 (1.17)	35.64 (10.92)
Jyndevad	19	45.0 (32.3)	1.61 (0.26)	4.87 (1.34)	5.17 (0.59) b	27.28 (8.61)
Estrup	16	99.2 (100.7)	2.97 (0.96)	3.79 (1.64)	5.17 (1.01) b	35.40 (6.74)
Varde	20	88.5 (80.8)	1.18 (0.92)	2.83 (1.84)	5.80 (1.28) b	30.11 (14.69)
Odder	7	94.0 (29.3)	2.31 (1.27)	2.63 (1.09)	3.99 (2.43) b	41.75 (12.41)

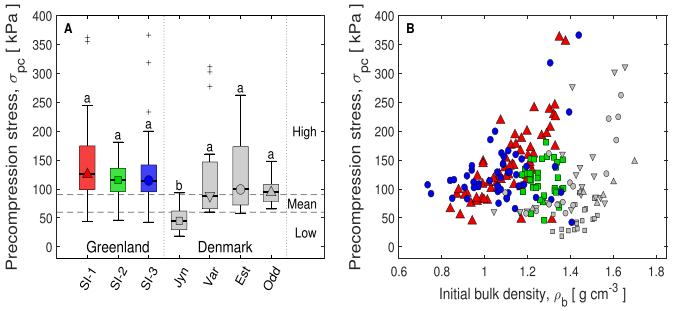

Fig. 4. Precompression stress (σ_{pc}, kPa) as a measure of soil strength. **A**; Box-Whisker plot of σ_{pc} for the different sites, including levels of soil strength as proposed by Horn and Fleige (2003) marked by horizontal dashed lines. Columns bearing the same letters were not statistically different on a 5% significance level. **B**; σ_{pc} as a function of the initial bulk density (ρ_b, g cm^{-3}). Greenland: ▲ South-Igaliku 1 (SI-1), ■ South-Igaliku 2 (SI-2), ● South-Igaliku 3 (SI-3); Denmark: □ Jyndevad (Jyn), ○ Estrup (Est), ▽ Varde (Var) and △ Odder (Odd).

wise comparison test revealed that SI-2 exhibited significantly lower C_c than the other two Greenlandic fields.

Good agreements between the determination of C_c using the methods described in Gregory et al. (2006) or Keller et al. (2011) (tangent at the inflection point of the fitted Gompertz function to the stress-void ratio curve) and the method used in this study (r = 0.92***, data not shown).

The linear correlation of the Greenlandic C_c (dependent variable, DV) with ρ_b (independent variable, IV) could be described by a significant linear regression with excellent goodness of fit given in Eq. (2).

$$C_c = 1.22^{***} - 0.81^{***} \times \rho_b;\ (\mathrm{RMSE}=0.04;\ R^2 = 0.92) \quad (2)$$

where ρ_b is in g cm^{-3}.

Several other studies reported a linear dependence of C_c on ρ_b or on the initial void ratio (e_0) (Salire et al., 1994; Keller et al., 2011). The Danish soils followed a linear trend, exhibiting a considerably lower slope, as can be seen in Fig. 5B. The regression equation determined for the C_c of the Danish soils ($C_c = 0.79 - 0.41 \times \rho_b$) was similar to the findings of Salire et al. (1994), $C_c = 0.89 - 0.44 \times \rho_b$; the goodness of fit and the significance levels were omitted due to the high degree of heteroscedasticity.

Higher C_c values indicated that the considered soil changed its volume to a larger extend for a given applied load. The low ρ_b resulted in a large amount of void space in the soil matrix. The irreversible reduction in volume at field conditions and relatively small applied stresses compared to the maximum applied stress during the UCCT (800 kPa) was mainly attributed to a reduction in the macro-porosity (Pagliai et al., 2003; Schäffer et al., 2007) and thus affecting soil aeration and hydraulic conductivity (Ahuja et al., 1984; Heard et al., 1988; Moldrup et al., 2001). Although the aggregate stability was not measured, the relatively low clay contents of the Greenlandic soils, as well as the intense freeze and thaw cycles in the region of interest, result in low aggregate stability (Lehrsch et al., 1991; Oztas and Fayetorbay, 2003) and once the bearing capacity of the top-soil overcome, the sandy Greenlandic soils are easily compacted.

3.4. Swelling index

Field-specific average C_s of the Greenlandic soils ranged between 3.59×10^{-2} kPa^{-1} (SI-2) and 5.64×10^{-2} kPa^{-1} (SI-3) kPa^{-1} with an overall median of 4.56×10^{-2} kPa^{-1} (absolute values). The site-specific C_s are listed in Table 3, and Fig. 6A shows a box-whisker plot of C_s for the different sites. The variation of C_s with ρ_b of the complete dataset (SI + DK) could be best explained by a reciprocal relation; it is given in Eq. (3).

$$C_s = 0.03^{***}/(\rho_b - 0.52^{***});\ (\mathrm{RMSE}=0.01;\ R^2 = 0.64) \quad (3)$$

where ρ_b is in g cm^{-3}. The lowest ρ_b exhibited the highest C_s, and the reciprocal nature of the relationship indicated a relatively abrupt change in the magnitude of C_s (decrease), once a certain ρ_b was exceeded.

The Danish soils generally exhibited lower C_s than the Greenlandic

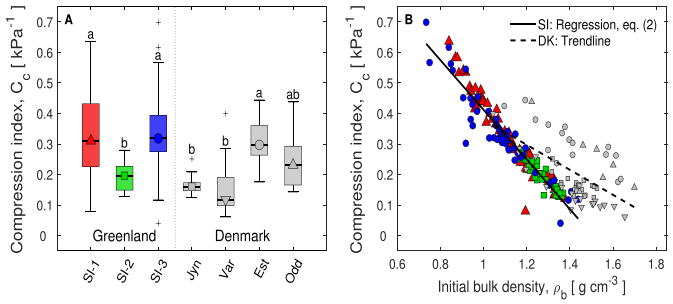

Fig. 5. Compression index (C_c, kPa^{-1}) as a measure of compressibility. **A**; Box-whisker plot of C_c. Columns bearing the same letter are not statistically different on a 5% significance level. **B**; C_c as a function of the initial bulk density (ρ_b, g cm^{-3}). Solid regression line describes the trend of C_c of the Greenlandic soils (SI) with ρ_b as the independent variable; the dashed trend line shows the same for the Danish soils (DK). Greenland: ▲ South-Igaliku 1 (SI-1), ■ South-Igaliku 2 (SI-2), ● South-Igaliku 3 (SI-3); Denmark: □ Jyndevad (Jyn), ○ Estrup (Est), ▽ Varde (Var) and △ Odder (Odd).

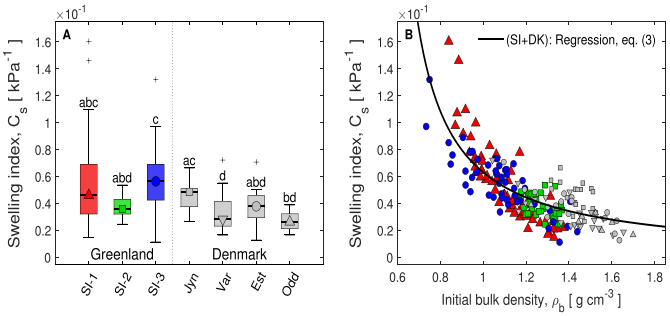

Fig. 6. The swelling index (C_s,kPa^{-1}) as a measure of resilience to compaction. **A**; Box-whisker plot of C_s. Columns bearing the same letter are not statistically different on a 5% significance level. **B**; C_s versus the initial bulk density (ρ_b, kPa^{-1}) and a regression line showing the reciprocal correlation of C_s with ρ_b, valid for both datasets (SI + DK). Greenland: ▲ South-Igaliku 1 (SI-1), ■ South-Igaliku 2 (SI-2), ● South-Igaliku 3 (SI-3); Denmark: □ Jyndevad (Jyn), ○ Estrup (Est), ▽ Varde (Var) and △ Odder (Odd).

soils, and a Kruskal–Wallis test indicated that the C_s of the Greenlandic soils (mean rank = 116.03, n = 148) were statistically significantly higher than the C_s of the Danish dataset (mean rank = 80.35, n = 62), χ^2 = 15.06, p < 0.0001. Following the assumptions of the elasto-plastic model, the Greenlandic soils were more resilient to compaction than the Danish cultivated soils. This is in accordance with several other studies (Gregory et al., 2009; Dörner et al., 2011) in which pasture soils of temperate regions showed higher resilience to compaction than regularly tilled soils.

A significant positive correlation could be found between C_c and C_s (r = 0.80***), with C_c being approximately six times higher than C_s (C_c = 6.26(1.73) × C_s, figure in brackets denotes the interquartile range) for all the soils considered in this study clearly showing that the elastic behaviour was closely linked to the plastic deformation and did not consist of two separated events, as already pointed out by other authors (Keller et al., 2004). During the relatively fast compaction procedure used in this study, the redistribution of soil water needed to overcome the hydraulic impedance of the soil matrix, leading to reduced effective stress (Terzaghi, 1925) on the soil skeleton and thus to less plastic deformation and particle rearrangements. This may be one reason for the high correlation between C_c and C_s, meaning that the resilience to compaction (i.e., the elastic energy stored in the soil matrix) persisted, although the σ_{pc} was well exceeded.

3.5. Rebound

Field-specific average Δε of the Greenlandic soils ranged between 5.67 × 10^{-2} (SI-2) and 9.14 × 10^{-2} (SI-3) with an overall median of 7.77 × 10^{-2} units of strain. All the site-specific Δε are listed in Table 3. The Greenlandic soils exhibited generally higher Δε than the Danish soils, and a Kruskal–Wallis test confirmed that the Δε of the Greenlandic soils (mean rank = 124.20, n = 148) were statistically significantly higher than the Δε of the Danish dataset (mean rank = 60.87, n = 62), χ^2 = 47.45, p < 0.0001.

Fig. 7A shows the linear relation between Δε and ρ_b for the Greenlandic soils given in Eq. (4), exhibiting markedly higher intercept and slope than the shown trend-line of the Danish cultivated soils.

$$\Delta\varepsilon = 0.\,24^{***} - 0.\,14^{***} \times \rho_b;\ (\mathrm{RMSE}{=}0.01;\ R^2 = 0.85) \quad (4)$$

where ρ_b is in g cm^{-3}. The most intuitive explanation and reason for the higher Δε of the Greenlandic soils are their significantly lower ρ_b. A less-dense soil needs less energy input to be moved, disregarding the direction of the movement, but the lower ρ_b might not be the only reason. Zhang et al. (May 2005) reported that high organic matter contents increased the rigidity of pores and that a large amount of particulate organic matter would act as a spring. The relatively high amounts of particulate organic matter present in the Greenlandic pasture soils could, therefore, be partly responsible for the relatively high measured rebound.

It is not completely clear what caused the higher Δε of the Greenlandic pasture soils specifically, as hydraulic parameters like the soil water potential were not monitored or controlled during the compression tests. Measurements of the saturated hydraulic conductivity were low for the Greenlandic soils (data not shown), despite their high total porosity (data not shown) what might indicate the presence of dead-end pores, resulting in entrapped air pockets contributing to a larger rebound after the release of the stress.

Fig. 7B shows the relation between Δε and C_c. A significant linear regression could be found for the Greenlandic soils, given in Eq. (5), whereas the Danish cultivated soils showed only marginal sensitivity to C_c.

$$\Delta\varepsilon = 0.\,03^{***} + 0.\,16^{***} \times C_c;\ (\mathrm{RMSE}{=}0.01;\ R^2 = 0.83) \quad (5)$$

where C_c is in kPa^{-1}. This suggests that the mechanisms involved in the relaxation after compression were of different nature for the soils from two different land uses and climatic regions.

3.6. Bulk densities during compression and recovery potential after compression

In the following, ρ_b and changes in ρ_b due to compression were used instead of e_0 and changes in e, because all of those parameters were directly measured or calculated and not estimated from other parameters, reducing the risk of introducing artefacts in the shown relations. The rebound, technically not being a level of compaction as no stress is applied to the soil, was included in the terms levels or degrees of compaction for better legibility.

The bulk densities at 800 kPa ($\rho_{b,800\,kPa}$) and after rebound ($\rho_{b,\Delta\varepsilon}$) as a function of the initial bulk density ρ_b are presented in Fig. 8A. To improve readability, only every third data-point was plotted. The $\rho_{b,m}$ at the two levels of compaction, were calculated via the compressive strain, ε, and ρ_b, according to Eq. 6.

$$\rho_{b,m} = \rho_b[1/(1 - \varepsilon_m)] \quad (6)$$

where m denotes a given compaction level. Examination of ρ_b at the two levels of compaction revealed that the relationship was best described by including the squared initial ρ_b as IV in the regression. Hence, the complete dataset could be adequately described by one regression for each of the two compaction levels (Eqs. (7) and (8)).

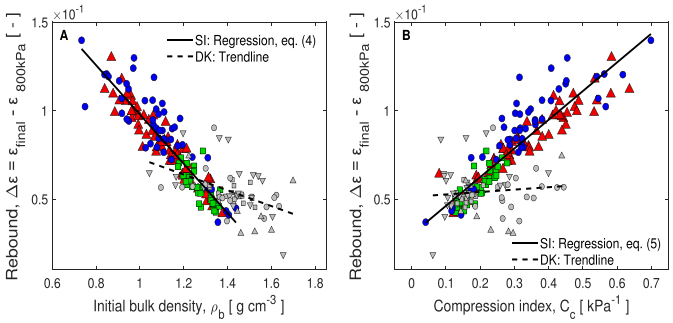

Fig. 7. The rebound ($\Delta\varepsilon$, –) expressed in terms of compressive strain as a measure of short term recovery from compaction. **A**; $\Delta\varepsilon$ as a function of the initial bulk density (ρ_b, g cm^{-3}) and the corresponding linear regression for the Greenlandic data (SI); the dashed line shows the general trend of the Danish dataset. **B**; $\Delta\varepsilon$ versus the compression index (C_c, kPa^{-1}) and a linear regression for the Greenlandic data (SI); the dashed line shows the trend for the Danish dataset. Greenland: ▲ South-Igaliku 1 (SI-1), ■ South-Igaliku 2 (SI-2), ● South-Igaliku 3 (SI-3); Denmark: □ Jyndevad (Jyn), ○ Estrup (Est), ▽ Varde (Var) and △ Odder (Odd).

$$\rho_{b,800kPa} = 0.90^{***} + 0.39^{***} \times (\rho_b)^2;\ (RMSE=0.07;\ R^2 = 0.87) \quad (7)$$

$$\rho_{b,\Delta\varepsilon} = 0.71^{**} + 0.43^{***} \times (\rho_b)^2;\ (RMSE=0.06;\ R^2 = 0.91) \quad (8)$$

where ρ_b is in g cm^{-3}.

For the given data, the plotted regression lines (Fig. 8A) approached each other with increasing ρ_b; the difference between $\rho_{b,800\,kPa}$ and $\rho_{b,\Delta\varepsilon}$ decreased with increasing initial ρ_b. This vertical distance between the two lines is a measure of how much a soil sample can recover from compaction.

Fig. 8B shows to what extent the different sites were able to recover from $\rho_{b,800\,kPa}$ back towards their initial bulk densities (ρ_b). By taking the ratio, $\Delta\rho = [\rho_{b,800\,kPa} - \rho_{b,\Delta\varepsilon}]/[\rho_{b,800\,kPa} - \rho_b]$, the effect of the significantly lower initial bulk density of the Greenlandic pasture soils could be eliminated. According to a Kruskal–Wallis test, $\Delta\rho$ of the Greenlandic soils (mean rank = 128.56, n = 148) was statistically significantly higher than $\Delta\rho_b$ of the Danish soils (mean rank = 50.45, n = 62), χ^2 = 72.19, $p < 0.0001$. The site-specific values of $\Delta\rho$ are given in Table 3. The values of recovery were very high in this study compared to other studies (Stone and Larson, 1980; Keller et al., 2011). This differences can be explained by that the Stone and Larson (1980) and Keller et al. (2011) studies used a sequential loading procedure with relatively long loading times, in contrast to the relatively fast strain-controlled procedure used in this study (Ghezzehei and Or, 2001).

Interestingly, among the Danish soils, Varde exhibited the highest recovery potential (not significantly different from SI-1 and SI-2), and it shared the most similar particle size distribution and similar OC content with the Greenlandic soils. This indicates that the recovery potential is dependent on both soil texture and OC, although it was not possible to find a simple statistically significant relationship between the three parameters for the used dataset.

4. Conclusion

The Greenlandic pasture soils exhibited significantly higher pre-compression stress, σ_{pc}, than the Danish cultivated soils despite markedly lower initial bulk densities, ρ_b. A main reason for the higher σ_{pc} of the Greenlandic soil is likely a large amount of non-complexed, particulate organic matter in the soil matrix. For some of the Greenlandic soils, a significant positive correlation between ρ_b and σ_{pc} could be found (r = 0.74).

The compression indices, C_c, of the Greenlandic pasture soils were significantly higher than for the Danish cultivated soils, and lower ρ_b gave higher C_c, likely due to a relatively large volume of easily compressible void space in the soil matrix. A strong linear relation between ρ_b and C_c for the Greenlandic soils was found (R^2 = 0.92).

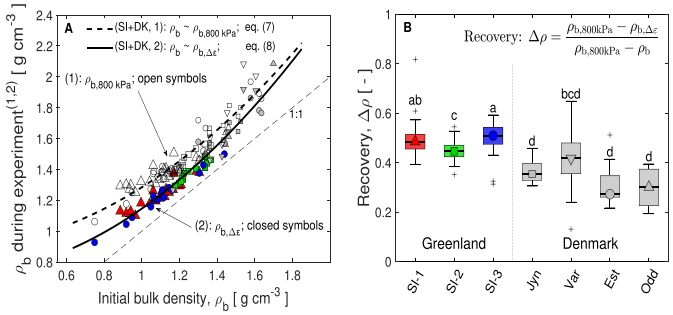

Fig. 8. Bulk density history at different stages (1 and 2) of the compression experiment. **A**; ρ_b at a normal stress of 800 kPa (1, open symbols; $\rho_{b,800kPa}$, g cm^{-3}) and after the relaxation time (2, closed coloured symbols; $\rho_{b,\Delta\varepsilon}$, g cm^{-3}) as a function of ρ_b. The 1:1 line represents the initial ρ_b. Data reduced for better legibility (each third point). **B**; Recovery ($\Delta\rho_b$, -), defined as the ability of a sample to return to its initial ρ_b during the relaxation time. Columns bearing the same letters are not statistically different on a 5% significance level. Greenland: ▲ South-Igaliku 1 (SI-1), ■ South-Igaliku 2 (SI-2), ● South-Igaliku 3 (SI-3); Denmark: □ Jyndevad (Jyn), ○ Estrup (Est), ▽ Varde (Var) and △ Odder (Odd).

The swelling indices, C_s, of the Greenlandic soils were also significantly higher than for the Danish soils. Lower ρ_b gave higher C_s due to increased pore rigidity and the relatively large amounts of particulate organic matter stemming from the permanent soil cover (grass). A reciprocal relation for the pooled (Greenlandic and Danish) dataset between ρ_b and C_s was found (R^2 = 0.64).

The rebound in terms of unit strain, $\Delta\varepsilon$, of the Greenlandic soils was significantly higher than the $\Delta\varepsilon$ of the Danish cultivated soils. The Greenlandic $\Delta\varepsilon$ showed a significant negative linear dependence on ρ_b (R^2 = 0.85). The recovery in terms of % of initial ρ_b, $\Delta\rho$, showed that the Greenlandic pasture soils could recover significantly better from severe compaction than the Danish cultivated soils.

For the Greenlandic pasture soils, the initial bulk density was overall a good predictor for all the mechanical properties considered in this study. Differences to Danish cultivated soils were associated with nature of the organic matter (particulate organic matter in the arctic pasture/grassland soils) and low bulk densities.

In perspective, a future land-use change from pasture to more intense cultivation together with rising temperatures in South Greenland would result in a reduction of particulate organic matter and thereby decrease the σ_{pc} of the sandy Greenlandic soils. The low clay contents, together with a reduction in organic matter, could further result in a weakly structured soil matrix, and the present high resilience and recovery potential to compaction would decline.

Declaration of Competing Interest

The authors declare that they have no known competing financial interests or personal relationships that could have appeared to influence the work reported in this paper.

Acknowledgements

This research was financed by the Danish Council for Independent Research, Technology and Production Sciences via the project: Glacial flour as a new, climate-positive technology for sustainable agriculture in Greenland: NewLand.

References

Ahuja, L.R., Naney, J.W., Green, R.E., Nielsen, D.R., 1984. Macroporosity to characterize spatial variability of hydraulic conductivity and effects of land management. Soil Sci. Soc. Am. J. 48 (4), 699–702.
Ajayi, A.E., Horn, R., 2016. Transformation of ex-arable land to permanent grassland promotes pore rigidity and mechanical soil resilience. Ecol. Eng. 94, 592–598.
Al Majou, H., Bruand, A., Duval, O., 2008. Use of in situ volumetric water content to improve prediction of soil water retention properties. Can. J. Soil Sci. 88, 533–541.
Alakukku, L., Elonen, P., 1995. Long-term effects of a single compaction by heavy field traffic on yield and nitrogen uptake of annual crops. Soil Tillage Res. 36 (3), 141–152.
Arvidsson, J., Keller, T., 2004. Soil precompression stress: I. A survey of Swedish arable soils. Soil Tillage Res. 77 (1), 85–95.
Austrheim, G., Asheim, L., Bjarnason, G., Feilberg, J., Fosaa, A.M., Holand, O., Høegh, Jónsdóttir, I., Magnusson, B., Mortensen, L., Mysterud, A., Olsen, E., Skonhoft, A., Steinheim, G., Thorhallsdottir, A., 2008. Sheep grazing in the North Atlantic region: a long term perspective on management, resource economy and ecology. Rapport Zool. Seri. 3, 1–82.
Bachmann, J., Zhang, H., 1991. Die Stabilität von Sandböden in Abhängigkeit vom Gehalt an organischer Substanz und deren Humifizierungsgrad. Zeitschrift für Pflanzenernährung und Bodenkunde 154 (1), 47–52.
Barral, M.T., Arias, M., Guërif, J., 1998. Effects of iron and organic matter on the porosity and structural stability of soil aggregates. Soil Tillage Res. 46 (3), 261–272.
Benbi, D.K., Boparai, A.K., Brar, K., 2014. Decomposition of particulate organic matter is more sensitive to temperature than the mineral associated organic matter. Soil Biol. Biochem. 70, 183–192.
Besnard, E., Chenu, C., Balesdent, J., Puget, P., Arrouyas, D., 1996. Fate of particulate organic matter in soil aggregates during cultivation. Eur. J. Soil Sci. 47 (4), 495–503.
Beylich, A., Oberholzer, H.-R., Schrader, S., Höper, H., Wilke, B.-M., 2010. Evaluation of soil compaction effects on soil biota and soil biological processes in soils. Soil Tillage Res. 109 (2), 133–143.
Cappelen, J., 2008. Guide to climate data and information from the Danish Meteorological Institute. Tech. Rep. 12-08, DMI, Danish Meteorological Institute, Copenhagen, from http://www.dmi.dk/dmi/tr12-08 (visited online: Feb. 2019).
Cappelen, J., 2019. Guide to climate data and information from the Danish Meteorological Institute. Tech. Rep. 19–10, DMI, Danish Meteorological Institute, Copenhagen, from http://www.dmi.dk/dmi/tr19-10 (visited online: Feb. 2019).
Casagrande, A., 1936. The determination of pre-consolidation load and its practical significance. In: Proceedings of the First International Conference on Soil Mechanics and Foundation Engineering, vol. 3. Harvard University, Cambridge, MA, USA, pp. 60–64.
Caviezel, C., Hunziker, M., Kuhn, N.J., 2017. Bequest of the Norseman-The potential for agricultural intensification and expansion in southern Greenland under climate change. Land 6 (4), 1–20.
Chan, K.Y., 2001. Soil particulate organic carbon under different land use and management. Soil Use Manage. 17 (4), 217–221.
Dawidowski, J.B., Koolen, A.J., 1994. Computerized determination of the preconsolidation stress in compaction testing of field core samples. Soil Tillage Res. 31 (2), 277–282.
Dexter, A.R., Richard, G., Arrouays, D., Czyż, E.A., Jolivet, C., Duval, O., 2008. Complexed organic matter controls soil physical properties. Geoderma 144 (3), 620–627.
Dörner, J., Dec, D., Zúñiga, F., Sandoval, P., Horn, R., 2011. Effect of land use change on Andosol's pore functions and their functional resilience after mechanical and hydraulic stresses. Soil Tillage Res. 115–116, 71–79.
Dunnett, C.W., 1955. A multiple comparison procedure for comparing several treatments with a control. J. Am. Stat. Assoc. 50 (272), 1096–1121.
Federer, C.A., Turcotte, D.E., Smith, C.T., 1993. The organic fraction–bulk density relationship and the expression of nutrient content in forest soils. Can. J. For. Res. 23 (6), 1026–1032.
Flint, L.E., Flint, A.L., 2002. Particle density. In: Dane, J.H., Topp, G.C. (Eds.), Methods of Soil Analysis: Part 4 Physical Methods. Vol. 4 of 5. SSSA Book Series, Madison, Wisconsin, Ch. 2.2, pp. 229–240.
Gee, G.W., Or, D., 2002. Particle-size analysis. In: Dane, J.H., Topp, G.C. (Eds.), Methods of Soil Analysis: Part 4 Physical Methods. Vol. 4 of 5. SSSA Book Series, Madison, Wisconsin, Ch. 2.4, pp. 255–293.
Ghezzehei, T.A., Or, D., 2001. Rheological properties of wet soils and clays under steady and oscillatory stresses. Soil Sci. Soc. Am. J. 65 (3), 624–637.
Gregory, A.S., Watts, C.W., Griffiths, B.S., Hallett, P.D., Kuan, H.L., Whitmore, A.P., 2009. The effect of long-term soil management on the physical and biological resilience of a range of arable and grassland soils in England. Geoderma 153 (1), 172–185.
Gregory, A.S., Whalley, W.R., Watts, C.W., Bird, N.R.A., Hallett, P.D., Whitmore, A.P., 2006. Calculation of the compression index and precompression stress from soil compression test data. Soil Tillage Res. 89 (1), 45–57.
Gupta, S.C., Bradford, J.M., Drescher, A., 2002. Soil compressibility. In: Dane, J.H., Topp, G.C. (Eds.), Methods of Soil Analysis: Part 4 Physical Methods. Vol. 4 of 5. SSSA Book Series, Madison, Wisconsin, Ch. 2.10, pp. 399–415.
Gupta, S.C., Larson, W.E., 1979. A model for predicting packing density of soils using particle-size distribution. Soil Sci. Soc. Am. J. 43 (4), 758–764.
Heard, J.R., Kladivko, E.J., Mannering, J.V., 1988. Soil macroporosity, hydraulic conductivity and air permeability of silty soils under long-term conservation tillage in Indiana. Soil Tillage Res. 11 (1), 1–18.
Henriksen, N. nad Higgins, A.K., Kalsbeek, F., Pulvertaft, T.C.R., 2009. Greenland from Archaean to Quaternary. Descriptive text to the 1995 Geological map of Greenland, 1:2 500 000. Geological Survey of Denmark and Greenland Bulletin 18, 126 pp. + map.
Håkansson, I., Voorhees, W.B., Riley, H., 1988. Vehicle and wheel factors influencing soil compaction and crop response in different traffic regimes. Soil Tillage Res. 11 (3), 239–282, proceedings 11th Conference of ISTRO: Tillage and Traffic in Crop Production.
Hollander, M., Wolfe, D.A., Chicken, E., 2013. Nonparametric statistical methods, third ed., vol. 751. John Wiley & Sons, Hoboken, New Jersey.
Horn, R., 2003. Stress-strain effects in structured unsaturated soils on coupled mechanical and hydraulic processes. Geoderma 116 (1–2), 77–88.
Horn, R., Domżał, H., Słowińska-Jurkiewicz, A., van Ouwerkerk, C., 1995. Soil compaction processes and their effects on the structure of arable soils and the environment. Soil Tillage Res. 35 (1), 23–36.
Horn, R., Fleige, H., 2003. A method for assessing the impact of load on mechanical stability and on physical properties of soils. Soil Tillage Res. 73 (1–2), 89–99.
Imhoff, S., Da Silva, A.P., Fallow, D., 2004. Susceptibility to compaction, load support capacity, and soil compressibility of Hapludox. Soil Sci. Soc. Am. J. 68 (1), 17–24.
Inouye, D.W., 2000. The ecological and evolutionary significance of frost in the context of climate change. Ecol. Lett. 3 (5), 457–463.
Jacobsen, N.K., 1987. Studies on soils and potential for soil erosion in the sheep farming area of South Greenland. Arct. Alp. Res. 19 (4), 498–507.
Junior, M.S.D., Pierce, F.J., 1995. A simple procedure for estimating preconsolidation pressure from soil compression curves. Soil Technol. 8 (2), 139–151.
Keller, T., Arvidsson, J., Dawidowski, J.B., Koolen, A.J., 2004. Soil precompression stress: II. A comparison of different compaction tests and stress-displacement behaviour of the soil during wheeling. Soil Tillage Res. 77 (1), 97–108.
Keller, T., Lamandé, M., 2010. Challenges in the development of analytical soil compaction models. Soil Tillage Res. 111 (1), 54–64.
Keller, T., Lamandé, M., Schjønning, P., Dexter, A.R., 2011. Analysis of soil compression curves from uniaxial confined compression tests. Geoderma 163 (1), 13–23.
Kirschbaum, M.U.F., 1995. The temperature dependence of soil organic matter decomposition, and the effect of global warming on soil organic C storage. Soil Biol. Biochem. 27 (6), 753–760.
Koolen, A.J., 1974. A method for soil compactibility determination. J. Agric. Eng. Res. 19 (3), 271–278.
Kruskal, W.H., Wallis, W.A., 1952. Use of ranks in one-criterion variance analysis. J. Am. Stat. Assoc. 47 (260), 583–621.
Lamandé, M., Schjønning, P., Labouriau, R., 2017. A novel method for estimating soil

precompression stress from uniaxial confined compression tests. Soil Sci. Soc. Am. J. 81 (5), 1005–1013.
Lebert, M., Horn, R., 1991. A method to predict the mechanical strength of agricultural soils. Soil Tillage Res. 19 (2), 275–286.
Lehrsch, G.A., Sojka, R.E., Carter, D.L., Jolley, P.M., 1991. Freezing effects on aggregate stability affected by texture, mineralogy, and organic matter. Soil Sci. Soc. Am. J. 55 (5), 1401–1406.
Lindhardt, B., Abildtrup, C., Vosgerau, H., Olsen, P., Torp, S., Iversen, B.V., Jørgensen, J. O., Plauborg, F., Rasmussen, P., Gravesen, P., 2001. The Danish pesticide leaching assessment programme. Site characterization and monitoring design, GEUS, Copenhagen, Denmark.
Lipiec, J., Stepniewski, W., 1995. Effects of soil compaction and tillage systems on uptake and losses of nutrients. Soil Tillage Res. 35 (1), 37–52.
Mann, H.B., Whitney, D.R., 1947. On a test of whether one of two random variables is stochastically larger than the other. Ann. Math. Stat. 18 (1), 50–60.
Masís-Mendélez, F., Deepagoda, T.K.K.C., de Jonge, L.W., Tuller, M., Moldrup, P., 2014. Gas diffusion-derived tortuosity governs saturated hydraulic conductivity in sandy soils. J. Hydrol. 512, 388–396.
MATLAB and Statistics Toolbox, 2018. version 9.5.0 (R2018b). The MathWorks Inc., Natick, Massachusetts.
McBride, R.A., Watson, G.C., 1990. An investigation of the re-expansion of unsaturated, structured soils during cyclic static loading. Soil Tillage Res. 17 (3), 241–253.
Moldrup, P., Olesen, T., Komatsu, T., Schjønning, P., Rolston, D.E., 2001. Tortuosity, diffusivity, and permeability in the soil liquid and gaseous phases. Soil Sci. Soc. Am. J. 65 (3), 613–623.
Oztas, T., Fayetorbay, F., 2003. Effect of freezing and thawing processes on soil aggregate stability. Catena 52 (1), 1–8.
Pagliai, M., Marsili, A., Servadio, P., Vignozzi, N., Pellegrini, S., 2003. Changes in some physical properties of a clay soil in central Italy following the passage of rubber tracked and wheeled tractors of medium power. Soil Tillage Res. 73 (1), 119–129.
Paradelo, M., Norgaard, T., Moldrup, P., Ferré, T.P.A., Kumari, K.G.I.D., Arthur, E., de Jonge, L.W., 2015. Prediction of the glyphosate sorption coefficient across two loamy agricultural fields. Geoderma 259–260, 224–232.
Park, T., Ganguly, S., Tømmervik, H., Euskirchen, E.S., Høgda, K.-A., Karlsen, S.R., Brovkin, V., Nemani, R.R., Myneni, R.B., 2016. Changes in growing season duration and productivity of northern vegetation inferred from long-term remote sensing data. Environ. Res. Lett. 11 (8), 084001.
Perie, C., Ouimet, R., 2008. Organic carbon, organic matter and bulk density relationships in boreal forest soils. Can. J. Soil Sci. 88 (3), 315–325.
Peth, S., Horn, R., 2006. Consequences of grazing on soil physical and mechanical properties in forest and tundra environments. In: Forbes, B.C., Bölter, M., Müller-Wille, L., Hukkinen, J., Müller, F., Gunslay, N., Konstantinov, Y. (Eds.), Reindeer Management in Northernmost Europe: Linking Practical and Scientific Knowledge in Social-Ecological Systems. vol. 184, Springer, Berlin Heidelberg, Berlin, Heidelberg, Ch. 11, pp. 217–243.
Ramesh, T., Bolan, N.S., Kirkham, M.B., Wijesekara, H., Kanchikerimath, M., Rao, C.S., Sandeep, S., Rinklebe, J., Ok, Y.S., Choudhury, B.U., Wang, H., Tang, C., Wang, X., Song, Z., Freeman, O.W., 2019. Soil organic carbon dynamics: Impact of land use changes and management practices: A review. In: Sparks, D.L. (Ed.), Advances in Agronomy. Vol. 156 of Advances in Agronomy. Academic Press, Ch. 1, pp. 1–107.
Rücknagel, J., Hofmann, B., Paul, R., Christen, O., Hülsbergen, K.-J., 2007. Estimating precompression stress of structured soils on the basis of aggregate density and dry bulk density. Soil Tillage Res. 92 (1), 213–220.
Reykdal, I., Sveinsson, S., Dalmannsdóttir, S., Martin, P., íGerðinum, J.I., Kavanagh, V., Frederiksen, A., Hermannsson, J., Apr. 2016. Northern cereals - New opportunities. Final report, NORA.
Rousseeuw, P.J., Croux, C., 1993. Alternatives to the median absolute deviation. J. Am. Stat. Assoc. 88 (424), 1273–1283.
Salire, E.V., Hammel, J.E., Hardcastle, J.H., 1994. Compression of intact subsoils under short-duration loading. Soil Tillage Res. 31 (2), 235–248.
Sandén, T., Lair, G.J., Van Leeuwen, J.P., Gísladóttir, G., Bloem, J., Ragnarsdóttir, K.V., Steffens, M., Blum, W.E.H., 2017. Soil aggregation and soil organic matter in conventionally and organically farmed Austrian Chernozems. Die Bodenkultur: J. Land Manage. Food Environ. 68 (1), 41–55.
Schäffer, B., Stauber, M., Müller, R., Schulin, R., 2007. Changes in the macro-pore structure of restored soil caused by compaction beneath heavy agricultural machinery: a morphometric study. Eur. J. Soil Sci. 58 (5), 1062–1073.
Schjønning, P., van den Akker, J.J.H., Keller, T., Greve, M.H., Lamandé, M., Simojoki, A., Stettler, M., Arvidsson, J., Breuning-Madsen, H., 2015. Driver-Pressure-State-Impact-Response (DPSIR) analysis and risk assessment for soil compaction - A European perspective. In: Sparks, D.L. (Ed.), Advances in Agronomy. Vol. 133 of Advances in Agronomy. Academic Press, Ch. 5, pp. 183–237.
Schjønning, P., McBride, R.A., Keller, T., Obour, P.B., 2017. Predicting soil particle density from clay and soil organic matter contents. Geoderma 286, 83–87.
Six, J., Elliott, E.T., Paustian, K., Doran, J.W., 1998. Aggregation and soil organic matter accumulation in cultivated and native grassland soils. Soil Sci. Soc. Am. J. 62 (5), 1367–1377.
Soil Survey Staff, 1999. A basic system of soil classification for making and interpreting soil surveys. Agricultural Handbook 436, Natural Resources Conservation Service, USDA, Washington DC, USA.
Stone, J.A., Larson, W.E., 1980. Rebound of five one-dimensionally compressed unsaturated granular soils. Soil Sci. Soc. Am. J. 44 (4), 819–822.
Terzaghi, K., 1925. Erdbaumechanik auf bodenphysikalischer Grundlage. F. Deuticke, Leipzig, Vienna.
Styrelsen for Dataforsyning og Effektivisering, 2018. Grønland 1:250.000. https://download.kortforsyningen.dk/content/groenland-1250000, (Agency for Data Supply and Efficiency; visited online: Feb. 2019).
Trükmann, K., Horn, R., Reintam, E., 2009. Impact of roots on soil stabilization in grassland. ISTRO 18th Triennial Conference Proceedings T4-022, 1–7.
Tukey, J.W., 1977. Exploratory Data Analysis. Addison-Wesley, Boston, Bonn.
Whalley, W.R., Dumitru, E., Dexter, A.R., 1995. Biological effects of soil compaction. Soil Tillage Res. 35 (1), 53–68.
Wiesmeier, M., Steffens, M., Mueller, C.W., Kölbl, A., Reszkowska, A., Peth, S., Horn, R., Kögel-Knabner, I., 2012. Aggregate stability and physical protection of soil organic carbon in semi-arid steppe soils. Eur. J. Soil Sci. 63 (1), 22–31.
IUSS Working Group WRB, 2015. World Reference Base for Soil Resources 2014, update 2015 International soil classification system for naming soils and creating legends for soil maps. World Soil Resources Reports No. 106. FAO, Rome.
Xie, S.-B., Jian-jun, Q., Yuan-ming, L., Zhi-wei, Z., Xiang-tian, X., 2015. Effects of freeze-thaw cycles on soil mechanical and physical properties in the Qinghai-Tibet plateau. J. Mt. Sci.-Engl. 12 (4), 999–1009.
Zhang, B., Horn, R., Hallett, P.D., May 2005. Mechanical resilience of degraded soil amended with organic matter. Soil Sci. Soc. Am. J. 69 (3), 864–871.
Zhang, H.Q., Hartge, K.H., 1990. Die Kohäsion ungesättigter Sandböden und deren Beeinflussung durch organische Substanz. Zeitschrift für Pflanzenernährung und Bodenkunde 3 (4), 311–326.
Zhang, X.-H., Li, L.-Q., Pan, G.-X., 2007. Topsoil organic carbon mineralization and CO2 evolution of three paddy soils from South China and the temperature dependence. J. Environ. Sci. 19 (3), 319–326.

C. Paper III

published as:
Pesch, C., Weber, P. L., de Jonge, L. W., Greve, M. H., Norgaard, T., & Moldrup, P. (2021). Soil–air phase characteristics: Response to texture, density, and land use in Greenland and Denmark. *Soil Science Society of America Journal*, *85*(5), 1534–1554. doi: 10.1002/saj2.20284

Received: 5 March 2021 | Accepted: 27 May 2021

DOI: 10.1002/saj2.20284

Soil Science Society of America Journal

SOIL PHYSICS & HYDROLOGY

Soil–air phase characteristics: Response to texture, density, and land use in Greenland and Denmark

Charles Pesch[1] | **Peter Lystbæk Weber**[2] | **Lis Wollesen de Jonge**[2] | **Mogens Humlekrog Greve**[2] | **Trine Norgaard**[2] | **Per Moldrup**[1]

[1] Dep. of the Built Environment, Faculty of Engineering and Science, Aalborg Univ., Thomas Manns Vej 23, Aalborg DK-9220, Denmark

[2] Dep. of Agroecology, Faculty of Techincal Sciences, Aarhus Univ., Blichers Allé 20, P.O. Box 50, Tjele DK-8830, Denmark

Correspondence
Charles Pesch, Dep. of the Built Environment, Faculty of Engineering and Science, Aalborg Univ., Thomas Manns Vej 23, Aalborg, Denmark, DK-9220.
Email: cp@civil.aau.dk

Assigned to Associate Editor Xiao Yan Li.

Funding information
Teknologi og Produktion, Det Frie Forskningsråd, Grant/Award Number: 8022-00184B

Abstract

Soil aeration is a key parameter for sustainable and productive agriculture. The intensification of agricultural activity in Greenland involves land use (LU) and LU change, affecting the soil–air phase. The combined effects of natural compaction (bulk density, ρ_b), texture (texture uniformity index; TUI), and LU on the soil–air phase of subarctic soils are not well known. This study aims to identify and compare the main drivers for air-filled porosity (ε) and soil-structure changes within and across sites in Greenland and Denmark. We analyzed comprehensive data sets of ε, relative gas diffusivity D_p/D_o), and air-permeability (k_a) measured on intact soil samples from South Greenland (pasture) and Denmark (cultivated, urban, and forest). The mechanical robustness of the air phase was evaluated by linear models of ε as a function of ρ_b (*H*-model). The ratio of k_a to D_p/D_o served as a soil-structure index (Ω); the latter significantly correlated to TUI. The Greenlandic pasture soils did not show signs of well-developed soil structure (low Ω-values), whereas low *H*-values suggested the soils were mechanically robust compared to similar-textured cultivated soils. The soil–air characteristic curve (ε vs. pF) was parameterized, and the moisture control parameter was accurately predicted by TUI and LU (R^2 = .95). Overall, the ρ_b was found to control the air-phase functions within a field. However, considering changes in ε-levels across different fields, texture, LU, and other environmental factors became statistically more relevant than ρ_b. A modeled response surface for changes in ε with soil conditions may, in perspective, be useful for better-predicting gas transport in soil, both within and across fields.

1 | INTRODUCTION

For many decades, soil aeration has been extensively studied in relation to plant and root growth (Cannon & Free, 1917; Stepniewski et al., 2011; Williamson, 1964) or for monitoring and remediation of subsurface contamination (Poulsen et al., 1998, 1999). The climatic effects due to the emissions of radiatively active gases from the subsurface to the atmosphere have been widely acknowledged (Ball, 2013; Gregorich et al., 2005; Smith et al., 2012), and methods to estimate, simulate, and reduce these emissions are continuously being refined (e.g., Deepagoda et al., 2011b; Johnson et al., 2007; Li et al., 2017).

Abbreviations: LU, land use; MRS, modeled response surface; OC, organic carbon content; SL-SAC, soil–air characteristic curve; TUI, texture uniformity index.

The soil's structure plays a paramount role in soil aeration and gas-exchange processes, and a multitude of factors controls it. The underlying controlling and regulating entities are the geological background, which governs the availability of the basic mineral material; the climatic conditions, which control weathering, biological. and anthropogenic processes (Folkoff & Meentemeyer, 1987; Kerr, 1952; Reynolds, 1971); and time (Egli et al., 2018; Uteau et al., 2013).

A major component of soil-structure development is the soil's potential to form aggregates. The formation and stability of soil aggregates are to a large extent controlled by texture (Wagner et al., 2007), microbial activity, and soil-organic matter quality (Annabi et al., 2011), whereby the latter two, in particular, are substantially influenced by land use (LU) and land management (Ball et al., 1997; Bottinelli et al., 2017).

To study the effect of cold climatic conditions and time on the development of agriculturally exploited soils, the western part of South Greenland is ideal. With an annual average temperature of 1.2 ˚C and a cumulative precipitation of 612.9 mm (Narsarsuaq, 1961–2018; Cappelen, 2019), the area is situated at the climatic limits at which agricultural production is feasible. In some areas, the rather recent retraction of glaciers (Carlson et al., 2014) formed relatively young soils compared to soils found in temperate regions. Agricultural activity in Greenland mainly consists of sheep-husbandry. The necessary winter-fodder production is carried out on low-lying, more or less fertile, generally sandy lands, whereas the areas at higher elevations are used as summer pastures. Climate change might alter the accustomed agricultural methods toward a more labor-intensive practice and entail a change in LU and land management, which, in turn, eventually will change the current soil-ecological equilibrium.

Changes in soil structure can be characterized by changes in the pore-size distribution of the porous soil-matrix. The pore size distribution may be altered by compaction due to climate, land-cover, and agricultural activity by, for example, cattle and field-traffic. Changes in bulk density (ρ_b) are directly reflected in the pore-size distribution. Compaction obviously results in an overall reduction of the total porosity (Φ), but more importantly, it results in a shift in the pore-size distribution with a reduction of the macroporosity ($D_\phi > 30$ µm, pore diameter D_ϕ) and an increase in micro-porosity ($D_\phi <$ 6 µm) (Lipiec et al., 2012). Dörner et al. (2016) and Dlapa et al. (2020) showed that LU and LU change had significant negative effects on the water-retention and air-phase characteristics in terms of soil-aeration processes.

Several studies have shown that soil structure and air-phase tortuosity could be quantified and qualified by gas-flow measurements (e.g., air permeability, relative gas diffusivity, and combinations of both) through the porous medium. Deepagoda et al. (2012) revealed that changes in the connectivity-tortuosity parameter X (Buckingham, 1904; Currie, 1960a), along a moisture gradient, could be used to differentiate between inter- and intra-aggregate pore space. Moldrup et al. (2003a) used the equivalent pore diameter to characterize the pore connectivity, and thus the presence of soil structure, along a soil–water potential gradient of differently textured soils exhibiting different LU and management. A similar approach was used by Kawamoto et al. (2006), who related air permeability to relative diffusivity measurements, where the latter was estimated by the relation suggested by Moldrup et al. (2000b) and solely relying on ε measurements at a fixed soil–water potential.

More complex prediction models incorporate soil-type dependent information (Moldrup et al., 2000b), generally in the form of a parameter describing the water retention characteristic. Moldrup et al. (1996) used the well-known Campbell (1974) water retention model to predict gas diffusivity; Moldrup et al. (1999) extended the approach into the Buckingham–Burdine–Campbell gas diffusivity model. Similar power law models exist for modeling the air permeability of variably saturated soils (Assouline et al., 2016; Kawamoto et al., 2006). The interested reader may also refer to the comprehensive work on air permeability models carried out by Yang et al. (2021).

The above-mentioned studies revealed that the gaseous exchange processes within the soil and between soil and atmosphere heavily rely on the pore-space available for gas transport (i.e., the air space not filled by water). However, many of the available prediction models for gas transport parameters incorporate some form of water-retention parameters, which do not represent the air-filled, but the water-filled, porosity and thus not taking into account the potentially significant differences in the variability of the air-filled porosity compared to water-filled porosity.

Instead of parameters derived from the soil–water retention curve, the use of derived parameters from a soil–air characteristic curve (SL-SAC) in soil–air function predictions would be more straightforward and might eventually reduce the not-explained variability of those models.

Core Ideas

- We analyzed air-phase characteristics of Danish and Greenlandic soils.
- The air phase revealed within-field variability not captured by the water phase.
- Structure-related fingerprints differentiated between land use and texture.
- The across-field air-phase characteristic was accurately predicted by land use and texture.
- The air-filled porosity was precisely estimated by a modeled response surface.

TABLE 1 Geographical information of the sites the samples were collected from and the soil classification according to Soil Survey Staff (1999)

Site	Country	Coordinates	Soil classification[a]	Reference
Jyndevad*		54°53′37″, 9°7′12″ E	Humic Psammentic Dystrudept	Masís-Meléndez et al. (2014)
Tylstrup*		57°10′47″ N, 9°57′24″ E	Abrupt/Aqua Argiudoll, Frangiaquic Glossudalf	Karup et al. (2016)
Estrup*	Denmark	55°29′10″ N, E 9°4′9″ E	Alfic Argiudoll, Typic Hapludoll	Paradelo et al. (2015)
Silstrup*		56°55′56″ N, E 8°38′44″ E	Aquic Palehumults	Norgaard et al. (2013)
Voldbjerg		56°18′71″ N, E 8°54′87″ E	Lithic Dystrocryept	Karup et al. (2016)
South Igaliku 1 & 2	Greenland	60°53′29″ N, 45°16′28″ W	Psammentic Dystrocryept	Weber et al. (2020); Pesch et al. (2020)
South Igaliku 3		60°51′39″ N, 45°16′26″ W	Typic Dystrocryept	
Igaliku 1		61°1′9″ N, 45°27′39″ W	Typic Dystrocryept	Weber et al. (2020)
Igaliku 2		60°59′51″ N, 45°26′55″ W	Filled Anthropic soil	
Skellingsted	Denmark	55°35′25″ N, 11°27′44″ E	Mixed Anthropic soil	Poulsen et al. (2001)
Hjørring		57°27′34″ N, 10°0′1″ E	Spodosol (not further specified)	Moldrup et al. (2000b)
Poulstrup		57°21′30”N, 10°0′38″ E	Humic Psammentic Dystrudept	Kruse et al. (1996); Moldrup et al. (1996)

*Detailed monitoring site description can also be found in Lindhardt et al. (2001).

[a]If more than one classification per site is given, more than one soil profile was evaluated and different results were obtained.

The objective of this study is to understand how soil texture (texture uniformity), compaction (dry bulk density), and LU (LU type) combined affect key soil–gas phase parameters across moisture conditions (at different levels of soil–water matric potential, as quantified by pF). Specifically, we aim to

1. provide a dual-fingerprint for soil structure that in perspective may allow us to better predict the key soil–gas transport parameters (diffusivity and permeability), and
2. understand and quantify (by a modeled response surface) combined effects of dry bulk density and pF on air-filled porosity at given indices for LU and texture.

First, we illustrate that the water retention curve, the derived SL-SAC, and gas transport parameter curves (gas diffusivity and air permeability) vary considerably across and within fields with very different texture and LU. Second, we combine soil–gas phase parameters to make a dual-fingerprint of soil–gas phase behavior related to soil moisture level (pF). Third, and based on these analyses, we develop and verify a modeled response surface for the soil air-filled porosity by combining two linear models for changes in air-filled porosity with dry bulk density and with pF and with the slopes in the two models related to texture or LU indices, or both.

We base this three-part analyses on data from 966 intact soil core samples from 14 differently textured South Greenlandic (pasture) and Danish (cultivated, urban, and forest) soils, hereby representing a wide range of soil texture, compaction, and LU.

2 | MATERIAL AND METHODS

2.1 | Soils and soil sampling

In total, data from 966 individual, intact soil core samples (6.05 cm in diam., 3.48 cm height, resulting in a volume of 100 cm^3) was collected and evaluated. The soil cores originated from 14 different sites located across southwest Greenland and Denmark and included four different LU (cultivated, pasture, urban, and forest). Table 1 gives an overview of the sampling sites and soils used in this study. The Greenlandic data set consisted of five perennial pasture soils, and the sampling locations are shown in Figure 1. The Danish data set comprised five conventionally cultivated, two urban, and one forest soil. For the localization of the Danish soils, the reader may refer to the geographical coordinates given in Table 1.

The Greenlandic pasture and Danish cultivated soils were sampled in rectangular grids (15 m × 15 m, except South Igaliku 2, which was sampled in a 7.5-m × 7.5-m grid). The grid-sampled soil-cores were extracted from the soil's upper horizon from a depth varying between 5 and 15 cm.

The Danish cultivated soils were sampled throughout the peninsula of Jutland, and, in total, 551 individual soil cores were included in this study (226 individual sampling points, varying number of replicates per point). The soil textures

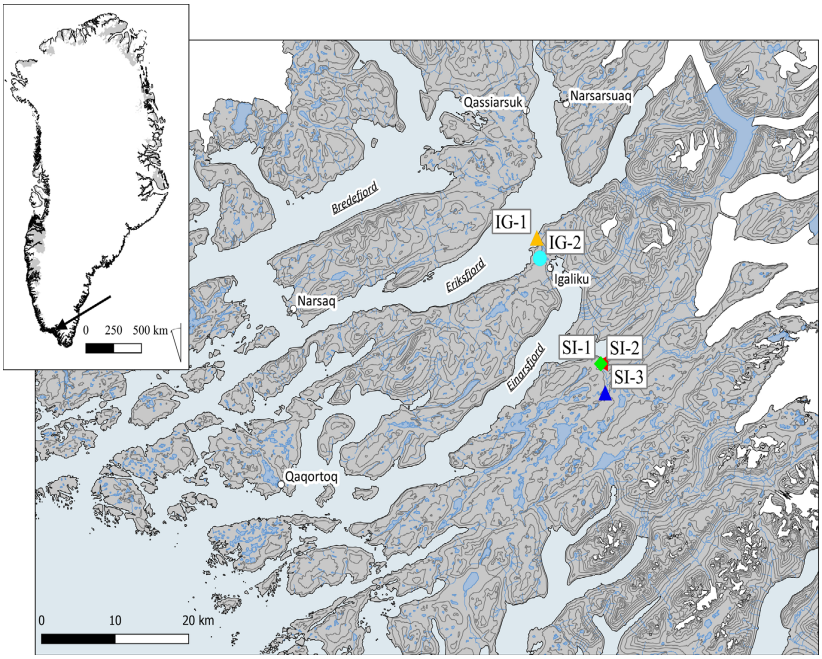

FIGURE 1 The five sampling sites in South Greenland

ranged from coarse sand (Jyndevad) to silty clay loam (Voldbjerg), covering the most abundant soil-textural classes of agriculturally exploited soils in Denmark. The sampling of the Danish cultivated soils was carried out between 2010–2014, and none of the fields were cultivated (plowed) approximately 1 yr prior to the sampling. The cultivated soils were previously published in other studies, and a detailed description of the different sites' geological background and land management can be found in the relevant studies (Hermansen et al., 2017; Karup et al., 2016; Katuwal et al., 2015; Masís-Meléndez et al., 2014; Norgaard et al., 2013; Paradelo et al., 2015). In addition, Jyndevad, Tylstrup, Estrup, and Silstrup are part of the Danish Pesticide Leaching Assessment Program, and detailed information about the specific sites can be found in Lindhardt et al. (2001).

The Greenlandic sites are described in Weber et al. (2020) and Pesch et al. (2020). In total, 396 individual soil core samples from five pasture fields from south-west Greenland were included in this study (132 individual sampling points, three replicates per point). The sampling was carried out in 2015 (South Igaliku 1, 2, and 3) and 2017 (Igaliku 1 and 2); the soil cover during sampling consisted of perennial grass, and besides field Igaliku-1, no cultivation or tillage was carried out at least 3 yr prior to the sampling. The grass cover is occasionally resown, especially if frost and water damage becomes prevalent. Tillage consists of disc harrowing (5-to-10-cm depth); plowing is generally avoided due to the high wind erosion hazard of the sandy to sandy-loamy soils, especially in combination with the frequent, intense katabatic winds in the area. To our knowledge, South Igaliku 1 and 2 have not been subjected to tillage during the last 20 yr and are used as pastures for grazing sheep. The fields Igaliku-1, Igaliku-2, and South Igaliku-3 are mainly used for winter fodder production.

To broaden the range of covered LU within this study, three additional sites exhibiting two different LU were included.

The soils categorized as urban soils were collected from a soil profile (Hjørring, North Jutland, Denmark) and from a subsoil transect (Skellingsted, Zealand, Denmark). The samples from Hjørring were collected during the drilling of a monitoring well on a former manufactured gas plant site. Subsamples of the initial drilling core samples (4-to-5- and 6-to-7-m soil depth) were taken at equal distance (0.4 m) throughout the soil profile. The samples from Skellingsted were collected along a transect on an abandoned landfill site from a depth of 70 cm, consisting of an artificially compacted, industrial sand cover-layer.

The forest soil samples (Poulstrup, North Jutland, Denmark) were collected from four different depth-intervals (0-to-5-, 5-to-10-, 10-to-15-, and 15-to-20-cm soil depth) below a deciduous forest. The forest soil data set was subdivided into two subsets due to the very distinct soil properties of the top and subsoil: Poulstrup topsoil comprised the two depth-intervals down to 10 cm, and Poulstrup subsoil consisted of the remaining 10-to-15-cm and 15-to-20-cm depth-intervals.

Along with the intact soil core samples, bulk soil from the same depth was collected at each sampling point for texture analysis in the laboratory. For the data analysis, the intact soil-core replicates per sampling point were treated as individual samples.

2.2 | Laboratory methods

2.2.1 | Basic soil characteristics

The bulk soil samples collected at each sampling point were air-dried and presieved (<2 mm) prior to texture analysis and organic carbon content (OC, in g g^{-1}) determination. The texture was determined using a combination of wet sieving and the hydrometer or pipette method, according to Gee and Or (2002). Total carbon was measured on ball-milled samples by dry combustion in combination with an infrared CO_2 detector. All the soils were free of carbonates, and the measured total carbon was thus set equal to organic carbon. The average particle density, ρ_s (g cm^{-3}), was estimated from organic matter and clay contents, according to Schjønning et al. (2017).

2.2.2 | Soil–water retention characteristics

To determine the water-retention characteristics, the intact soil core samples were saturated from below on a tension table and subsequently drained to all or to a selection of the following matric-potentials: ψ(cm H_2O) $\in\{-10, -30, -50, -100, -300, -500, -1{,}000\}$. The drainage procedure followed the procedure given in Dane and Hopmans (2002). Based on the magnitude of the intended negative soil–water potentials (ψ), different apparatus and procedures were used: hanging water column for $-100 \leq \psi \leq -10$, suction plate for $-500 \leq \psi \leq -100$, and pressure plates for $\psi \leq -500$.

After equilibration of the soil sample with the applied negative potential, the mass loss was determined on a laboratory scale and set equal to the gravimetric soil–water release during the drainage step. The volumetric water content, θ (cm^3 cm^{-3}) was obtained by multiplication of the gravimetric water content with the dry bulk density. The air-filled porosity, ε ($cm^3 \cdot cm^{-3}$) was obtained by $\varepsilon = \Phi - \theta$, with Φ ($cm^3 \cdot cm^{-3}$) being the total porosity.

2.2.3 | Soil–air phase functions

At each drainage step, the air permeability and the relative gas diffusivity were determined. The air permeability (k_a in μm^2) of the forest and urban soils were measured by the steady-state method, according to the procedure and device described in Iversen et al. (2001) and Ball and Schjønning (2002); the k_a of the cultivated and pasture soils was measured using the device described in Schjønning and Koppelgaard (2017), following the guidelines given in Ball and Schjønning (2002). The gaseous phase's diffusive movement through the unsaturated soil matrix was assessed by the non-steady, single-chamber method suggested by Taylor (1950) and further developed by Schjønning (1985). Oxygen was used as the diffusing agent, and the apparent diffusion coefficient of the soil, D_p (cm^2 s^{-1}) was calculated, according to Taylor (1950). The relative diffusivity, D_p/D_o (dimensionless), was then obtained by dividing D_p by the diffusion coefficient of oxygen in free air, $D_o = 0.205$ cm^2 s^{-1} at 20 °C (Schjønning et al., 2013). A comprehensive description of the different aspects and procedures of the measurement can be found in Rolston and Moldrup (2002).

After the final drainage step, the dry bulk density of the intact soil-core samples, ρ_b (g cm^{-3}), was measured after oven-drying for 24 to 48 h at 105 °C.

For the sake of simplicity, the soil–water potential is given as $pF = \log(-\psi)$ (Schofield, 1935).

In addition, two notations need to be defined: the notation across-field variation was defined as the variation of the field-averaged parameter in question between at least two fields, whereas the within-field variation covered variations inherent to one specific field. The field-average value of a soil property was calculated as the arithmetic mean of all the individual measurements available for the relevant property for a given field; its variation was assessed by the standard deviation and illustrated by error-bars in the figures.

2.3 | Models

2.3.1 | H-model

The within-field dependence of the air-filled porosity (ε) on the bulk density (ρ_b) for each soil–water potential level (pF) was assessed by fitting the linear function given in Equation 1 to the measured ε at each available drainage level and ρ_b. The model will hereafter be referred to as the *H*-model:

$$\varepsilon = -H \cdot \rho_b + C \quad (1)$$

where H and C represent the slope and the intercept, respectively. We thus obtained a maximum of seven individual

TABLE 2 *H*-indices for a theoretical pure sand from assumed ρ_b and θ_g ranges, determined by using Equation 1

θ_g	P_b	Φ	θ_v	ε	H
g g^{-1}	g cm^{-3}	cm^3 cm^{-3}			
0.05[a]	1.4	0.47	0.07	0.40	0.43
	1.6	0.40	0.08	0.32	
0.20[b]	1.4	0.47	0.28	0.19	0.58
	1.6	0.40	0.32	0.08	

Note. ρ_s was fixed to 2.65 g cm^{-3}. θ_g and θ_v denote the gravimetric and volumetric water contents, respectively.
[a]Dry soil, high pF.
[b]Wet soil, low pF.

regression lines per field (maximum of seven drainage steps), where *H* describes the sensitivity of the air-filled porosity to changes in natural compaction (ρ_b).

The *H*-range of a theoretical pure sand will be used to evaluate and contrast the *H*-values obtained on intact soil cores. The expected *H*-range for a pure sand at low and high moisture conditions can be estimated by assuming reasonable ρ_b and a θ_g ranges for such material. We used the soil conditions and properties given in Table 2. The *H*-values of the resulting theoretical pairs of measurements (ρ_b, ε) at the two moisture levels were then determined by fitting the *H*-model as given in Equation 1.

2.3.2 | Soil–air characteristic model

Similar to the Gregson et al. (1987) semilogarithmic model for soil–water retention, the variation of ε with varying moisture conditions can be approximated in the $\log(-\psi) - \varepsilon$ domain.

The resulting log-linear (semilogarithmic) SL-SAC exhibits two parameters: the reference air-filled porosity, ε_{ref}, which is the ε at the reference soil–water potential, pF_{ref}, and the soil–air characteristic parameter, *A*. The *A*-model is fully defined if ε_{ref} (location parameter) and *A* (shape parameter) are known:

$$\varepsilon = \varepsilon_{ref} - A \cdot \left(pF_{ref} - pF\right) \quad (2)$$

The introduction of a reference point other than the phase content at saturation [which would be $\varepsilon(\psi = 0) = 0$ in this case] is not a new concept, as it was already applied with success by other authors (Pittaki-Chrysodonta et al., 2018).

2.3.3 | Modeled response surface

The *A*- and *H*-models were eventually combined to express the air-filled porosity as a function of ρ_b and pF only. Substituting ε_{ref} in Equation 2 by the relation given in Equation 1 generates the multi-variable function given in Equation 3, and its output will be referred to as modeled response surface (MRS):

$$\varepsilon = [-H \cdot \rho_b + C] - A \cdot \left(pF_{ref} - pF\right) \quad (3)$$

The main model parameters *A* and *H* need to be known beforehand, and we will show over the course of this study that it is possible to predict both very accurately from basic soil properties.

2.3.4 | Gas-diffusion model

The diffusive gas movement in the soil–air phase, which originates from concentration gradients within the porous matrix, is the principal gaseous exchange process in the soil (Rolston & Moldrup, 2002). It can be evaluated by the relative gas diffusion coefficient or gas diffusivity, D_p/D_o, with D_p and D_o being the gas diffusion coefficient in the soil and in free air, respectively. Many studies (e.g., Buckingham, 1904; Currie, 1960b, 1961; Millington & Quirk, 1961; Moldrup et al., 2003b, 2004; Thorbjørn et al., 2008) have assumed or ascertained that D_p/D_o is governed to a large extend by texture, soil–air content (ε) and total porosity (Φ). Buckingham (1904) suggested that D_p/D_o follows a power function of ε:

$$D_p/D_o = \varepsilon^X \quad (4)$$

where *X* was later referred to as the connectivity-tortuosity parameter (Currie, 1960b, 1961).

2.3.5 | Ω-model

The contrasting behavior of advective and diffusive flows to the pore geometry (Millington & Quirk, 1964; Ball, 1981) enables a direct assessment of soil structure (Kawamoto et al., 2006; Eden et al., 2011; Arthur et al., 2012). Kawamoto et al. (2006) derived a prediction model for k_a from D_p/D_o, and a simplified version of the model is given in Equation 5:

$$k_a = \Omega \cdot \varepsilon^X, \quad \text{with } \varepsilon^X = (D_p/D_o) \quad (5)$$

where ε and *X* are the air-filled porosity and the connectivity-tortuosity parameter, respectively, and Ω is a soil-structure index. Kawamoto et al. (2006) found the best agreement between k_a and D_p/D_o for $\Omega = 700$, based on 25 differently textured soil layers. For soils exhibiting $\Omega > 700$, the advective flow exceeds the diffusive flow, and a more pronounced soil structure can be expected (larger connected macroporosity).

2.3.6 | TUI

Soil texture was characterized by the field-average ratios of the gravimetric contents of fine sand ($50 < D_e < 200$ µm, $D_e \times 50 < D_e < 200$ µm, where D_e denotes the equivalent particle diameter) and fine particles (fines, $D_e < 20$ µm), referred to as soil texture uniformity index (TUI, dimensionless). Fines and D_e represent the sum of the clay and fine silt fractions and the equivalent particle diameter, respectively:

$$\mathrm{TUI} = \mathrm{fS}/\mathrm{fines} \quad (6)$$

The fine fraction of the mineral soil ($D_e < 20$ µm) largely controls soil-aggregate formation, primarily by self-aggregation and complexation with available soil-organic matter (Chesters et al., 1957; Schjønning et al., 1999; Dexter et al., 2008). Because the soils considered in this study generally exhibited high ratios of organic matter to fine particles, the differences in the composition of the fine-textured mineral phase ($D_e < 200$ µm) become the main driver for aggregation and structure formation; the TUI describes these differences in a simple way. In addition, relations between coarse and fine particles were already found to be useful for successfully predicting hydraulic soil properties, which are undoubtedly closely related to soil structure (Arya & Paris, 1981; Nielsen et al., 2018).

2.4 | Statistical analysis

The Pearson correlation coefficient r assessed the linear correlation between two continuous variables. The significance level of any fitted or estimated parameter was depicted by asterisks appended as an exponent to the parameter in question, according to the levels of significance: $p \geq .05$; $*.01 \leq p < .05$; $**.01 < p \leq .001$; $***p < .001$; ns, no significance.

The linear relations between the investigated properties and parameters were evaluated by simple or multiple ordinary least-squares regressions. The goodness-of-fit and the model performance were judged by the ordinary and adjusted coefficient of determination, R^2 (simple) and R^2_{adj} (multiple), respectively, the root mean square error, and the Akaike information criterion (Sakamoto et al., 1986), specifically by the corrected Akaike information criterion, accounting for small sample sizes according to Sugiura (1978).

For determining the confidence and prediction intervals of the H-model's regression coefficients (Equation 1), we deployed a nonparametric bootstrapped regression scheme. The base for the computation of the required bootstrapped regression coefficients and statistics was the random resampling of pairs of observations with replacement (Efron, 1979, 1983; Stine, 1985). The resampling was based on 75% of the total number of available observations, and the resampling was repeated 1,000 times. The confidence and prediction intervals were computed as the 5.0% and 95.0% percentiles of the relevant bootstrapped parameter, leading to 90.0% ($\alpha = .10$) confidence and prediction intervals. The goodness-of-fit (only R^2) and the overall significance of the regression (p-value of the F-statistic) were given as mean values of the bootstrapped results.

The statistical analysis was entirely carried out in MATLAB and Statistics Toolbox (MathWorks, 2018).

3 | RESULTS AND DISCUSSION

3.1 | Combined effects of texture, density, and LU on gas-phase behavior

Table 3 lists the different particle size fractions, along with the number of samples and soil types (Soil Survey Staff, 1999). The sites were grouped according to their LU and ordered with an increasing fine particle content (fines, equivalent particle diameter $D_e < 20$ µm, i.e., the sum of the clay and fine silt fractions) within each group. For better legibility, texture and OC contents in Table 3 were given in grams per 100 grams. Following the definition of TUI, an additional subdivision had to be made within the silt and sand fractions: fine and coarse silt (2–20 and 20–50 µm), and fine and coarse sand (50–200 and 200–2,000 µm).

According to Table 3, the cultivated and urban soils generally showed lower OC contents than the pasture or forest soils; the opposite was true for the ρ_b. The field-average ρ_b were nonlinearly correlated to OC, as shown in Figure 2a. We chose to fit a power function to illustrate the nonlinear trend between OC and ρ_b, which has been expressed by exponential or reciprocal functions by other studies (Federer et al., 1993; Perie & Ouimet, 2008).

The fine sand/fines ratio (TUI) of the pasture soils exhibited a significant negative linear correlation with OC ($r = -.97^{***}$), and a linear regression based on the pasture soils resulted in a coefficient of determination of $R^2 = .95$, as shown in Figure 2. The forest soils followed the same linear trend as the pasture soils, whereas only a weak linear correlation between TUI and OC could be observed for the cultivated and urban soils (cultivated soils: $r = -.67$, ns), mainly due to the relatively small OC range of the latter (not shown).

The measured water- and air-phase parameters of all the samples used in this study are shown in Figure 3: the volumetric water content (θ, $cm^3\ cm^{-3}$), the air-filled porosity (ε, $cm^3\ cm^{-3}$), the relative gas-diffusivity (D_p/D_o, dimensionless), and the air-permeability (k_a, μm^2). The abscissa values (pF) of θ and ε in subfigures Figure 3a and 3b were shifted randomly within a narrow range (pF ± 0.5) around the true pF value to emphasize the number of measurements per soil–water potential. The used soils spanned a wide range of θ

TABLE 3 Summary table of the basic soil properties and the number of individual undisturbed soil core samples (number of sampling points per site in parentheses); soil type and particle size distribution; texture uniformity index, TUI (dimensionless); the organic carbon content (OC); the bulk density (ρ_b)

				Silt (2–50 µm)		Sand (50–2,000 µm)				
Site	Samples (& points)	Soil type USDA	Clay (< 2 µm)	Fine (<20 µm)	Coarse	Fine (<200 µm)	Coarse	TUI	OC	ρ_b
			g 100 g^{-1}						g 100 g^{-1}	g cm^{-3}
Jyndevad	88 (88)	S	4.2 (0.4)	3.7 (0.4)	1.0 (0.0)	23.4 (0.9)	64.4 (1.2)	3.0 (0.2)	1.8 (0.2)	1.38 (0.04)
Tylstrup	72 (36)	lS-sL	3.8 (0.2)	7.0 (0.9)	12.4 (1.5)	63.7 (1.8)	9.9 (1.3)	6.0 (0.7)	1.8 (0.1)	1.34 (0.05)
Estrup	135 (45)	sL-lS	10.9 (2.1)	12.4 (2.4)	12.5 (2.6)	22.5 (1.2)	37.0 (5.6)	1.0 (0.2)	2.6 (0.7)	1.36 (0.10)
Silstrup	180 (60)	sL-L	15.8 (1.3)	16.5 (1.0)	13.6 (1.3)	28.9 (1.4)	21.8 (1.8)	0.9 (0.1)	1.9 (0.1)	1.43 (0.07)
Voldbjerg	36 (9)	cL-ucL	31.5 (1.4)	22.9 (1.1)	18.8 (3.6)	13.0 (3.6)	9.3 (2.2)	0.3 (0.1)	2.6 (0.4)	1.26 (0.06)
South Igaliku-2	54 (18)	lS-sL	2.2 (0.4)	3.1 (0.5)	20.6 (1.6)	51.3 (3.5)	20.3 (3.8)	9.7 (0.9)	1.5 (0.3)	1.25 (0.06)
South Igaliku-1	96 (32)	lS-sL-S	2.9 (0.6)	3.5 (0.5)	18.0 (2.9)	48.4 (8.3)	23.3 (10.8)	7.8 (1.7)	2.2 (0.7)	1.07 (0.14)
South Igaliku-3	72 (24)	sL-lS	3.9 (0.8)	4.4 (1.4)	19.9 (3.2)	43.1 (4.6)	22.8 (7.4)	5.6 (1.5)	3.4 (1.1)	1.05 (0.16)
Igaliku-1	84 (28)	sL	4.4 (0.8)	8.7 (0.7)	22.8 (2.3)	37.2 (4.2)	15.5 (5.8)	3.0 (0.4)	6.6 (1.1)	0.92 (0.11)
Igaliku-2	90 (30)	sL	4.9 (0.7)	9.1 (0.6)	22.6 (1.3)	36.8 (3.0)	16.4 (2.3)	2.8 (0.4)	5.9 (1.0)	0.95 (0.08)
Skellingsted	9 (t[a])	lS	5.0 (–)	2.0 (–)	6.4 (–)	23.8 (—)	61.1 (–)	3.4 (–)	1.0 (–)	1.71 (0.04)
Hjørring	10 (2[b])	L-sL	13.6 (2.3)	8.3 (2.9)	24.6 (5.0)	50.6 (10.8)	0.9 (0.4)	2.8 (1.7)	1.1 (0.1)	1.69 (0.08)
Poulstrup subsoil	18 (2[b])	lS	3.8 (0.3)	2.7 (0.3)	11.1 (0.2)	56.0 (0.1)	12.3 (0.2)	9.3 (0.2)	2.3 (0.1)	1.22 (0.06)
Poulstrup top-soil	18 (2[b])	ND	ND	ND	ND	ND	ND	ND	10.9 (3.5)	0.59 (0.08)

Note. All displayed figures are mean values, and the figures in parentheses represent the standard deviation. S, sand; lS, loamy sand; SL, sandy loam; L, loam; cL, clay loam; ucL, uncultivated clay loam; ND, not determined.

[a]Transect.

[b]Number of sampled soil-horizons (depths).

and of ε, and the median θ and ε at each soil–water potential of three selected soils (A: Igaliku-2, subarctic pasture; B: Skellingsted, urban; and C: Poulstrup, subsoil, temperate forest) were connected by a stepwise linear interpolation polynomial to illustrate the evolution of θ and ε of the three soil-types during drainage. The diffusive and convective mass transport parameters in the gas phase, D_p/D_o and k_a, respectively, are displayed in Figure 3c and 3d. As an illustrative example, the best-fit lines of the D_p/D_o and k_a models (Equation 4 and Equation 5) for the three above-mentioned soils were added to Figure 3c and 3d, respectively.

The fitted connectivity-tortuosity parameter, X (Figure 3c), significantly correlated to ρ_b ($r = -.81^{***}$); furthermore, a linear regression explained 79% of the variation (Figure 4a). Several other studies (Deepagoda et al., 2011a; Masís-Meléndez et al., 2015) found similar linear correlations between the total porosity or derivations of the latter and X; given the direct linear dependence of Φ on ρ_b, those correlations can be considered as equivalent. Soils showing high X exhibited a more tortuous pore network (Deepagoda et al., 2012), which basically could be traced back to an increase in the amount of parallel and well-connected pores with increasing bulk density, according to Poulsen et al. (2001). In general, the pasture and forest soils showed a more tortuous pore network than the cultivated and urban soils.

The fitted soil-structure index, Ω (Figure 3d), correlated significantly with the TUI (both in log-scale, $r = -.84^{***}$), and a linear regression resulted in a coefficient of determination of $R^2 = .75$ as shown in Figure 4b. A well-developed soil structure ($\Omega > 700$) could be observed for soils exhibiting a gravimetric fine sand content smaller than 1.54 times the fine particles content (intersection of the trend-line $\Omega = f$(fine sand/fines) and the dashed horizontal line at $\Omega = 700$). The significant correlation suggested that the amount of fine material was a strong driver for soil-structure development. The Greenlandic pasture soils exhibited relatively high fine sand contents compared to the amount of fines, and none of the pasture soils showed signs of well-developed soil structure. The trend-line given in Figure 4b indicated that the proportionality between D_p/D_o and k_a was highly dependent on the soil's aggregation potential, especially considering the logarithmic scale of both variables.

The considerable effect of compaction (ρ_b) on the air-phase parameters (ε, D_p/D_o, and k_a) is illustrated in Figure 5. For this purpose, we chose the relatively homogeneous Silstrup field and defined three levels of compaction (low, median, and high), where the degree of compaction was represented by ρ_b. The θ, ε, D_p/D_o, and k_a of each level of compaction was represented by the arithmetic average of the measures of three samples exhibiting the lowest,

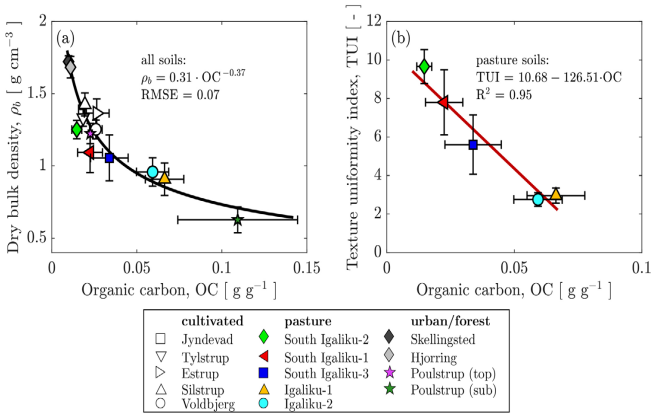

FIGURE 2 (a) The nonlinear relation between field-averaged organic carbon content (OC) and bulk density (ρ_b). (b) Across-field relation between the OC and the ratio of fine sand to fines (texture uniformity index, TUI) and best linear fit for the pasture soils (five soils). RMSE, root mean square error of approximation. The symbols are within-field mean values, and the error-bars depict the standard deviation

the closest to the calculated median, and the highest ρ_b, respectively.

The soil–water retention curves at the three levels of compaction, given in Figure 5a, were only marginally different from each other, whereas the air-filled porosity curves (Figure 5b) showed considerable differences between each other. The simultaneous look at the water retention and air-filled porosity curves clearly revealed that the differences in available space for gaseous exchange could not be captured by the positions (vertical displacement) of the water retention curves. The ρ_b primarily acts on the total porosity (Φ) and, by that, defining the total void space. The effect of decreasing ρ_b was carried over to the air-phase functions via a higher available pore space for gas transport at each moisture level, as shown in Figure 5c and 5d. It was evident that the within-field variation could not be neglected for either the diffusive or the advective flows.

3.2 | Dual-fingerprint for functional soil structure (air space and gas transport)

In the following, the *H*-model will be applied to investigate further the dependence of ε on ρ_b for different moisture conditions.

3.2.1 | Application of the H-model

Figure 6 visualizes the considerable differences in the gradual increase of air-filled porosity during drainage for two typical soils: a relatively compact and homogeneous, conventionally cultivated temperate soil which was classified as a sandy loam (Silstrup, Denmark) and a perennial pasture soil, which showed considerably lower ρ_b, classified as sandy loam from subarctic South Greenland (Igaliku-2, Greenland). Note that no measurements at pF 1.0 of the Silstrup soil were available.

We observed not only an overall dependence of ε on ρ_b, but the different soils also exhibited a different dependence on ρ_b, if subjected to different moisture conditions (e.g., monotonically increasing absolute slope versus variable slope with increasing absolute soil–water potential for Silstrup and Igaliku-2, respectively). As an illustrative example, the *H*-model (Equation 1) was applied to the pairs of measurements at pF 3.0. It is clear from Figure 6a and 6b that, although the subarctic pasture soil exhibited significantly lower ρ_b, and therefore a greater Φ than the cultivated sandy loam, the lack of soil structure and the high tortuosity of the pore network had significant effects on the drainage behavior, especially at lower soil–water potentials (pF $\leq$ 1.7).

The dependencies of ε on ρ_b at pF 2.7 ($\psi = -500$ cm H_2O) for all the soils used in this study are shown in Figure 6c, and the applied *H*-model for the chosen pF-level is displayed in Figure 6d as an illustrative example. At pF 2.7, the pores exhibiting a diameter of $D_\phi \geq 6$ µm were drained, according to the capillary rise equation (Schjønning, 1992).

The *H*-model was fitted using a bootstrapped regression scheme to the pairs of (ρ_b, ε) of each soil at each available drainage level, and both, the goodness of fits and significance criteria, were generally high with an increased performance for higher pF. The detailed results of the bootstrapped regression analysis can be found in Supplemental Table S1 in the appendix.

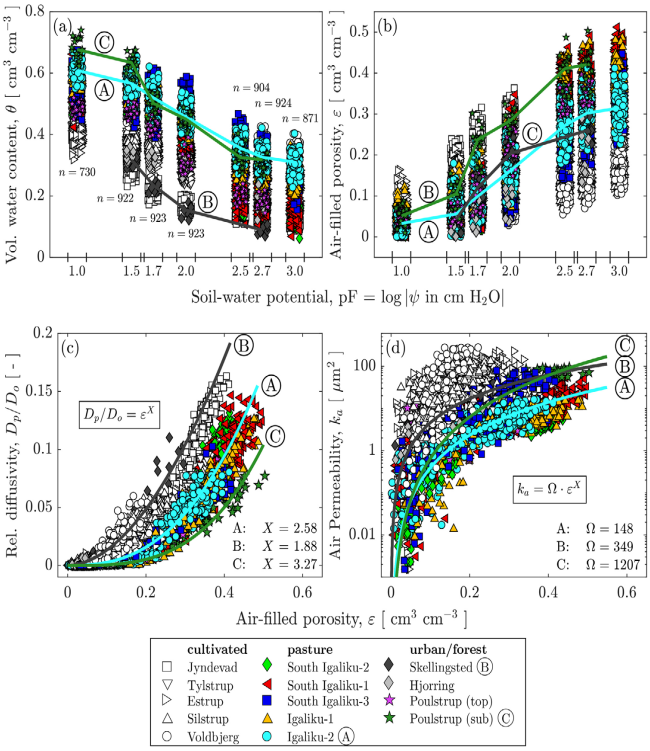

FIGURE 3 Phase distributions and air-phase functions. (a) Volumetric water content, θ, and (b) air-filled porosity, ε, vs. soil–water potential levels (pF) and the number of valid measurements per pF (*n*). The connecting lines for three soils (A: Igaliku-2, B: Skellingsted, C: Poulstrup-sub) are linearly interpolated. (c) Relative diffusivity (D_p/D_o) and applied gas-diffusion model Equation 4; (d) air permeability (k_a) and applied Ω-model (five) for three selected soils. The parameter Ω was fitted, whereas *X* was fixed to the values obtained in subfigure (c)

The main parameter of the *H*-model (*H*) reflected the sensitivity of ε to changes in natural compaction, quantified by ρ_b, at a given drainage step. Observing the *H* index from wet to dry soil conditions enabled to evaluate which faction of the pore size distribution was most vulnerable to changes in ρ_b.

3.2.2 | Dual fingerprint

The decadal logarithm of the Kawamoto et al. (2006) soil-structure index, Ω, determined at each soil–water potential level after rearranging Equation 5 ($\Omega = k_a/[D_p/D_o]$) are given in the left-hand subplots of Figure 7. The dashed horizontal line highlights the threshold value, Ω = 700, in each subplot. The right-hand subplots of Figure 7 show the variation of *H* with the soil–water potential; as a reference for *H*, the expected *H*-range for a theoretical pure and uniform sand (see Table 2) was indicated by the shaded area in the plots.

The soils were grouped according to their LU, and the connecting lines were interpolated. The measurements at pF 1.0 were omitted due to the relatively large associated measurement uncertainties at such low suctions.

From a soil-textural perspective, the soil from Jyndevad showed the most narrow and uniform particle-size distribution (>80% sand) among the cultivated soils, which was also reflected in its pore-size distribution (Schjønning, 1992; Jensen et al., 2019) and eventually in the range of the calculated *H*-values, comprised within the boundaries of the expected *H*-range of pure sands. The relatively low Ω-values (Figure 7b) throughout the complete moisture range could be associated with the low aggregation potential and noncohesive nature of the Jyndevad coarse sandy soil (Schjønning, 1992).

The fine sandy Tylstrup soil exhibited considerably higher *H*-values between pF 1.7 and pF 2.5 than the other cultivated soils, indicating that a change in ρ_b mainly affected the volume

TABLE 4 Results of the linear regressions to predict the field-averaged soil–air characteristic curve parameter $\bar{A}$

	Model	*n*	R^2/R^2_{adj}	RMSE	AICc
Equation 7, Figure 9a	$A = 0.073^{**} + 0.024^{***}$ (TUI)	13	$R^2 = 0.844$	0.032	−49.83
Equation 8, Figure 9b	$A = 0.061^{**} + 0.017^{***}$ (TUI)	13	$R^2_{adj} = 0.955$	0.016	−57.88
	+0.071 #pasture[a]				
	+0.036 #urban[a]				
	+0.044 #forest[a]				

Note. Equation 7 with the texture uniformity index, TUI, as independent variable; Equation 8 also including a factor accounting for land use (LU[a]). *n*, number of observations included in the regression; R^2 and R^2_{adj}, ordinary and adjusted coefficient of determination, respectively; RMSE, root-mean-square error; AICc, Akaike information criterion adjusted for small sample numbers; exponents of regression coefficients depict the significance levels according to the rules given in the Methods section.
[a]LU is expressed explicitly, omitting the reference level #cultivated, as #pasture takes the value of 1 if the land use is pasture and 0 if not; the same for #urban and #forest.

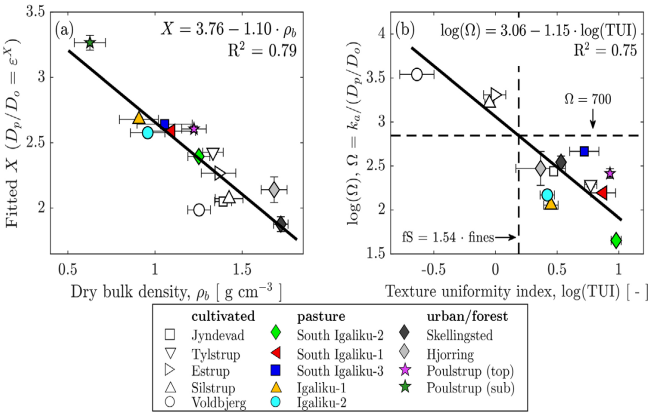

FIGURE 4 (a) Connectivity-tortuosity parameter *X* (Equation 4 and Figure 3c) vs. bulk density (ρ_b) and (b) soil-structure index Ω (Equation 5 and Figure 3d) as a function of the texture uniformity index (TUI) (both in log-scale). Dashed horizontal line at the threshold Ω-value for soils exhibiting developed structure. Vertical dashed line depicts the threshold TUI-value at which well-developed soil structure can be expected. Error-bars depict the within-field standard deviation of ρ_b and TUI (horizontal) and the 95% confidence interval of the fitted connectivity-tortuosity parameter *X* and soil structure parameter Ω (vertical)

of the pore-size classes exhibiting a pore diameter between 10 and 60 µm. Further, the Ω-values below the threshold of Ω = 700 indicated a lack of soil structure for the Tylstrup soils as well.

The finer-grained cultivated soils (Estrup, Silstrup, and Voldbjerg) exhibited a lower *H*, indicating that the ε at each soil–water potential were less susceptible to changes in ρ_b. The Ω-values above Ω = 700 throughout the whole moisture range implied the presence of a developed soil structure; that is, the larger k_a to D_p/D_o ratio indicated a dual-porosity network, exhibiting inter- and intra-aggregate porosity, arising from aggregate formation amplified by the relatively high OC and fines contents (Six et al., 1998; Dexter et al., 2008).

The low Ω-values of the sandy Jyndevad and Tylstrup soils were a direct consequence of the only marginally differing dominating particle (dispersed particles) sizes compared to the dominating aggregate (nondispersed) sizes (236 vs. 420 µm and 125 vs. 250 µm for the two soils, respectively). The Silstup soil on the other hand, showed considerable differences between particle and aggregate sizes (120 vs. 6,300 µm) (Schjønning, 1992).

The sensitivity of ε to changes in ρ_b of the arctic pasture soils was generally lower (Figure 7c) compared to the temperate cultivated soils, although the low Ω-values pointed toward a lack of soil structure. Weber et al. (2020) investigated the pore-network connectivity of the herein presented arctic pasture soils and concluded that the pasture soils showed only little to no soil-structure development, which is in accordance with the low Ω-values found in this study.

The forest soils showed *H*-values similar to the arctic pasture soils. However, the Ω-values of the forest top-soil were consistently higher compared to the pasture soils, mainly due

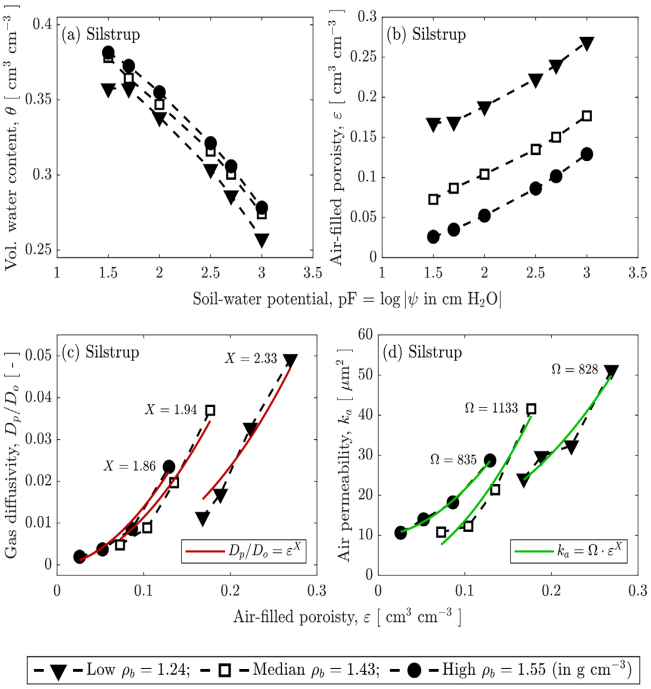

FIGURE 5 Phase distributions and air-phase functions for three levels of natural within-field compaction (Silstrup: low, median, and high bulk density [ρ_b]). (a) Volumetric water content, θ, and (b) air-filled porosity, ε, for wet to dry moisture conditions. Air-phase functions as a function of ε: (c) gas diffusivity (D_p/D_o) and fitted model according to Equation 4 (fitted connectivity-tortuosity parameter *X*); (d) air permeability (k_a) and applied Ω-model (Equation 5), with fitted structure parameter Ω and fixed *X* as obtained in subfigure (c)

to the low diffusivity compared to the high air permeability of this organic matter-dominated soil. High ε throughout the complete moisture range promoted k_a of the forest top-soil, although D_p/D_o was impeded by the pore-tortuosity presumably created by the high organic matter content (Iiyama & Hasegawa, 2005; Hamamoto et al., 2012). Although the organic matter of the forest soils had not been characterized, it is plausible that it consisted of relatively large amounts of nondecomposed organic matter fragments and a relatively dense root zone. The Greenlandic pasture soils likely exhibited similar characteristics (especially SI-1, SI-2, and SI-3; Pesch et al., 2020), which might be the reason for the similarities between the pasture and forest soils in terms of $\rho_b - \varepsilon$ dynamics.

As expected, the samples from Skellingsted, consisting of an artificially compacted, industrial sand cover-layer with low OC, showed *H*-values in the same order of magnitude as the theoretical sand and the Jyndevad soil. The Hjorring subsoil samples showed a distinct evolution of *H*. The high stress at the deeper soil layers caused by the overlying soil probably resulted in a homogeneous pore-size distribution dominated by small pores ($D_\phi \leq 6$ μm) and a shift of high *H*-values toward smaller pore-sizes (higher pF). Moldrup et al. (2000a) reported silt-lenses within the soil profile, which most likely had a notable but unspecified effect on the relation between ρ_b and ε. The urban soils showed both relatively low Ω-values, similar to the sandy Jyndevad and Tylstrup soils.

3.3 | Two-dimensional, modeled response surface for soil air-filled porosity

3.3.1 | Application of the A-model

As shown in the first part of this study, ρ_b could explain the intra-field variation of ε to a large extent, especially at dry soil-conditions. We deployed the earlier introduced *A*-model (Equation 2) to evaluate the within-field variation of ε for varying moisture conditions. The SL-SAC parameter determined on field-averaged ε were referred to as $\bar{A}$, to avoid confusion with the sample specific *A*.

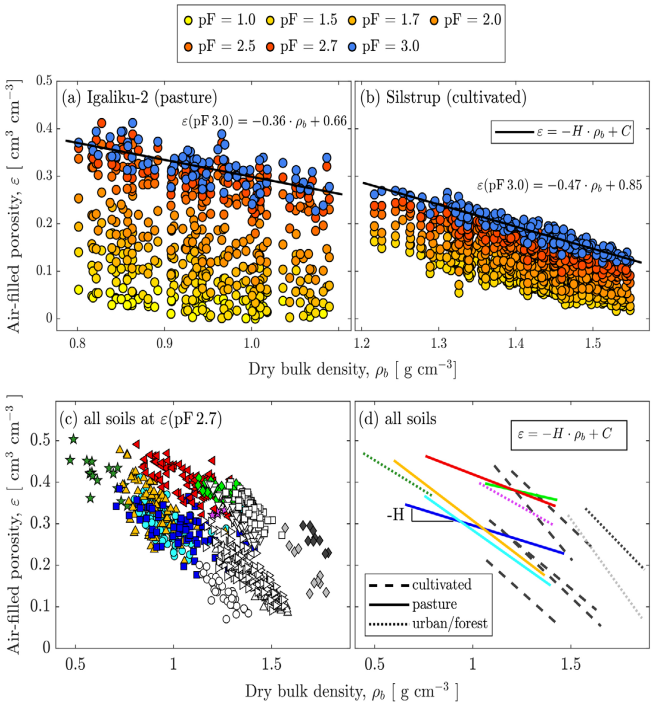

FIGURE 6 Evolution of the air-filled porosity, ε, as a function of dry bulk density, ρ_b, and soil–water potential (pF, color gradient, blue for measurements at pF 3) for a subarctic pasture (a) and a temperate cultivated soil (b). Solid lines show the applied *H*-model (Equation 1) at pF 3.0. (c) Scatter plot of ε versus bulk density (ρ_b) at pF 2.7 for the complete data set and the corresponding *H*-model for each field (d). Open symbols: cultivated soils; closed colored symbols: pasture and forest soils; closed black and gray symbols: urban soils

The *A*-model was fitted to ε values measured at soil–water potentials varying between pF 1.5 and pF 3.0, and the reference soil-matric potential was fixed at $\varepsilon_{ref} = \varepsilon(\text{pF } 2.7)$. The choice of $\text{pF}_{ref} = 2.7$ was related to data availability; it was the lowest (most negative) soil–water potential at which data was available for all the soils. In principle, pF_{ref} did not necessarily need to be fixed at the highest pF to yield satisfactory regression results. However, the goodness-of-fit improved markedly for $\text{pF}_{ref} \geq 2$.

The *A*-model was applied to the measured ε of the same collection of samples from Silstrup as in Figure 5, covering the complete within-field ρ_b-range (Figure 8a). As expected, the effect of ρ_b on the sample-specific average ε (horizontal shift of the SL-SAC lines in Figure 8a) was distinct and also well explained by ρ_b, given the significant correlation between ρ_b and ε(pF 2.7) of $r = -.81^{***}$ or the high explained variation by the linear regression (*H*-model) given in Table S1 (Silstrup at pF 2.7, $R^2 = .88$).

The performance of the *A*-model, fitted to the field-averaged ε of three differently textured soils, is displayed in Figure 8b. The corresponding field-averaged SL-SAC parameters ($\bar{A}$) and R^2 are given in the plot area. The model represented the data of the cultivated loamy to clayey soils fairly well (Silstrup and Voldbjerg), whereas the model could not entirely capture the pronounced curvature of the sandy-loamy pasture soil (Igaliku-2). The $\bar{A}$ of all the 14 soils varied between 0.064 (Voldbjerg) and 0.28 (South-Igaliku 2) and, while being inversely proportional to the gravimetric fines content, a significant linear correlation between $\bar{A}$ and the TUI could be observed ($r = .92^{***}$). Because of the similarity of the *A*-model to well-known water-retention models, the correlation of the parameter *A* with TUI was not surprising because other studies found similar correlations between water-retention-model parameters and soil-texture criteria (Clapp & Hornberger, 1978; Vereecken et al., 1989; Pittaki-Chrysodonta et al., 2018).

The dependence of the field-averaged *A*-model parameter on basic soil properties was evaluated via linear regressions, and it could be accurately predicted by a regression including the texture uniformity parameter, TUI (Figure 9a and

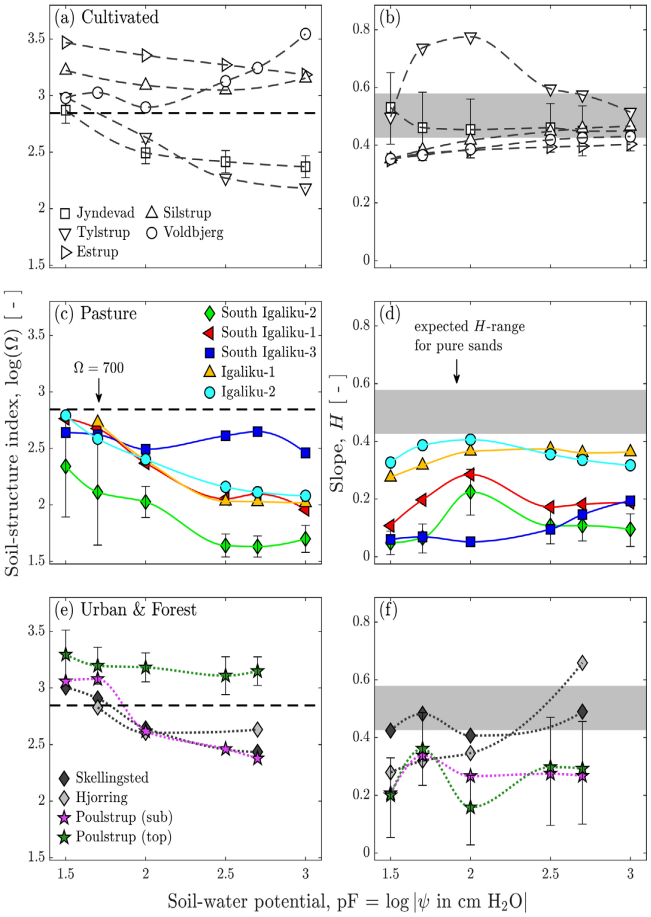

FIGURE 7 The soil-structure index given by the Ω-model (b, d, f) from wet (pF 1.5) to dry (pF 3.0) moisture conditions. The dashed line represents the threshold of Ω = 700 for soil-structure effects on air-phase functional parameters (Kawamoto et al., 2006). The sensitivity of air-filled porosity (ε) to ρ_b (bulk density; a, c, e) is given by the main parameter of the *H*-model. The shaded area corresponds to the expected range of *H* for a pure sand (see Table 2). The error-bars depict the intra-field standard deviation of Ω at each soil–water potential (a, c, e) and the 90% confidence intervals (b, d, f) of *H*. For better legibility, only one set of error-bars is shown per subfigure

Equation 7). However, including a nominal categorical variable accounting for the LU (cultivated, pasture, urban, forest) increased the explained variation from 86% to 98% and the model performance by more than 20% compared to the initial model (Figure 9b and Equation 8). The ANOVA of the regression model (Equation 8) showed that the categorical variable was significant at the 1% significance level (LU: $p[>F]) = .003$). Significant collinearity among the predictors could be safely rejected because of the invertibility of the predictor matrix. The effect of the LU on the marginal means of the LU-grouped *A* compared to the reference level given by the mean *A* of the cultivated soils was given explicitly in the model function Equation 8 in Table 4 (regression coefficients associated with the levels of the categorical factor).

The outcome of the multiple linear regressions revealed that the variation of the across-field $\bar{A}$ was explained by the LU factor at a precision-level, which could not be achieved by ρ_b and TUI alone (nonsignificant ρ_b, if included in the regression, not shown), indicating that the LU-factor incorporated information which was not captured by the continuous independent variables.

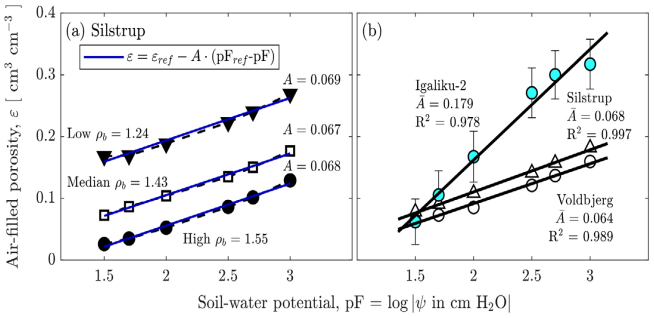

FIGURE 8 Semilogarithmic soil–air characteristic curve (SL-SAC). Fitted log-linear air-filled porosity model (2) (*A*-model) to (a) samples from Silstrup, spanning the field's complete bulk density (ρ_b)-range to depict the within-field variation, and to (b) the within-field mean ε of three differently textured soils to depict the across-field variation (error bars depict the standard deviation and are given for one soil only)

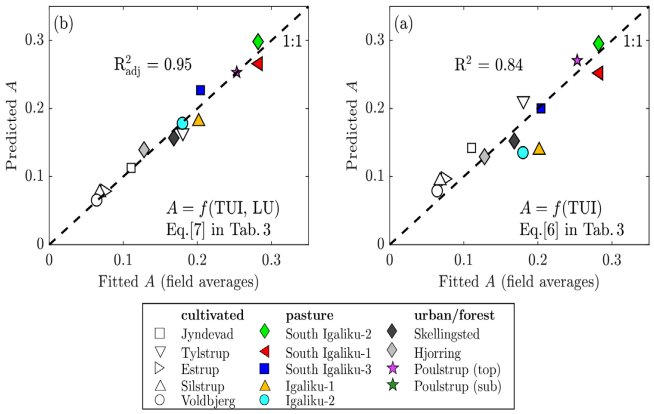

FIGURE 9 Prediction of the field-averaged semilogarithmic soil–air characteristic curve (SL-SAC) parameter $\bar{A}$ by (a) linear regression with the texture uniformity index, TUI (fine sand/fines), and (b), including the land use index, LU, as predictors; detailed statistics in Table 4; no texture data for Poulstrup (top)

From the linear regressions established in the first part of the study, ε could be accurately predicted from ρ_b, so that, it was possible to predict the complete SL-SAC for any ρ_b by combining the *H*- and *A*-models.

3.3.2 | MRS

The expression for ε_{ref} in the *A*-model (Equation 2, reference fixed at pF 2.7) was substituted by the *H*-model (Equation 1), which permitted the generation of a MRS (Equation 3). The SL-SAC parameter *A* was estimated from the linear model (Equation 8) with field-average TUI and LU as predictors.

The estimated ε for simulated ρ_b, spanning the soils ρ_b-range and from wet to dry soil conditions for Igaliku-2 and Silstrup, are shown in Figure 10. Negative outputs were set to null. The fitted and estimated parameter inputs are given in Table 5; the relevant *H* were obtained from Supplemental Table S1 (*H*[pF 2.7] for Igaliku-2 and Silstrup, respectively).

The *A*-model, in combination with the *H*-model, could thus accurately predict the ε for samples exhibiting a wide ρ_b-range for wet to dry conditions. To be able to predict the air-characteristic curve completely from texture and LU, a prediction model for the parameter *H* would be needed. It can be shown that *H* can be very accurately predicted from the gravimetric OC and fine sand (D_e < 200 µm) contents, along with the LU factor (R^2_{adj} = .94, not shown).

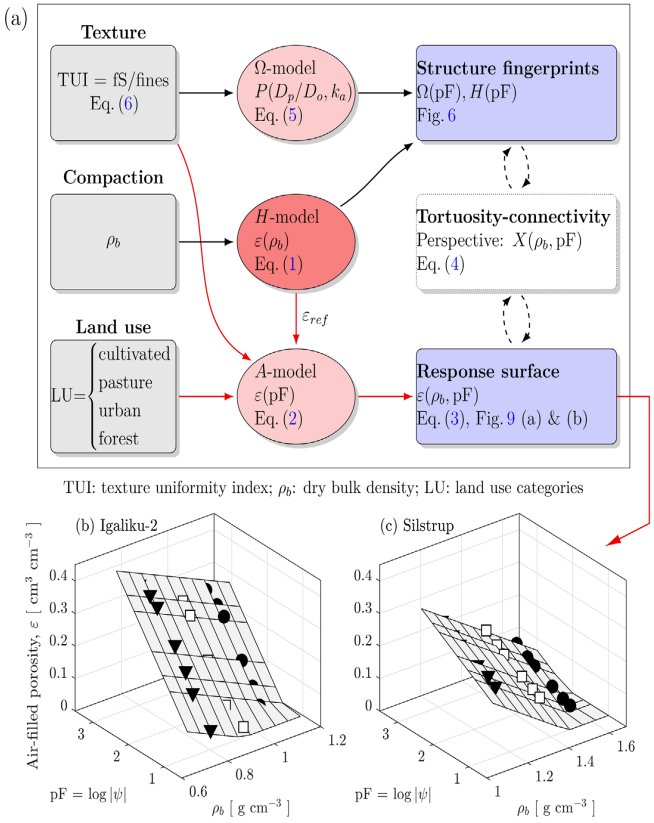

FIGURE 10 (a) Relational concept map elucidating the connections between soil state variables (texture, compaction, and land use), the deployed models, and the resulting descriptive entities. Estimated ε for varying bulk density (ρ_b) and pF. Symbols: measured ε corresponding to lowest (▼), median (□) and highest (●) ρ_b of (b) Igaliku-2 and (c) Silstrup. Plane: estimated ε from *A*-model (2) in combination with the *H*-model (1) for simulated ρ_b spanning the ρ_b-range of the two selected fields. Model parameters and relative error (RMSE) are given in Table 5

TABLE 5 Fitted and estimated values to compute the response plane in Figure 10 from the *A*-model (to estimate A) in combination with the *H*-model (to estimate ε_{ref})

	H	ε_{ref}		$\bar{A}$		RMSE(ε)		
Site	**Fitted**	**Measured**	***f*(*H*, $\bar{\rho}_b$)**	**Fiitted**	***f*(TUI, LU)**	**Low ρ_b**	**Median ρ_b**	**High ρ_b**
Igaliku-2	0.336	0.302	0.304	0.180	0.179	0.021	0.023	0.015
Silstrup	0.458	0.157	0.154	0.068	0.077	0.011	0.010	0.013

Note. The measured (fitted) variables (ε_{ref} and $\bar{A}$, both field-averages) are given as reference. The error of the estimated ε using the modeled response surface model compared to the measured ε at three bulk density (ρ_b)-levels is given by the root mean square error (RMSE).

However, the nominal land-use variable, LU, differentiated not only between the different LU but also between the climatic regions (arctic and temperate) and most likely included hidden components that influenced the ε evolution during drainage. In addition, the sample sizes between the different LU groups differed to such an extent that a reliable, unbiased prediction model could not be established. To avoid a gray-box and heavily biased model, it was preferred not to elaborate further on the prediction model at this time.

The concept map given in Figure 10a elucidates the relations between the different controls (texture, compaction, and LU) and the resulting soil structure fingerprints and final response surface for ε. Organic matter was not used as a control parameter; however, from Figure 2, it was apparent that OC was strongly connected to TUI and ρ_b. Furthermore, many studies have shown that the quantity and quality of the organic matter fractions are ultimately controlled by LU (Parfitt et al., 1997; Leifeld & Kögel-Knabner, 2005; Yeasmin et al., 2020) and, also, have a distinct effect on the air-phase functions (Resurreccion et al., 2007). Especially in regard to climate and potential LU changes at high latitudes, the effect on the organic matter pools and subsequent changes in soil structure and related soil-functional parameters and gas-exchange processes may eventually be modeled and simulated by the combination of the presented soil-structure fingerprints (Ω[pF]) and *H*[pF]) and simple ε-response surface via the connectivity-tortuosity factor *X*, which, in turn, was shown to be correlated to ρ_b (Figure 4).

4 | CONCLUSION

From comprehensive soil physical data measured at different moisture conditions on 14 different soils representing four different LU, two climatic zones, and a wide range of soil texture and bulk density (ρ_b), we conclude:

1. Bulk density (ρ_b) was strongly and nonlinearly related to OC across the fields, but only weakly within the fields for some of the South Greenlandic pastures. The ratio of fine sand to fines, referred to as the TUI, exhibited different relations with OC across the LU and climate zones.
2. The connectivity-tortuosity parameter, *X*, was significantly negatively correlated to ρ_b, whereas, on the other hand, the soil-structure index, Ω, was significantly negatively correlated to the TUI. For the herein used soils, no signs of structure development were observed for the pasture soils.
3. The simultaneous display of the soil–water retention curve (volumetric water content, θ) along with the SL-SAC (air-filled porosity, ε) revealed that the SAC varied significantly for varying levels of compaction, whereas the water retention curve varied only marginally. The air-phase functions (relative diffusivity and air permeability, D_p/D_o and k_a, respectively) showed relatively large variations along the ρ_b-gradient, mainly due to the considerable effect of ρ_b on ε, and hence on the available void-space for gaseous exchanges.
4. The air-filled porosity (ε) of the different soils exhibited distinct linear dependencies on ρ_b at changing moisture conditions. The slopes, *H*, of these linear dependencies (*H*-model) showed different magnitudes for contrasting soil-types and LU. The *H*-parameter, interpreted as a measure of the sensitivity of ε to changes in ρ_b, revealed that the ε at each pF of the subarctic pasture soils were less sensitive to changes in ρ_b than similarly textured cultivated soils.
5. The soil-structure index, Ω, calculated as the ratio of k_a to D_p/D_o for each soil–water potential level, enabled to differentiate between the textures of the cultivated soils. The pasture soils, on the other hand, did not show signs of a developed soil structure.
6. The semilogarithmic SL-SAC could be reasonably well described by the developed *A*-model (two parameters: *A* and ε_{ref}). For the herein used soils, the model parameter, *A*, could be accurately predicted by the TUI and a factor accounting for environmental properties, including LU, achieving a coefficient of determination of $R^2 = .95$.
7. The combination of the *H*-model (to estimate ε_{ref}) and the *A*-model (to simulate the response of ε to changes in pF) was successfully applied to model a response surface of ε as a function of ρ_b and pF (MRS).

The dry bulk density, ρ_b, turned out to be the chief parameter explaining the within-field variation of ε, and thus, to a large extent, also the levels of air-exchange processes within a field. On the contrary, the across-field variation was better explained by texture together with a categorical factor accounting for environment-specific properties (including LU and management). The effect size of ρ_b on the field-averaged ε was statistically less significant than texture and environmental factors.

In perspective and toward actual use, the MRS concept should be further tested, validated against independent data, and extended to include nonlinear ε-pF models. The combined controls of soil compaction (density), type (texture), and environmental factors, including LU, on the three air-phase parameters (ε, D_p/D_o, and k_a) will be a key to predict future changes in soil ecosystem services.

ACKNOWLEDGMENTS

The research was financed by the Danish Council for Independent Research, Technology, and Production Sciences via the project "Glacial Flour as a New, Climate-Positive Technology for Sustainable Agriculture in Greenland: NewLand."

AUTHOR CONTRIBUTIONS

Charles Pesch: Conceptualization; Data curation; Formal analysis; Investigation; Methodology; Visualization; Writing-original draft; Writing-review & editing. Peter Lystbæk Weber: Data curation; Investigation; Validation. Lis Wollesen de Jonge: Conceptualization; Data curation; Funding acquisition; Project administration; Resources; Supervision. Mogens Humlekrog Greve: Funding acquisition; Resources. Trine Norgaard: Data curation; Validation. Per Moldrup:

Conceptualization; Formal analysis; Investigation; Methodology; Project administration; Resources; Supervision; Writing-review & editing.

CONFLICTS OF INTEREST

The authors declare that there is no conflicts of interest.

ORCID

Trine Norgaard https://orcid.org/0000-0001-7669-3841

REFERENCES

Annabi, M., Le Bissonnais, Y., Le Villio-Poitrenaud, M., & Houot, S. (2011). Improvement of soil aggregate stability by repeated applications of organic amendments to a cultivated silty loam soil. *Agriculture, Ecosystems & Environment*, *144*(1), 382–389.

Arthur, E., Moldrup, P., Schjønning, P., & Jonge, L. W. (2012). Linking particle and pore size distribution parameters to soil gas transport properties. *Soil Science Society of America Journal*, *76*(1), 18–27. https://doi.org/10.2136/sssaj2011.0125

Arya, L. M., & Paris, J. F. (1981). A physicoempirical model to predict the soil moisture characteristic from particle-size distribution and bulk density data. *Soil Science Society of America Journal*, *45*(6), 1023–1030. https://doi.org/10.2136/sssaj1981.03615995004500060004x

Assouline, S., Tuli, A., & Hopmans, J. W. (2016). Evaluating the relative air permeability of porous media from their water retention curves. *Water Resources Research*, *52*(5), 3428–3439. https://doi.org/10.1002/2015WR018286

Ball, B. C. (1981). Modelling of soil pores as tubes using gas permeabilities, gas diffusivities and water release. *Journal of Soil Science*, *32*(4), 465–481. https://doi.org/10.1111/j.1365-2389.1981.tb01723.x

Ball, B. C. (2013). Soil structure and greenhouse gas emissions: A synthesis of 20 years of experimentation. *European Journal of Soil Science*, *64*(3), 357–373. https://doi.org/10.1111/ejss.12013

Ball, B. C., Campbell, D. J., Douglas, J. T., Henshall, J. K., & O'sullivan, M. F. (1997). Soil structural quality, compaction and land management. *European Journal of Soil Science*, *48*(4), 593–601. https://doi.org/10.1111/j.1365-2389.1997.tb00559.x

Ball, B. C., & Schjønning, P. (2002). Air permeability. In J. H. Dane & C. G. Topp (Eds.), *Methods of soil analysis: 4. Physical methods* (pp. 1141—1158). SSSA.

Bottinelli, N., Angers, D. A., Hallaire, V., Michot, D., Le Guillou, C., Cluzeau, D., Heddadj, D., & Menasseri-Aubry, S. (2017). Tillage and fertilization practices affect soil aggregate stability in a. *Humic Cambisol of northwest France*. *Soil and Tillage Research*, *170*, 14–17. https://doi.org/10.1016/j.still.2017.02.008

Buckingham, E. (1904). *Contributions to our knowledge of the aeration of soils* (Tech. Rep. 25). Bureau of Soils, USDA.

Campbell, G. S. (1974). A simple method for determining unsaturated conductivity from moisture retention data. *Soil Science*, *117*(6), 311–314. https://doi.org/10.1097/00010694-197406000-00001

Cannon, W. A., & Free, E. E. (1917). The ecological significance of soil aeration. *Science*, *45*(1156), 178–180. https://doi.org/10.1126/science.45.1156.178

Cappelen, J. (2019). *Guide to climate data and information from the Danish Meteorological Institute* (Tech. Rep. 19-10). Danish Meteorological Institute. http://www.dmi.dk/dmi/tr19-10

Carlson, A. E., Winsor, K., Ullman, D. J., Brook, E. J., Rood, D. H., Axford, Y., Legrande, A. N., Anslow, F. S., & Sinclair, G. (2014). Earliest Holocene south Greenland ice sheet retreat within its late holocene extent. *Geophysical Research Letters*, *41*(15), 5514–5521. https://doi.org/10.1002/2014GL060800

Chesters, G., Attoe, O. J., & Allen, O. N. (1957). Soil aggregation in relation to various soil constituents. *Soil Science Society of America Journal*, *21*(3), 272–277. https://doi.org/10.2136/sssaj1957.03615995002100030007x

Clapp, R. B., & Hornberger, G. M. (1978). Empirical equations for some soil hydraulic properties. *Water Resources Research*, *14*(4), 601–604. https://doi.org/10.1029/WR014i004p00601

Currie, J. A. (1960a). Gaseous diffusion in porous media: 1. A non-steady state method. *British Journal of Applied Physics*, *11*(8), 314–317. https://doi.org/10.1088/0508-3443/11/8/302

Currie, J. A. (1960b). Gaseous diffusion in porous media: 2. Dry granular materials. *British Journal of Applied Physics*, *11*(8), 318–324. https://doi.org/10.1088/0508-3443/11/8/303

Currie, J. A. (1961). Gaseous diffusion in porous media. Part 3 - Wet granular materials. *British Journal of Applied Physics*, *12*(6), 275–281. https://doi.org/10.1088/0508-3443/12/6/303

Dane, J. H., & Hopmans, J. W. (2002). Water content. In J. H. Dane & C. G. Topp (Eds.), *Methods of soil analysis: 4. Physical methods* (pp. 417–545). SSSA.

Deepagoda, T. K. K. C., Moldrup, P., Schjønning, P., De Jonge, L. W., Kawamoto, K., & Komatsu, T. (2011a). Density-corrected models for gas diffusivity and air permeability in unsaturated soil. *Vadose Zone Journal*, *10*(1), 226–238. https://doi.org/10.2136/vzj2009.0137

Deepagoda, T. K. K. C., Moldrup, P., Schjønning, P., Kawamoto, K., Komatsu, T., & De Jonge, L. W. (2011b). Generalized density-corrected model for gas diffusivity in variably saturated soils. *Soil Science Society of America Journal*, *75*(4), 1315–1329. https://doi.org/10.2136/sssaj2010.0405

Deepagoda, T. K. K. C., Moldrup, P., Schjønning, P., Kawamoto, K., Komatsu, T., & De Jonge, L. W. (2012). Variable pore connectivity model linking gas diffusivity and air-phase tortuosity to soil matric potential. *Vadose Zone Journal*, *11*(1). https://doi.org/10.2136/vzj2011.0096

Dexter, A. R., Richard, G., Arrouays, D., Czyż, E. A., Jolivet, C., & Duval, O. (2008). Complexed organic matter controls soil physical properties. *Geoderma*, *144*(3), 620–627. https://doi.org/10.1016/j.geoderma.2008.01.022

Dlapa, P., Hriník, D., Hrabovský, A., Šimkovic, I., Žarnovičan, H., Sekucia, F., & Kollár, J. (2020). The impact of land-use on the hierarchical pore size distribution and water retention properties in loamy soils. *Water*, *12*(2). https://doi.org/10.3390/w12020339

Dörner, J., Dec, D., Thiers, O., Paulino, L., Zúñiga, F., Valle, S., Martínez, O., & Horn, R. (2016). Spatial and temporal variability of physical properties of Aquands under different land uses in southern Chile. *Soil Use and Management*, *32*(3), 411–421. https://doi.org/10.1111/sum.12286

Eden, M., Schjønning, P., Moldrup, P., & De Jonge, L. W. (2011). Compaction and rotovation effects on soil pore characteristics of a loamy sand soil with contrasting organic matter content. *Soil Use and Management*, *27*(3), 340–349. https://doi.org/10.1111/j.1475-2743.2011.00344.x

Efron, B. (1979). Bootstrap methods: Another look at the jackknife. *Annals of Statistics*, *7*(1), 1–26. https://doi.org/10.1214/aos/1176344552

Efron, B. (1983). Estimating the error rate of a prediction rule: Improvement on crossvalidation. *Journal of the American Statistical Association*, *78*(382), 316–331. https://doi.org/10.1080/01621459.1983.10477973

Egli, M., Hunt, A. G., Dahms, D., Raab, G., Derungs, C., Raimondi, S., & Yu, F. (2018). Prediction of soil formation as a function of age using the percolation theory approach. *Frontiers in Environmental Science*, *6*, 108. https://doi.org/10.3389/fenvs.2018.00108

Federer, C. A., Turcotte, D. E., & Smith, C. T. (1993). The organic fraction–bulk density relationship and the expression of nutrient content in forest soils. *Canadian Journal of Forest Research*, *23*(6), 1026–1032. https://doi.org/10.1139/x93-131

Folkoff, M. E., & Meentemeyer, V. (1987). Climatic control of the geography of clay minerals genesis. *Annals of the Association of American Geographers*, *77*(4), 635–650. https://doi.org/10.1111/j.1467-8306.1987.tb00185.x

Gee, G. W., & Or, D. (2002). Particle-size analysis. In J. H. Dane & C. G. Topp (Eds.), *Methods of soil analysis: 4. Physical methods* (pp. 255–293). SSSA.

Gregorich, E., Rochette, P., Vandenbygaart, A. & Angers, D. (2005). Greenhouse gas contributions of agricultural soils and potential mitigation practices in Eastern Canada. *Soil and Tillage Research*, *83*(1), 53–72. https://doi.org/10.1016/j.still.2005.02.009

Gregson, K., Hector, D. J., & Mcgowan, M. (1987). A one-parameter model for the soil water characteristic. *Journal of Soil Science*, *38*(3), 483–486. https://doi.org/10.1111/j.1365-2389.1987.tb02283.x

Hamamoto, S., Moldrup, P., Kawamoto, K., & Komatsu, T. (2012). Organic matter fraction dependent model for predicting the gas diffusion coefficient in variably saturated soils. *Vadose Zone Journal*, *11*(1). https://doi.org/10.2136/vzj2011.0065

Hermansen, C., Knadel, M., Moldrup, P., Greve, M. H., Karup, D., & De Jonge, L. W. (2017). Complete soil texture is accurately predicted by visible near-infrared spectroscopy. *Soil Science Society of America Journal*, *81*(4), 758–769. https://doi.org/10.2136/sssaj2017.02.0066

Iiyama, I., & Hasegawa, S. (2005). Gas diffusion coefficient of undisturbed peat soils. *Soil Science and Plant Nutrition*, *51*(3), 431–435. https://doi.org/10.1111/j.1747-0765.2005.tb00049.x

Iversen, B. V., Moldrup, P., Schjønning, P., & Loll, P. (2001). Air and water permeability in differently textured soils at two measurement scales. *Soil Science*, *166*(10), 643–659. https://doi.org/10.1097/00010694-200110000-00001

Jensen, J. L., Schjønning, P., Watts, C. W., Christensen, B. T., & Munkholm, L. J. (2019). Soil water retention: Uni-modal models of pore-size distribution neglect impacts of soil management. *Soil Science Society of America Journal*, *83*(1), 18–26. https://doi.org/10.2136/sssaj2018.06.0238

Johnson, J. M.-F., Franzluebbers, A. J., Weyers, S. L., & Reicosky, D. C. (2007). Agricultural opportunities to mitigate greenhouse gas emissions. *Environmental Pollution*, *150*(1), 107–124. https://doi.org/10.1016/j.envpol.2007.06.030

Karup, D., Moldrup, P., Paradelo, M., Katuwal, S., Norgaard, T., Greve, M. H., & De Jonge, L. W. (2016). Water and solute transport in agricultural soils predicted by volumetric clay and silt contents. *Journal of Contaminant Hydrology*, *192*, 194–202. https://doi.org/10.1016/j.jconhyd.2016.08.001

Katuwal, S., Arthur, E., Tuller, M., Moldrup, P., & De Jonge, L. W. (2015). Quantification of soil pore network complexity with X-ray computed tomography and gas transport measurements. *Soil Science Society of America Journal*, *79*(6), 1577–1589. https://doi.org/10.2136/sssaj2015.06.0227

Kawamoto, K., Moldrup, P., Schjønning, P., Iversen, B.o V., Komatsu, T., & Rolston, D. E. (2006). Gas transport parameters in the vadose zone: Development and tests of power-law models for air permeability. *Vadose Zone Journal*, *5*(4), 1205–1215. https://doi.org/10.2136/vzj2006.0030

Kerr, P. F. (1952). Formation and occurrence of clay minerals. *Clays and Clay Minerals*, *1*(1), 19–32. https://doi.org/10.1346/CCMN.1952.0010104

Kruse, C. W., Moldrup, P., & Iversen, N. (1996). Modeling diffusion and reaction in soils: II. Atmospheric methane diffusion and consumption in a forest soil. *Soil Science*, *161*(6), 355–365. https://doi.org/10.1097/00010694-199606000-00002

Leifeld, J., & Kögel-Knabner, I. (2005). Soil organic matter fractions as early indicators for carbon stock changes under different land-use? *Geoderma*, *124*(1), 143–155. https://doi.org/10.1016/j.geoderma.2004.04.009

Li, Z., Zhang, X., & Liu, Y. (2017). Pore-scale simulation of gas diffusion in unsaturated soil aggregates: Accuracy of the dusty-gas model and the impact of saturation. *Geoderma*, *303*, 196–203. https://doi.org/10.1016/j.geoderma.2017.05.008

Lindhardt, B., Abildtrup, C., Vosgerau, H., Olsen, P., Torp, S., Iversen, B. V., Jørgensen, J. O., Plauborg, F., Rasmussen, P., & Gravesen, P. (2001). *The Danish pesticide leaching assessment programme*. GEUS.

Lipiec, J., Hajnos, M., & Świeboda, R. (2012). Estimating effects of compaction on pore size distribution of soil aggregates by mercury porosimeter. *Geoderma*, 179–180, 20–27. https://doi.org/10.1016/j.geoderma.2012.02.014

Masís-Meléndez, F., Chamindu Deepagoda, T. K. K., De Jonge, L. W., Tuller, M., & Moldrup, P. (2014). Gas diffusion-derived tortuosity governs saturated hydraulic conductivity in sandy soils. *Journal of Hydrology*, *512*, 388–396. https://doi.org/10.1016/j.jhydrol.2014.02.063

Masís-Meléndez, F., De Jonge, L. W., Chamindu Deepagoda, T. K. K., Tuller, M., & Moldrup, P. (2015). Effects of soil bulk density on gas transport parameters and pore-network properties across a sandy field site. *Vadose Zone Journal*, *14*(7), 1–12. https://doi.org/10.2136/vzj2014.09.0128

MathWorks. (2018). *MATLAB and statistics toolbox* (version 9.5.0 [R2018b]). The MathWorks Inc.

Millington, R. J., & Quirk, J. P. (1964). Formation factor and permeability equations. *Nature*, *202*, 143–145. https://doi.org/10.1038/202143a0

Millington, R. J., & Quirk, J. P. (1961). Permeability of porous solids. *Transactions of the Faraday Society*, *57*, 1200–1207. https://doi.org/10.1039/tf9615701200

Moldrup, P., Kruse, C. W., Rolston, D. E., & Yamaguchi, T. (1996). Modeling diffusion and reaction in soils: III. Predicting gas diffusivity from the Campbell soil–water retention model. *Soil Science*, *161*(6), 366–375. https://doi.org/10.1097/00010694-199606000-00003

Moldrup, P., Olesen, T., Gamst, J., Schjønning, P., Yamaguchi, T., & Rolston, D. E. (2000a). Predicting the gas diffusion coefficient in repacked soil: Water-induced linear reduction model. *Soil Science Society of America Journal*, *64*(5), 1588–1594. https://doi.org/10.2136/sssaj2000.6451588x

Moldrup, P., Olesen, T., Schjønning, P., Yamaguchi, T., & Rolston, D. E. (2000b). Predicting the gas diffusion coefficient in undisturbed soil

from soil water characteristics. *Soil Science Society of America Journal*, *64*(1), 94–100. https://doi.org/10.2136/sssaj2000.64194x

Moldrup, P., Olesen, T., Yamaguchi, T., Schjønning, P., & Rolston, D. E. (1999). Modeling diffusion and reaction in soils: IX. The Buckingham-Burdine-Campbell equation for gas diffusivity in undisturbed soil. *Soil Science*, *164*(8), 542–551. https://doi.org/10.1097/00010694-199908000-00002

Moldrup, P., Olesen, T., Yoshikawa, S., Komatsu, T., & Rolston, D. E. (2004). Three-porosity model for predicting the gas diffusion coefficient in undisturbed soil. *Soil Science Society of America Journal*, *68*(3), 750–759. https://doi.org/10.2136/sssaj2004.7500

Moldrup, P., Yoshikawa, S., Olesen, T., Komatsu, T., & Rolston, D. E. (2003a). Air permeability in undisturbed volcanic ash soils. *Soil Science Society of America Journal*, *67*(1), 32–40.

Moldrup, P., Yoshikawa, S., Olesen, T., Komatsu, T., & Rolston, D. E. (2003b). Gas diffusivity in undisturbed volcanic ash soils. *Soil Science Society of America Journal*, *67*(1), 41–51.

Nielsen, J. E., Karup, D., De Jonge, L. W., Ahm, M., Bentzen, T. R., Rasmussen, M. R., & Moldrup, P. (2018). Can the volume ratio of coarse to fine particles explain the hydraulic properties of sandy soil? *Soil Science Society of America Journal*, *82*(5), 1093–1100. https://doi.org/10.2136/sssaj2018.02.0083

Norgaard, T., Moldrup, P., Olsen, P., Vendelboe, A. L., Iversen, B.o V., Greve, M. H., Kjaer, J., & De Jonge, L. W. (2013). Comparative mapping of soil physical–chemical and structural parameters at field scale to identify zones of enhanced leaching risk. *Journal of Environmental Quality*, *42*(1), 271–283. https://doi.org/10.2134/jeq2012.0105

Paradelo, M., Norgaard, T., Moldrup, P., Ferré, T. P. A., Kumari, K. G. I. D., Arthur, E., & De Jonge, L. W. (2015). Prediction of the glyphosate sorption coefficient across two loamy agricultural fields. *Geoderma*, 259–260, 224–232. https://doi.org/10.1016/j.geoderma.2015.06.011

Parfitt, R. L., Theng, B. K. G., Whitton, J. S., & Shepherd, T. G. (1997). Effects of clay minerals and land use on organic matter pools. *Geoderma*, *75*(1), 1–12. https://doi.org/10.1016/S0016-7061(96)00079-1

Périé, C., & Ouimet, R. (2008). Organic carbon, organic matter and bulk density relationships in boreal forest soils. *Canadian Journal of Soil Science*, *88*(3), 315–325. https://doi.org/10.4141/CJSS06008

Pesch, C., Lamandé, M., De Jonge, L. W., Norgaard, T., Greve, M. H., & Moldrup, P. (2020). Compression and rebound characteristics of agricultural sandy pasture soils from South Greenland. *Geoderma*, *380*, 114608. https://doi.org/10.1016/j.geoderma.2020.114608

Pittaki-Chrysodonta, Z., Moldrup, P., Knadel, M., Iversen, B.o V., Hermansen, C., Greve, M. H., & De Jonge, L. W. (2018). Predicting the Campbell soil water retention function: Comparing visible–near-infrared spectroscopy with classical pedotransfer function. *Vadose Zone Journal*, *17*(1), 170169. https://doi.org/10.2136/vzj2017.09.0169

Poulsen, T. G., Christophersen, M., Moldrup, P., & Kjeldsen, P. (2001). Modeling lateral gas transport in soil adjacent to old landfill. *Journal of Environmental Engineering*, *127*(2), 145–153. https://doi.org/10.1061/(ASCE)0733-9372(2001)127:2(145)

Poulsen, T. G., Moldrup, P., Yamaguchi, T., Massmann, J. W., & Hansen, J. A. (1998). VOC vapor sorption in soil: Soil type dependent model and implications for vapor extraction. *Journal of Environmental Engineering*, *124*(2), 146–155. https://doi.org/10.1061/(ASCE)0733-9372(1998)124:2(146)

Poulsen, T. G., Moldrup, P., Yamaguchi, T., Schjønning, P., & Hansen, J. A. (1999). Predicting soil–water and soil–air transport properties and their effects on soil-vapor extraction efficiency. *Groundwater Monitoring & Remediation*, *19*(3), 61–70.

Resurreccion, A. C., Kawamoto, K., Komatsu, T., Moldrup, P., Sato, K., & Rolston, D. E. (2007). Gas diffusivity and air permeability in a volcanic ash soil profile: Effects of organic matter and water retention. *Soil Science*, *172*(6), 432–443. https://doi.org/10.1097/SS.0b013e3180471c94

Reynolds, R. C. (1971). Clay mineral formation in an alpine environment. *Clays and Clay Minerals*, *19*(6), 361–374. https://doi.org/10.1346/CCMN.1971.0190604

Rolston, D. E., & Moldrup, P. (2002). Gas diffusivity. In J. H. Dane & C. G. Topp (Eds.), *Methods of soil analysis: 4. Physical methods* (pp. 1113—1139). SSSA.

Sakamoto, Y., Ishiguro, M., & Kitagawa, G. (1986). *Akaike information criterion statistics: Vol. 1. Mathematics and its applications*. Reidel Publishing Company.

Schjønning, P. (1985). *A laboratory method for determination of gas diffusion in soil* (Tech. Rep. S 1773). Statens Planteavlsforsøg.

Schjønning, P., & Koppelgaard, M. (2017). The Forchheimer approach for soil air permeability measurement. *Soil Science Society of America Journal*, *81*(5), 1045–1053. https://doi.org/10.2136/sssaj2017.02.0056

Schjønning, P., Thomsen, I. K., Møberg, J. P., De Jonge, H., Kristensen, K., & Christensen, B. T. (1999). Turnover of organic matter in differently textured soils: I. Physical characteristics of structurally disturbed and intact soils. *Geoderma*, *89*(3), 177–198. https://doi.org/10.1016/S0016-7061(98)00083-4

Schjønning, P. (1992). Size distribution of dispersed and aggregated particles and of soil pores in 12 Danish soils. *Acta Agriculturae Scandinavica, Section B–Soil & Plant Science*, *42*(1), 26–33.

Schjønning, P., Eden, M., Moldrup, P., & De Jonge, L. W. (2013). Two-chamber, two-gas and one-chamber, one-gas methods for measuring the soil–gas diffusion coefficient: Validation and inter-calibration. *Soil Science Society of America Journal*, *77*(3), 729–740. https://doi.org/10.2136/sssaj2012.0379

Schjønning, P., Mcbride, R. A., Keller, T., & Obour, P. B. (2017). Predicting soil particle density from clay and soil organic matter contents. *Geoderma*, *286*, 83–87. https://doi.org/10.1016/j.geoderma.2016.10.020

Schofield, R. K. (1935). The pF of the water in soil. In *Transactions of the Third International Congress of Soil Science* (Vol. 2, pp. 37–48). International Society of Soil Science, Thomas Murby & Company.

Six, J., Elliott, E. T., Paustian, K., & Doran, J. W. (1998). Aggregation and soil organic matter accumulation in cultivated and native grassland soils. *Soil Science Society of America Journal*, *62*(5), 1367–1377. https://doi.org/10.2136/sssaj1998.03615995006200050032x

Smith, K., Watts, D., Way, T., Torbert, H., & Prior, S. (2012). Impact of tillage and fertilizer application method on gas emissions in a corn cropping system. *Pedosphere*, *22*(5), 604–615. https://doi.org/10.1016/S1002-0160(12)60045-9

Soil Survey Staff. (1999). A basic system of soil classification for making and interpreting soil surveys *(Agricultural Handbook 436)*. USDA-NRCS.

Stepniewski, W., Stepniewska, Z., & Rozej, A. (2011). Gas exchange in soils. In J. L. Hatfield & T. J. Sauer (Eds.), *Soil management: Building a stable base for agriculture* (pp. 117–144). SSSA.

Stine, R. A. (1985). Bootstrap prediction intervals for regression. *Journal of the American Statistical Association*, *80*(392), 1026–1031. https://doi.org/10.1080/01621459.1985.10478220

Sugiura, N. (1978). Further analysts of the data by Akaike's information criterion and the finite corrections. *Communications in Statistics–Theory and Methods*, *7*(1), 13–26. https://doi.org/10.1080/03610927808827599

Taylor, S. A. (1950). Oxygen diffusion in porous media as a measure of soil aeration. *Soil Science Society of America Journal*, *14*(C), 55–61. https://doi.org/10.2136/sssaj1950.036159950014000C0013x

Thorbjørn, A., Moldrup, P., Blendstrup, H., Komatsu, T., & Rolston, D. E. (2008). A gas diffusivity model based on air-, solid-, and water-phase resistance in variably saturated soil. *Vadose Zone Journal*, *7*(4), 1276–1286. https://doi.org/10.2136/vzj2008.0023

Uteau, D., Pagenkemper, S. K., Peth, S., & Horn, R. (2013). Root and time dependent soil structure formation and its influence on gas transport in the subsoil. *Soil and Tillage Research*, *132*, 69–76. https://doi.org/10.1016/j.still.2013.05.001

Vereecken, H., Maes, J., Feyen, J., & Darius, P. (1989). Estimating the soil moisture retention characteristic from texture, bulk density, and carbon content. *Soil Science*, *148*(6), 389–403. https://doi.org/10.1097/00010694-198912000-00001

Wagner, S., Cattle, S. R., & Scholten, T. (2007). Soil-aggregate formation as influenced by clay content and organic-matter amendment. *Journal of Plant Nutrition and Soil Science*, *170*(1), 173–180. https://doi.org/10.1002/jpln.200521732

Weber, P. L., Jonge, L. W., Greve, M. H., Norgaard, T., & Moldrup, P. (2020). Gas diffusion characteristics of agricultural soils from South Greenland. *Soil Science Society of America Journal*, *84*(5), 1606–1619. https://doi.org/10.1002/saj2.20114

Williamson, R. E. (1964). The effect of root aeration on plant growth. *Soil Science Society of America Journal*, *28*(1), 86–90. https://doi.org/10.2136/sssaj1964.03615995002800010039x

Yang, Z., Mohanty, B. P., Tong, X., Kuang, X., & Li, L. (2021). Effects of water retention curves and permeability equations on the prediction of relative air permeability. *Geophysical Research Letters*, *48*(10). https://doi.org/10.1029/2021GL092459

Yeasmin, S., Singh, B., Smernik, R. J., & Johnston, C. T. (2020). Effect of land use on organic matter composition in density fractions of contrasting soils: A comparative study using 13C NMR and DRIFT spectroscopy. *Science of The Total Environment*, *726*, 138395. https://doi.org/10.1016/j.scitotenv.2020.138395

SUPPORTING INFORMATION

Additional supporting information may be found online in the Supporting Information section at the end of the article.

How to cite this article: Pesch C, Weber P L, de Jonge L W, Greve M H, Norgaard T, & Moldrup P. Soil–air phase characteristics: Response to texture, density, and land use in Greenland and Denmark. *Soil Sci Soc Am J*. 2021;1−21. https://doi.org/10.1002/saj2.20284

D. Paper IV

submitted version of:
Pesch, C., Weber, P. L., de Jonge, L. W., Greve, M. H., Lamandé, M., & Moldrup, P. (n.d.). Changes in pore-network and mechanical properties after Greenlandic rock flour addition to repacked sands and soils [submitted]. *Soil Science Society of America Jounal*, *n/a*(n/a)

Core ideas

- Air-filled porosity decreased with increasing rock flour concentration
- Air-phase tortuosity increased with increasing rock flour concentration
- Compression index was not affected by low rock flour concentrations

Abbreviations

Abbr.	Explanation
GRF	Glacial rock flour
OM_{LOI}	Organic matter (loss-on-ignition)
PSD	Particle size distribution
C_c	Compression index
ΔE	Rebound

Changes in pore-network and mechanical properties after Greenlandic rock flour addition to repacked sands and soils

Charles Pesch*[1], Peter L. Weber[2], Lis W. de Jonge[2], Mogens H. Greve[2], Mathieu Lamandé[2,3] and Per Moldrup[1]

[1]Aalborg Univ., Dep. of the Built Environment, Thomas Manns Vej 23, DK-9220 Aalborg, Denmark
[2]Aarhus Univ., Dep. of Agroecology, Blichers Allé 20, P.O. Box 50, DK-8830 Tjele, Denmark
[3]Norwegian Univ. of Life Sciences, Faculty of Environmental Sciences and Natural Resource Management, Campus Ås, Universitetstunet 3, 1430 Ås, Norway

Abstract

Soil melioration by adding mineral material to improve crop production has a long tradition in agriculture. Recent studies investigated the potential of readily available fine-grained mineral material (glacial rock flour, GRF) as soil amendment in South Greenland. The addition of mineral material changes soil texture, thereby affecting its mechanical and pore-network properties. We determined the compression index (C_c) and the rebound after compaction (ΔE) on repacked soil cores of four differently textured soils (sand to sandy loam) amended with three different levels (G0, G1, and G2 with 0, 3.5, and 10 % w/w, respectively) of GRF. The gas exchange parameters, air permeability (k_a) and gas diffusivity (D_p/D_o) were measured at a fixed soil water potential before and after compression. The pore-network tortuosity-connectivity parameter (X, derived from D_p/D_o) increased from G0 to G1 but did not further increase for G2. No significant effect of GRF on the effective diameter for gas transport (d_{eff}, derived from k_a) was observed. The C_c only increased significantly from G1 to G2 for the coarse-grained soils. The ΔE was not significantly affected by GRF. The C_c was related by a power law to the grading of the particle size distribution; well graded soils exhibited lower compressibility than poorly graded soils. ΔE showed a linear increase with increasing organic matter contents.

Keywords: Soil functions, glacial rock flour amendment, compression index, gas diffusivity, pore-network tortuosity

*Corresponding author: cmep@build.aau.dk

1 Introduction

Soil melioration techniques for ensuring optimal yield harvests have been employed since the beginning of agriculture. One of such techniques is providing mineralogically depleted soils with minerals by adding ground rock flour, first described by Missoux (1853) and Hensel (1894). In more recent years, van Straaten (2002, 2007) revived the idea of using ground rock for remineralizing depleted soils in the tropics and subtropics. Bakken et al. (1997) and Gautneb et al. (1995) investigated the potential of using mine tailings in Nordic countries to provide the regional agriculture with a source of potassium, reporting that the crushed rocks could potentially serve as long term K-fertilizer. Kleiv et al. (2007) reported an increase of the leachability of potassium after mechanical activation of the substrate by ultra-fine milling.

In Greenland, the perpetual movement of the ice sheet produces fine-grained glacial rock flour (GRF) by abrading the underlying bedrock. The material is eventually transported by glacial meltwater streams and deposited in the fjords (Bennike et al., 2019). Existing submarine deposits appeared at the surface after isostatic rebound and continental uplift about $\sim 11\,\mathrm{ka\,BP}$ (Bennike et al., 2002). A recent publication (Pesch et al., 2022) investigated 16 deposits of GRF in South Greenland. The fine particle fraction (particles with an equivalent diameter $< 20\,\mu\mathrm{m}$) of the investigated GRFs ranged between 31 and 82 % w/w. The mineralogical analysis revealed that the fine fraction of the sediments contained relatively large amounts of quartz and feldspars, but also clay minerals (kaolinite, chlorite), micas (biotite, muscovite) and amphiboles which significantly contribute to the chemical activity of the mineral fraction of a soil (Kennedy, 1965; Malcolm et al., 1970).

The soils used for agricultural production in Greenland are often characterized by a coarse texture and relatively high contents of particulate organic matter; furthermore, Greenlandic agriculture is entirely dependent on imports of mineral fertilizers. Considering that large deposits of GRF are readily available within the major agricultural areas of South Greenland, GRF could be an interesting and sustainable complement to artificial mineral fertilizers, eventually increasing their efficiency, as reported by Sukstorf et al. (2020). The potential of GRF as soil amendment has been investigated by several authors (Gunnarsen, 2020; Gunnarsen et al., 2019; Sukstorf et al., 2020), but none of the studies investigated

the effect of GRF on soil functional and mechanical properties.

The addition of GRF to a soil as amendment modifies its particle size distribution, which might affect the soil's pore network, as the texture (including soil organic matter, OM) partly governs the arrangement and shape of the pores (Arthur et al., 2012; Fujikawa et al., 2005; Nimmo, 2004). Several authors (e.g., Hamamoto et al., 2008; Moldrup et al., 2003; Poulsen, 2013; Tuli et al., 2005) suggested the use of air-phase parameters to assess the properties of the pore network, because gas transport through soil is inseparably connected to the pore network characteristics (Buckingham, 1904; Katuwal et al., 2015). Generally, the air-phase parameters include the air-filled porosity (ε), the air permeability (k_a, as a measure for the pressure-driven mass transport), and the gas diffusivity (D_p/D_o, as a measure for the density-driven mass transport). k_a and D_p/D_o are controlled to a large extent by ε and are thus dependent on the soil's moisture status (McCarthy et al., 1992). Recently, Pesch et al. (2021) and Weber et al. (2020) used the connectivity-tortuosity parameter ($X = \log(D_p/D_o)/\log\varepsilon$) to assess the tortuosity and connectivity of the pore network of undisturbed Greenlandic pasture soils. Kawamoto et al. (2006) and Pesch et al. (2021) used the ratio of k_a to D_p/D_o (Ω) as a soil structure index in cultivated and pasture soils.

As for the air-phase, changes in particle size distribution also affect the mechanical properties of soil (Keller et al., 2012; Salire et al., 1994). Some mechanical properties of soil can be derived from stress-strain curves, which can be obtained from uniaxial confined compression tests (UCCT, Lamandé et al., 2017).

The plastic deformation of a soil sample is generally quantified by the compression index (C_c), a measure for the soil's compressibility. The partly irreversible plastic deformation is strongly affected by texture (including OM, Etana et al., 1997; Soane, 1990), soil moisture (Larson et al., 1980) and land use and management (Batey, 2009). Several studies investigated the texture dependence of a soil's compressibility (e.g., Etana et al., 1997; Larson et al., 1980) who found a positive correlation between the C_c and the fine mineral fraction (clay) and the opposite effect for increasing OM, while keeping the fine fraction constant. An increase in OM of the tested samples generally led to larger C_c, which was mainly attributed to the lower dry bulk densities associated with higher OM contents and thus to higher void ratios (Pesch et al., 2020; Zhang et al., 2005).

The soil's recovery from compression (i.e., the rebound) can be characterized by the expansion of the soil after the applied stress has been released and is a function of the elasticity of the soil matrix and the pore water pressure (Stone et al., 1980; Zhang et al., 2005). For undisturbed sandy Greenlandic pasture soils, Pesch et al. (2020) recently reported a significant rebound after severe compaction ($\sigma_{max} = 800\,\text{kPa}$) and attributed it mainly to the presence of organic fibers originating from the root zone in the soil matrix and the low dry bulk density.

The melioration of Greenlandic sandy soils by the addition of the fine grained GRF may be an opportunity to optimize the soils for agricultural production by increasing the reactivity of the soil's mineral phase and, by that, reducing the water repellency (Ward et al., 1993), which was reported to be significant by Weber et al. (2021). Furthermore, GRF amendment might, with time, induce soil aggregation by organo-mineral complexation (Eusterhues et al., 2003) and thus improving soil aeration and water-holding capacity of Greenlandic agricultural soils. However, the addition of GRF to sandy soil might have undesired effects on the pore network and mechanical stability, which need to be assessed prior to application.

This study investigated the effects of adding low and high doses of GRF on soil functional behavior. Glacial rock flour was added to three soils (two from Greenland and one from Denmark) and one techno-sand (Sweden) to investigate how the GRF-induced change in particle size distribution affected different soil types. The pore-network was described by the soil-gas diffusivity, the soil-air permeability, and the derived indices for tortuosity (X) and effective pore diameter for gas transport (d_{eff}). In addition, the effect of adding GRF on the soil mechanical behavior was investigated using the compression index (C_c) and soil rebound after compaction (ΔE). The experiments were performed on repacked samples under well-controlled conditions.

2 Materials and Methods

2.1 Soils and rock flour

The soil from Upernaviarsuk was collected during a field trip in 2013 and was first described in Hermansen et al. (2017); it was classified as a Lithic

Table 1: Background information on sites, soils, and GRF.

Site		Origin	Geographical coordinates		Geological origin	Land/material use
Upernaviarsuk	(U)	South Greenland	N60°45′19.7″	W45°53′36.5″	glacial till	cultivated
South Igaliku	(S)	South Greenland	N60°53′29.2″	W45°16′27.8″	periglacial aeolian/fluvial	pasture
Jyndevad	(J)	Denmark	N54°53′36.9″	E9°7′12.0″	periglacial fluvial/aeolian	cultivated
Baskarp	(B)	Sweden	N58°1′6.1″	E14°10′18.0″	lacustrine	geotechnical sand
Iterlak	(IK-4)	South Greenland	N60°55′4.9″	W45°17′19.7″	uplifted marine	soil amendment

Dystrocryepts. The soil type ranged from loamy sand to sandy loam (Soil Survey Division Staff, 1999). At the time of sampling, the vegetation consisted of common oat (*Avena sativa*, L.).

The South Igaliku field is used as a long-term summer pasture for sheep, and the soil was described in Weber et al. (2020). It was classified as Lithic Dystrocryepts, and the soil type ranged from loamy sand to sandy loam (Pesch et al., 2021). The sampling took place in 2017, and the vegetation consisted of a typical mix of high latitude (or altitude in temperate regions) grassland species (further details in Weber et al., 2020).

The soil from Jyndevad is part of the Danish Pesticide Leaching Assessment Program and was classified as Typic Haplorthods. The sampling was carried out in spring 2012, and the soil was classified as coarse sand (Masís-Meléndez et al., 2014).

All the soil samples used in this study consisted of loose bulk samples ($5-15\,\mathrm{cm}$ depth); the material was air dried, crushed in a mortar to eliminate aggregates if necessary (only the soil from Upernaviarsuk), sieved to $< 2\,\mathrm{mm}$, and stored in plastic bags until further testing.

The construction sand Baskarp (Baskarp Sand No. 15) was obtained from the manufacturer (Baskarpsand AB, Habo, Sweden); a detailed description of its geotechnical properties is given in Nielsen et al. (2018).

We used fine-grained physically abraded mineral material (glacial rock flour, GRF) from South Greenland as a soil amendment and to alter the texture of the pure soils and sands. We collected loose bulk samples ($20-30\,\mathrm{cm}$ depth) from a deposit (IK-4) in South Greenland during a sampling campaign in 2019. The volume of the deposit was estimated at $360\times10^3\,\mathrm{m}^3$. The samples were stored in sealed plastic bags during the transport to the laboratory and subsequently air dried, crushed in a mortar, and stored in sealed containers until further

testing. A detailed description and its potential as soil amendment of the herein used GRF (IK-4) can be found in Pesch et al. (2022).

2.2 Laboratory methods

A flow chart outlines the test procedures deployed in this study (Figure 1).

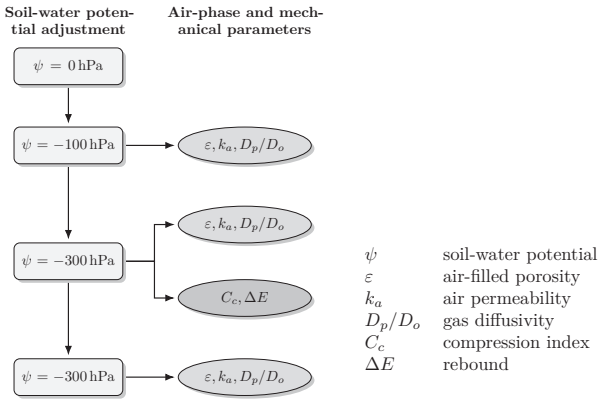

Figure 1: Flow diagram of measurements; available measurements for each test stage are given in Table 2.

Table 2: Overview of the parameters measured at different soil water potentials (ψ) and before (bC) and after compression and rebound (aR).

	k_a	D_p/D_o	C_c	ΔE
$\psi = -100\,\mathrm{hPa}$, bC	J, B	J, B	not applicable	
$\psi = -300\,\mathrm{hPa}$, bC	U, S, J, B	U, S, J, B	not applicable	
$\psi = -300\,\mathrm{hPa}$, aR	U, S, J, B*	U, S, J, B*	U, S, J, B*	U, S, J, B*

k_a: air permeability; D_p/D_o: diffusivity; C_c: compression index; ΔE: rebound
bC: before compression; aR: after compression, rebound and readjustment of ψ
U: Upernaviarsuk; S: South Igaliku; J: Jyndevad; B: Baskarp
B*: samples B 0 % collapsed during testing

Repacking

We prepared triplicates of repacked (disturbed) samples exhibiting three levels of GRF-concentration (per weight): 0, 3.5, and 10 % using 100 cm^3 steel soil

core cylinders (diameter: 6.01 cm, height 3.41 cm). Three replicates of each mixture were prepared, resulting in 36 soil core samples (four soils – three GRF concentrations – three replicates each).

The air–dried components (soils and GRF) were mixed by hand and passed through a 2 mm sieve two times to ensure homogeneity. To facilitate the repacking process, the cohesion of the soil-GRF mixtures was increased by the adjustment of the gravimetric water content to $\sim 0.02\,\mathrm{kg\,kg^{-1}}$. The soil cores were repacked layer by layer, where each layer consisted of approximately 25 mL of loose material and was proctor compacted using a hammer with a sliding weight of 0.190 kg and a falling height of 0.40 m. Each layer received ten blows, resulting in a total energy input of approximately 7 J per layer and a layer height between $0.5 - 0.7$ cm, depending on the soil type. To reduce a potential layering effect caused by the repacking procedure, the surface of each layer was carefully loosened using a spatula in order to achieve a more or less uniform transition between each layer. The procedure was repeated until the soil core was filled beyond the cylinder edge; the excess soil was removed with a spatula to end up with an exact volume of $100\,\mathrm{cm^3}$.

Soil air-phase parameters

The repacked samples were saturated from below and subsequently drained to the soil water potentials of $\psi = -100$ hPa and $\psi = -300$ hPa on suction tables, according to Dane et al. (2002). After equilibration with the applied negative pressure head, the water content (θ), the air permeability (k_a), and relative diffusivity (D_p/D_o) were determined.

The k_a in $\mu\mathrm{m}^2$ was determined, according to Ball et al. (2002), using the device and procedure as described in Schjønning et al. (2017). The gas diffusion coefficient (D_p in $\mathrm{cm^2\,s^{-1}}$) using O_2 as diffusing gas was determined by the one-chamber steady-state method as described in Schjønning (1985). The relative gas diffusivity (D_p/D_o) was obtained by dividing the D_p by the diffusion coefficient of O_2 in free air at 20 °C, $D_o = 0.205\,\mathrm{cm^2\,s^{-1}}$ (Schjønning et al., 2013). Due to technical problems, not all the air-phase parameters could be measured at the two soil water potentials (see Table 2).

The initial dry bulk density (ρ_b in $\mathrm{Mg\,m^{-3}}$) was determined after oven drying the samples at 105 °C for 24 h. The total porosity was calculated from ρ_b

and the average particle density (mass of soil solids per unit volume), ρ_s, as $\Phi = 1 - \rho_b/\rho_s$, and given in $m^3\,m^{-3}$. The air-filled porosity, ε in $m^3\,m^{-3}$, was determined as the difference between Φ and the volumetric water content (θ in $m^3\,m^{-3}$).

Soil mechanical parameters

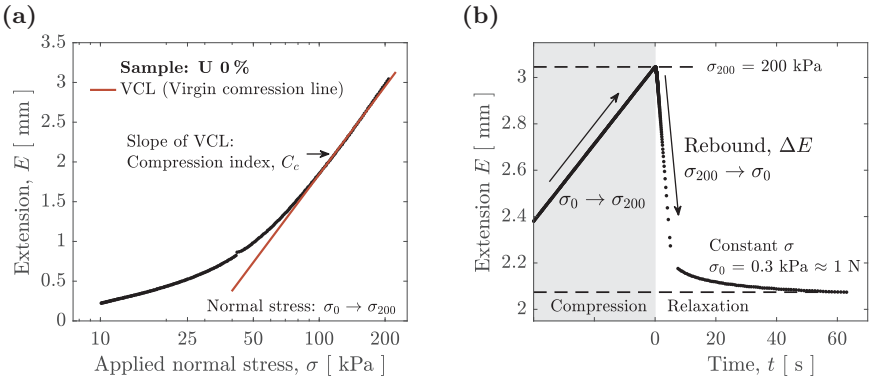

Figure 2: Compression and relaxation test exemplified by a pure soil sample (Upernaviarsuk 0 %). (a) Compression curve with indicated virgin compression line (VCL), and (b) active measurement of relaxation, quantified by the rebound, ΔE.

The strain-controlled, undrained uniaxial confined compression tests (UCCT) were performed on soil samples drained to $\psi = -300$ hPa using a fully automated dual column table frame extensometer (Instron series 5960, Illinois Tool Works Inc.) mounted with a 5 kN static load cell, using a constant strain rate of $1\,mm\,min^{-1}$, as suggested by Koolen (1974) and Lamandé et al. (2017) and a maximum applied stress of 200 kPa. Figure 2 a shows a typical compression curve plotted in a semi-logarithmic domain with the applied normal stress (σ in kPa, log-scale) on the x-axis and the position of the compression piston relative to the sample surface (compressive extension, E in mm) on the y-axis. The compression index, C_c [$mm\,(10\,kPa)^{-1}$], was calculated as the slope of the linear part of the compression curve at high applied stress, generally referred to as the virgin compression line (VCL; Keller et al., 2011).

The rebound after relaxation, ΔE in mm, was actively measured by keeping a constant load of approximately 1 N on top of the sample's surface for 60 s and

simultaneously measuring the expansion of the soil sample by the extensometer. The procedure is visualized in Figure 2 b.

After the completion of the UCCT, the matric potentials of the samples were slowly readjusted to −300 hPa as described in the previous section and, after equilibration, the air-phase parameters (ε, k_a, and D_p/D_o) were measured again. The samples were intentionally not re-saturated then drained to −300 hPa after the compression tests to avoid substantial alteration of the pore network.

Soil solid-phase parameters

Particle size distribution (PSD), organic matter content (OM), and average particle density (mass of solid particles per unit volume, ρ_s) were measured on triplicates of loose bulk soil.

The OM was determined by ignition at 550 °C for at least 12 h and was referred to as OM_{LOI} and given in % w/w (Hoogsteen et al., 2018). The particle density, ρ_s in Mg m^{-3}, was measured on oven-dry (105 °C) material by water displacement according to Flint et al. (2002). In short, a pyknometer (60 cm^3) was filled with approximately 7 g of air dried soil and mixed with demineralized and degassed water. To ensure the sedimentation of the organic fraction and to remove entrapped air, the pyknometer was subjected to a partial vacuum in a desiccator for 30 min.

The volume-weighted particle size distribution was measured by low angle light scattering (laser diffraction, LD) using a Mastersizer 2000 coupled to the wet dispersion unit Hydro 2000MU (both Malvern Instruments Ltd, Worcestershire, UK). Prior to the measurements, the OM was removed by hydrogen peroxide, and the material was dispersed by the addition of $Na_4P_2O_7$ and two hours of horizontal shaking. The device stored the measurements internally in 100 particle size bins resulting in 100 measured points between 0.02 and 2000 µm.

The gravimetric clay content (clay in % w/w) was estimated from the volumetric fraction of particles < 4.4 µm determined by LD, as proposed by Di Stefano et al. (2010) and Pesch et al. (2022). The gravimetric sand content was set equal to the volumetric fraction of particles > 50 µm, as proposed by Di Stefano et al. (2010). The estimated gravimetric clay and sand fractions were used to determine the texture classes according to Soil Survey Division Staff (1999).

The solid phase properties of the used GRF were determined by the same methods as described above (see Pesch et al., 2022)

2.3 Modeling soil parameters

Rosin-Rammler particle size distribution function

The frequency size distribution measured by LD was converted to the cumulative particle size distribution by cumulative summation. The Rosin-Rammler size distribution function (RR; Rosin et al., 1933), as given in Equation 1 was fitted to the cumulative distributions.

$$F(d < D) = 1 - \exp\left(-\frac{d}{\alpha_R}\right)^{\beta_R}, \tag{1}$$

with $F(d < D)$ representing the cumulative fraction of particles exhibiting a diameter d (in linear scale) smaller than D (here: upper boundary of the relevant particle size class). The fitting parameters α_R and β_R represent the location and shape parameters of the distribution, respectively. In particular, α_R represents the particle diameter of the 0.632 or $1 - 1/e$ (e being the Euler number) fraction; β_R is a measure for the grading (or spread) of the distribution with well-graded material exhibiting high and poorly graded low values of β_R, respectively (see Figure 3).

Pore network models

The Buckingham (1904) connectivity-tortuosity parameter X was either determined by fitting Equation 2 to the entire or part of the dataset or, for individual pairs of measurements, by linearization of Equation 2 into Equation 3.

$$D_p/D_o = \varepsilon^X \tag{2}$$

$$X = \frac{\log(D_p/D_o)}{\log \varepsilon} \tag{3}$$

The diameter of pores allowing air-flow through the soil sample was assessed by the effective pore diameter, d_{eff} [µm], derived independently by Ball (1981) and Millington et al. (1964) by combining Poiseuille's (convective) and Fick's (diffusive) laws for fluid transport (Moldrup et al., 2001); it was calculated according to Equation 4.

$$d_{eff} = 2 \cdot \sqrt{\frac{8 \cdot k_a}{(D_p/D_o)}} \tag{4}$$

2.4 Statistical analysis

The linear and non-linear relation between dependent and independent variables was assessed via linear and non-linear least-squares regression, respectively. The goodness of fit of a relation including an intercept was given by the ordinary (R^2) and adjusted coefficient of determination (R^2_{adj}) in the case of single independent or multiple independent variables, respectively. The root-mean square error, RMSE, was used to quantify the deviation of a predicted to an observed value and is given in Equation 5.

$$\mathrm{RMSE} = \sqrt{\sum_{i=1}^{n} \frac{(\hat{y}_i - y_i)^2}{n}}, \tag{5}$$

with $\hat{y}_i$ being the predicted value of the observed y_i and n the number of observations. The RMSE takes the same physical units (if any) as the observed and predicted values.

The linear correlation between two variables was assessed by the Pearson correlation coefficient denoted by r.

We used a non-parametric bootstrap scheme to artificially augment the number of samples to compute a density distribution of the regression parameters (Efron, 1979; Stine, 1985).

The statistical significance of differences among means was assessed by analysis of variance (ANOVA). We applied Tukey's HSD test (Tukey Honest Significant Differences; Tukey, 1977) for the pair-wise comparisons. The assumptions of normality of the ANOVA residuals and homogeneity of variances were assessed

by the Shapiro-Wilk test (Shapiro et al., 1965) and the Levene test (Brown et al., 1974), respectively. Statistical significance was reached if the p-value was below .05.

3 Results and discussion

3.1 Effects of glacial rock flour (GRF) addition on soil solid-phase parameters

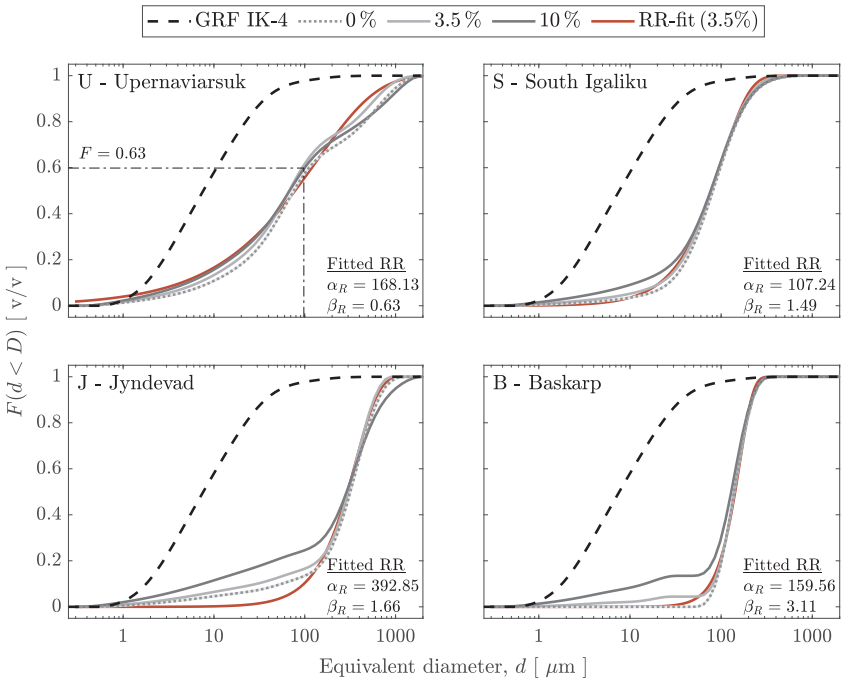

Figure 3: Cumulative particle size distribution (PSD) of the used materials and mixes. Location parameter of the RR-distribution at $F = 1 - 1/e = 0.63$ in the U sub-plot. The GRF concentrations are given in the legend above the plot area. The Rosin-Rammler distribution function (RR, Equation 1) was fitted to the 3.5 % GRF-amended samples of each material to depict the variation of the fitting parameters α_R and β_R. The PSD of IK-4 was taken from Pesch et al. (2022).

The different GRF-amendment levels could be identified as vertical shifts of the cumulative particle size distributions, especially in the grain size range below 100 µm, as shown in Figure 3. The PSD of the pure materials exhibited multimodal distributions, except the Baskarp sand; the addition of GRF increased

Table 3: Soil texture classes according to Soil Survey Division Staff (1999); clay ($< 2\,\mu m$), silt ($2 - 50\,\mu m$), and sand ($> 50\,\mu m$) contents; fitting parameters of the Rosin-Rammler particle size distribution function (α_R and β_R); organic matter based on loss on ignition at 550 °C (OM_{LOI}); ρ_s and ρ_b, particle and initial dry bulk density, respectively; Φ, initial total porosity.

Material	GRF-Level	Abb.	Class	Clay*	Silt	Sand*	α_R	β_R	OM_{LOI}	ρ_s	ρ_b	Φ
	%				% w/w		µm		% w/w	Mg m^{-3}		m^3 m^{-3}
Upernaviarsuk	0	U 0	SL	5.92	30.85	63.23	168.13	0.63	5.02	2.58	1.32	0.49
	3.5	U 3.5	SL	7.55	32.51	59.94	136.99	0.65	4.91	2.60	1.33	0.49
	15	U 15	SL	9.35	31.72	58.93	151.94	0.57	4.60	2.60	1.32	0.49
South Igaliku	0	S 0	LS	1.96	23.69	74.35	107.24	1.49	2.97	2.67	1.31	0.51
	3.5	S 3.5	SL	3.07	25.42	71.51	102.94	1.43	3.05	2.67	1.31	0.51
	15	S 15	SL	5.72	25.35	68.93	102.34	1.26	2.85	2.68	1.31	0.51
Jyndevad	0	J 0	S	2.91	6.41	90.68	392.85	1.66	3.63	2.58	1.41	0.45
	3.5	J 3.5	S	4.20	8.30	87.50	365.52	1.71	3.52	2.59	1.42	0.45
	15	J 15	LS	7.68	12.78	79.54	376.30	1.00	3.35	2.60	1.45	0.44
Baskarp	0	B 0	S	0	0	100	159.56	3.11	0.18	2.64	1.29	0.51
	3.5	B 3.5	S	1.60	2.83	95.57	161.22	2.97	0.28	2.65	1.27	0.52
	15	B 15	LS	5.78	7.69	86.52	150.85	2.42	0.37	2.66	1.38	0.48
Glacial rock flour	—	IK-4	SiCL	32.09	61.24	6.67	12.62	0.99	—	2.63	—	—

* gravimetric clay and sand: estimated from volumetric fraction $d < 4.4\,\mu m$ and $d > 50\,\mu m$, respectively (measured by LD).

the amplitude and number of modes, which resulted in poorer fits of the RR distribution function with increasing GRF concentration. The RMSE of the fitted RR distribution function ranged between $0.011 - 0.064$, with a mean value of $0.035\,v/v$.

Apart from the loamy U soil, the texture shifted to finer classes with increasing GRF concentration (Table 3).

The addition of GRF replaced an equal amount of soil and OM. The lower density of the OM than that of the added mineral fraction explained the slight increase of the ρ_s of the mixtures.

The constant energy input repacking procedure resulted in fairly constant ρ_b for the loamy soils (U and S), whereas an increase was observed for the sandy material (Table 3). This corroborates the findings of Sohn et al. (1968), who attributed the increase of the packing density to an increased spread of the distribution (here: decreasing parameter β_R) and the shape of the particles (not considered or measured in this study). No significant correlation could be found between the OM_{LOI} and the ρ_b, neither for the pooled nor for the individual soils (except B sands: $r = .70^*$).

The apparent cohesion of the pure Baskarp sand at $\psi = -300\,hPa$ was low, which resulted in the collapse of all of the three replicates of the 0 % GRF amended material before the air-phase, and mechanical parameters could be

measured (Table 2). The addition of 3.5 % of GRF per weight of dry sand increased the cohesion so that the samples did not collapse.

3.2 Combined effects of GRF addition and soil OM on soil air-phase parameters

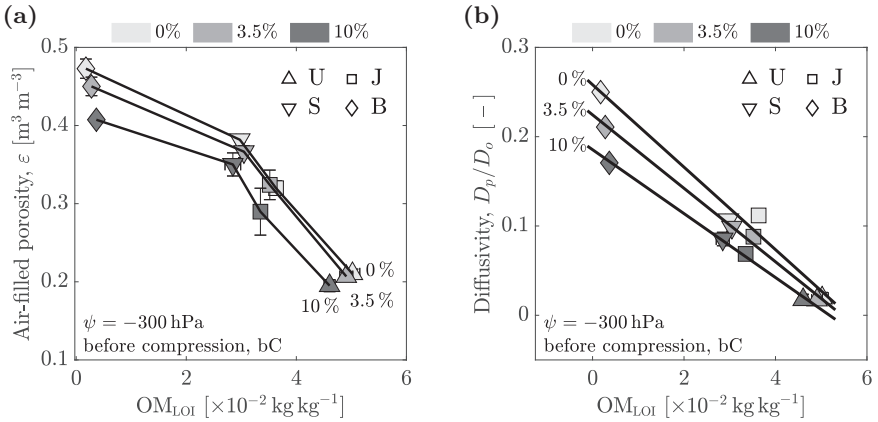

FIGURE 4: Air phase parameters of the repacked soil samples versus OM_{LOI} (loss-on-ignition) at the three GRF concentrations (see labels above figures). (a) Air-filled porosity, ε, and (b) gas diffusivity, D_p/D_o, both at $\psi = -300$ hPa and before compression, versus OM_{LOI}.

The volume of pores > 10 µm drained at an applied negative pressure of $\psi = -300$ hPa (Schjønning, 1992) decreased with increasing fine particle fractions. The soil type governed the general level of available pore space for gas exchange at $\psi = -300$ hPa; for the prepared mixtures, the initial soil type prevailed over the GRF effect on ε.

The decreasing curvilinear dependence of ε on the OM_{LOI} was well depicted by the connecting lines in Figure 4 a. Generally, the 0 and 3.5 % GRF levels did not exhibit considerable differences in ε at $\psi = -300$ hPa, whereas the 10 % GRF amended soils seemed to have reduced available pore space for gas transport at the given matric potential, most likely due to a shift in the pore size distribution towards smaller pores caused by the preferential filling of the voids between larger (sand-sized) particles by the added fine material. The higher amount of available fine grained material might have partly closed those larger pores.

It should be noted that the OM_{LOI} did not only account for the organic fraction; it also contained the loss of structural water (crystal lattice water and interlayer water molecules of mainly clay minerals) during the ignition process (Sun et al., 2009), thus including additional information about the mineral phase of the soil.

The D_p/D_o of each GRF level exhibited a significant negative linear correlation with OM_{LOI}, as depicted by the trend lines in Figure 4 b. The technical sands (B) exhibited the largest decrease in D_p/D_o with increasing GRF concentration which could be attributed to the reduced ε as shown in Figure 4 a. The effect of GRF on D_p/D_o decreased with increasing fine mineral fraction of the pure soils and sands.

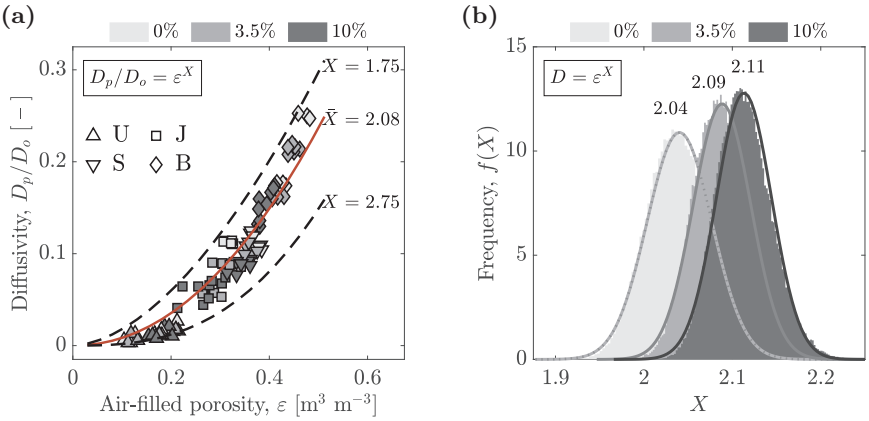

FIGURE 5: Relative diffusivity (a) as a function of the air-filled porosity (ε) and Equation 2 using $X = \bar{X} = 2.08$ (solid red line, see text); extrema (dashed lines, estimated by eye) and their respective X values; (b) result of the bootstrapped non-linear regression given as the frequency distributions of the fitted regression coefficients (X); mean X values for each GRF level are given above the distributions.

Equation 2 was fitted to the resampled D_p/D_o measurements of all the experimental stages combined (Figure 1) but separated according to the GRF concentration (0, 3.5, and 10 %). The resulting means of the bootstrapped X of the individual GRF-level datasets increased with increasing GRF-concentration. The frequency distribution and the fitted normal distribution function of the bootstrapped X-fit are shown in Figure 5 b. The mean and standard deviation (in parentheses) of the fitted normal distribution for the three increasing GRF levels were 2.04 (0.04), 2.09 (0.03), and 2.11 (0.03), respectively. The frequency distributions of the bootstrapped X and the associated standard deviations

revealed a relatively narrow distribution of each of the GRF-levels. Figure 5 a shows that the simple power-law (Equation 2) well described the D_p/D_o as a function of ε across soil types, moisture, and compaction levels. Deepagoda et al. (2018) reported similar results for mixtures of differently textured sands. The mean and standard deviation of the resampled complete dataset (all GRF, moisture and compaction levels combined) resulted in $\bar{X} = 2.08\,(0.02)$; it is depicted by the solid red line in Figure 5 a.

The comparison with existing D_p/D_o data from literature of undisturbed soil samples from the U (Weber et al., 2020) and S (Pesch et al., 2021; Weber et al., 2020) pasture fields in South Greenland revealed that the D_p/D_o were in the same order of magnitude for the herein measured ε-range. Although this might be surprising, Pesch et al. (2021) and Weber et al. (2020) also noted that the Greenlandic soils showed modest signs of soil-structure development, with similar air-phase parameters to the repacked soils.

Increasing X with increasing GRF and thus increasing fine particle fraction indicated an increase in the tortuosity and a decrease of the pore network's connectivity. The addition of the fine grained GRF reduced the void space between larger particles as those are preferentially filled by the smaller fraction (Sohn et al., 1968); additionally, the repacking procedure by individual layers most likely created a layered structure within the cores which contributed to the slightly larger observed X, despite the precautions taken during the repacking as described in the methods section. The tortuosity decreased with increasing texture uniformity, represented by the parameter β_R ($r = -.83^{***}$); a similar trend of X with β_R was also reported by Chamindu Deepagoda et al. (2020).

In contrast to D_p/D_o, k_a clearly differentiated between the different initial soil types as shown in Figure 6 b. The fitting of the Ω-model ($k_a = \Omega \cdot \varepsilon^X$, Kawamoto et al., 2006; Pesch et al., 2021) revealed the differences between the repacked Greenlandic and Danish sands and soils, as shown in Figure 6 a; X was kept constant and set to $X = 2.08$ as determined and explained earlier in the text and shown in Figure 5 a. The magnitude of k_a was highly dependent on soil type, as shown by the significantly different fitted Ω-values obtained for the sands (J & B) and loams (U & S), as depicted by the dashed lines in Figure 6 a. For the sandy soils (J & B), the steps of the experiment (1 to 2: drying; 2 to 3: compression) could be approximated by linear trend lines, and they were clearly distinguishable from each other (solid colored lines 1, 2, and 3 in Figure 6 b).

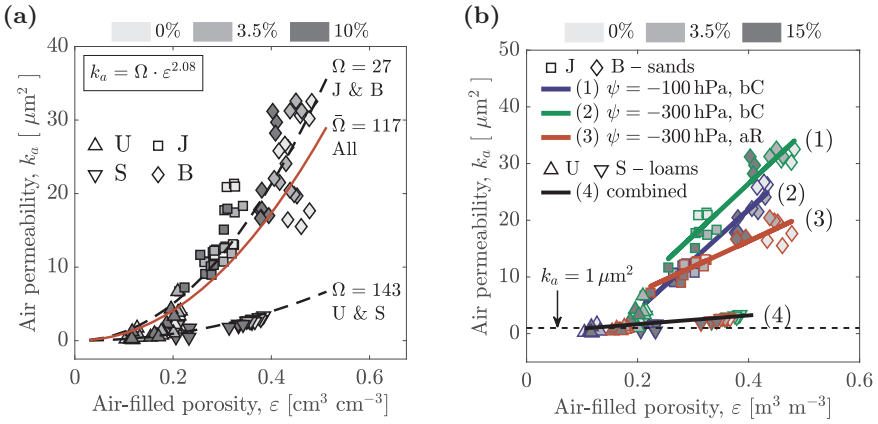

Figure 6: Air permeability as a function of the air-filled porosity (ε) and Kawamoto et al. (2006) (Ω) model fitted to the sands (J & B), sandy loams (U & S), and the complete dataset (All). X was fixed to 2.08, as shown in Figure 5 (a); (b) combined effects of moisture (ψ) and compression (bC and aC) only evident for the sands (J & B) and no clear influence of GRF-level.

The samples exhibited similar ε ranges before and after compression, but k_a was reduced by compression. This reduction in k_a could be attributed to a shift in the pore size distribution towards smaller pore diameters due to the compression (Pulido-Moncada et al., 2019; Schäffer et al., 2008). The general limit of impermeability for undisturbed soil is $k_a < 1\,\mu\text{m}^2$ (Ball et al., 1988) and is depicted in Figure 6 b. The low k_a of the Greenlandic material (U & S) indicated that the repacked soils were susceptible to degradation in terms of soil aeration even at $\psi = -300$ hPa (trend-line 4 in Figure 6 b).

Figure 7 (top) shows the connectivity-tortuosity parameter X at $\psi = -300$ hPa before (left-hand symbol) and after compression (right-hand symbol). For each soil, an ANOVA followed by Tukey's HSD test was used to examine the significance of the means for each GRF amendment level (bC and aR combined). The results were given as letter notation in the plot areas. The X of the loamy U soil was not significantly affected by the GRF concentration, whereas, for the remaining soils, a positive trend with increasing GRF concentration was observed, which, however, did not persist for the 10 % GRF concentration.

For the pooled dataset, the linear model including the factors GRF concentration (3 levels: 0, 3.5 and 10 %), compression (2 levels: bC and aR), and the factor soil (representing texture, OM and other intrinsic properties, 4 levels: U, S, J,

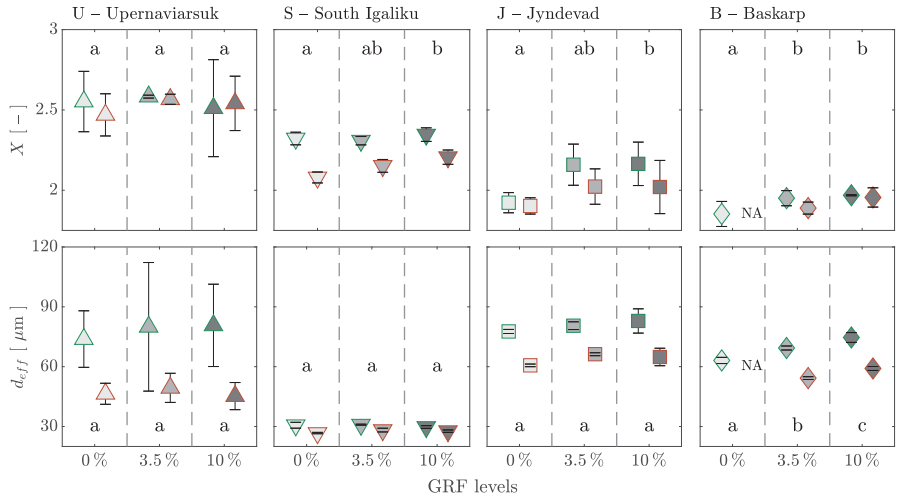

Figure 7: Pore network parameters at $\psi = -300$ hPa: X (upper plots) and d_{eff} (lower plots) before (left-hand symbol of each GRF level, green outline, bC) and after compression and rebound (right-hand symbol, red outline, aR). Symbols are mean values; error bars represent the standard deviation. Groups bearing the same letters were not statistically different from each other (each soil type was tested individually, bC and aR were combined).

Table 4: ANOVA table for X and d_{eff} including all relevant and significant factors (pooled dataset).

Factor/model	Sum of Squares	df	Mean Square	F	p
Linear model:	$X \sim 1 +$ GRF conc. $+$ compression $+$ soil				
GRF conc.	0.137	2	0.068	5.874	.005
compression	0.129	1	0.129	11.074	.001
soil	3.868	3	1.289	110.853	<.000
Error	0.721	62	0.012		
Linear model:	$d_{eff} \sim 1 +$ compression $+$ soil				
compression	4320.192	1	4320.192	45.782	<.000
soil	19 230.707	3	6410.236	67.931	<.000
Error	6039.334	64	94.365		

and B) as predictors revealed that X increased significantly with increasing GRF concentration and was significantly reduced by compression (Table 4). The factor soil had the largest impact on the magnitude of X. None of the

relevant interactions between the categorical predictors had a significant effect on X.

The effective pore diameter of the agricultural soils, d_{eff}, determined according to Equation 4, was not affected by the GRF concentration. However, a significant increase was observed for the geotechnical sand from Baskarp.

For the pooled dataset, the linear model including the factors compression (2 levels: bC and aR) and the factor soil (4 levels: U, S, J, and B) as predictors revealed that d_{eff} was significantly reduced by compression (Table 4) and that the factor soil-type had the biggest impact on the magnitude of d_{eff}. The d_{eff} was neither affected by the GRF concentration nor by any of the relevant interactions between the categorical predictors.

3.3 Effect of GRF addition on soil mechanical parameters

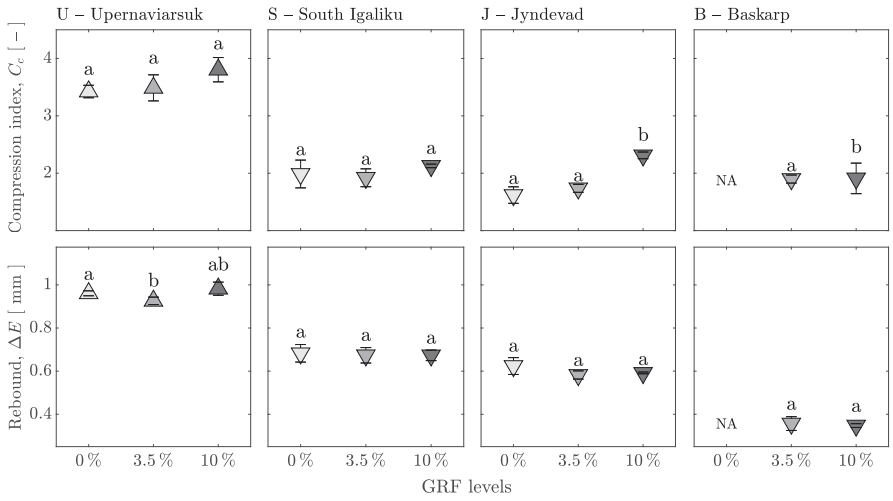

Figure 8: (top) Compression index, C_c, and (bottom) rebound, ΔE, in mm. Samples B 0 % collapsed before the compression test could be performed. Symbols are mean values; error bars represent the standard deviation; symbols bearing the same letter are not statistically different from each other (each soil was tested individually).

The compression index as a measure of irreversible deformation was highest for the loamy U soils, and the 3.5 % GRF-level had no significant effect on the C_c compared to the 0 % GRF-level. The C_c of the 10 % GRF amended soils

Table 5: ANOVA table for C_c and ΔE including all relevant and significant factors (pooled dataset).

Factor/model	Sum of Squares	df	Mean Square	F	p
Linear model:	$C_c \sim 1 + \text{GRF conc.} + \text{soil}$				
GRF conc.	0.756	2	0.378	10.451	<.000
soil	17.812	3	5.937	164.159	<.000
Error	0.976	27	0.036		
Linear model:	$\Delta E \sim 1 + \text{soil}$				
soil	1.389	3	0.463	564.974	<.000
Error	0.024	27	0.001		

exhibited an increasing tendency, which was significant for the sands, J & B. The result of the Tukey's HSD test following the one-way ANOVA for each soil using the GRF concentration as grouping variable is given as letter notation in Figure 8 (top).

For the pooled dataset, the linear model including the factors GRF concentration (3 levels: 0, 3.5 and 10 %) and soil (4 levels: U, S, J, and B) as categorical predictors revealed that C_c increased significantly with increasing GRF concentration (Table 5). The factor soil had the largest impact on the magnitude of C_c; however, the pair-wise comparison showed that only the C_c of the loamy U soil was significantly higher than the remaining soils. None of the relevant interactions between the categorical predictors had a significant effect on C_c.

The magnitude of ΔE was highest for the loamy U soils and only the 3.5 % GRF-level of the U soils was significantly lower compared to the 0 % GRF-level. The remaining soils and sands were not affected by the GRF concentration, as shown in Figure 8 (bottom).

For the pooled dataset, the magnitude of ΔE was not affected by the GRF concentration, and it was again the factor soil which had the most significant impact on the magnitude of ΔE (Table 5). The pairwise comparison revealed that ΔE significantly decreased following U > S > J > B.

C_c could be well described by a power-law function using the RR shape-parameter, β_R, as the independent variable, as shown in Figure 9 a and Table 6. The increasing C_c with increasing GRF concentration did not only affect the

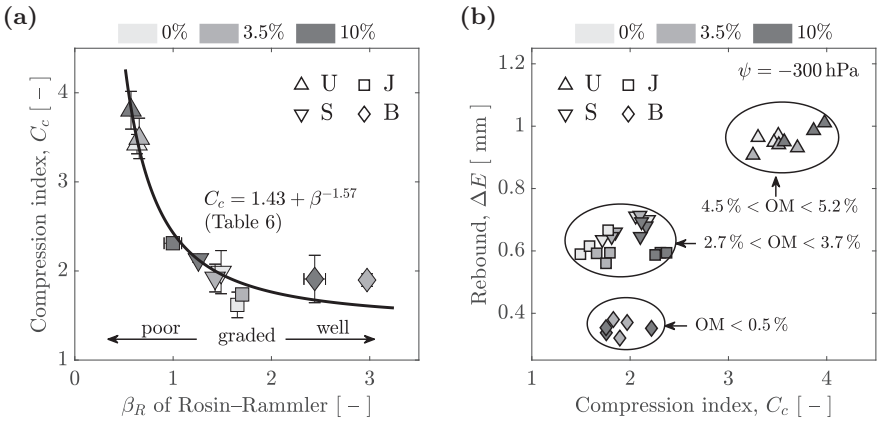

Figure 9: Influence of basic soil properties on mechanical parameters. (a) The non-linear relation of C_c to the texture grading (bars depict the standard deviation) and (b) the dependence of ΔE on the organic matter content (OM) and the compressibility of the material (C_c). Regression statistics are given in Table 6

Table 6: Simple linear regression statistics showing the dependence of C_c and ΔE on basic soil properties. N is the number of observations included in each regression.

Regression equation	N	R^2	RMSE
$C_c = 1.43^{***} + \beta_R^{-1.57^{***}}$	11	.95	0.17
$\Delta E = 0.28^{***} + 12.56^{***} \cdot \mathrm{OM_{LOI}}$	11	.86	0.09

β_R: grading coefficient of RR-fit; $\mathrm{OM_{LOI}}$: organic matter (loss on ignition)

sample's behavior during compression but also during the sample preparation (same energy input for each sample during repacking). Sohn et al. (1968) observed an increasing packing density with a decreasing grading of the PSD, resulting in higher C_c. No significant correlation could be found between the C_c and the ρ_b, neither for the pooled nor for the individual soils, which was also mainly due to the repacking procedure. Changes in soil water pressure and resistance to redistribution of soil water (both dependent on the hydraulic properties of the material) during compression are a well known parameters affecting the magnitude of C_c (e.g., Fazekas et al., 2005; Keller et al., 2007) but have not been considered in this study.

ΔE was significantly correlated to the $\mathrm{OM_{LOI}}$ ($r = .92^{***}$), and a simple linear regression resulted in excellent goodness of fit as shown in Table 6. Figure 9 b

reveals the influence of the OM content on the magnitude of ΔE related to the compressibility (C_c) of the material. Even though the resistance to the compressibility of soil decreased with increasing OM content, the recovery from compaction increased too. Increasing OM contents generally lead to decreasing ρ_b (Ruehlmann et al., 2009) and thus to higher void ratios, leaving more space to soil deformation and a reduced resistance to compression (Keller et al., 2011). Similar patterns regarding the relationship between ΔE and basic soil properties were observed by Zhang et al. (2005) on repacked, peat amended soils, and by Pesch et al. (2020) on undisturbed pasture samples; the observations were attributed to the elastic spring effect of soil organic matter. Additionally, a lower ρ_b requires less energy for the soil to be deformed either by internal forces (ΔE) or external forces (C_c).

The diameter to height ratio of the herein used soil core cylinders ($D/h = 1.76$) was below the range of $2.5 - 4$ as suggested by de Lima et al. (2019) and Koolen (1974), to reduce the impact of wall-friction effects on the results. Additionally, the nonuniform bulk densities after compression and concomitant gradients in air-filled porosity eventually affecting the air-phase and mechanical parameters were disregarded in this study, because no comparisons with other studies using different soil core dimensions were performed.

4 Summary and conclusions

We measured air-filled porosity (ε), diffusivity (D_p/D_o), and air permeability (k_a) of repacked soils and sands amended with three concentrations of glacial rock flour (GRF; 0 %, 3.5 %, and 10 % per weight) before (at $\psi = -100$ hPa and $\psi = -300$ hPa) and after uniaxial confined compression tests (only at $\psi = -300$ hPa). We determined the compression index (C_c) and the rebound after compression (ΔE) from the compression curves.

Effects of glacial rock flour (GRF) addition on soil solid-phase parameters

The parameters α_R and β_R of the fitted Rosin-Rammler distribution function were lowest for the highest GRF-concentrations. Only the bulk densities (ρ_b) of the sandy soils were markedly affected by the addition of GRF and were significantly correlated to the soil organic matter content.

Combined effects of GRF addition and soil OM on soil air-phase parameters

We found consistently lower ε for the highest GRF-level. The addition of GRF reduced the OM by the same amount and affected both the ε and the D_p/D_o. A simple power-law model could adequately describe the D_p/D_o of the combined dataset. On the other hand, the k_a clearly differentiated between the different experimental stages (drainage, before compression, after compression) and between the different soil types. We found that the repacked Greenlandic soils, independent of GRF-concentration were susceptible to degradation in terms of soil aeration.

The tortuosity of the pore network generally increased with increasing GRF concentration and was significantly reduced by compression. The effective pore diameter for gas transport (d_{eff}) was not affected by GRF addition but was, however, significantly decreased by compression.

Effects of GRF addition on soil mechanical parameters

The compressibility (C_c) of the 10 % amended mixtures increased markedly compared to the other two levels of GRF. The rebound after compaction, ΔE, did not show any significant variation related to the GRF concentration. The poorly graded and finer textured soils exhibited larger C_c than the more sandy materials, and ΔE was significantly correlated to the organic matter content. The reduction of the resistance to compression with increasing organic matter contents was accompanied by greater recovery from compression.

Perspectives

The amount of GRF should be adapted to the soil type so that adequate aeration and compressibility are not negatively affected. This is especially important for future changes in land use and management (e.g., conversion from pasture to cultivated land). This study showed that the addition of only 3.5 % GRF per weight did not greatly negatively affect the mechanical properties of the repacked soils but induced changes in the pore network such that the tortuosity increased, while the d_{eff} was not affected. However, repacked soil core samples do not perfectly reflect the in-situ conditions, not even right after tillage. External factors like temperature and precipitation, among others, have

a significant impact on soil properties which cannot entirely be captured by laboratory testing. The temporal interaction between OM and GRF needs to be further investigated to be able to assess potential soil aggregation by OM-complexation and subsequent soil structure formation, which ultimately could increase soil strength and optimize soil aeration and water-holding capacity markedly, especially for sandy Greenlandic cultivated soils.

References

Arthur, E., Moldrup, P., Schjønning, P. & de Jonge, W., Lis. (2012). Linking particle and pore size distribution parameters to soil gas transport properties. *Soil Science Society of America Journal*, *76*(1), 18–27.

Bakken, A. K., Gautneb, H. & Myhr, K. (1997). Plant available potassium in rocks and mine tailings with biotite, nepheline and K-feldspar as K-bearing minerals. *Acta Agriculturae Scandinavica, Section B — Soil & Plant Science*, *47*(3), 129–134.

Ball, B. C. (1981). Modelling of soil pores as tubes using gas permeabilities, gas diffusivities and water release. *Journal of Soil Science*, *32*(4), 465–481.

Ball, B. C., O'Sullivan, M. F. & Hunter, R. (1988). Gas diffusion, fluid flow and derived pore continuity indices in relation to vehicle traffic and tillage. *Journal of Soil Science*, *39*(3), 327–339.

Ball, B. C. & Schjønning, P. (2002). 4.4 Air Permeability. In J. H. Dane & C. G. Topp (Eds.), *Methods of Soil Analysis: Part 4 Physical Methods* (pp. 1141–1158). Soil Science Society of America.

Batey, T. (2009). Soil compaction and soil management – a review. *Soil Use and Management*, *25*(4), 335–345.

Bennike, O., Björck, S. & Lambeck, K. (2002). Estimates of South Greenland late-glacial ice limits from a new relative sea level curve. *Earth and Planetary Science Letters*, *197*(3), 171–186.

Bennike, O., Jensen, J. B., Næsby Sukstorf, F. & Rosing, M. T. (2019). Mapping glacial rock flour deposits in Tasersuaq, southern West Greenland. *GEUS Bulletin*, *43*.

Brown, M. B. & Forsythe, A. B. (1974). Robust tests for the equality of variances. *Journal of the American Statistical Association*, *69*(346), 364–367.

Buckingham, E. (1904). *Contributions to our knowledge of the aeration of soils* (tech. rep. No. 25). Bureau of Soils, US Deptartment of Agriculture. Washington.

Chamindu Deepagoda, T. K. K., Clough, T. J., Jayarathne, J. R. R. N., Thomas, S. & Elberling, B. (2020). Soil-gas diffusivity and soil-moisture effects on N2O emissions from repacked pasture soils. *Soil Science Society of America Journal*, *84*(2), 371–386.

Dane, J. H. & Hopmans, J. W. (2002). 3.1 Water Content. In J. H. Dane & C. G. Topp (Eds.), *Methods of Soil Analysis: Part 4 Physical Methods* (pp. 417–545). Soil Science Society of America.

de Lima, R. P. & Keller, T. (2019). Impact of sample dimensions, soil-cylinder wall friction and elastic properties of soil on stress field and bulk density in uniaxial compression tests. *Soil and Tillage Research*, *189*, 15–24.

Deepagoda, T. K. K. C., Smits, K., Jayarathne, J. R. R. N., Wallen, B. M. & Clough, T. J. (2018). Characterization of grain-size distribution, thermal conductivity, and gas diffusivity in variably saturated binary sand mixtures. *Vadose Zone Journal*, *17*(1), 180026.

Di Stefano, C., Ferro, V. & Mirabile, S. (2010). Comparison between grain-size analyses using laser diffraction and sedimentation methods. *Biosystems Engineering*, *106*(2), 205–215.

Efron, B. (1979). Bootstrap methods: Another look at the jackknife. *Annals of Statistics*, *7*(1), 1–26.

Etana, A., Comia, R. A. & Håkansson, I. (1997). Effects of uniaxial stress on the physical properties of four Swedish soils. *Soil and Tillage Research*, *44*(1), 13–21.

Eusterhues, K., Rumpel, C., Kleber, M. & Kögel-Knabner, I. (2003). Stabilisation of soil organic matter by interactions with minerals as revealed by mineral dissolution and oxidative degradation. *Organic Geochemistry*, *34*(12), 1591–1600.

Fazekas, O. & Horn, R. (2005). Zusammenhang zwischen hydraulischer und mechanischer Bodenstabilität in Abhängigkeit von der Belastungsdauer. *Journal of Plant Nutrition and Soil Science*, *168*(1), 60–67.

Flint, L. E. & Flint, A. L. (2002). 2.2 Particle Density. In J. H. Dane & C. G. Topp (Eds.), *Methods of Soil Analysis. part 4 Physical Methods.* (pp. 229–240). Soil Science Society of America.

Fujikawa, T. & Miyazaki, T. (2005). Effects of bulk density and soil type on the gas diffusion coefficient in repacked and undisturbed soils. *Soil Science*, *170*(11), 892–901.

Gautneb, H. & Bakken, A. K. (1995). Crushed rocks, minerals and mine tailings as sources of potassium in agriculture. *Norges Geologiske Undersøkelse*, (427), 119–122.

Gunnarsen, K. C. (2020). *Plant nutritional value of Greenlandic glacial rock flour: An amendment to improve weathered and nutrient poor soils* (Doctoral dissertation). Department of Plant and Environmental Sciences. Faculty of Science, University of Copenhagen.

Gunnarsen, K. C., Jensen, L. S., Gómez-Muñoz, B., Rosing, M. T. & de Neergaard, A. (2019). Glacially abraded rock flour from Greenland: Potential for macronutrient supply to plants. *Journal of Plant Nutrition and Soil Science*, *182*(5), 846–856.

Hamamoto, S., Tokida, T., Miyazaki, T. & Mizoguchi, M. (2008). Dense gas flow in volcanic ash soil: Effect of pore structure on density-driven flow. *Soil Science Society of America Journal*, *72*(2), 480–486.

Hensel, J. (1894). *Bread from Stones. New and Rational System of Land Fertilization and Physical Regeneration.* (A) [Translated from German]. A. J. Tafel.

Hermansen, C., Knadel, M., Moldrup, P., Greve, M. H., Karup, D. & de Jonge, L. W. (2017). Complete soil texture is accurately predicted by visible near-infrared spectroscopy. *Soil Science Society of America Journal*, *81*(4), 758–769.

Hoogsteen, M. J. J., Lantinga, E. A., Bakker, E. J. & Tittonell, P. A. (2018). An evaluation of the loss-on-ignition method for determining the soil organic matter content of calcareous soils. *Communications in Soil Science and Plant Analysis*, *49*(13), 1541–1552.

Katuwal, S., Arthur, E., Tuller, M., Moldrup, P. & de Jonge, L. W. (2015). Quantification of soil pore network complexity with X-ray computed tomography and gas transport measurements. *Soil Science Society of America Journal*, *79*(6), 1577–1589.

Kawamoto, K., Moldrup, P., Schjønning, P., Iversen, B. V., Komatsu, T. & Rolston, D. E. (2006). Gas transport parameters in the vadose zone: Development and tests of power-law models for air permeability. *Vadose Zone Journal*, *5*(4), 1205–1215.

Keller, T. & Arvidsson, J. (2007). Compressive properties of some Swedish and Danish structured agricultural soils measured in uniaxial compression tests. *European Journal of Soil Science*, *58*(6), 1373–1381.

Keller, T. & Dexter, A. R. (2012). Plastic limits of agricultural soils as functions of soil texture and organic matter content. *Soil Research*, (50), 7–17.

Keller, T., Lamandé, M., Schjønning, P. & Dexter, A. R. (2011). Analysis of soil compression curves from uniaxial confined compression tests. *Geoderma*, *163*(1), 13–23.

Kennedy, V. C. (1965). *Mineralogy and cation-exchange capacity of sediments from selected streams* (Professional paper No. 433D). United States Department of the Interior, Geological Survey.

Kleiv, R. A. & Thornhill, M. (2007). Production of mechanically activated rock flour fertilizer by high intensive ultrafine grinding. *Minerals Engineering*, *20*(4), 334–341.

Koolen, A. J. (1974). A method for soil compactibility determination. *Journal of Agricultural Engineering Research*, *19*(3), 271–278.

Lamandé, M., Schjønning, P. & Labouriau, R. (2017). A novel method for estimating soil precompression stress from uniaxial confined compression tests. *Soil Science Society of America Journal*, *81*(5), 1005–1013.

Larson, W. E., Gupta, S. C. & Useche, R. A. (1980). Compression of agricultural soils from eight soil orders. *Soil Science Society of America Journal*, *44*(3), 450–457.

Malcolm, R. L. & Kennedy, V. C. (1970). Variation of cation exchange capacity and rate with particle size in stream sediment. *Journal (Water Pollution Control Federation)*, *42*(5), R153–R160.

Masís-Meléndez, F., Chamindu Deepagoda, T. K. K., de Jonge, L. W., Tuller, M. & Moldrup, P. (2014). Gas diffusion-derived tortuosity governs saturated hydraulic conductivity in sandy soils. *Journal of Hydrology*, *512*, 388–396.

McCarthy, K. P. & Brown, K. W. (1992). Soil gas permeability as influenced by soil gas-filled porosity. *Soil Science Society of America Journal*, *56*(4), 997–1003.

Millington, R. J. & Quirk, J. M. (1964). Formation factor and permeability equations. *Nature*, *202*, 143–145.

Missoux, M. (1853). Sur l'emploi de la poudre des roches granitiques comme excitant de la végétation. *Compt Rend Acad Sci*, *36*(1), 1136.

Moldrup, P., Olesen, T., Komatsu, T., Schjønning, P. & Rolston, D. E. (2001). Tortuosity, diffusivity, and permeability in the soil liquid and gaseous phases. *Soil Science Society of America Journal*, *65*(3), 613–623.

Moldrup, P., Yoshikawa, S., Olesen, T., Komatsu, T. & Rolston, D. E. (2003). Air permeability in undisturbed volcanic ash soils. *Soil Science Society of America Journal*, *67*(1), 32–40.

Nielsen, S. & Nielsen, B. (2018). *Data report on Baskarp Sand No. 15: 2018 Delivery*. Aalborg Universitet, Institut for Byggeri og Anlæg.

Nimmo, J. R. (2004). Porosity and pore size distribution. *Encyclopedia of Soils in the Environment*, *3*, 295–303.

Pesch, C., Lamandé, M., de Jonge, L. W., Norgaard, T., Greve, M. H. & Moldrup, P. (2020). Compression and rebound characteristics of agricultural sandy pasture soils from South Greenland. *Geoderma*, *380*, 114608.

Pesch, C., Weber, P. L., de Jonge, L. W., Greve, M. H., Norgaard, T. & Moldrup, P. (2021). Soil–air phase characteristics: Response to texture, density, and land use in Greenland and Denmark. *Soil Science Society of America Journal*, *85*(5), 1534–1554.

Pesch, C., Weber, P. L., Moldrup, P., de Jonge, L. W., Arthur, E. & Greve, M. H. (2022). Physical characterization of glacial rock flours from fjord deposits in south greenland–toward soil amendment. *Soil Science Society of America Journal*, *86*(2), 407–422.

Poulsen, T. G. (2013). Gas Permeability in Soils as Related to Soil Structure and Pore System Characteristics. In S. Logsdon, M. Berli & R. Horn (Eds.), *Quantifying and Modeling Soil Structure Dynamics* (pp. 155–185). Soil Science Society of America, Inc.

Pulido-Moncada, M., Munkholm, L. J. & Schjønning, P. (2019). Wheel load, repeated wheeling, and traction effects on subsoil compaction in northern Europe. *Soil and Tillage Research*, *186*, 300–309.

Rosin, P., Rammler, E. & Sperling, K. (1933). *Korngrossenprobleme des Kohlenstaubes und ihre Bedeutung für die Vermahlung* (Bericht des Reichkohlerates No. 52). Reichkohlerat. Berlin.

Ruehlmann, J. & Körschens, M. (2009). Calculating the effect of soil organic matter concentration on soil bulk density. *Soil Science Society of America Journal*, *73*(3), 876–885.

Salire, E. V., Hammel, J. E. & Hardcastle, J. H. (1994). Compression of intact subsoils under short-duration loading. *Soil and Tillage Research*, *31*(2), 235–248.

Schäffer, B., Stauber, M., Mueller, T. L., Müller, R. & Schulin, R. (2008). Soil and macro-pores under uniaxial compression. I. Mechanical stability of repacked soil and deformation of different types of macro-pores. *Geoderma*, *146*(1), 183–191.

Schjønning, P. (1992). Size distribution of dispersed and aggregated particles and of soil pores in 12 Danish soils. *Acta Agriculturae Scandinavica, Section B — Soil & Plant Science*, *42*(1), 26–33.

Schjønning, P. (1985). *A laboratory method for determination of gas diffusion in soil* (tech. rep. S 1773) [in Danish with English summary]. Beretning. Statens Planteavlsforsøg (Denmark).

Schjønning, P., Eden, M., Moldrup, P. & de Jonge, L. W. (2013). Two-chamber, two-gas and one-chamber, one-gas methods for measuring the soil-gas diffusion coefficient: Validation and inter-calibration. *Soil Science Society of America Journal*, *77*(3), 729–740.

Schjønning, P. & Koppelgaard, M. (2017). The Forchheimer approach for soil air permeability measurement. *Soil Science Society of America Journal*, *81*(5), 1045–1053.

Shapiro, S. S. & Wilk, M. B. (1965). An analysis of variance test for normality (complete samples). *Biometrika*, *52*(3-4), 591–611.

Soane, B. D. (1990). The role of organic matter in soil compactibility: A review of some practical aspects [A Tribute to Prof. IR. H. Kuipers]. *Soil and Tillage Research*, *16*(1), 179–201.

Sohn, H. Y. & Moreland, C. (1968). The effect of particle size distribution on packing density. *The Canadian Journal of Chemical Engineering*, *46*(3), 162–167.

Soil Survey Division Staff. (1999). *A basic system of soil classification for making and interpreting soil surveys* (Agricultural Handbook No. 436). Natural Resources Conservation Service, USDA. Washington DC, USA.

Stine, R. A. (1985). Bootstrap prediction intervals for regression. *Journal of the American Statistical Association*, *80*(392), 1026–1031.

Stone, J. A. & Larson, W. E. (1980). Rebound of five one-dimensionally compressed unsaturated granular soils. *Soil Science Society of America Journal*, *44*(4), 819–822.

Sukstorf, F. N., Bennike, O. & Elberling, B. (2020). Glacial rock flour as soil amendment in subarctic farming in South Greenland. *Land*, *9*(6).

Sun, H., Nelson, M., Chen, F. & Husch, J. (2009). Soil mineral structural water loss during loss on ignition analyses. *Canadian Journal of Soil Science*, *89*(5), 603–610.

Tukey, J. W. (1977). *Exploratory Data Analysis*. Addison-Wesley.

Tuli, A., Hopmans, J. W., Rolston, D. E. & Moldrup, P. (2005). Comparison of Air and Water Permeability between Disturbed and Undisturbed Soils. *Soil Science Society of America Journal*, *69*(5), 1361–1371.

van Straaten, P. (2002). *Rocks for Crops: Agrominerals of sub-Saharan Africa*. ICRAF.

van Straaten, P. (2007). *Agroecology: The use of rocks for crops*. Enviroquest.

Ward, P. R. & Oades, J. M. (1993). Effect of clay mineralogy and exchangeable cations on water repellency in clay-amended sandy soils. *Soil Research*, *31*(3), 351–364.

Weber, P. L., de Jonge, L. W., Greve, M. H., Norgaard, T. & Moldrup, P. (2020). Gas diffusion characteristics of agricultural soils from South Greenland. *Soil Science Society of America Journal*, *84*(5), 1606–1619.

Weber, P. L., Hermansen, C., Norgaard, T., Pesch, C., Moldrup, P., Greve, M. H., Müller, K., Arthur, E. & de Jonge, L. W. (2021). Moisture-dependent water repellency of Greenlandic cultivated soils. *Geoderma*, *402*, 115189.

Zhang, B., Horn, R. & Hallett, P. D. (2005). Mechanical resilience of degraded soil amended with organic matter. *Soil Science Society of America Journal*, *69*(3), 864–871.

ISSN (online): 2446-1636
ISBN (online): 978-87-7573-882-3

AALBORG UNIVERSITY PRESS